Preparation and Characterization of Rare Earth Ion Doped Luminescent Materials for Optoelectronic Device Applications

Thesis

Submitted to the Delhi Technological University

for the Award of the Degree of

DOCTOR OF PHILOSOPHY

in

APPLIED PHYSICS

Submitted by

RAVITA
(2K18/PhD/AP/02)

Under the Supervision of

Prof. A.S. RAO

Department of Applied Physics, Delhi Technological University
Bawana Road, Delhi-110042, India

July-2022

This thesis is dedicated to

my family

DECLARATION

This is to certify that the thesis entitled ***"Preparation and characterization of Rare Earth Ion-Doped Luminescent Materials for Optoelectronic Device Applications"*** submitted to the Delhi Technological University, Delhi for the award of the degree of Doctor of Philosophy is based on original research work carried out by me under the supervision of Prof. A. S. Rao, Department of Applied Physics, Delhi Technological University, Delhi. It is further certified that the work embodied in this thesis has not been submitted in part or fully to any other University or Institute for the award of any degree or diploma.

RAVITA
Candidate
Roll No. 2K18/PhD/AP/02

Delhi Technological University
Formerly Delhi College of Engineering

(Govt. of National Capital Territory of Delhi)
Shahbad daulatpur, Bawana Road, Delhi-110042

CERTIFICATE

This is to certify that the thesis entitled ***"Preparation and characterization of Rare Earth Ion-Doped Luminescent Materials for Optoelectronic Device Applications"*** submitted to the Delhi Technological University, Delhi for the award of the degree of Doctor of Philosophy is based on original research work carried out by me under the supervision of Prof. A. S. Rao, Department of Applied Physics, Delhi Technological University, Delhi. It is further certified that the work embodied in this thesis has not been submitted in part or fully to any other University or Institute for the award of any degree or diploma.

Ravita

RAVITA
Candidate
Roll No. 2K18/PhD/AP/02

This is to certify that the above statement made by the candidate is correct to the best of our knowledge.

Rao
28/07/2022

Prof. A.S. Rao
Supervisor (Professor)
Department of Applied Physics
Delhi Technological University
Delhi, India

Rinku
28th July 2022

Prof. Rinku Sharma
Head,
Department of Applied Physics
Delhi Technological University
Delhi, India

ACKNOWLEDGMENTS

I feel obligated to thank everyone who has helped me to complete my thesis work, whether directly or indirectly. First and foremost, I would like to convey my heartfelt gratitude and sincere thanks to my supervisor, Professor A. S. Rao, Department of Applied Physics at Delhi Technological University. He has always been helpful and encouraging, providing me with all the necessary instruction while also allowing me the freedom to follow my research interests. I am grateful for all of his contributions to my Ph.D. work, including his time, valuable recommendations, and facilities. I shall be eternally grateful for the time I spent under his guidance.

I am thankful to Prof. Rinku Sharma, Head of the Department of Applied Physics and Prof. S.C. Sharma, DRC chairman for their encouragement and valuable advice.

I am also thankful to Dr. Nisha Deopa, Dr. Swapna Koneru, Dr. Mahmuda Shek and Dr. M. Venkateswarulu for their help and suggestions during my research work.

I would like to thank to Dr. Kanika Bhatiya and Dr. Arti Yadav, postdoctoral colleagues, for their professionalism and dedication to maintaining a relaxed environment.

I am also grateful to my seniors Dr. Sumandeep Kaur, Dr. Aman Prasad, Dr. Harpreet Kaur, Mr. Mukesh Sahu, Ms. Yasha Tayal, Ms. Kartika Maheshwari, Mr. Mohit Tyagi, for their kind support and valuable suggestions.

I am also thankful to all the teaching and non-teaching staff of Delhi technological university for their help whenever and wherever I needed it.

It is my pleasure to thank all my fellow researchers Ms. Pooja Rohilla, Ms. Shristy Malik, Mr. Rajat Bajaj, Ms. Deepali, Ms. Shweta Kumari, Ms. Anu, Ms. Sheetal Kumari, Mr. Sandeep Sharma, Mr. Mohit Mann, Mr. Vikash Sangwan, Mr. Videsh, Mr. Inderjeet Maurya and Ms. Vertika for their support and help as and when required during my research work.

I owe this effort to my family, friends, and colleagues, whose persistent encouragement and cooperation enabled me to complete it. I am grateful to my parents, Mr. Vijay Singh and Mrs. Kamlesh Devi, for their devotion and hard work in getting me to where I am now. I want to

convey my heartfelt gratitude to my husband, Mr. Sachin, and my little daughters, Maanvi and Vaanya Kadyan. They have always been a real inspiration to me. Their consistent love and support prompted me to finish my research.

Last but not least, I consider myself fortunate to be able to thank my mother-in-law, Mrs. Nirmala Devi, for her unconditional love and assistance during this journey. In every circumstance, whether financial or psychological, she always stood up for me. I owe her a great deal of credit for my degree.

I am so grateful to the University Grants Commission (UGC), Govt. of India, New Delhi for the award of Junior Research Fellowship (JRF) (1471/(CSIRNETJUNE2019)).

These accomplishments are all virtue of God's grace.

Ravita

LIST OF PUBLICATIONS

1. "Effective Sensitization of Eu^{3+} Visible Red emission by Sm^{3+} in thermally stable Potassium Zinc Alumino Borosilicate Glasses for Photonic Device Applications"
   Ravita, *A. S. Rao*
   Journal of Luminescence, 244 (2022) 118689 (I.F. = 4.171)

2. "Effective energy transfer from Dy^{3+} to Tb^{3+} ions in thermally stable KZABS glasses for intense green-emitting device applications"
   Ravita, *A. S. Rao*
   Journal of Luminescence, 239 (2021) 118325 (I.F. = 4.171)

3. "Color tunable photoluminescence in KZABS: Tm^{3+} glasses under different sources of excitation for photonic applications"
   Ravita, *A. S. Rao*
   Journal of Non-Crystalline Solids, 585 (2022) 121532 (I.F. = 4.458)

4. "Tunable photoluminescence studies of KZABS: RE^{3+} (RE^{3+} = Tm^{3+}, Tb^{3+} and Sm^{3+}) glasses for w-LEDs based on energy transfer"
   Ravita, *A. S. Rao*
   Accepted in Journal of Luminescence, manuscript ID: LUMIN-D-22-00843 (I.F. = 4.171)

5. "Green-emitting Tb^{3+} doped LaP_3O_9 phosphors for the plasma display panel"
   V. Singh, ***Ravita****, S. Kaur, A.S. Rao, H. Jeong*
   Optik, 244 (2021) 167323 (I.F. = 2.840)

6. "Spectral characteristics of Tb^{3+} doped ZnF2–K2O–Al2O3–B2O3 glasses for epoxy-free tricolour w-LEDs and visible green laser applications"
   A. Kumar, Anu, M.K. Sahu, ***Ravita,*** *S. Dahiya, N. Deopa, A. Kumar, R. Punia, A.S. Rao*
   Journal of luminescence, 43 (2017) 118676 (I.F. = 4.171)

7. "Effect of Annealing on Structural Properties of Fe3O4 Ferrite Nanoparticles"
   Ravita, *Amita, A. Kumar, P.S. Rana*
   Journal of Computational and Theoretical Nanoscience, 24 (2018) 5748-5751, (I.F. = 1.3)

8. "Luminescent studies on Sm^{3+} doped Alkali Zinc Alumino Borosilicate (AZABS) Glasses for w-LED Applications"
   Rajat Bajaj, Pooja Rohilla, Aman Prasad, ***Ravita,*** *Ankur Shandilya, A.S. Rao*
   Communicated to Journal of non-crystalline solids, (I.F. = 4.538)

9. "Luminescent studies on Tm^{3+}/Dy^{3+}/Eu^{3+}doped Potassium Zinc Alumino Borosilicate (KZABS) glasses for color tunability and warm white light generation"
   Ravita, *Aman Prasad, A.S. Rao*
   Communicated to Journal of Luminescence, (I.F. = 4.171)

10. "Cool white light generation from thermally stable Dy^{3+} doped CABS glasses for epoxy-free lighting applications"
    Ravita, *Aman Prasad, Pooja Rohilla, Rajat Baja, Ankur Shandilya, A.S. Rao*
    Communicated to Optical materials, (I.F. = 3.754)

ABSTRACT

Potassium Zinc Alumino Borosilicate (KZABS) glasses doped with different concentrations of various rare-earth ions such as Sm^{3+}, Eu^{3+}, Dy^{3+}, Tb^{3+} and Tm^{3+} ions were prepared by the conventional melt quenching technique. The glassy nature of KZABS host glass has been confirmed through XRD measurements. FT-IR and Raman spectra for the KZABS host glass have been recorded to know the presence of various functional groups and phonon energy of the host glass. FT-IR spectrum helps to evaluate the OH content present in the host glass. Archimedes' principle and Brewster's angle method were employed to estimate the physical parameters such as density and refractive index for the as-prepared glasses, respectively. The optical absorption, excitation, emission and lifetime measurements were carried out to find the suitability of these glasses for designing and developing various optoelectronic devices. Absorption spectra were used to estimate the energy bandgap of the synthesized glasses.

The PL emission profiles were subjected to Dexter's theory in order to elucidate the mechanism involved in the energy transfer process between various rare-earth ions. The Inokuti-Hirayama model was applied to the PL decay profiles one mare in order to understand the energy transfer mechanism and confirm the conclusions of Dexter's theory. The temperature-dependent emission profiles have been recorded to check the thermal stability of the as prepared glasses. Further, it will also be used to evaluate the activation energy of the as-prepared glasses. Furthermore, CIE chromaticity coordinates were also evaluated to understand the suitability of these glasses for various visible emission applications. CIE points help to assess the color purity and color-correlated temperature of the as-prepared glasses. All these parameters are essential to know the suitability of these glasses for various photonic device

applications such as solid-state lightings, fiber amplifiers and white light emitting diodes (w-LEDs).

TABLE OF CONTENTS

Chapter 2. Experimental Section

Chapter 3. ***Effective sensitization of Eu^{3+} Red emission by Sm^{3+} in thermally stable Potassium Zinc Alumino Borosilicate Glasses for Photonic Applications***

Chapter 4. *Effective energy transfer from Dy^{3+} to Tb^{3+} ions in thermally stable KZABS glasses for intense green-emitting device applications*

Chapter 5. *Colour tunable photoluminescence in KZABS: Tm^{3+} glasses under different sources of excitation for Photonic Applications*

LIST OF FIGURES

LIST OF TABLES

Chapter 1
Introduction

This chapter deals with the lighting technology, a basic idea for the vast requirement of white light emission materials in the current scenario, ways of generating white light, properties of rare-earth ions, RE doped glasses and their colorimetric properties, followed by the objectives of this thesis work.

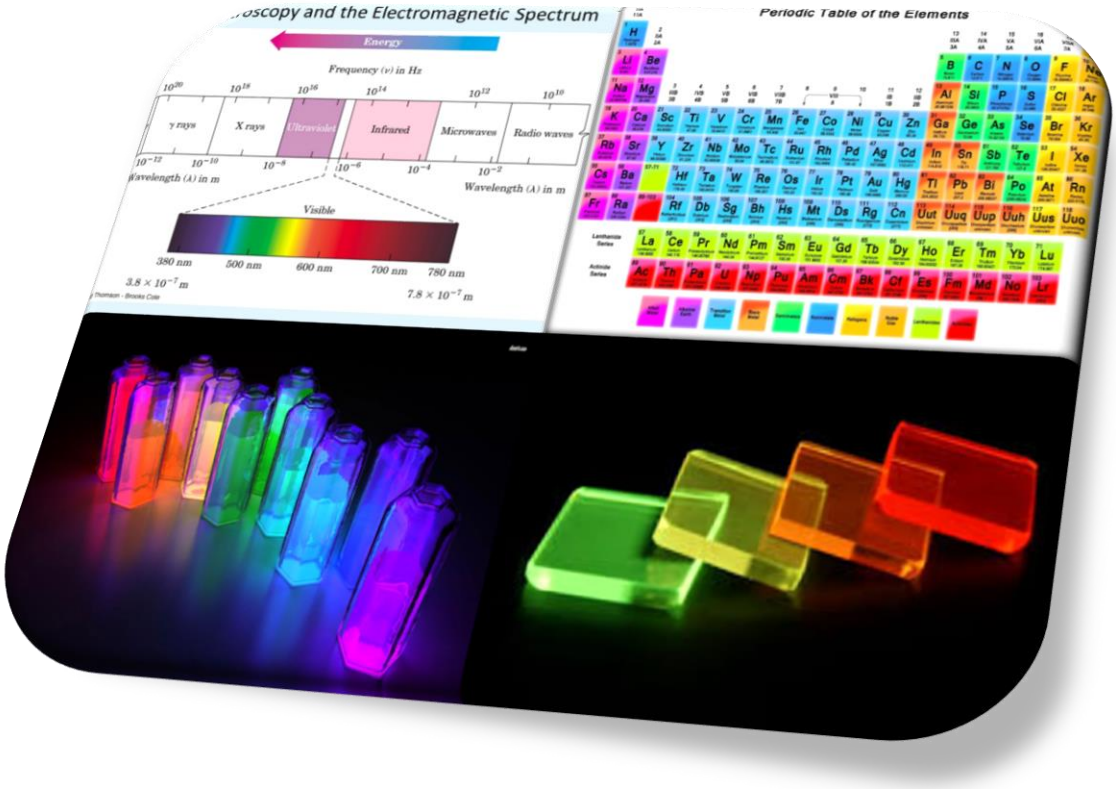

1.1 . Basic introduction

In today's world, lighting uses more than 19% of total global electrical energy consumption, and this percentage is increasing day by day. Lighting technology is basically divided into four types: incandescent, fluorescent, halogen, and light emitting diode (LED). Each uses a different method to produce light. Incandescent and fluorescent lamps produce a lot of heat resulting into insufficient efficiency. Halogen lamps also emit a lot of heat; it could explode due to high pressure result into fire. LEDs are the most widespread form of artificial lighting among these four technologies and are crucial to modern civilization. LEDs are seeking the attention of the researchers in subsequent illumination sources because of their characteristic features such as long lifecycle, low energy consumption, high stability, high efficiency, eco-friendly, and many more [1–3]. Nowadays, white LEDs (w-LEDs) can be made-up by coating a yellow phosphor on a blue LED chip. Indium galillium nitride (InGaN) and yttrium aluminium garnet (YAG) activated with Ce^{3+} ions have commonly used as blue and yellow color emission sources respectively [4,5]. The light obtained using this method contrasts with the natural light and has other drawbacks like color in-stability, short lifecycle, poor color rendering index (CRI), and high correlated color temperature (CCT). CRI and CCT ratings reveal a lot of things about the device's capabilities. The earlier mentioned problems arise due to the deficiency of red components [6]. To obtain w-LEDs with high CRI, the RGB (red, green, and blue) phosphor method may be an appropriate one because of their durability and high efficiency [7,8]. Still, it has various downsides because of high temperature and the epoxy resin requirement, which degrades lifetime, efficiency and quite danger for healthiness (due to high temperature) [9,10]. One more considerable drawback is that green and red light absorbed the blue color, which cause oxidative degradation observed in commercially available $BaMgAl_{10}O_{17}:Eu^{2+}$ phosphor [11]. Rare-earth (RE) doped glasses may be better alternatives to rectify this kind of problems due to the low cost, simple synthesis techniques, safer environment, and no epoxy resin

required [12–17]. We have gone through literature to know about the work being done on RE doped glasses in luminescence.

1.2. Literature survey

It includes several investigations by various researchers to examine the photoluminescence (PL) characteristics of different RE ions in multiple materials.

S. Nayab Rasool et al. (2013) studied the PL properties of Sm^{3+} ions in phosphate glasses. They observed the emission in the orangish-red region corresponding to the $^4G_{5/2} \rightarrow {}^6H_{7/2}$ (596 nm) transition. The non-exponential decay profiles were analyzed from the $^4G_{5/2}$ level and the energy transfer mechanism between Sm^{3+} ions was observed via dipole-dipole interaction [18]. Y. Ye et al. (2019) studied Dy^{3+} doped fluoride glasses and observed white light emission. They reported the J-O parameter using absorption spectra to calculate the relation between Dy^{3+} ion content and the Y/B color ratio. The chromaticity 1931 diagram has been used to show the emitted color suitable for white light applications [19]. F. Grum et al. (1974) reported the basic colorimetry concerning the CIE recommendations. They primarily focused on the standard illuminations and observers, tristimulus values, chromaticity points, the conditions for views and illustrations, and many other formulae [20]. K. El-Egili et al. (2003) reported the infra-red (IR) spectroscopy of borosilicate glasses. They observed that the structure of borosilicate is affected by the addition of Al_2O_3. The author found the Si-O-Si bonds vibrating and containing SiO_4 tetrahedral units [21].

Kh. A. Bhaskar et al. (2020) studied the singly doped and co-doped borosilicate glasses with Dy^{3+} and Tb^{3+} ions, which were found suitable for white color applications. The author revealed the non-crystalline nature of the prepared glasses by recording X-ray diffraction (XRD) spectra. The radiative properties have been estimated using the J-O theory on absorption spectra. The variation in PL intensities confirms the mutual energy transfer between Dy^{3+} and Tb^{3+} ions.

Based on the estimated CIE coordinates and CCT values, the author claimed their usage for standard white color applications [12]. A. A. Ali et al. (2017) reported the Fourier transform infrared (FT-IR) studies on borate glasses. The author observed the presence of BO_4 and BiO_6 at lower concentrations of Bi_2O_3 in the FT-IR spectrum and BiO_3 appeared at higher concentrations. They have estimated various physical parameters such as density, refractive index and band gap using absorption spectrum fitting (ASF) and derivation of ASF (DASF). All the values calculated from ASF and DASF are in good agreement with each other [22].

L. Krishna Bharat et al. (2016) investigated the thermoluminescence, cathodoluminescence and PL characteristics of Y_6WO_{12} phosphors activated with different RE^{3+} (RE^{3+} = Tm^{3+}, Tb^{3+} and Sm^{3+}) ions. The morphology of the prepared phosphors has been studied by transmission electron microscopy (TEM) and structure analysis by recording XRD patterns. The calculated color coordinates were comparable to the standard phosphor useful for lighting applications [23]. R. T. Alves et al. (2020) investigated the Tm^{3+}/Tb^{3+}/Sm^{3+} doped telluride glasses with a typical UV excitation for white light emission applications. The author demonstrated the luminescence characteristics of singly-doped and tri-doped glasses under the same excitation and observed the intense emission. The studies also support energy transfer from $Tm^{3+} \rightarrow Tb^{3+}$ and $Tm^{3+} \rightarrow Sm^{3+}$ via three routes [24].

Tong Wang et al. (2020) analyzed the crystal phase of $NaY(MoO_4)_2$ glass-ceramics by using XRD. The author prepared glass ceramics by applying an optimal heat treatment for 2.5 hr and detected increased luminescence. They demonstrated the energy transfer mechanism between Tm^{3+}, Dy^{3+} and Eu^{3+} ions. The color of the Tm^{3+}-Dy^{3+} co-doped glasses shifts from blue to white region with an increase in Dy^{3+} ion concentration whereas in the tri-doped glass-ceramics it move towards the warm white region with an increase in Eu^{3+} ion concentration [25]. P. Rekha Rani et al. (2019) studied the spectroscopic properties of borate glasses doped with Dy^{3+} ions for white light-emitting diodes (w-LEDs) and laser applications. The author demonstrated

the absorption spectra, PL emission and PL decay characteristics to understand the utility of the as-prepared glasses in photonic devices. The estimated color parameters agree with the standard white color parameters [26].

After surveying the literature, it is observed that white light emission plays a crucial role in the performance of modern lighting devices. Many researchers devoted their time to get better results and focused on it because of their potential applications. This has motivated us to take up research on RE doped glasses suitable for white LED applications. For this some of the basic concepts involved in producing white light and the necessary theories needed to be understood throughly. This has been enumerated in the following sections of this chapter.

1.3. Luminescence

It is the emission of light when a luminescent material is excited by some form of energy. Based on the type of excitation energy, it can be of many types as follows:

- **Cathodoluminescence:** The emission of light from a substance in response to excitation by incident electrons is known as cathodoluminescence.
- **Chemiluminescence:** It is the emission of light caused by a chemical reaction.
- **Photoluminescence:** It is emission of light after the absorption of photons.
- **Electroluminescence:** The ability of a material, often a semiconductor, to generate light in response to an electrical current or a strong electrical field is known as electroluminescence.
- **Radioluminescence:** It is emission of light after ionizing the radiations with matter.
- **Thermoluminescence:** It refers to the process through which a mineral emits light when heated.

1.4. Photoluminescence (PL)

In this process, an electron gets excited to higher levels by absorbing some photons and then relaxing to the ground state by emitting light energy equal to the difference between those energy levels.

Fig. 1.1. Examples of photoluminescence

Further, it can be classified into two types:

(i) **Fluorescence:** In this phenomenon, electrons get excited by absorbing many photons and return to the lower energy states. The emission is immediate and spin remains the same throughout this process. The emitted electrons have a longer wavelength and are lower in energy.

(ii) **Phosphorescence:** The material can store energy relatively for more time in this phenomenon. Here, electrons get excited by absorbing appropriate energy and then relaxing to the lower energy states by changing their spin multiplicity. It is also termed as afterglow. In other words, phosphorescence is a delayed fluorescence.

The difference between fluorescence and phosphorescence can be easily understood from the Jablonski diagram in Fig. 1.2

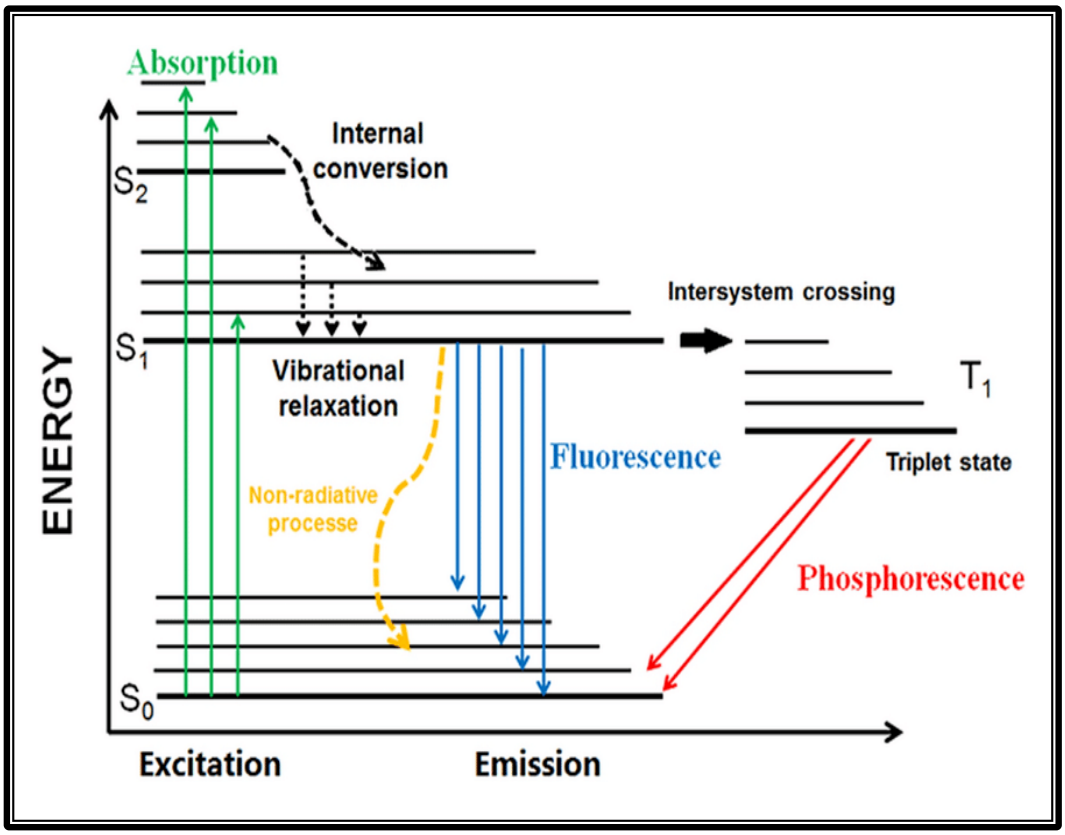

Fig. 1.2. Jablonski diagram showing various processes involved in PL

Some of the essential terms mentioned in the Jablonski diagram are explained below:

(a) Absorption: This is a process in which light gets absorbed by the material and attenuates. One typical example of absorption is how the grass is visible green in color. Out of seven distinct shades of white, the grass absorbed all six except the green one. It reflects the green color and our eyes detect it.

(b) Excitation: In this process, a system or an electron absorbs energy and gets excited to a higher level. Jablonski diagram show various singlet (S1, S2) and triplet (T1) excited states**.**

(c) Emission: After excitation, a molecule tries to return to the ground state by emitting a certain amount of energy in terms of photons. If it returns to the same spin state (S1→S0), emission will be termed as fluorescence and phosphorescence to the different spin state (T1→S0). This results in a loss of energy.

(d) Vibrational relaxation: After exciting an electron, there are many ways to dissipate that energy. It may be through vibrational relaxation, which is a non-radiative process. It is shown in Fig. 1.2 by the straight dotted line. In this process, the energy of the excited electron is given away to the other vibrational modes of the same electronic state as kinetic energy. It is an immediate process taking time $\approx 10^{-13}$ seconds.

(e) Internal conversion: This process is similar to vibrational relaxation and a non-radiative process. The excited electrons can transfer their energy to the lower vibration states in the same and different electronic states. This transition is shown by the curved dotted arrow in the Jablonski diagram. It occurs because of the overlapping of vibrational and electronic energy levels.

(f) Intersystem crossing: This is another path an electron can follow to dissipate energy. Here, the electron changes its spin multiplicity along with the vibrational or electronic levels. This is a relatively slow process that is forbidden transition. It leads to the various routes back to the ground state. Phosphorescence is one such a route in which an electron goes from a triplet excited state to the singlet ground state through a radiative transition.

1.4.1. Applications

Photoluminescent materials are used in various applications such as fluorescent lights, emissive displays, and LEDs. The systems that detect X-rays or γ-rays used in medical imaging also use luminescent materials. Television and computer monitor screens, oscilloscope and radar screens, electron microscope screens, and LEDs for general illumination and specialized applications are all examples of luminescent materials that are in use today. Synthesis and characterization of luminescent materials attracted many scientific groups phenomenally due to their significant and widespread applications in fascinating fields like lasers, optical fiber amplifiers, display devices and other lighting devices such as w-LEDs [1–4].

1.5. White light emission

White light is just daylight that has been filtered via a filter. It contains all visible spectrum wavelengths at the same intensity. White light, in simple words, is light that appears white to the retina. It encompasses all electromagnetic energy in the visible spectrum at all wavelengths.

1.5.1. Why white light

The growing demand for fossil fuels and the environmental consequences of their use continue to put a strain on an already overburdened global energy infrastructure. Heat or gas discharge is used in traditional incandescent and fluorescent lamps. Both phenomena result in significant energy losses due to enormous heat and massive Stokes shifts. To overcome these limitations, a new lighting device was invented in 1996 using a blue InGaN light-emitting diode (LED) chip with a yellow phosphor. The InGaN chip emits blue light when operated at a particular current due to electron-hole recombination in the p–n junctions. A schematic diagram of the phosphor-converted white LEDs is shown in Fig. 1.3.

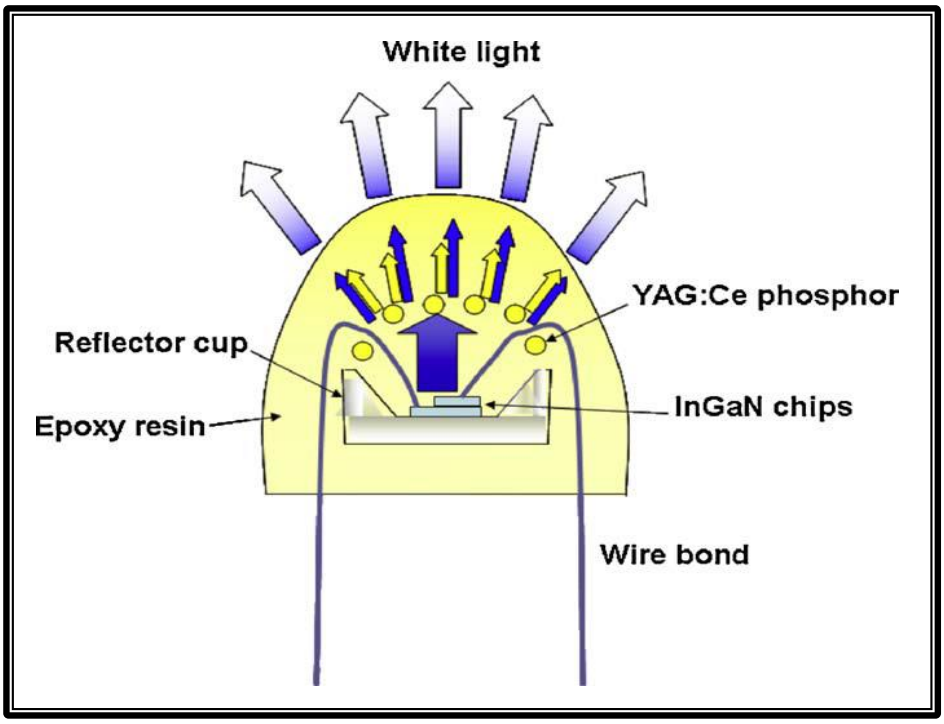

Fig. 1.3. Schematics of pc-white LEDs

The YAG: Ce^{3+} phosphor is excited by some of the blue light from the LED, which emits yellow light, and the remainder of the blue light is combined with the yellow light to produce white light. This LED-based lighting type is known as solid-state lighting (SSL).

High luminous brightness, fuel savings, environmental friendliness, compact volume, and extended persistence are all the advantages of SSL. Traditional white light sources have virtually reached their physical efficiency limits. However, white LEDs have not yet reached to their highest efficiency limits. In conventional incandescent and fluorescent lamps, energy is wasted in heat radiation and efficiency is poor.

1.5.2. White light generation

As illustrated in Fig. 1.4, three alternative ways may be employed to generate white light using LEDs:

(1) utilizing red–green–blue (RGB) LEDs

(2) employing an ultraviolet (UV) LED to stimulate RGB phosphors

(3) Using blue light to excite a yellow-emitting phosphor implanted in the epoxy resin

A 450–470 nm blue GaN LED chip is frequently coated with a yellowish phosphor coating. At present Yttrium Aluminium Garnet (YAG) activated with Ce^{3+} is the commercially available yellow phosphor used in pc-wLEDs. Yellow phosphors have various drawbacks, such as a low CRI and color temperature stability due to the absence of a red component. Color temperature instability may also be found in RGB LEDs leading to degradation of different color LEDs or fluctuations in driving current. Furthermore, various driving currents are required for distinct RGB LEDs, making their development more difficult.

The third method in which white UV-LEDs are fabricated by UV-LED chips coated with white light-emitting single-phased phosphors or RGB tri-color phosphors might have some earlier pitfalls. But this is far better due to the relatively high CRI, significant efficiency, and tunable

color temperature. Because of their excellent features, white UV-LEDs are thought to represent the future of SSL advancement.

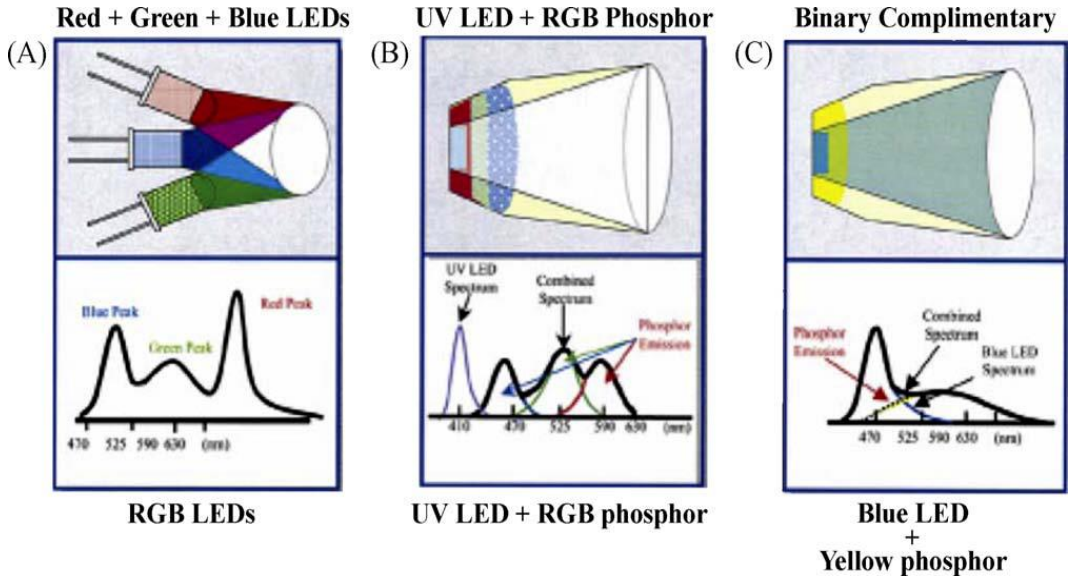

Fig. 1.4. Three methods of generating white light from LEDs: (a) red + green + blue-LEDs, (b) UV-LED + RGB phosphors, and (c) blue-LED + yellow phosphor

In phosphor-based LEDs, epoxy resins are required, which degrade the devices with time. The Halo effect is another drawback of the use of phosphor materials. To avoid these problems, people are searching for glass-based LEDs [27,28]. The primary benefit of glass-based LEDs is that they are simple to produce, cost-effective, healthy, environment friendly and do not require any epoxy resins.

1.6. Glasses

Glass is an amorphous material with short-range order and a non-periodic arrangement of atoms exhibiting the transition temperature.

1.6.1. Glass components

Glass components are classified into three groups based on their essential characteristics, such as electronegativity and their bond strength. They are glass formers, network modifiers and intermediates.

1.6.1.1. Glass formers

These are the primary components of the glass network, which form glasses without the help of additional elements following the melting and cooling process. They have cation-oxygen bond strengths of more than 80 Kcal/mol, and cations have large electronegativity, with 50% of bonds being ionic.

1.6.1.2. Network modifiers

When added to the network producing oxides in modest amounts (10 mol percent to 15 mol percent), these are the oxides that substantially affect and modify the glass network. These are generally oxides of small-charged cations. These oxides have the lowest bond strength, ranging between 10 and 60 Kcal/mol, and do not engage in network creation, instead assist in structural alteration. These cations are very ionic and have shallow electronegativity values. The choice of modifier cation allows the glass to be used in various applications, including optoelectronic devices, sensors, solid-state ionic conductors, and more.

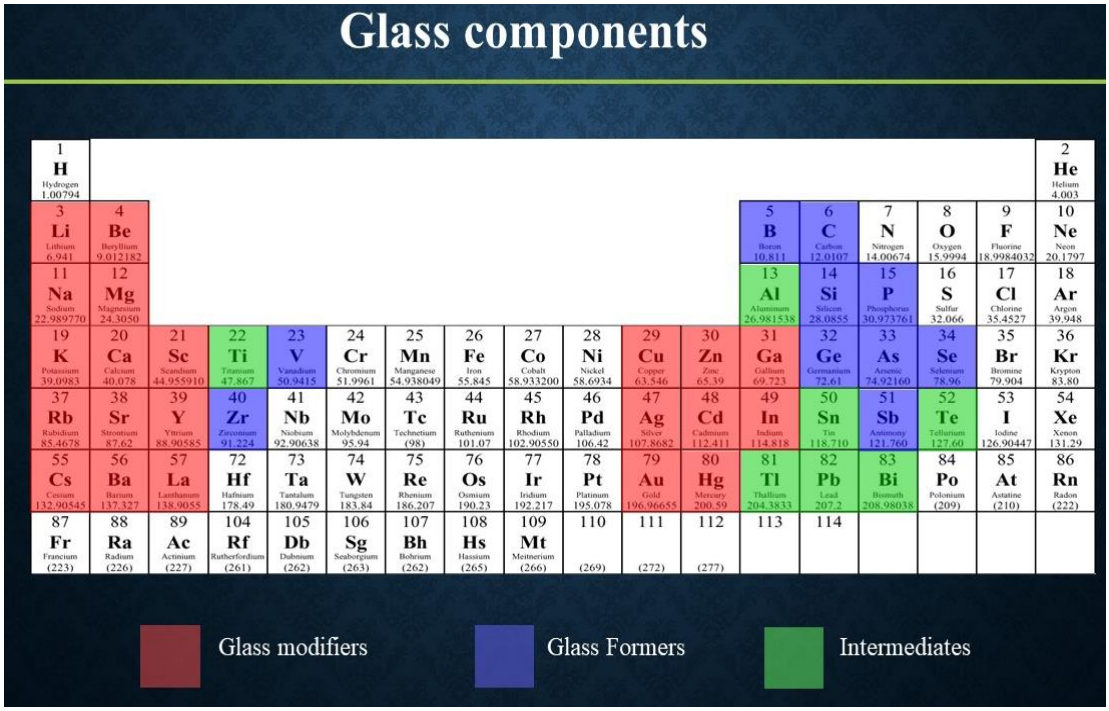

Fig. 1.5. Highlighted different chemicals that can be used as glass formers, network modifiers and intermediates

1.6.1.3. Intermediates

These oxides are in the middle of the glass formers and modifiers spectrum. Their binding strength and electronegativity values are similar between glass formers and modifiers. Intermediate cations can enter the glass network and take up former glass locations. Depending on their chemical properties, the elements can be used as glass formers, modifiers, and intermediates. Fig. 1.5 shows the distribution of elements depending on their electronegativity and bond strength. The elements highlighted by red, blue and green color can be utilized as glass modifiers, network formers, and intermediates, respectively.

1.6.2. Types of glasses

Glasses are made from a variety of different materials. They can be divided into several categories:

1.6.2.1. Silicate glasses

Silica (SiO2) is a standard oxide that forms networks. Vitreous silica is the only commercial glass made from naturally occurring minerals and includes only one significant chemical component. The basic building unit of silica-based glasses is the SiO_4 tetrahedron. Silicate glasses have a low coefficient of thermal expansion, making them resistant to thermal shock and allowing them to be used at temperatures above 1000°C. Because they are optically transparent throughout a wide spectral range, these glasses are utilized as optical fibers for telecommunications, windows, lenses, and other optical devices.

1.6.2.2. Borate glasses

Borate glasses have structural components of boric oxide (B_2O_3) and a low melting point. Various structural groups and compounds made in borate glasses as discussed below. When oxygen from a modifier oxide is introduced into boric oxide glass, one of two things happens:

a) Produces non-bridging oxygen (NBO)

b) Changes the three-coordination units (B_3) of boron (B) to the four-coordination units (B_4)

1.6.2.3. Telluride glasses

Tellurite glasses are oxide glasses that include a significant amount of TeO_2, which is more stable, with a melting point of about 730 degrees Celsius. These glasses feature a wide transparency range (0.35–5.0 m), low phonon cut-off energy of about 800 cm^{-1}, large refractive indices, excellent corrosion resistance, and increased mechanical stability.

1.6.2.4. Phosphate glasses

The oxide used in these glasses is P_2O_5 and can quickly melt around 800-1000 degrees Celsius. These glasses are heat resistant to hydrofluoric acid. Phosphate glasses can act as heat absorbers when added with iron oxide. One problem is that incorporating molecular structure into the model is challenging and phosphate glasses gets moisturized quickly.

1.6.2.5. Borosilicate glasses

These glasses contain silicon and boron oxide as the main glass-forming ingredients. It's widely utilized in the chemical sector for laboratory apparatus, ampules and other pharmaceutical containers, high-intensity lighting applications, glass fibers for textile and plastic reinforcement, and ornamental and architectural industries. They are of technical and scientific interest due to their high density, high chemical resistance, low coefficient of thermal expansion, and numerous applications in everyday life.

1.7. Host glass

We have selected the following materials due to their vital ability in various fields for the investigation.

a) Boron trioxide (B_2O_3): It is a material of white color with amorphous nature. It can get crystalline nature after some heat treatment. B_2O_3 is a superior glass former because of its

excellent transparency, durability, thermal and mechanical characteristics. Boron has a +3 oxidation state, which results in a strong covalent bond, which accounts for its great heat stability. These glasses have BOB links in BO_3 triangles and BO_4 pyramids [29].

b) **Aluminium Oxide (Al_2O_3):** Generally, it is called alumina. It has a high melting point, leading to a refractory material having significant hardness and high mechanical strength. Al_2O_3 acts as a network modifier, reinforcing the chemical stability. Also, an optimal quantity of Al_2O_3 in a host glass helps to enhance its mechanical resistance.

c) **Silicon Dioxide (SiO_2):** It is also referred to as silica. It is most commonly used in structural materials. SiO_2 in borate glasses makes the glasses more useful for applications of optical devices. Adding SiO_2 to a borate glass enhances the index of refraction with good dispersal features [30].

d) **Potassium Carbonate (K_2CO_3):** It is an inorganic compound available in white color with a low melting point. It is a network modifier that enhances chemical stability and helps to minimize redundant phonon energies [31].

e) **Zinc Oxide (ZnO):** Heavy metal oxides with relatively low phonon energies are often introduced to eliminate the redundant and undesired phonon energy in primary networks. ZnO is a critical metal oxide with low phonon energy and excellent RE ion solubility. Adding ZnO to a borosilicate network eliminates redundant phonon energy and improves quantum efficiency [32,33]. ZnO is a widely used comprehensive bandgap semiconductor due to its optical and electrical properties. The ZnO-based materials can easily absorb the UV light for several optical applications [34].

Using the above-explained chemical species, we fabricated a host matrix namely Potassium Zinc Alumino Borosilicate (KZABS) glass.

1.8. RE elements

RE elements are the seventeen-member family containing scandium (Sc), yttrium (Y), and the lanthanide series. These elements are relatively abundant. The RE ions occur primarily in their most stable trivalent oxidation state as RE^{3+} ions with their electronic configurations as $4f^n$ $5s^2$ $5p^6$ (n =1 to 14 for lanthanides). The RE ions have chemical properties alike because of the same number of electrons except for the 4f valence cell. The 4f orbitals are well shielded by fully filled octet $5s^2$ $5p^6$ which is responsible for the unique optical behaviors of RE ions. The trivalent RE ions have been widely helpful as activators due to the following characteristic features:

- Long emission lifetimes
- Emit almost monochromatic light (narrow lines)
- Intra configurational f-f transitions
- Unique electronic energy distribution
- High stability
- High solubility

The RE^{3+} ions possess their distinctive color emission in the visible spectrum because of the internal transitions of the 4*f* electrons. As earlier, we have selected the UV+ RGB method to produce white light. The detailed discussion of different RE ions used in the present investigation is given below:

i) Samarium oxide (Sm_2O_3)

The RE element samarium (Sm) has the electrical configuration [Xe] $4f^6 6s^2$. It can exist in divalent and trivalent oxidation states. Due to its closely lying energy level structure, trivalent samarium (Sm^{3+}) is a prominent active RE^{3+} ion in the lanthanide family that has five electrons in the f-shell ($4f^5$) (Carnall et al. 1968). Due to electronic transitions from $^4G_{5/2} \rightarrow {}^6H_{5/2}$, $^6H_{7/2}$, and $^4G_{5/2}$, it shows a robust orangish-red fluorescence. Sm^{3+} ions

behave well as a spectroscopic probe because of the electric dipole nature of the hypersensitive transition $^4G_{5/2} \rightarrow {}^6H_{5/2}$. These ions attracted researchers because of their potential applications in optical laser, high density optical storage, displays and w-LEDs.

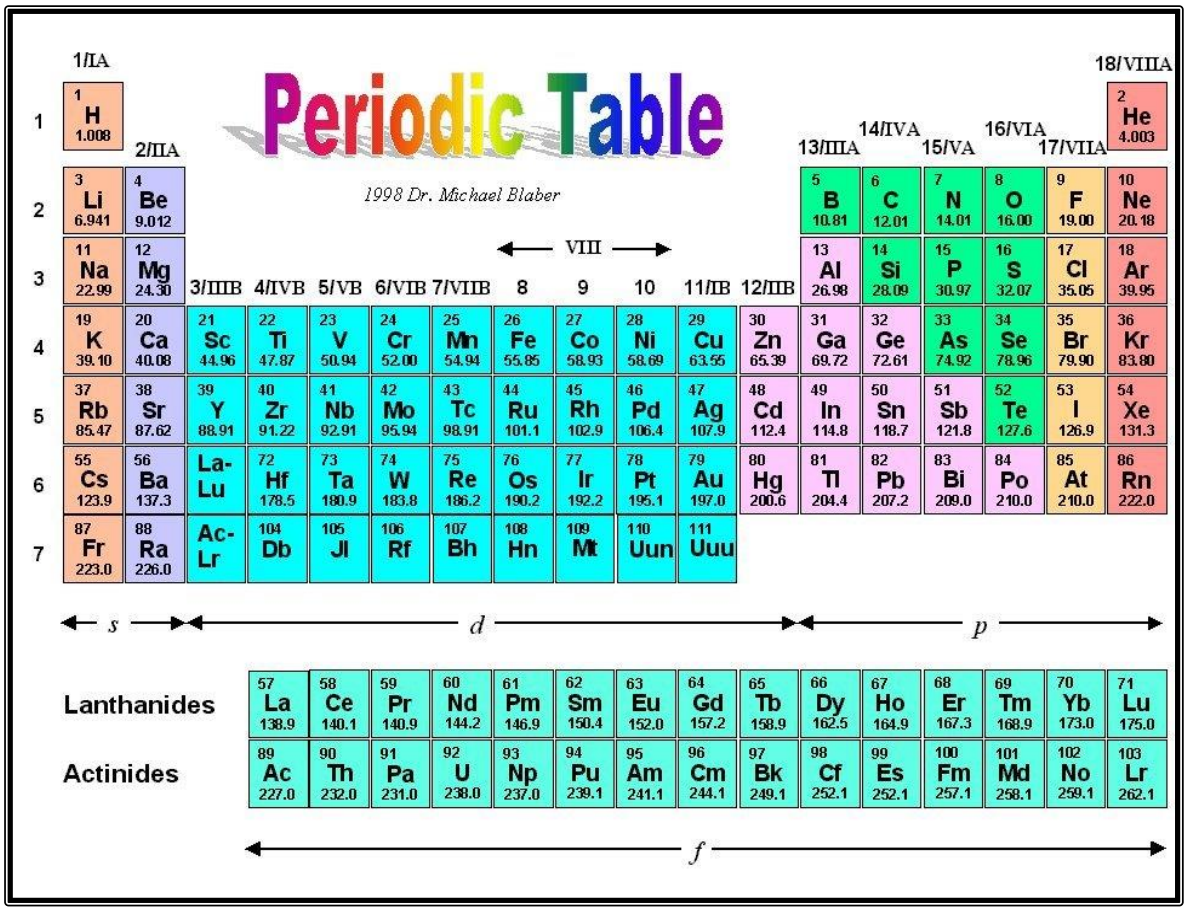

Fig. 1.6. Periodic table showing RE elements with their atomic and mass numbers

j) Europium oxide (Eu_2O_3)

Europium has its electronic configuration as [Xe] $4f^7 6s^2$ and Eu^{3+} ions as $4f^6$ in its valence shell. It shows its characteristic emission at 615 nm corresponding to the transition $^5D_0 \rightarrow {}^7F_0$ responsible for the dark red color in the visible spectrum, which makes the devices useful for red lasers, SSL devices and other optoelectronic devices.

k) Terbium oxide (Tb_2O_3)

Trivalent terbium (Tb^{3+}) ions possess their distinctive emission in the green region of the visible spectrum. Tb^{3+} ions exhibit sharp green emission at 545 nm pertaining to the

$^5D_4 \rightarrow {}^7F_5$ transition. We have used these RE ions in our work for the green component of white light emission applications.

l) Thulium oxide (Tm_2O_3)

Among different RE ions, Tm^{3+} has relatively fewer absorption bands in the visible region and huge energy gaps between other J states. Tm^{3+} ions exhibit different characteristic colors when excited under different wavelengths. Under suitable excitation wavelengths, Tm^{3+} ions can emit red and blue colors. Further, these ions can be used to tune the color of the devices, making the photonic devices more satisfactory to use in diversified fields.

m) Dysprosium oxide (Dy_2O_3)

Dy^{3+} ions have nine valence electrons in their 4*f* valence shell. It shows prominent emission at 575 nm, which is responsible for yellow color emission and beneficial in cool white light emission applications.

1.9. Energy levels of RE ions

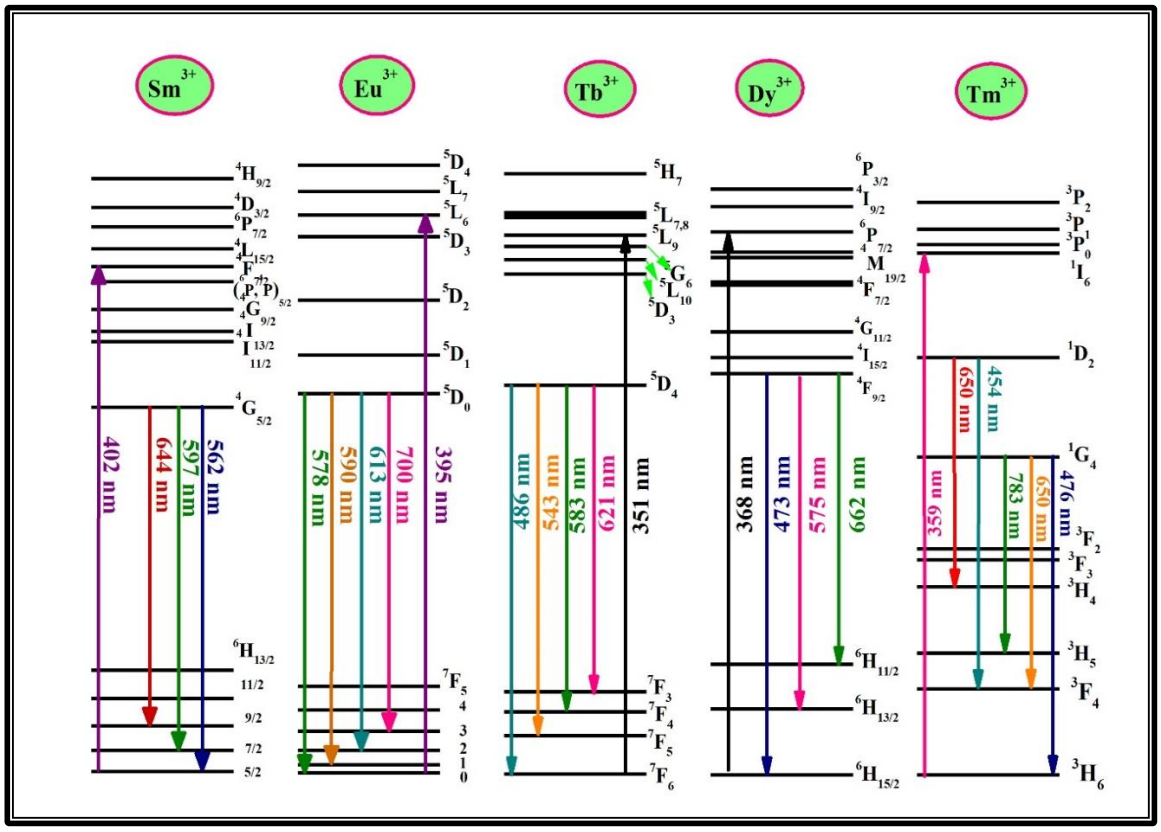

Fig. 1.7. Partial energy levels of some different RE ions with their characteristic emissions

Fig. 1.7 shows the energy levels of various RE ions used with their characteristic emissions. RE ions in modest concentrations can be considered isolated since they are well separated. The ion gap becomes sufficiently tiny for ion contact as concentration increases or if a non-random distribution emerges. Such ion interactions lead to the energy transfer between different energy levels of a RE ion or two different RE ions that influence the action of lasers and other fluorescence devices.

Fig. 1.8 shows the energy transfer to the activator ions from sensitizer ions or from the host itself via non-radiative transitions. The relaxation of RE ions to different energy states includes radiative and non-radiative decay.

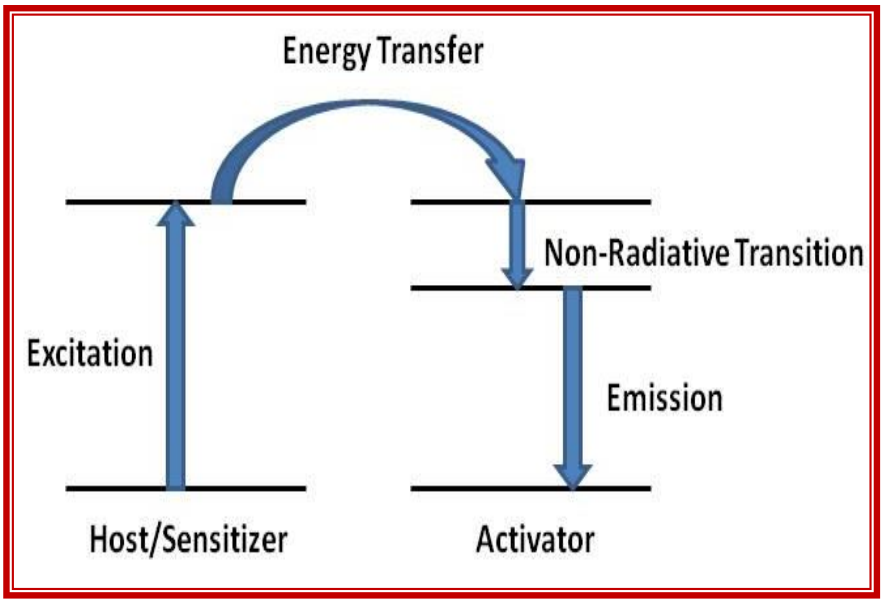

Fig. 1.8. Host lattice or sensitizer transferring energy to activator ions via non-radiative transitions

Radiative decay: When RE ion changes their energy state by absorbing and emitting a photon, such an optical transition is called radiative decay. Radiative decay of RE ions is predominantly due to electric dipole-dipole (EDD) in nature. The contribution due to magnetic dipole (MD) and electric quadrupole (EQ) are generally small and negligible, although they have allowed nature. Radiative decay may occur as follows:

(A) Transference of radiative energy between similar ions with possible decay of excited energy by emission of photons (Phosphorescence).

(B) Radiative energy transfer between unlike ions by EDD, MD and EQ interactions.

The radiative energy transfer process occurs merely by absorbing photons emitted by donors. The radiative transfer is easily determined by calculating the absorption and emission of ions involved. The rate of radiative transfer depends on the number of ions among the exciting volume and the absorber and their emission or absorption strength.

Non-Radiative Decay: The non-radiative transfer from donor to acceptors depletes the populated excited state of the donor and reduces the intensity and lifetime from the excited state to the lower state. For significant and measurable transfer, the rate of energy transfer must be of the same order of magnitude as the radiative transition in donor ion.

1.10. Type of Interactions

Broadly, the interaction between two different levels is classified based on the transition between *f-f* levels and $4f^{n-1}$-$4f^{n}5d^{0}$.

a) Intra-configurational (*f-f*) transition: Absorption and PL spectroscopy are two crucial techniques in investigating systems that have been doped with RE^{3+} ions because they make it possible to ascertain the RE^{3+} ions' native frequencies. Single crystals and glasses doped with RE^{3+} ions exhibit distinct thin line groups in their absorption spectra. However, the lines within a group are widened to a single absorption band in RE doped glasses. Electronic transitions occurring inside the 4*f* shell must be attributed to these bands and lines. Every band represents a change in energy between two $^{2S+1}L_J$ free ion levels, known as intra-configurational f-f transitions. These transitions are weak in intensity, and the interactions between RE ions and light can be induced by three mechanisms as mentioned below:

i) Electric dipole (ED) transitions: An ED transition occurs when RE ions interact with the electric field vector of electromagnetic radiation via an electric dipole. These are the

parity allowed transitions between the 4f and 5d states. The formation of an electric dipole necessitates a linear movement of charge with odd parity. As a result, the electric dipole operator has unusual transformation properties concerning an inversion center when inverted. These transitions are subjected to the selection rules as ($|\Delta s| = 0$, $|\Delta l| = \pm 1$, $|\Delta L| \leq 6$, $|\Delta J| \leq 6$).

ii) **Magnetic dipole (MD) transitions:** When the RE ions interact with the magnetic component of the incident light, the induced transitions are knowns as MD transitions. These transitions have slightly weaker intensity than the ED transitions, approximately to the order of 10^{-8}. MD transitions result in the rotational movement of charges and having even parity. It means transitions with same parity are allowed and endorsed by the selection rules ($|\Delta s| = 0$, $|\Delta l| = \pm 1$, $|\Delta L| \leq 0$, $|\Delta J| = 0, \pm 1$; $J = 0 \leftrightarrow 0$ is forbidden transition).

iii) **Electric quadrupole (EQ) transitions:** The displacement of quadrupole charges leads to the EQ transitions, which are much weaker than ED and MD transitions. These are parity allowed transitions with selection rules ($|\Delta S| = 0$, $|\Delta L| \leq 2$ and $|\Delta J| \leq 2$). So far, there is no evidence for the EQ transitions in RE ions spectra.

b) **Interconfigural (*f-d*) interaction:** In these transitions, the transfer of 4*f* electrons to the 5*d* shell is parity allowed. The transition between $4f^{n-1}5d^1$-$4f^n5d^0$ levels gives rise to a broad range of wavelengths compared to the 4*f*-4*f* transition. The host ions provided such an environment to the doped RE ions that led to the splitting of 5*d* energy levels due to the crystal field splitting. The magnitude of this crystal field effect depends on the bond length between acceptor ion and ligand, the nature of the bond, the surrounding environment and the site symmetry of acceptor ions. These transitions are highly energetic.

1.11. Energy transfer mechanism

Energy transfer between two neighboring ions can occur only if the resonance occurs in their ground and excited states energy difference and if suitable interaction exists between them. The energy transfer can occur via exchange or multipolar interactions when they are at the nearest neighbor sites. To identify the type of interactions involved in energy transfer, Dexter's theory and Reisfeld's approximation can be employed to the PL emission profiles or Inokuti Hirayama (I-H) model to the PL decay profiles.

I. Dexter's theory and Reisfield's approximation

To elucidate the multipolar interaction type involved in the energy transfer process, the Dexter theory has been applied to PL emission profiles.

In this process of identifying the type of mechanism involved in the energy transfer between different energy levels of a RE ion, the luminescence efficiency can be related to the concentration of RE ions as [35]:

$$\frac{I}{x} = k\left[1 + \beta(x)^{\frac{S}{3}}\right] \qquad (1.1)$$

Where I is the PL emission intensity, x is the dopant concentration in mol%, s represents the type of interaction, k and β are the arbitrary constants.

According to the Dexter theory, the probability of energy transfer via multipolar interaction between activator ions depends on the value of S. The interaction will be dipole-dipole (d-d), dipole-quadrupole (d-q) and quadrupole-quadrupole (q-q) corresponding to value S = 6, 8 and 10 respectively.

Now assuming the condition $\beta(x)^{\frac{S}{3}} >> 1$, Eq^{n} (1.1) can be simplified as:

$$log\left(\frac{I}{x}\right) = C - \frac{s\,log(x)}{3} \qquad (1.2)$$

Where *C* is a constant independent of *I* and *x.* A graph is plotted between the $log\left(\frac{I}{x}\right)$ and $log(x)$ to find the value of *s.* The slope of this graph will be equal to the value of *s/3*.

To reveal the nature of interaction involved in the energy transfer between the different energy levels of two distinct RE ions, the relation between luminescence efficiency and concentrations of doped RE ions is given below:

$$\frac{I_0}{I} \propto C^{\frac{\alpha}{3}} \qquad (1.3)$$

Where I_0 and *I* are the luminescent intensities of sensitizer/dopant ions in the absence and presence of activator/acceptor ions respectively. C is the sum of the donor and acceptor ion concentration, α = 6, 8 and 10 for d-d, d-q and q-q interactions respectively. To understand the mechanism, the graph will be plotted between $\frac{I_0}{I}$ and $C^{\frac{\alpha}{3}}$ and the best linear fit suggests the corresponding value of α that further indicates the energy transfer mechanism.

II. I-H model: The type of interaction that occurs in energy transfer can also be explained by employing I-H model to non-exponential decay curves. According to the I-H model, the decay of luminescence can be described by the equation given below [3]:

$$I = I_0 \exp\left\{-\frac{t}{\tau_0} - Q\left(\frac{t}{\tau_0}\right)^{\frac{3}{s}}\right\} \qquad (1.4)$$

Where I_0 and *I* are the luminescence intensity at time t=0 and t, t is the time after excitation, τ_0 is the average lifetime of donor in the absence of acceptor ions, and s denotes the multipole effect; it can take values 6, 8 and 10 for d-d, q-d and q-q interactions respectively. Q is the fitting parameter.

1.12. Colorimetric properties

The Commission Internationale de 1' Eclairage (CIE) format is used to describe the color of any material in terms of three primary colors. The PL emission spectral data can be modified into chromaticity coordinates (x, y and z) using the CIE 1931 standard procedure.

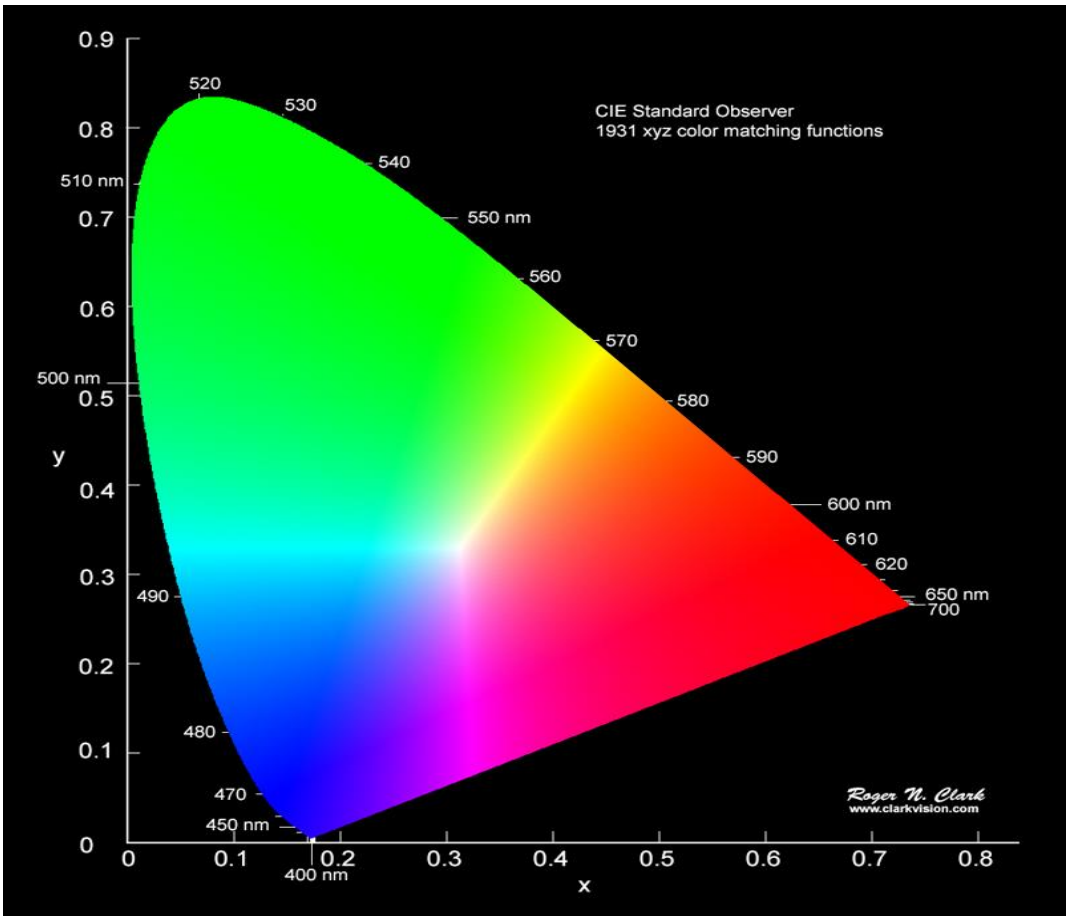

Fig. 1.9. CIE 1931 diagram showing colors corresponding to 400-700 nm wavelength

The equations given below can estimate the trichromatic color values [19]:

$$X = k\sum_{\lambda}\phi(\lambda)\bar{x}(\lambda)\Delta\lambda \tag{1.5}$$

$$Y = k\sum_{\lambda}\phi(\lambda)\bar{y}(\lambda)\Delta\lambda \tag{1.6}$$

$$Z = k\sum_{\lambda}\phi(\lambda)\bar{z}(\lambda)\Delta\lambda \tag{1.7}$$

Where $\bar{x}(\lambda)$, $\bar{y}(\lambda)\ and\ \bar{z}(\lambda)$ are the color matching functions of the 1931 CIE standard. $\phi(\lambda)$ is that the spectral distribution, i.e. ($\phi(\lambda) = \frac{d\phi(\lambda)}{d\lambda}$) and k is a normalized constant. $\Delta\lambda$ is the wavelength intervals at which the integration is carried out by numerical summations [20].

CIE chromaticity points are calculated from the trichromatic color values as given below:

$$x=X/(X+Y+Z) \quad (1.8)$$

$$y=Y/(X+Y+Z) \quad (1.9)$$

$$z=Z/(X+Y+Z) \quad (1.10)$$

The monochromaticity of the material can be ascertained by using the CIE coordinates in terms of color purity (CP) as per the following expression:

$$CP = \frac{\sqrt{(x-x_{ee})^2+(y-y_{ee})^2}}{\sqrt{(x_d-x_{ee})^2+(y_d-y_{ee})^2}} \quad (1.11)$$

where (x, y), (x_{ee}, y_{ee}) and (x_d, y_d) are the coordinates of the examined glass, white point and dominant wavelength point respectively.

For better consideration of different color emissions, CCT values can be estimated by the following McCamy's expression [36]:

$$CCT = -437z^3 + 3601z^2 - 6861z + 5514 \cdot 31 \quad (1.12)$$

where $z=\frac{x\ -x_e}{y\ -y_e}$ The coordinates of inverse slope line (x_e) and chromaticity epicenter (y_e) are located at (0.332, 0.186); x and y are coordinates of examined glass.

1.13. Objectives of the thesis

- ❖ To synthesize RE doped KZABS glasses with varying concentrations using sudden melt quenching technique.
- ❖ To investigate the structural, optical and luminescence behaviors of RE doped KZABS glasses for their suitable usage in modern SSL and photonic devices.
- ❖ To improve their illumination:
    - By varying different concentrations and finding the optimized one
    - By co-doping or tri-doping as per the emission requirement
    - By exciting at different wavelengths
- ❖ Preparation of KZABS glasses with many RE ions for all primary colors and optimizing all the respective ions to make them suitable for co-doped and tri-doped combinations so that desired color emission can be achieved.
- ❖ Thermal behaviors for all KZABS glasses with different combinations of RE ions will be checked to confirm their thermal stability.

  Finally, to suggest some environmentally safe and eco-friendly glass w-LEDs suitable to replace RE doped phosphors needed to fabricate w-LEDs.

Chapter 2
Experimental section

The progress of the glass systems needs appropriate manufacturing and characterization techniques. The procedures for synthesizing RE doped KZABS glasses and the characterization techniques used to explore their physical and photoluminescent properties are discussed in this chapter. This chapter also summarizes many experimental instruments used to characterize the as prepared glasses. The glass synthesis technique will be addressed first, followed by various spectroscopic techniques like XRD, FT-IR, Raman, absorption, PL excitation, PL emission and PL decay used to characterize the synthesized glasses. These studies helped us to investigate several characteristics such as structural behaviors, functional groups present, PL properties, Colorimetric properties, and spectral decay behaviors.

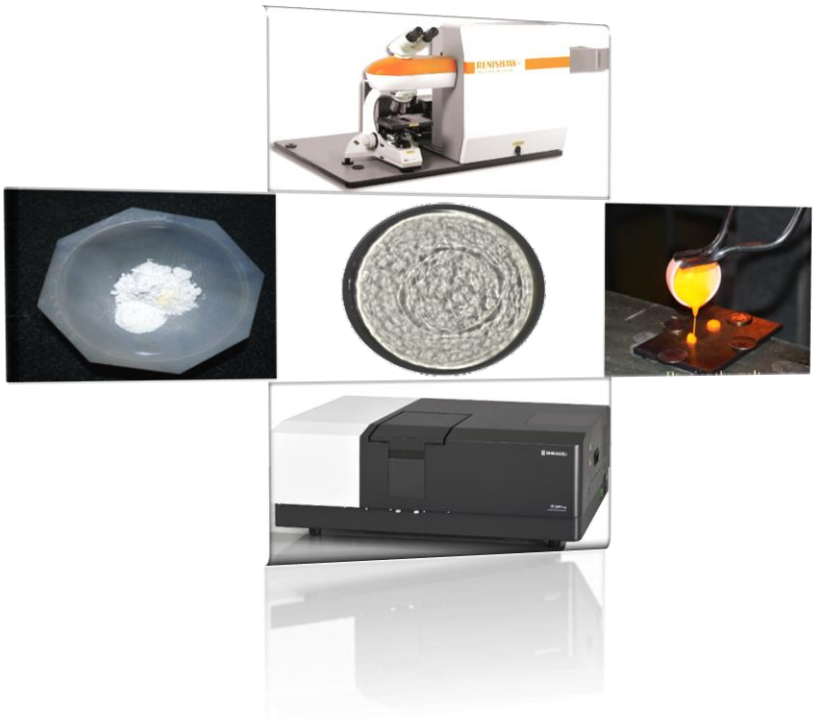

2.1. Glass synthesis

Glassy materials can be made using various techniques, including sol-gel, melt-quenching, thermal vapor deposition, and so on. The melt quenching procedure was employed to manufacture the glass samples used in this study. This is the simplest and oldest of the several glass preparation procedures utilized by glass manufacturing companies and researchers. Aside from that, the melt quench process allows for greater versatility in the manufacture of various glass compositions containing borates, silicates, phosphates, oxides, and non-oxides, among other materials. This method does not need stoichiometry among the ingredients, and glass can be made with various compositions and components, sometimes as many as ten. It also encourages the doping and co-doping of active ions such as transition metal and RE ions. When it comes to increasing luminescence efficiency, a host matrix must occasionally accept more significant doping concentrations, and the melt quench procedure favors this over other glass preparation techniques. The melt quench technique's only drawback is the lack of purity in the prepared glass. However, utilizing alumina, platinum, or gold crucibles can help to alleviate this difficulty.

2.1.1. Chemicals used

All chemicals used to prepare glasses were procured from many brands with high purity. The basic oxides B_2O_3, SiO_2, Al_2O_3, ZnO, and K_2CO_3 have been bought from Thermo Fischer and Alfa Aesar with 99% purity, whereas all RE oxides such as Sm_2O_3, Eu_2O_3, Dy_2O_3, Tb_4O_7 and Tm_2O_3 from Sigma-Aldrich with a purity of 99.99%.

2.1.2. Glass preparation

KZABS: RE^{3+} glasses were prepared by taking the constituent chemicals as per the following stoichiometric ratio given below:

50 B_2O_3 + 30 SiO_2 + 10Al_2O_3 + (4.5-x) ZnO + 5 K_2CO_3 + x RE_2O_3; where (x = 0.1, 0.25, 0.5, 0.75, 1.0, 1.25 and 1.5 mol% and RE_2O_3 = Sm_2O_3, Eu_2O_3, Dy_2O_3, Tb_4O7 and Tm_2O_3).

The digital balance (Shimadzu: ATX244, accuracy: 10^{-4} g) was used to weigh the raw materials according to their stoichiometric ratio. A batch of raw materials taken as 8gm was grounded to get smooth and homogeneous powder. The smooth mixture then shifts into an alumina crucible. The melting of the as-prepared mix was carried out in an alumina crucible at 1270˚C for 4 hours in an electronic furnace. After that, the melts were poured on a preheated brass plate and pressed quickly with another brass plate to get glass samples of uniform thickness.

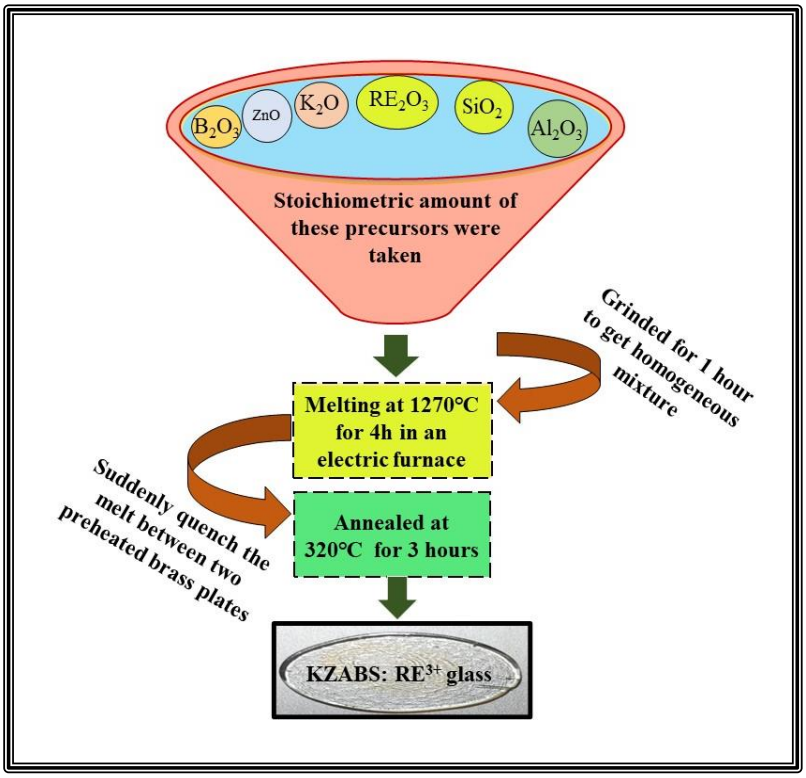

Fig. 2.1. Schematic diagram of melt-quenching technique.

The thermal and mechanical stability can be attained by annealing glasses further at 320˚C for 3 hours [40-43]. In conclusion, RE doped KZABS glass samples were prepared and found stable at ambient temperature to study their structural and PL properties. All these steps used to prepare glasses were drawn with the help of a schematic diagram, shown in the Fig. 2.1.

2.2. Physical and optical properties

The material's physical properties also play a vital role in investigating them for practical applications. Measurement of physical properties such as thickness, density, molar volume, and refractive index were discussed as given below. Further, by using them, many optical parameters will be evaluated and discussed.

2.2.1 Thickness

The as-prepared glasses' thickness or optical path length can be estimated using a Vernier caliper, shown in Fig. 2.2. The thickness of the as-prepared glass is observed to be ≈ 2.40 mm in the present work.

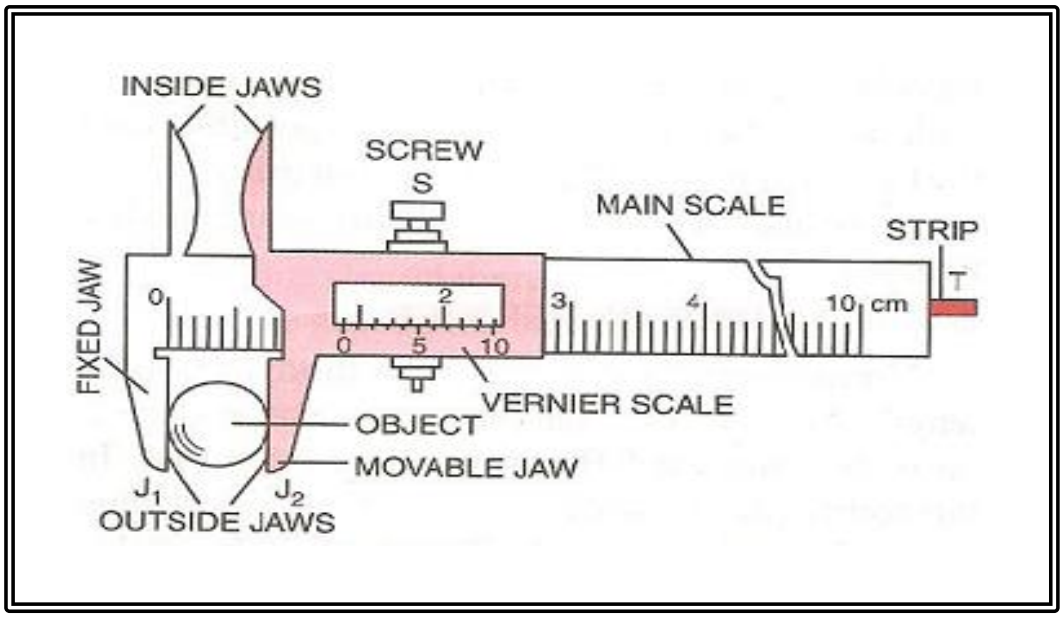

Fig. 2.2. Schematics of Vernier caliper

2.2.2 Molar volume

The molar volume of the glasses is estimated by employing the formula given below [22,41]:

$$Molar\ volume\ (V_m) = \frac{Molar\ mass\ of\ the\ glass\ (M)}{density\ of\ the\ glass\ (d)} \qquad (2.1)$$

2.2.3 RE ions concentration

In a particular glass sample, RE ions concentration (C^n) can be estimated using the below expression [105]:

$$C^n(mol/litre) = \frac{d}{MW} \times \frac{M_{RE}}{M_{TW}} \times 10^3 \quad (2.2)$$

where, d = density of the glass sample

MW = molecular weight of the RE oxide used

M_{RE} = mass of the RE oxide

M_{TW} = total weight of the glass sample

The units of concentration can be converted from $(mol/litre)$ to (*ions* cm^{-3}) by multiplying a factor of (N_A X 10^{-3}).

N_A = Avagadro's number = 6.022 X 10^{23}

2.2.4 Density

By employing the Archimedes principle, the density of the glasses was measured with the help of an electronic balance (Shimadzu, sensitivity: 10^{-4} mg) using double distilled water as an immersion fluid. Three *sets* of observations were recorded for each sample, and then an average of these values were taken. The following expression estimates the density (d) values:

$$d = \frac{(wt)_a}{(wt)_a - (wt)_w} \quad (2.3)$$

Where $(wt)_a$ and $(wt)_w$ denotes the weight of the glass sample in the presence of air and water respectively, at an ambient temperature.

2.2.5 Refractive index

It is the material property that describes the extent of bending of a light ray passing from one medium to another. Theoretically, it is given by

Refractive index = speed of light/phase velocity of light in that medium.

Experimentally, it can be estimated by two methods.

2.2.5.1 Using absorption spectrum

The value of the refractive index (n) can be estimated by using the bandgap energy (E_g) as per the following equation:

$$\frac{n^2-1}{n^2+1} = 1 - \sqrt{\frac{Eg}{20}} \qquad (2.4)$$

2.2.5.2 Brewster's angle method

In this method, a He-Ne laser (633 nm) with a photodetector is used to measure the refractive indices of the glass sample. The values of refractive indices for all glass matrices are found to be approximately equal to 2.9.

2.2.6 Bandgap energy (E_g)

The direct bandgap energy (E_g) values has been calculated from the absorption spectral data by using the equation below expression [117]:

$$(\alpha h\nu)^n = C\left(h\nu - E_g\right) \qquad (2.5)$$

Where α is the absorption coefficient, h is Planck's constant, n = ½ for direct allowed transitions, and *C* is a random constant..

2.2.7 Molar refractivity

The molar refractivity (R_m) can be estimated by using the Lorentz-Lorentz equation given below [42]:

$$R_m = \frac{n^2-1}{n^2+2}(V_m) \quad (2.6)$$

Which can be viewed as an instantaneous measure for the entire polarizability of 1 mole.

2.2.8 Electronic polarizability

The electronic polarizability (α_m) is calculated using molar refractivity (R_m) using the relation given below [42]:

$$\alpha_m = \frac{3}{4\pi N_A} R_m \quad (2.7)$$

Where N_A is an Avogadro's number.

2.3. Characterization techniques

2.3.1 X-Ray diffraction studies

XRD is a prerequisite technique to identify the structure of the material. In structural analysis, it can reveal various properties such as the nature of the material (crystalline or non-crystalline). The material should be finely powdered and homogenous to investigate under the XRD instrument. But it is easy to analyze the thin films with new XRD instruments. It is a non-destructive technique. In present work, XRD instrument has been used to reveal the amorphous nature of the as prepared glasses. Figure 2.3 represents the Bruker- D8 advanced X-ray diffractometer.

Fig. 2.3. Bruker-D8 Advance X-ray diffractometer.

2.3.2 FT-IR spectroscopy

FT-IR is a potential technique to identify the functional groups and bonding present in the synthesized materials. It is preferred because of several advantages:

- ❖ It does not destroy the sample
- ❖ Significantly faster
- ❖ Sensitive and precise

It can measure how much light a sample absorbs and scattered at each wavelength.

Principle: It works on the principle of Michelson's interferometer technique. The schematic diagram representing the working of the FT-IR instrument is shown in Fig. 2.4.

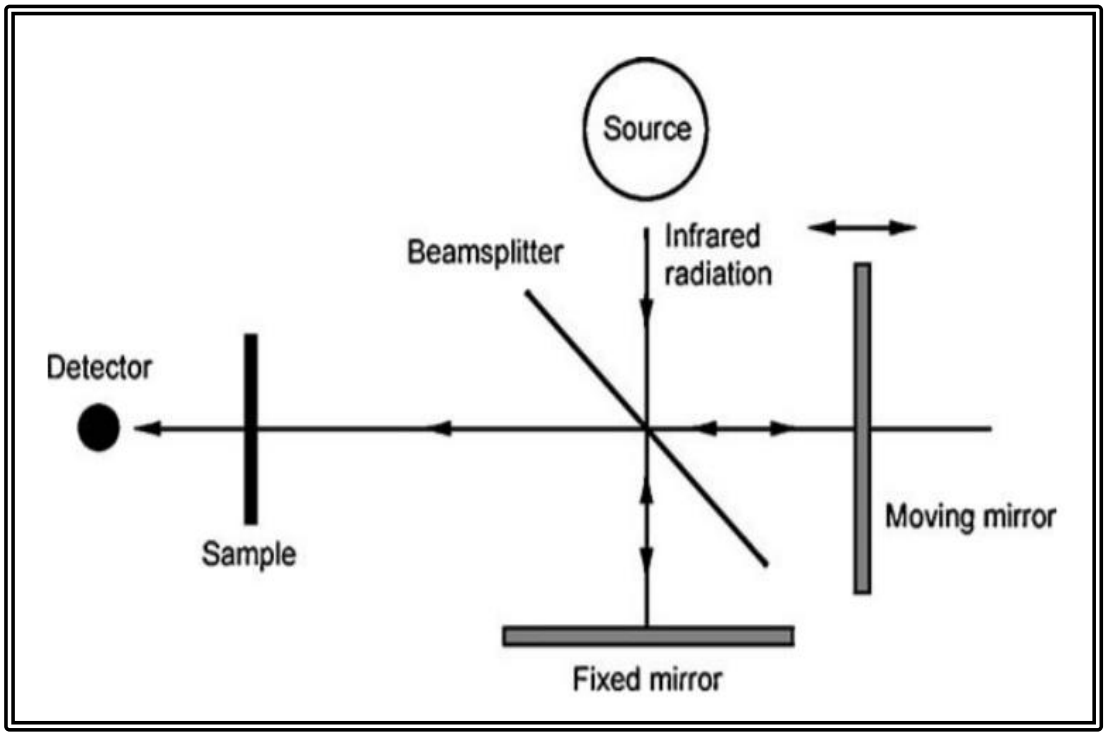

Fig. 2.4. Schematics for Michelson interferometer

Across the beam splitter, the interferometer comprises two mirrors that are at right-angled. The output beam is the consequence of interference of the reflected rays from both mirrors, with one mirror moving and the other stationary. The infrared spectrum of the material is produced by passing the beam across the sample and creating an interferogram using the Fourier transform technique. A molecule's total internal energy is made up of the sum of its rotational, vibrational, and electronic energy levels. The EM wave is primarily linked with molecular vibrations in the infrared area, and the molecule is stimulated to a higher vibration state by absorbing IR radiation. As a result, IR spectroscopy is an effective technique that provides crucial fingerprint information for sample structure. Fig. 2.5 shows the FT-IR instrument from Perkin Elmer used to perform the investigations on KZABS glasses.

Fig. 2.5. FT-IR from Perkins Elmer

2.3.3 Raman spectroscopy

Raman spectroscopy is identical to FI-IR because it gives structural information based on the molecular system's vibrational and rotational modes. When a laser photon interacts with materials in the near-infrared or ultraviolet range, the energy of the produced photon is dispersed elastically or inelastically, resulting in two options.

- Rayleigh scattering occurs when released photons have the same energy as absorbed photons.
- The released photons have lost or gained energy in the form of vibrational energy, resulting in Stokes and Anti-stokes lines in the Raman spectra, equal-spaced from the Rayleigh line.

These energy changes give crucial information about the material's vibrational modes and phonon energies. However, the fundamental distinction between Raman and FT-IR is the type

of chemical change can be seen by both the methods. A Raman active transition can only occur when a change in polarizability of the molecule is noticed during a vibration transition. It implies that the molecule's electron cloud must shift location. For an IR observable transition to occur, the dipole moment of a molecule must change during vibration. As a result, IR detection is not possible for symmetrical molecules like O_2, since O_2 cannot modify its dipole moment. Because the two techniques described, the complete information on a material's structural property when used simultaneously, FT-IR and Raman spectroscopy are complementary. In the present work, Raman spectral studies were performed with the help of the Renishaw Invia Raman Microscope, as shown in Fig. 2.6.

Fig. 2.6. Renishaw Invia Raman Microscope

2.3.4 Absorption spectrometer

Absorption spectroscopy gives the information pertaining to the interaction of electromagnetic radiation with matter in the UV-Vis-NIR spectral range. A molecule's absorption spectrum has many absorption bands used to calculate the bandgap of the materials in this thesis. As a result, proper measures were followed throughout the absorption spectral recording. This study

measured the optical absorption spectrum with a Jasco V-770 spectrophotometer with a spectral resolution of 0.1 nm. The Spectrophotometer determines the percentage of EM radiation absorbed or transmitted in the UV-Vis-NIR spectral band.

Fig. 2.7. Jasco V-770 spectrophotometer.

The absorption spectrometer from Jasco (V-770) has been shown in Fig. 2.7. Monochromators divide a comprehensive source signal into specific wavelengths, while optical filters prevent diffracted lines from overlapping in distinct orders. The essential function of this instrument is based on a double beam technique in which one beam passes through the sample. In contrast, the other beam passes through the reference before reaching the detector, with a Lead Sulphide (PbS) cell for the IR region and a photomultiplier tube (PMT) for the UV and visible regions.

2.3.5 PL spectral analysis

Its PL spectra describe RE doped material's excitation, emission, and decay profiles. When applied to a molecular system, PL is also referred to as fluorometry. When pulsed with adequate

stimulation, PL accounts for the spontaneous emission of light from any material. The material under examination absorbs a particular wavelength of light and re-emits it at various wavelengths. It is a fundamental contactless approach to exploring materials' electrical structure. When light strikes a substance, it is absorbed, and the extra energy is transferred to the material. Photoexcitation was observed due to electrons within the sample moving in the permitted excited states. Electrons return to the ground state from the excited state, and the excess energy is emitted in light (radiative transition) or heat (non-radiative transition). A schematic diagram related to the typical spectrometer configuration is depicted in Fig 2.8.

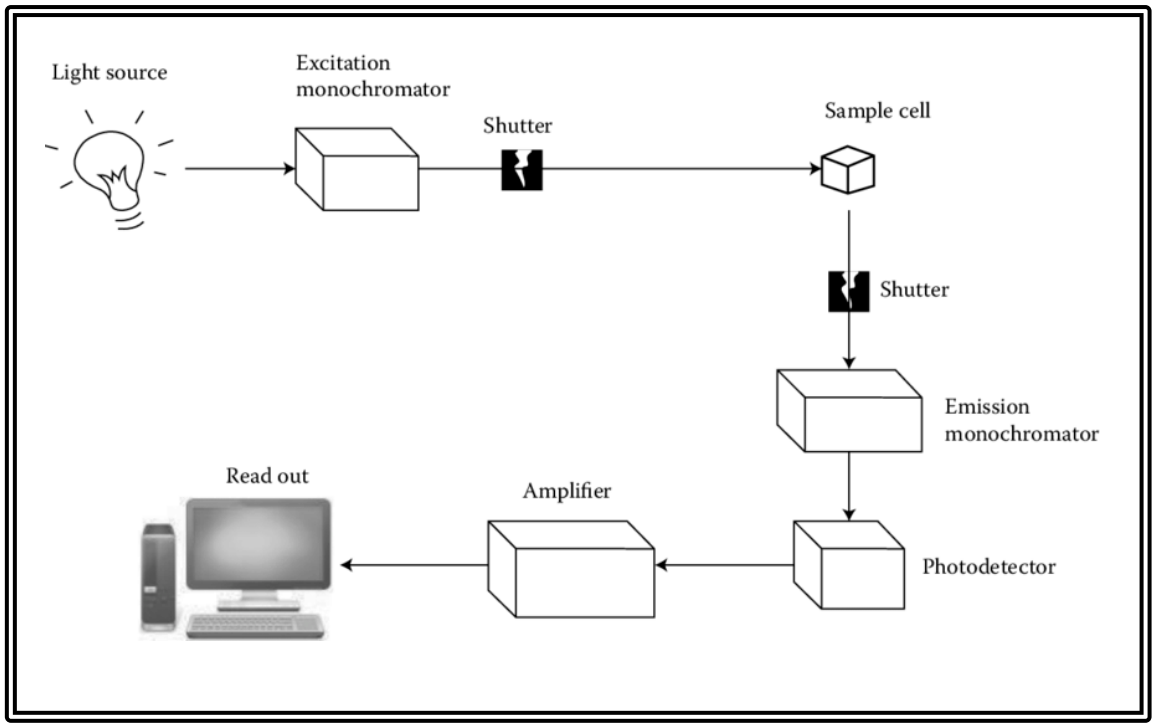

Fig. 2.8. Schematic diagram of spectrofluorophotometer.

It consists of an excitation source, a sample cell, a light dispersing element for the excitation radiation, a light spreading component for the emitted radiation, and a sensitive detector for determining the intensity of the emitted radiation. An amplifier is used to make signals readable and display unit. In most cases, RE doped material's excitation and emission spectra are recorded simultaneously. In emission spectroscopy, the emitted light is resolved by scanning

the emission dispersing component while the excitation source broadcasting part is fixed throughout the emission scanning. The emission spectrum offers data on the energy sites of optical transitions involved in light emission. In excitation spectroscopy, the emission monochromator is set at a wavelength corresponding to a strong emission line, and both monochromators have a spectral range from 200-900 nm. Fig. 2.9. shows the instrument used to carry out the work reported in this thesis.

Fig. 2.9. Spectrofluorometer from Jasco FP-8300.

The decay spectral recordings for the as-prepared glasses were done using an Edinburgh FLS 980 fluorescence spectrometer with a spectral resolution of 0.1 nm. A xenon lamp is used as an excitation source, as shown in Fig. 2.10.

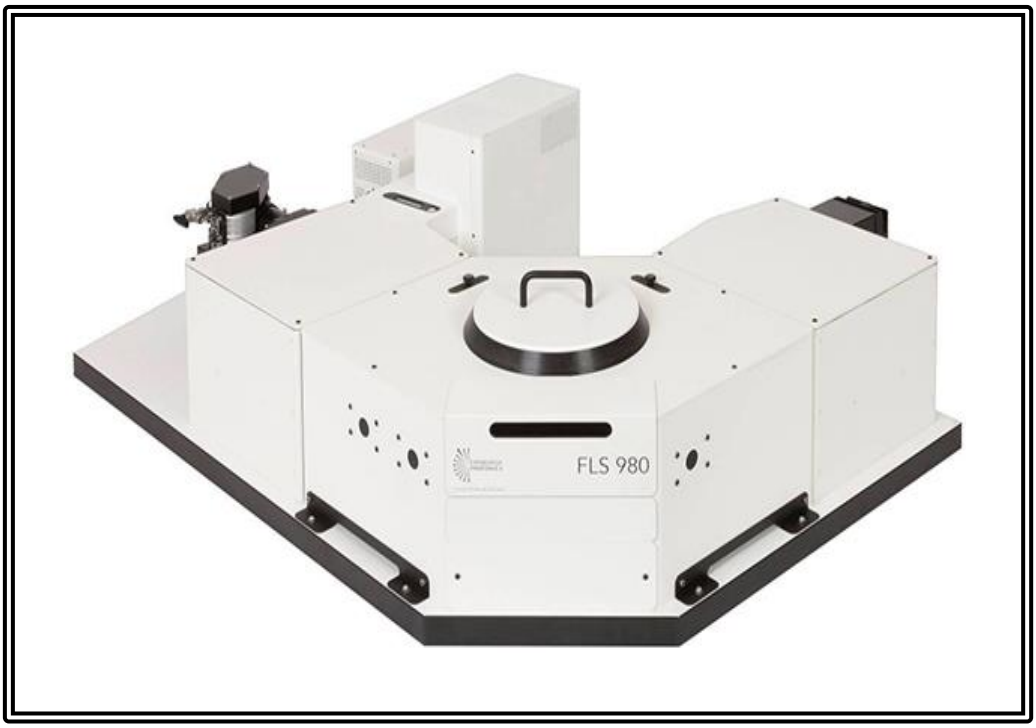

Fig. 2.10. Edinburgh FLS 980 fluorescence spectrometer.

Chapter 3

Effective sensitization of Eu^{3+} red emission by Sm^{3+} in thermally stable Potassium Zinc Alumino Borosilicate glasses for Photonic Applications

Sm^{3+}/Eu^{3+} co-doped KZABS glasses were prepared by the melt quenching method and characterized by spectroscopic techniques such as XRD, FT-IR, PL and PL decay to understand their photoluminescence behavior. The energy transfer from Sm^{3+} to Eu^{3+} ions has enhanced the red emission given by Eu^{3+} ions in the titled glasses. The bi-exponential time decay curves give decreasing lifetimes with an increase in Eu^{3+} ions concentration confirming the energy transfer. All the results obtained contemplate the suitability of the as prepared glasses for photonic device (red emitters) applications such as w-LEDs, solar cells, and display devices.

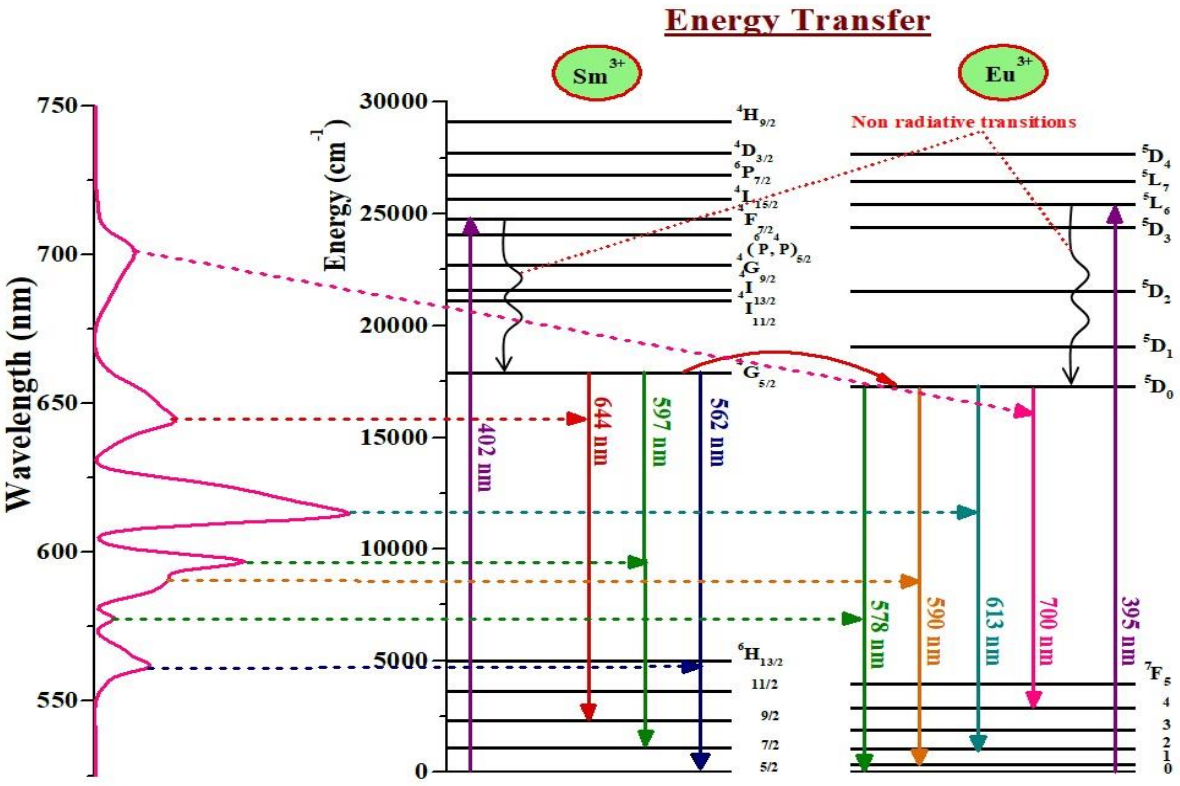

3.1. Introduction

Synthesis and characterization of RE ions doped glasses attracted many scientific groups phenomenally due to their significant and widespread applications in fascinating fields like lasers, optical fiber amplifiers, display devices and SSL devices such as w-LEDs [32,43–45]. Usage of RE doped glasses in SSL technology, especially in w-LEDs, is quite interesting because of their unique characteristics like high brightness, less power consumption, financial viability and environment-friendly nature [1–3]. Owing to these characteristic features, many researchers are paying attention to the RE doped glasses [8-12]. In literature, researchers have investigated several types of glasses such as fluoride, tellurite, halide, borate, silicate and borosilicate glasses for the aforementioned applications [13-15]. Among these, borate glasses have proved to be a competent candidate for device applications in ultraviolet optics, optical triggers, semiconductors, biomaterials and temperature-dependent sensors [29].

Further, these materials could be used as optical device substrates in reflecting windows owing to their unique properties like thermal stability, less reactivity, high transparency and high mechanical strength [48,49]. Many types of dopants have been used, like transition metals, heavy metals and RE ions [44,50]. Regarding high luminescence, RE ions are a unique and better choice as dopants. Broadly, RE ions have been used in all kinds of optical devices like optical fibers, optical detectors, optical amplifiers, and color displays [18,26]. RE metals are 17 elements, including Scandium and Yttrium, within the lanthanide family. RE ions are essential for optical and magnetic behavior due to their 4f valence shell. Out of these, the trivalent europium (Eu^{3+}) ion has six 4f valence electrons showing intense red emission in the visible range. Eu^{3+} doped materials are employed in solid-state lasers, w-LEDs, color displays and communication devices [7,22–24].

At present, w-LEDs can be fabricated by various methods. The first method is by exciting a yellow phosphor with a blue LED (or) near-ultraviolet (n-UV) LEDs [7]. Such types of phosphors exhibit relatively low CRI and CCT due to the absence of a red component [10]. CRI defines the quality of the devices; a high CRI value means high color emission or good quality of the devices. The more generalized way to fabricate w-LEDs is to combine tricolor (red, green and blue) LEDs, as they have better color stability and temperature than the blue LED chip-based w-LEDs [54]. However, epoxy resins are required in phosphor-based LEDs, which degrade the devices with time. To avoid these problems, people search for glass-based LEDs [27,28]. The greatest advantage of glass-based LEDs is that they are easy to prepare, financially supportive, and require no epoxy resins. The red one is more important for natural white light among the three prime colors needed to produce white light. Eu^{3+} ions are good red emitters to explore luminescence in a suitable host. The addition of trivalent Samarium (Sm^{3+}) ion makes it more efficient for lasers, optical storage devices. In glasses co-doped with Sm & Eu, the transfer of energy from samarium to europium ions results in the enhancement of emission intensity of Eu. Sm^{3+} ion acts as a decent sensitizer to Eu^{3+} ions capable of demonstrating reddish-orange emission through its emission transitions from $^5D_0$ to various ^7F_J (J=0,1,2,3,4) levels [55–59].

The selection of the host matrix is also equally important to enhance the luminescence behavior. B_2O_3 is superior to many glass formers due to its high transparency, high durability, and high thermal and mechanical strengths. Boron has a +3-oxidation state; hence, it forms a strong covalent bond, accounting for its high thermal stability. Such glasses contain BOB linkages in BO_3 triangles and BO_4 pyramids [29]. Incorporating SiO_2 in borate glasses makes the glasses more useful for applications of optical devices. The addition of SiO_2 to a borate glass enhances the index of refraction with good dispersal features [30].

Nevertheless, B_2O_3 and SiO_2 possess high phonon energies that increase non-radiative losses. Low phonon energies minimize non-radiative losses, resulting in higher luminescence efficiency [31,60]. To reduce such redundant and unwanted phonon energies of borosilicate glass networks, heavy metal oxides with relatively low phonon energies are added. Zinc oxide (ZnO) is a vital metal oxide with comparatively fewer phonon energies and good RE ion solubility. Adding ZnO to a borosilicate network certainly reduces its redundant phonon energies and helps in enhancing its quantum efficiency [32,33]. Al_2O_3 added to a borosilicate glass as a network modifier will reinforce its thermal and chemical stability. Also, an optimal quantity of Al_2O_3 helps to enhance the mechanical resistance [37-39]. The past research observed that the host glasses containing alkali metal ions give higher quantum efficiency because of relatively low phonon energies. Among all the alkali metals, potassium containing glasses are less reported than lithium and sodium. Potassium ions are relatively more efficient in enhancing a glass host's luminescence efficiency and facilitating large energy transfer [31]. The aforementioned interesting characteristic features of the constituent chemical species such as B_2O_3, SiO_2, K_2O, ZnO and Al_2O_3 prompted us to prepare an excellent optical glass system, namely KZABS glassy system, to understand its suitability for photonic device applications.

In this chapter, our primary focus is to synthesize Sm^{3+}/Eu^{3+} co-doped KZABS glasses and to understand their supremacy in producing intense visible red color useful for LEDs and other photonic devices. Various functional groups present in host glass have been obtained using FT-IR and Raman spectral recordings. Visible emission characteristic features and energy transfer efficiency of the as-synthesized glasses were obtained by recording PL and PL decay spectral features. The thermal stability of the as-synthesized KZABS glass has also been studied by recording the temperature-dependent PL.

3.2. Experimental work

The glass samples used in present investigation are prepared with the melt quench method as already been discussed in section 2.1.

Sm^{3+}/Eu^{3+} co-doped KZABS glasses were prepared by taking the constituent chemicals as per the following stoichiometric ratio given below:

$50B_2O_3 + 30\ SiO_2 + 10Al_2O_3 + (4.5\text{-}y)\ ZnO + 5K_2CO_3 + 0.5Sm_2O_3 + yEu_2O_3$; where (y = 0.25, 0.5, 0.75, 1.0, 1.25 mol%). The details of the sample IDs with composition are given in Table 3.1

Table 3.1

Composition with sample ID for the as-prepared KZABS glasses.

Sample ID	Composition (mol%)						
	B_2O_3	SiO_2	Al_2O_3	ZnO	K_2O	Sm_2O_3	Eu_2O_3
SmEu0	50	30	10	5	5	-	-
Sm1	50	30	10	4.75	5	0.25	-
Sm2	50	30	10	4.5	5	0.5	-
Sm3	50	30	10	4.25	5	0.75	-
Sm4	50	30	10	4	5	1.0	-
Sm5	50	30	10	3.75	5	1.25	-
Sm2Eu1	50	30	10	4.25	5	0.5	0.25
Sm2Eu2	50	30	10	4	5	0.5	0.5
Sm2Eu3	50	30	10	3.75	5	0.5	0.75
Sm2Eu4	50	30	10	3.5	5	0.5	1.0
Sm2Eu5	50	30	10	3.25	5	0.5	1.25

The XRD measurement was performed using Bruker model No: D-8 high-resolution X-ray using Cuα radiation (λ = 1.5406 Å) with an operating voltage of about 30 kV. FT-IR investigation has been done by using Perkin Elmer spectrum 2. The Raman spectrum has been recorded by using the Renishaw Invia Raman Microscope. The absorption spectral recording have been done with the help of absorption spectrometer (JASCO; Model Number: V-770). The PL excitation & emission spectral information were recorded using Spectrofluorometer (JASCO; Model Number: FP-8300). The decay curves were measured using an Edinburgh spectrophotometer model Number: FLS980. All the measurements were taken at an ambient temperature. The temperature-dependent PL was performed using a fiber integrated spectrometer (Model: FLAME-S-XR1-ES) from Ocean Optics with an operating resolution of 0.1 nm.

3.3 Results and discussion

3.3.1. Optimization of alkali metal ion in borosilicate glasses

Fig. 3.1 shows the PL spectra recorded for zinc alumino borosilicate (ZABS) glasses containing different alkali metals like lithium (Li), sodium (Na) and potassium (K) (LZABS, NZABS, and KZABS glasses) containing 0.5mol% of Sm^{3+} ion under 402 nm excitation wavelength. It was depicted that each sample consists of three peaks at 562, 597 and 644 nm pertaining to $^4G_{5/2} \rightarrow {}^6H_{5/2}$, $^6H_{7/2,}$ and $^6H_{9/2}$ transitions, respectively. From Fig. 3.1, it is conspicuous that KZABS glass shows relatively high luminescence emission than the remaining two alkali metal containing ZABS glasses, showing the KZABS glass's superior quality for further studies.

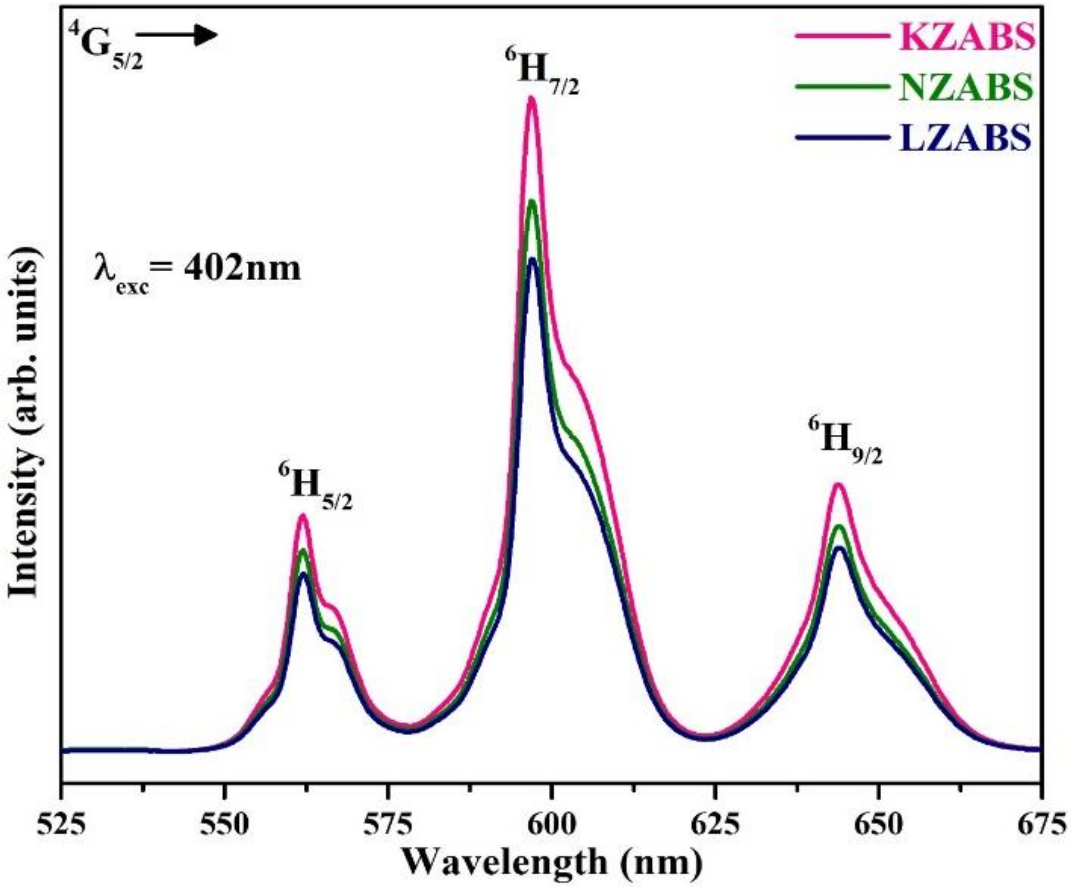

Fig. 3.1. Optimization of alkali metal ion in ZABS host glass.

3.3.2. Physical and optical properties characterization

By employing the equations described in chapter 2 (equation 2.1 to equation 2.7), we have determined various physical and optical properties for Sm-Eu co-doped KZABS glasses and given in Table. 3.2. Variation of molar volume and density of the titled glasses with Eu^{3+} ion concentration is shown in Fig. 3.2. As shown in Fig. 3.2, with an increase in Eu^{3+} ions concentration, density values increase, and molar volume values decrease in the titled glasses. This may be due to replacing some zinc ion sites (lower molecular weights) with europium ions having relatively greater molecular weights.

Table 3.2

Physical properties of Sm^{3+}/Eu^{3+} co-doped KZABS glasses.

Sample ID	Sm2Eu1	Sm2Eu2	Sm2Eu3	Sm2Eu4	Sm2Eu5
Thickness (mm)	2.46	2.46	2.46	2.46	2.46
Average molecular weight	73.82	74.49	75.12	75.85	76.52
Density (g/cm^3)	2.23	2.28	2.32	2.37	2.43
Molar Volume (cm^3)	33.08	32.67	32.42	31.98	31.48
Optical Band Gap (E_g)	2.99	3.00	3.03	3.07	3.12
Refractive Index (n)	2.39	2.39	2.38	2.37	2.36
Molar Refraction R_m (cm^3)	20.28	20.88	21.42	21.94	22.43
Polarizability α_m (10^{-24})	5.118	5.267	5.405	5.535	5.659

With the assistance of Brewster's angle method, the index of refraction (n) of titled glasses was measured using a He-Ne laser (650 nm. The band gap values values lie in the range of 2.99 to 3.12eV as plotted in Fig. 3.3. These values are enlisted in Table.3.2.

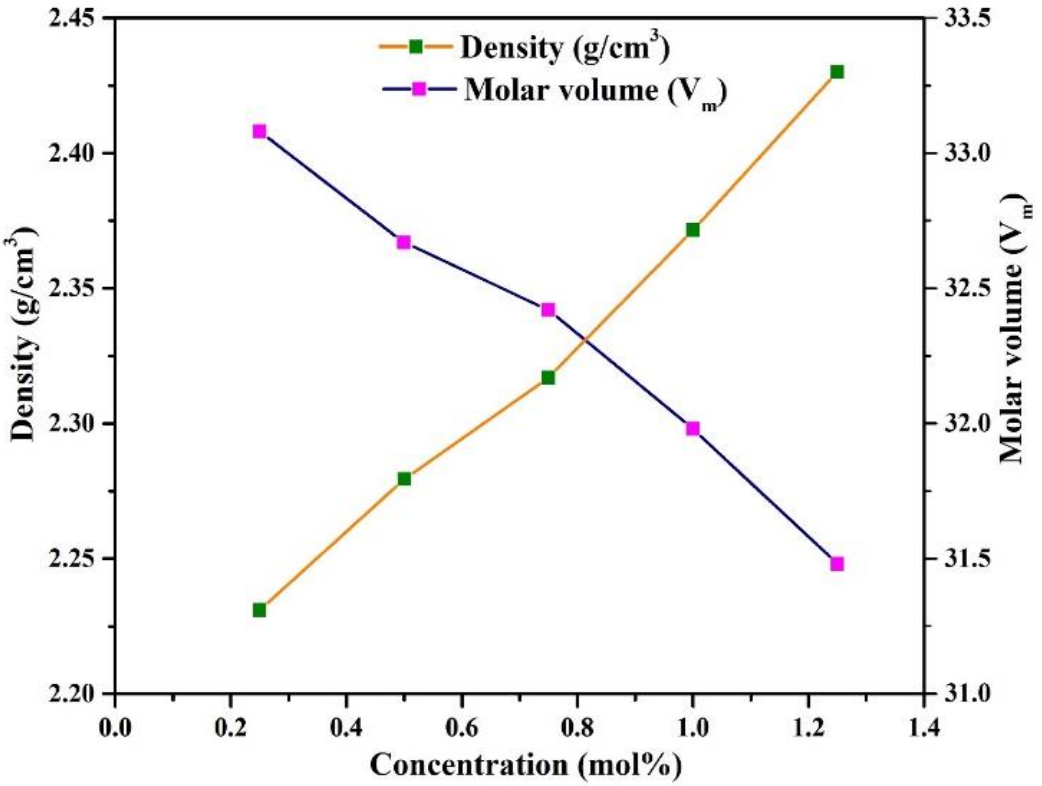

Fig. 3.2. Variation of density and molar volume with Eu^{3+} ions content in KZABS glasses.

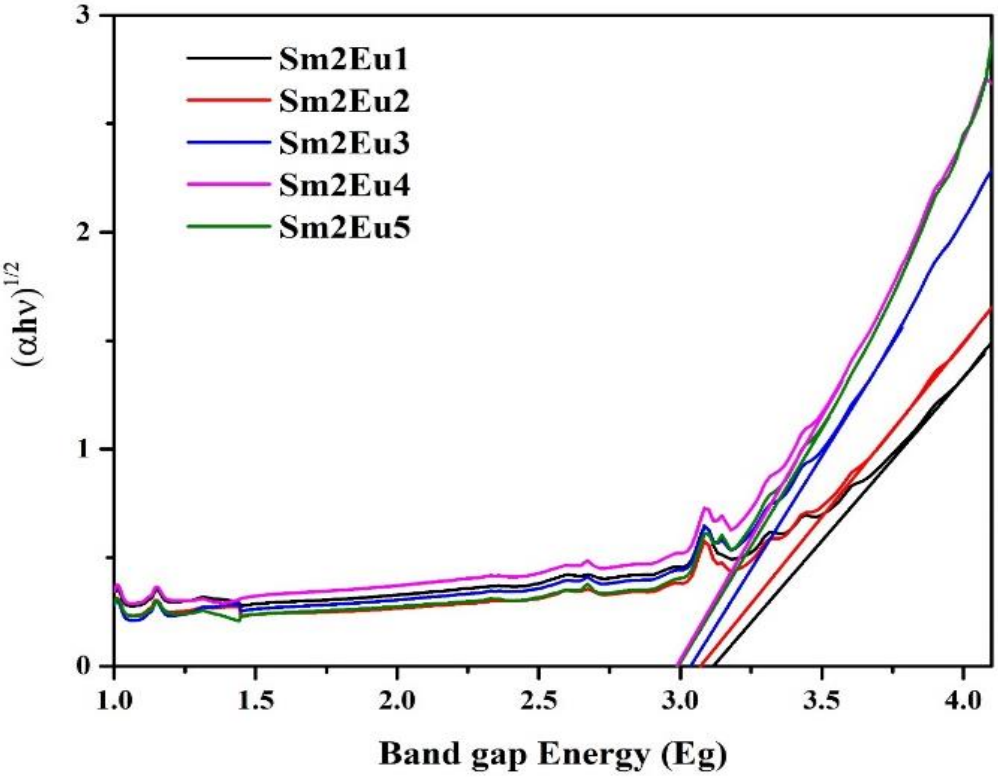

Fig. 3.3. Tauc plot for direct optical band gap for Sm^{3+}/Eu^{3+} co-doped KZABS glasses.

3.3.3 XRD spectral analysis

XRD pattern of an un-doped KZABS glass has been shown in Fig. 3.4. It contains a broad hump in a range of 20º-30º without any diffraction peak revealing the amorphous behavior of the host glass [42].

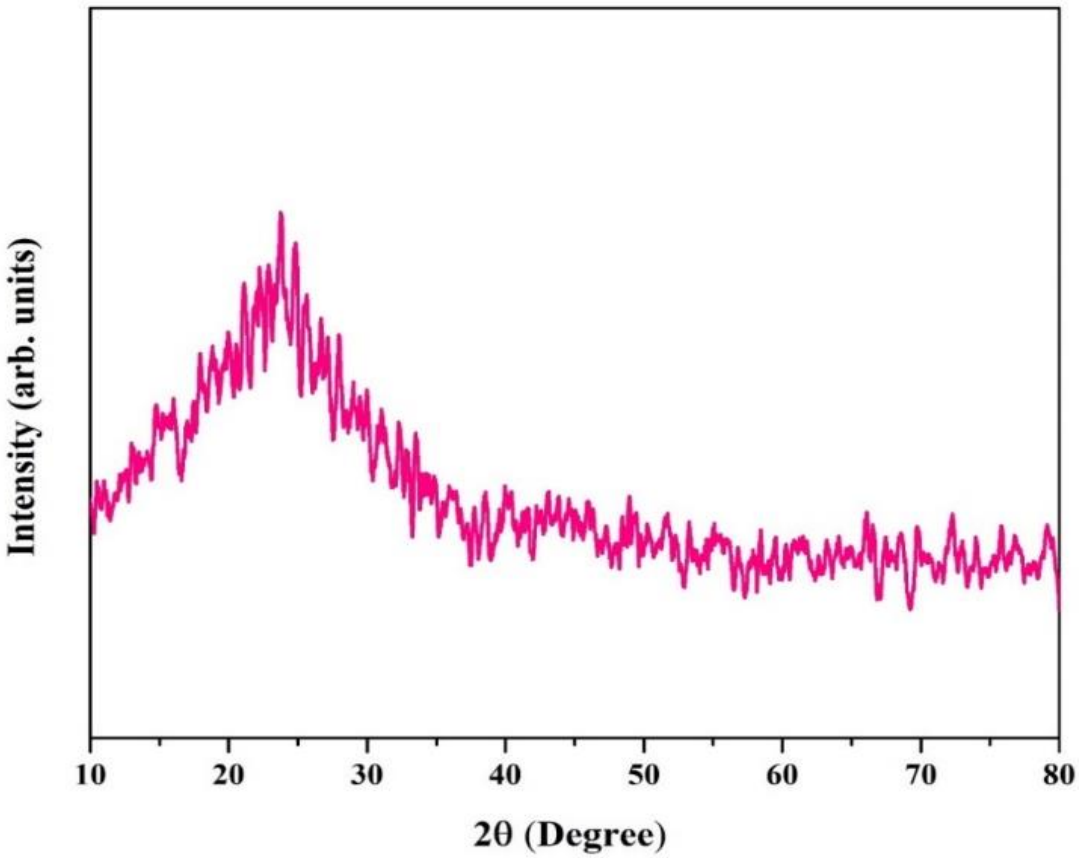

Fig. 3.4. XRD pattern of an un-doped KZABS glass.

3.3.4. FT-IR spectral analysis

FT-IR could be a powerful technique used to explore the varied functional groups and study the significant variation in the composition of the glass sample. It is evident from the literature that the FT-IR spectrum of a borate glass show three prime regions; the first one is at 600-800 cm^{-1} (different borate segments), the second one is at 800-1200 cm^{-1} (BO_4 units), and the third one at

1200-1600 cm^{-1} (BO_3 units) regions [42]. BO_3 triangle and BO_4 pyramid groups are the fundamental units of borate glasses. Fig. 3.5 shows the FT-IR spectrum recorded in 400-4000 cm^{-1} for a base glass with no Sm^{3+} and Eu^{3+} ions. It is noticed that the spectrum has many shoulders at around 436, 697, 804, 915, 1091, 1388, 1630 and 3488 cm^{-1}.

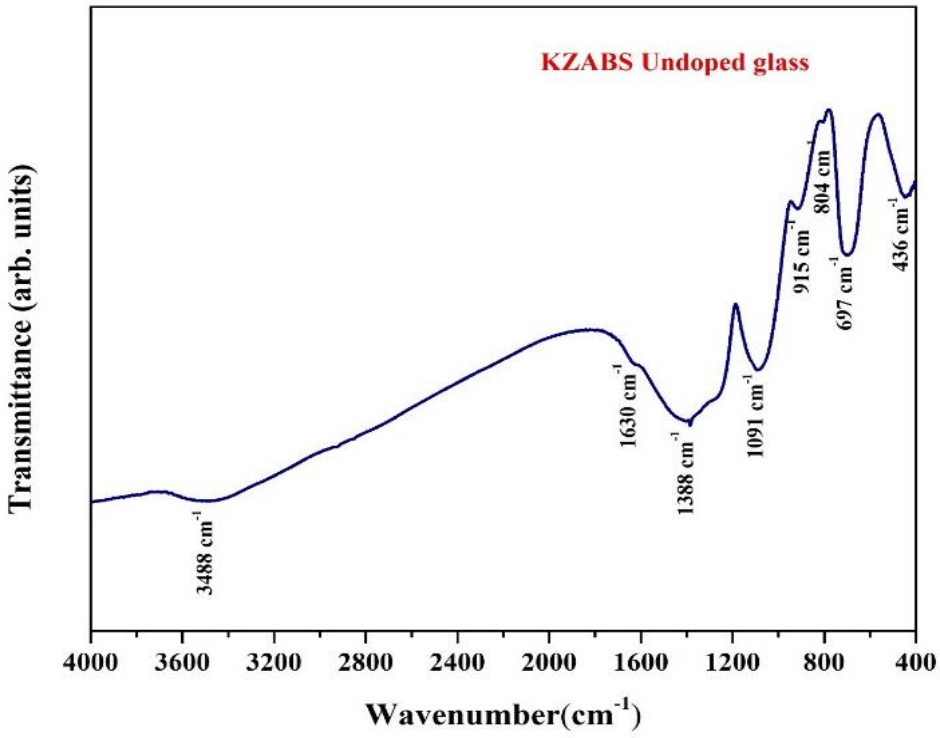

Fig. 3.5. The FT-IR spectrum of an un-doped KZABS glass.

The shoulder presented at 436 cm^{-1} may be because of the vibrations within the Zn-O bond [61]. The shoulder at 697 cm^{-1} may be due to B-O-B linkage and B-O bond. The transmittance shoulder at 804 cm^{-1} could be due to the bending of BO_3-O-BO_4 bond vibrations. The bands at 915 and 1091 cm^{-1} may be attributed to the stretching vibration in BO_4 units and Si-O-Si linkage generally present in many borosilicate hosts. The shoulder observed at 1388 cm^{-1} represents the vibration of BO_3 units [44,48-51].The shoulder at 1630 cm^{-1} represents the bending of O-H bonds that are introduced because of the

addition of some air during the preparation of the pellets by using KBr [45]. The OH groups are present at 3488 cm^{-1} with very low intensity implying less OH content. The value of OH content is beneficial in reducing radiation losses in glassy materials. The lower the OH content in glasses, the higher will be the quantum efficiency [67]. The band present at 1388 cm^{-1} has lower transmission, implying increased absorption. Thus, according to the value reported in the literature, the highest energy peak (1388 cm-1) represents the current system's phonon energy [68].

The OH content can be obtained by employing the equation given below:

$$\alpha_{OH} = \frac{\ln\left(\frac{T0}{TD}\right)}{l} \qquad (3.1)$$

Where T_0, T_D and l denote the highest transmission, transmission at 3000 cm^{-1} and thickness of the glass sample, respectively. The OH content for the KZABS host glass estimated using the aforementioned formula is 52.21 ppm, which is relatively smaller than the other reported values for glasses such as ZnAlBiB (65.48ppm) [15], NaBiSrP (58.14 ppm) [45] and GeS2 (175.5 ppm) [69]. Relatively less OH content present in KZABS glass allows us to contemplate that the as-prepared glasses can show good visible luminescence suitable for the fabrication of photonic devices.

3.3.5. Raman spectral analysis

Raman spectrum recorded in the range 200-2000 cm^{-1} for an un-doped KZABS glass show four peaks at 466, 549, 801 and 1391 cm^{-1}, as shown in Fig. 3.6. The spectrum confirms the presence of various borate functional groups. The Raman band observed at 466 and 549 cm^{-1} shows the B-O-B and Al-O-Al bending respectively [61,70]. The band presents at 801 cm^{-1} due to stretching vibrations in BO_4 tetrahedral units [71]. The Raman band attributed at 1391 cm^{-1} is because of vibrations in the B-O bond from diborate groups [58].

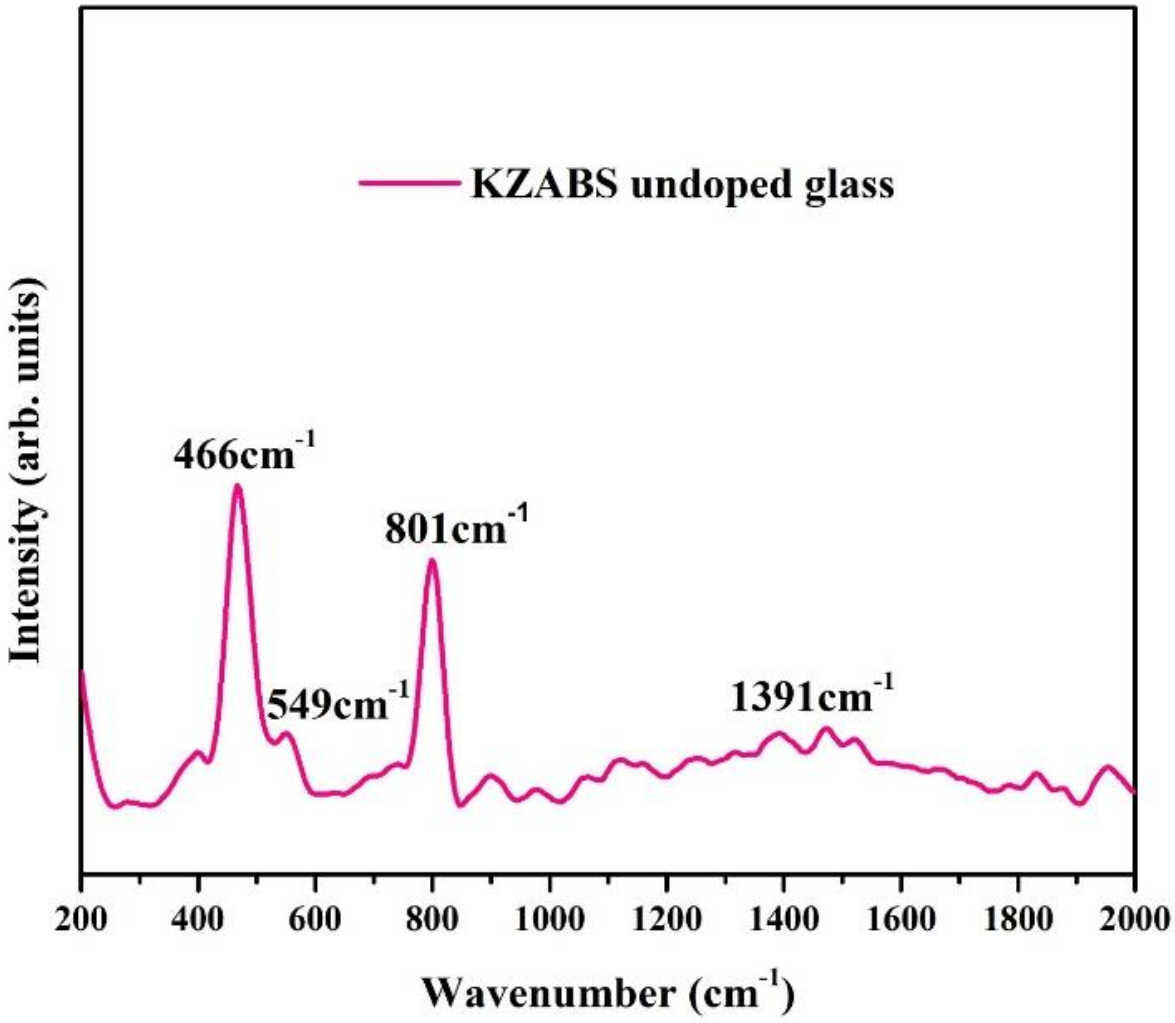

Fig. 3.6. Raman spectrum of an un-doped KZABS glass.

It is renowned that the alkali borate glasses (more than 25 mol% boron content) will display a band nearly at 800 $cm^{-1,}$ the characteristic of di-borate groups. Generally, extreme vibrational energy portrayed in the Raman spectrum gives the phonon energy of the material [30]. For the present glass, maximum vibrational energy was observed at 1391cm^{-1}, nearly equal to the phonon energy noticed from the FT-IR spectrum. This allows us to claim that the synthesized glasses are quite suitable for visible photonic device applications as they show relatively less phonon energies.

3.3.6. PL spectral analysis

3.3.6.1. PL studies of Sm^{3+} doped KZABS glasses

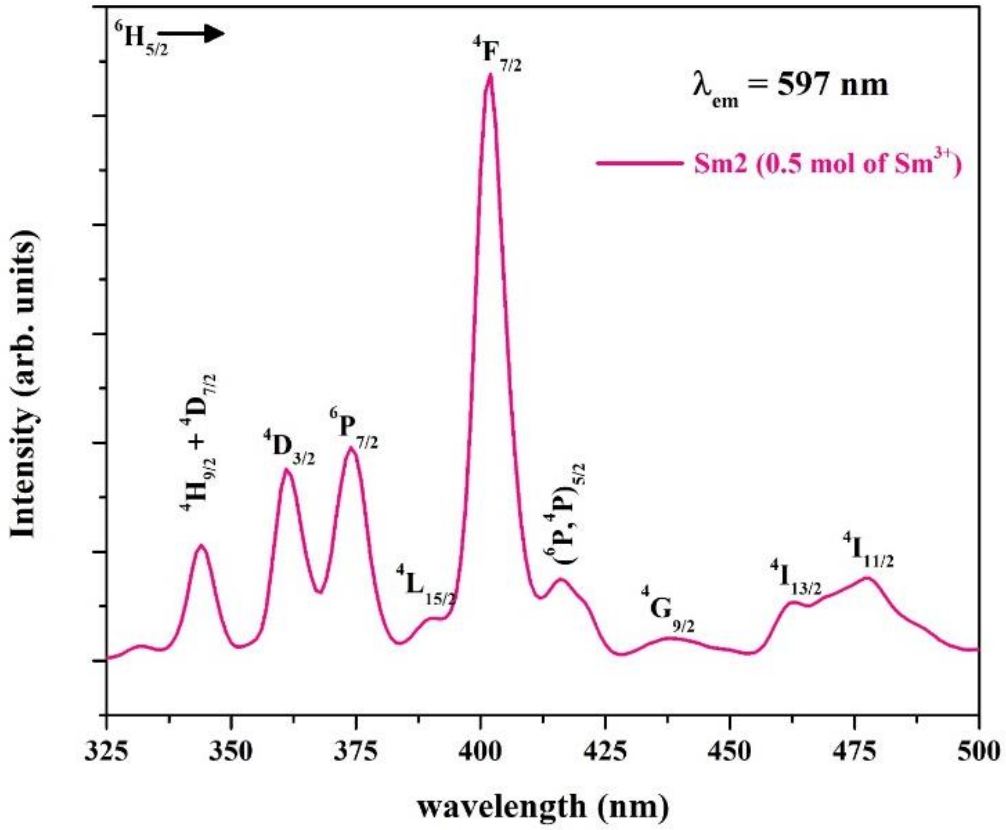

Fig. 3.7. The excitation spectrum of Sm2 glass under 597 nm emission wavelength.

The doping concentration of RE^{3+} ions in a host matrix is crucial for impressive performance and luminescence intensity. Fig. 3.7 shows the excitation spectrum of KZABS glasses doped with 0.5 mol% of Sm^{3+} ions under 597 nm emission wavelength.

The excitation spectra for the other KZABS glasses are similar in-band position except for some variation in their intensity; hence, they were not depicted in Fig. 3.7. The excitation spectrum depicted in Fig.3.7, show nine peaks at 344, 361, 374, 388, 402, 416, 438, 462, and 477 nm pertaining to

$^6H_{5/2} \rightarrow {}^4H_{9/2} + {}^4D_{7/2}$, $^4D_{3/2}$, $^6P_{7/2}$, $^4L_{15/2}$, $^4F_{7/2}$, $(^6P, {}^4P)_{5/2}$, $^4G_{9/2}$, $^4I_{13/2}$, and $^4I_{11/2}$ transitions respectively. The peak observed at 402 nm corresponding to the $^6H_{5/2} \rightarrow {}^4F_{7/2}$ transition is the most intense and is quite suitable for reading the emission spectra.

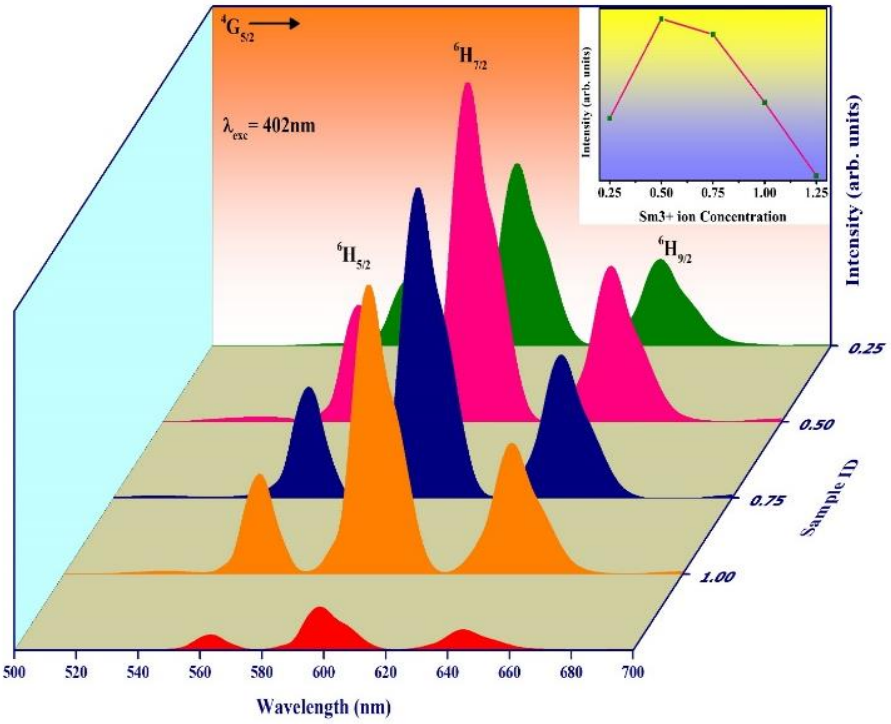

Fig. 3.8. Optimization of Sm^{3+} ion concentration in KZABS glass under 402 nm excitation wavelength (Inset: showing the emission intensity variation with Sm^{3+} ion concentration for 597 nm emission peak).

Fig. 3.8 depicts the emission spectra of KZABS glasses activated with Sm^{3+} ions under 402 nm excitation wavelength. The emission spectrum of each sample consists of three peaks at 562, 597 and 644 nm pertaining to $^4G_{5/2} \rightarrow {}^6H_{5/2}$, $^6H_{7/2}$, and $^6H_{9/2}$ transitions, respectively. The peak observed at 562 nm is magnetic dipole (MD) as per the selection rule ($\Delta J = 0$, J is angular momentum). Another peak observed at 644 nm is purely electric dipole (ED) following the selection rule ($\Delta J = \pm 2$). On the other hand, the most intense peak observed at 597 nm is because of both ED and MD transitions. As

shown in Fig. 3.8, the Sm^{3+} ion content entering the glass can only influence emission peak intensity without bringing any change to the peak position. As observed in Fig. 3.8, the emission intensity increases monotonically up to 0.5 mol% of Sm^{3+} ion content and diminishes beyond because of the concentration quenching effect [18,72,73]. The inset of Fig. 3.8 shows the quenching effect produced for the intense peak observed at 597 nm.

3.3.6.2. PL studies of Sm^{3+}/Eu^{3+} co-doped KZABS glasses

The excitation spectra recorded for 0.5 mol% of Sm^{3+}(blue line), 1.0 mol% of Eu^{3+} (red line) and Sm^{3+} (0.5 mol%)/Eu^{3+} (1.0 mol%) (green line) co-doped KZABS glass under 597 nm emission wavelength is shown in Fig. 3.9. The excitation spectral features for the remaining co-doped KZABS glasses are the same in peak position, expecting some intensity variation. From Fig. 3.9, it is conspicuous that the excitation spectrum of the co-doped glass corresponds to both Sm^{3+} and Eu^{3+} ion compared to Sm^{3+} and Eu^{3+}. The peaks observed exclusively at 344, 361, 374, 388, 402, 416, 438, 462, and 477 nm are due to Sm^{3+} ions, as already discussed in Fig. 3.7. The peaks observed at 361, 375, 394, 416, and 464 nm are exclusively due to Eu^{3+} ion corresponding to $^7F_0 \rightarrow {}^5D_4$, $^5L_7$, $^5L_6$, $^5D_3$, and $^5D_2$ transitions, respectively. It can be observed from the same figure that the excitation peak intensity of the Sm-Eu co-doped KZABS glass is more than Eu doped and less than Sm doped KZABS glasses.

It might be due to the transfer of excitation energy from Sm^{3+} ions to Eu^{3+} ions, which expands the excitation spectra of Eu^{3+} ions in KZABS glass. The enhancement observed in the excitation peak intensity of co-doped glass elucidates an ample scope for enhancing visible red emission shown by Eu^{3+} ions in the co-doped KZABS glasses.

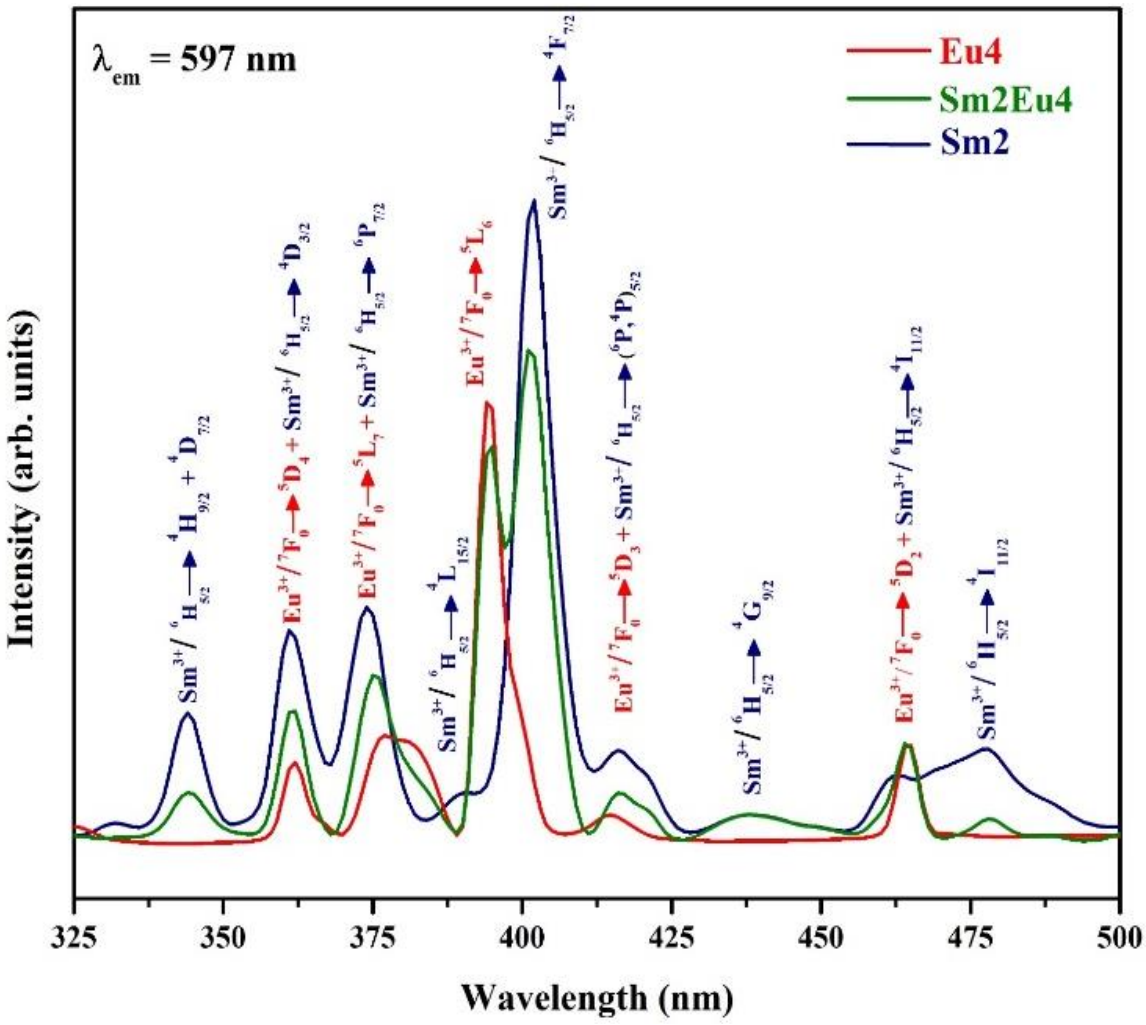

Fig. 3.9. Excitation spectra of Sm2, Eu4 and Sm2Eu4 glasses under 597 nm excitation.

The emission spectra of Sm^{3+}/Eu^{3+} co-doped KZABS glasses measured under 402 nm excitation wavelength are shown in Fig. 3.10. Seven emission peaks were observed, out of which three are due to Sm^{3+} ions at 562, 597, and 644 nm, corresponding to $^4G_{5/2} \rightarrow {}^6H_{5/2}$, $^4G_{5/2} \rightarrow {}^6H_{7/2}$, and $^4G_{5/2} \rightarrow {}^6H_{9/2}$ transitions, respectively. The remaining four are due to Eu^{3+} ions at 578, 590, 613, and 700 nm corresponding to $^5D_0 \rightarrow {}^7F_0$, $^5D_0 \rightarrow {}^7F_1$, $^5D_0 \rightarrow {}^7F_3$, and $^5D_0 \rightarrow {}^7F_4$ transitions respectively. With an increase in Eu^{3+} ion concentration, the intensity of the emission peaks pertaining to Sm^{3+} ions situated at 562, 597, and 644 nm decreases gradually.

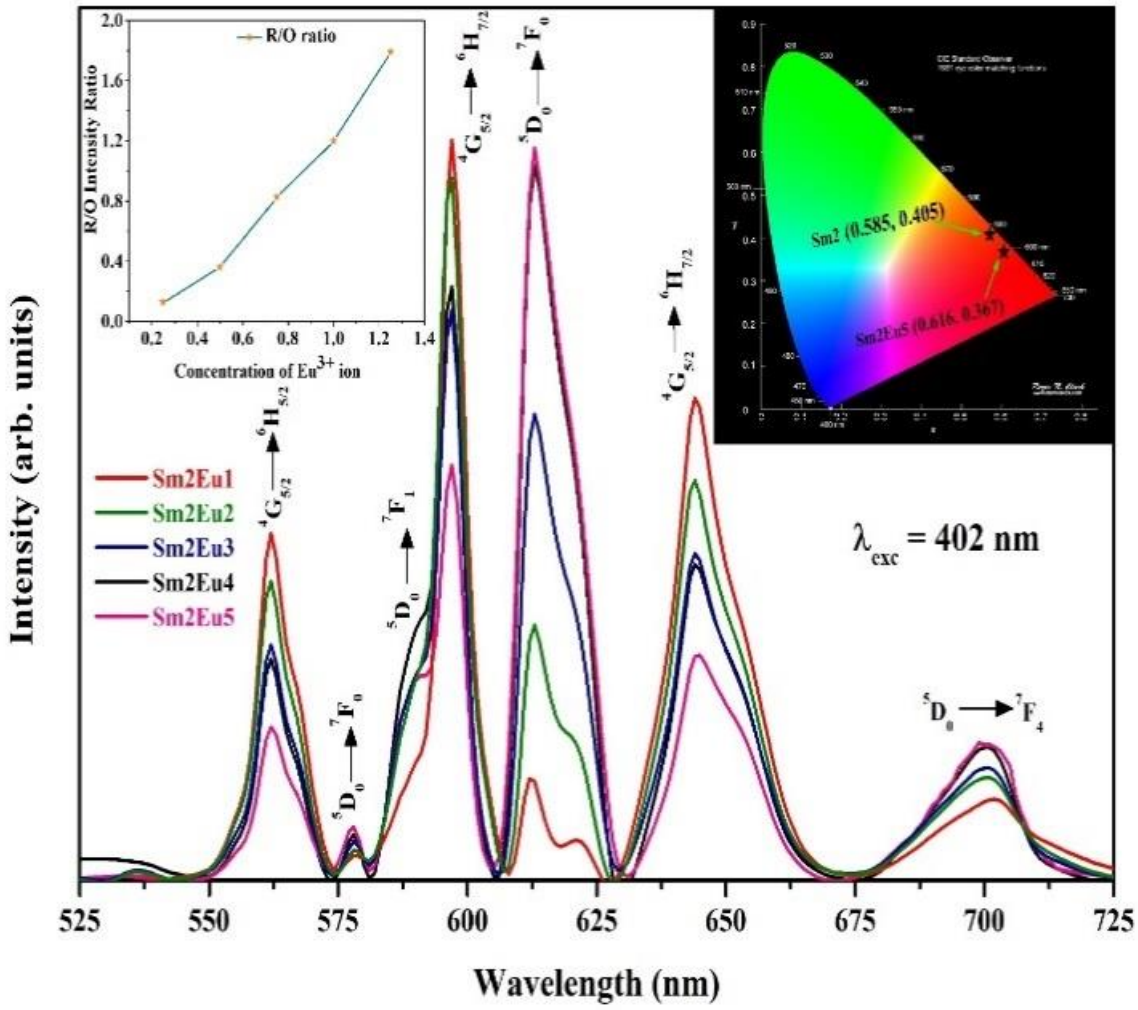

Fig. 3.10. Emission spectra of Sm^{3+}/Eu^{3+} co-doped KZABS glasses under 402 nm excitation [Inset (left side): Variation of R/O ratio with the Eu^{3+} ion concentration, Inset (right side): CIE chromaticity diagram for Sm-Eu co-doped KZABS glasses under 402 nm excitation].

In contrast, the intensity of peaks due to Eu^{3+} ions observed at 578, 613, and 700 nm increases slowly. This is happening because of the sensitization of Eu ions emission by the transfer of energy from Sm ions in the as-prepared glasses. The inset of Fig. 3.10 shows the increase in red to orange (R/O) emission intensity with Eu^{3+} ion concentration. This is a clear evidence for the energy transfer from Sm^{3+} to Eu^{3+} ions and enhancement in visible red luminescence.

3.3.7. Energy transfer dynamics and PL decay spectral analysis

In general, energy transfer between sensitizer and activator can occur via radiative transfer, exchange interaction and multipole-multipole interaction. The decay curves can confirm the energy transfer due to the radiative process. The possible energy transfer due to the radiative process can be discarded if the experimental lifetimes shown by the decay curves decrease gradually with an increase in dopant ion concentration [57]. In the present work, the observed lifetimes measured from the decay curves are gradually decreasing, indicating the transfer of energy not due to the radiative process [74]. On the other hand, exchange interaction is possible only when sensitizer and activator ions are in close proximity to each other.

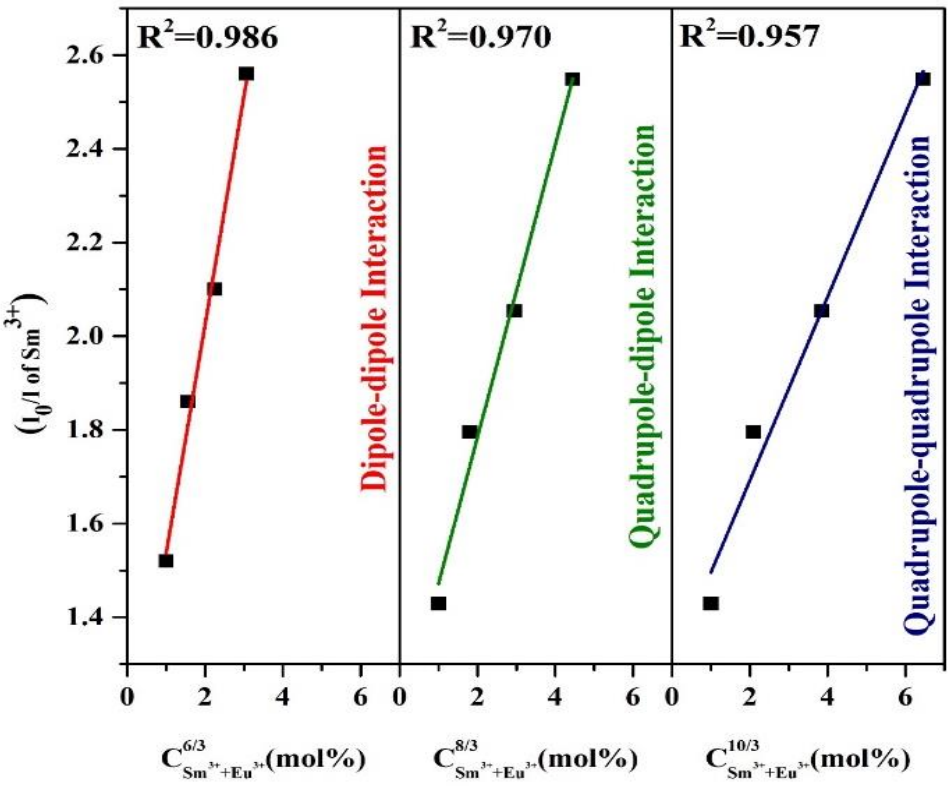

Fig. 3.11. Variation of I_0/I with $C^{\alpha/3}$ for different concentrations of Eu in Sm fixed at 0.5 mol% under 402 nm excitation

In the titled glasses, the possibility for energy transfer through multipole-multipole interaction is more than the aforementioned mechanisms. Further, to investigate the type of multipolar interaction involved in the energy transfer process, Dexter's theory was applied as per the equation (1.3), as explained in chapter 1. To understand the mechanism, the graph was plotted between $\frac{I_0}{I}$ and $C^{\frac{\alpha}{3}}$ and is shown in Fig. 3.11. The best linear fit was observed for $\alpha = 6$, indicating the non-radiative energy transfer through dipole-dipole interaction.

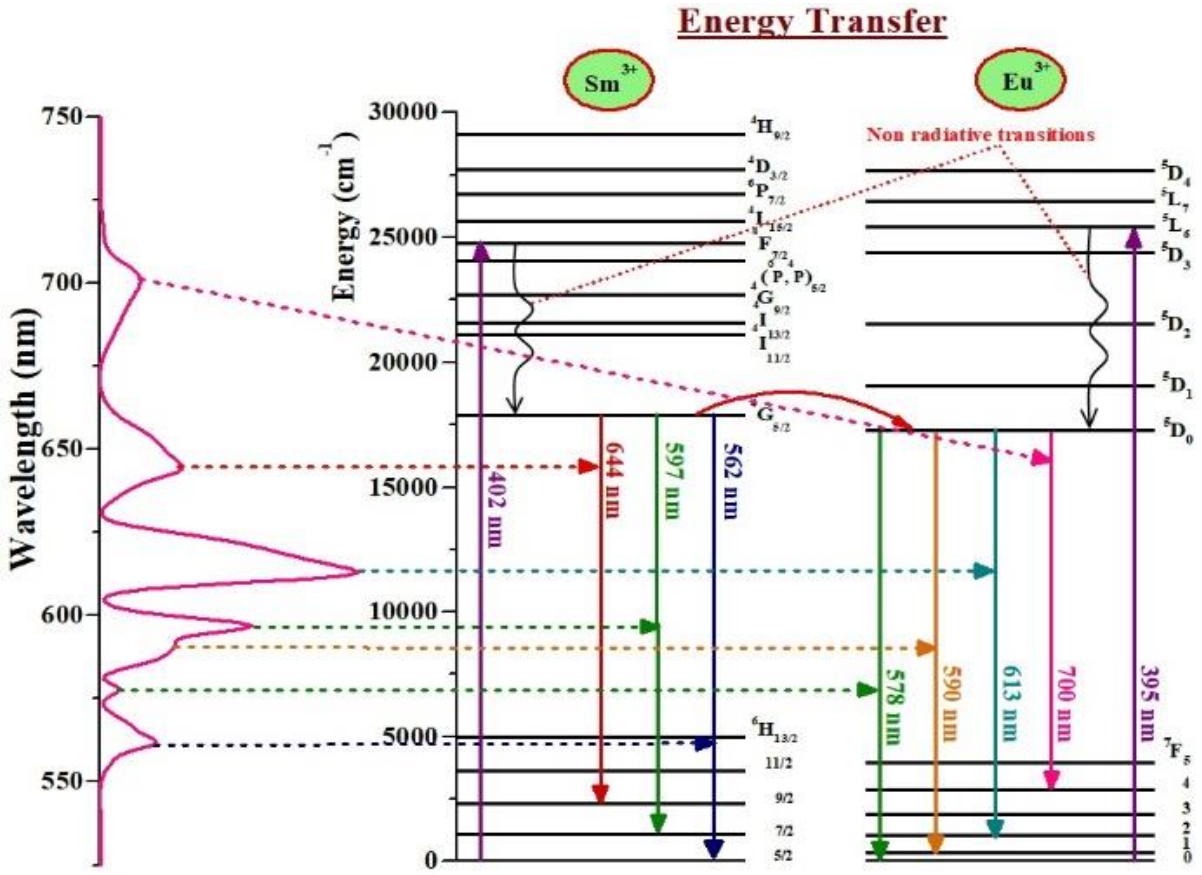

Fig. 3.12. Energy level diagram for Sm^{3+} and Eu^{3+} ions showing energy transfer via non-radiative transitions

With the help of Carnall's papers, energies (cm^{-1}) for Sm^{3+} and Eu^{3+} ions are used to design the energy level diagram shown in Fig. 3.12. With the help of the energy level diagram, it is easy to understand

the channels through which energy transfers from Sm^{3+} to Eu^{3+} [75,76]. Fig. 3.12 indicates the ground state absorption in Sm^{3+} and Eu^{3+} and energy transfer from $^4G_{5/2}$ (17900 cm^{-1}) to $^5D_0$ (17277 cm^{-1}) via non-radiative transitions. To understand the energy transfer mechanism, PL decay has been recorded. Fig. 3.13 shows the decay curves plotted for Sm2, Sm2Eu1, Sm2Eu2, Sm2Eu3, Sm2Eu4, and Sm2Eu5 samples for the emission peak at 597 nm from Sm^{3+} ion under 402 nm excitation wavelength. The decay curves are found to be non-exponential and are well fitted to the non-exponential equation given below[77]:

$$I = I_0 + A_1 exp(-t/\tau_1) + A_2 exp(-t/\tau 2) \quad (3.2)$$

Where I_0 and I are the luminescence intensities at zero and t time, A_1 and A_2 are the fitting constants, τ_1 and $\tau 2$ are fast and slow lifetime components.

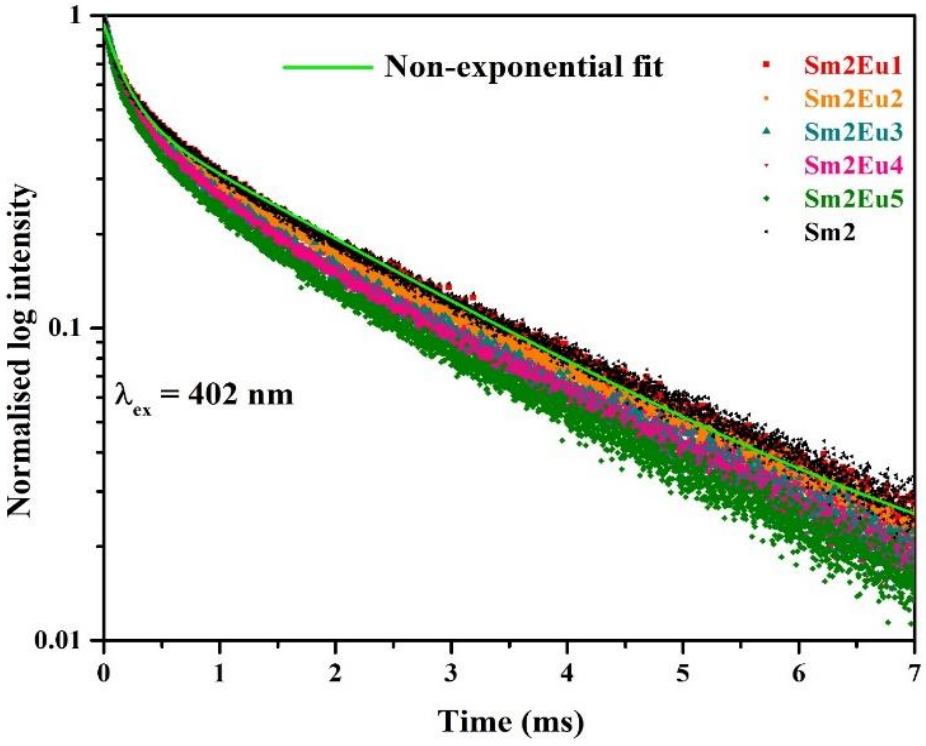

Fig. 3.13. Decay curves for Sm2 and series of SmEu glasses recorded at 597 nm under 402 nm excitation wavelength

Table 3.3

Average lifetime (τ_{avg}), energy transfer efficiency (η_T), energy transfer probability rate (P_T) and CIE coordinates of Sm-Eu co-doped KZABS glasses**.**

Sample ID	Concentration of Eu^{3+} ion (mol%)	τ_{avg} (ms)	$\eta_{T\,(\%)}$	P_T	CIE chromaticity coordinates (X, Y)
Sm2	0	1.35	-	-	0.585,0.405
Sm2Eu1	0.25	1.31	03.05	02.26	0.598, 0.392
Sm2Eu2	0.5	1.26	07.14	05.29	0.602, 0.384
Sm2Eu3	0.75	1.18	14.40	10.67	0.610, 0.378
Sm2Eu4	1.0	1.16	16.37	12.13	0.613, 0.372
Sm2Eu5	1.25	1.10	22.72	16.83	0.616, 0.367

With the help of Carnall's papers, energies (cm^{-1}) for Sm^{3+} and Eu^{3+} ions are used to design the energy level diagram shown in Fig. 3.12. With the help of the energy level diagram, it is easy to understand the channels through which energy transfers from Sm^{3+} to Eu^{3+} [75,76]. Fig. 3.12 indicates the ground state absorption in Sm^{3+} and Eu^{3+} and energy transfer from $^4G_{5/2}$ (17900 cm^{-1}) to $^5D_0$ (17277 cm^{-1}) via non-radiative transitions.

The type of interaction that occurs in energy transfer can also be explained by employing I-H model to non-exponential decay curves as per equation (1.4), mentioned in chapter 1. By following equation

(1.4), the decay profiles were fitted with I-H model and found best fit for S =6. that shows that energy transfers via dipole-dipole interaction. This result of the I-H model is in consonance with the result of Dexter's theory. The decay profiles fit with the I-H model have been depicted in Fig. 3.14.

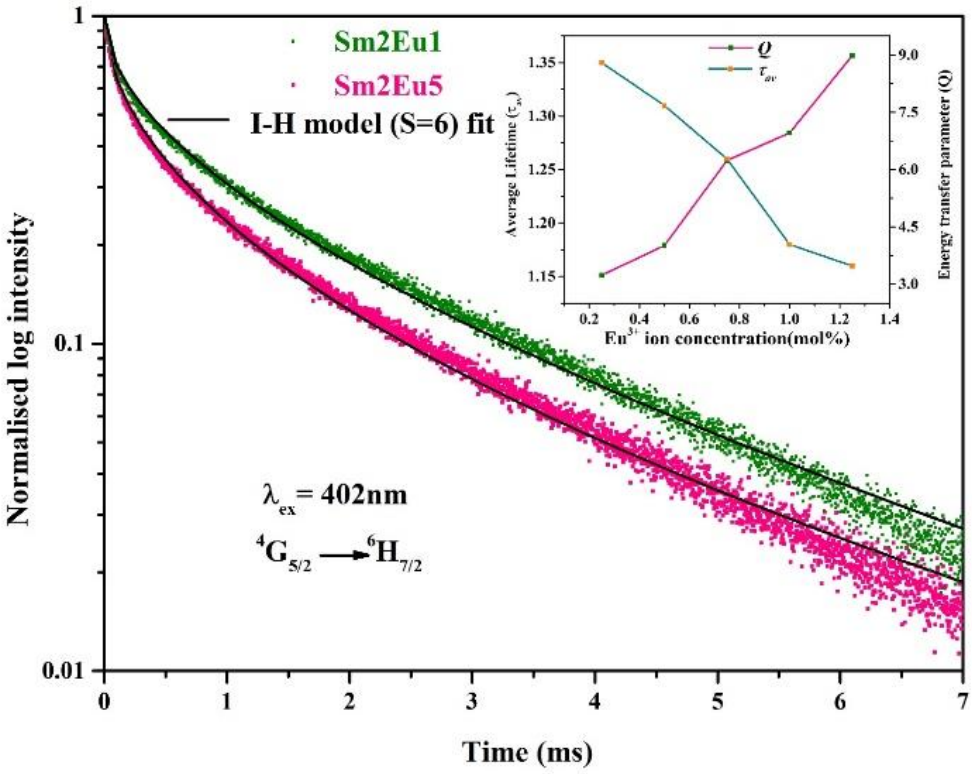

Fig. 3.14. Decay curves fitted with the I-H model (S=6) for Sm2Eu1 and Sm2Eu5 glasses under 402 nm excitation (Inset: Variation of an average lifetime (τ_{av}) and energy transfer parameter (Q) with Eu^{3+} ion concentration)

The energy transfer parameter (Q) can be found by using the expression:

$$Q = \frac{4\Pi}{3}\Gamma\left(1-\frac{3}{s}\right)\cdot N_0 R_0^3 \qquad (3.6)$$

Where $\Gamma(s)$ is the gamma function, whose value is 1.77 for (s=6). N_0 is the acceptor ion concentration, and R_0 is the separation between donor and acceptor when the rate of energy transfer is equal to the

rate of intrinsic decay time. The value of Q was obtained by fitting decay curves and further using this Q value in equation (3.6) to find out R_0. The inset of Fig. 3.14 shows the variation of Q and τ_{av} with the Eu^{3+} ion concentration. The inset figure shows that the value of Q increases with an increase in Eu^{3+} ion concentration. This can be attributed to relatively more energy transfer.

The interaction parameter value between donor & acceptor (C_{DA}) can be estimated by using R_0 in the following expression:

$$C_{DA} = R_0^s \cdot \tau_0^{-1} \qquad (3.7)$$

The values of Q, N_0, R_0 and C_{DA} were placed in Table 3.4. Increasing values of these parameters with Eu^{3+} ion concentration indicate that energy transfer is more dominant [80].

Table 3.4

Energy transfer parameter (Q), acceptor-ion concentration (N_0), critical transfer distance (R_0) and donor-acceptor interaction parameter (C_{DA}) for Sm-Eu co-doped KZABS glasses.

Sample ID	Q	N_0(10^{19} ions/cm^3)	R_0 (Å)	C_{DA} (10^{-44} cm^6 s^{-1})
Sm2Eu1	3.24	0.765	1.78	4.34
Sm2Eu2	4.01	1.530	1.91	6.67
Sm2Eu3	6.24	2.314	2.21	15.8
Sm2Eu4	6.96	3.124	2.28	19.27
Sm2Eu5	8.98	3.969	2.47	31.07

3.3.8. Colorimetry and CIE chromaticity analysis

The PL emission spectral data can be modified into chromaticity coordinates (x, y and z) using the CIE 1931 standard procedure discussed in chapter 1 to explore the color emitted by the co-doped glasses The CIE points measured using the aforementioned procedure are depicted in Fig. 3.10 as an inset. As shown in the inset of Fig. 3.10, the CIE points are shifting towards an intense red region with an increase in Eu^{3+} ion concentration in the titled glasses.

3.3.9. Temperature-dependent PL studies

To explore the potential applications of the as-prepared glass in w-LEDs and other optical devices, temperature-dependent PL for Sm2Eu5 (Sm^{3+} 0.5 mol% and Eu^{3+} 1.25 mol%) glass was recorded in the range 25-175°C under 402 nm excitation and is depicted in Fig. 3.15(a). As the temperature increases, the emission intensity decreases. With an increase in temperature, the emission intensity changes without changing peak position. As shown in Fig. 3.15(a), the thermal quenching is due to the temperature-dependent non-radiative relaxations. The probability rate (R) for non-radiative relaxation can be estimated by using the following equation [81]:

$$R = A \exp\left(-\frac{\Delta E}{k_B T}\right) \qquad (3.8)$$

Where ΔE, k_B, and T stand for activation energy corresponding to thermal quenching, Boltzmann's constant, temperature respectively and A is constant. According to the above equation, R will increase with a rise in temperature, which eventually escalates the probability of non-radiative relaxations and thus emission intensity decreases, as shown in Fig. 3.15(a). The emission intensity retains 72.3% at 175°C as compared to the initial temperature (25 °C).

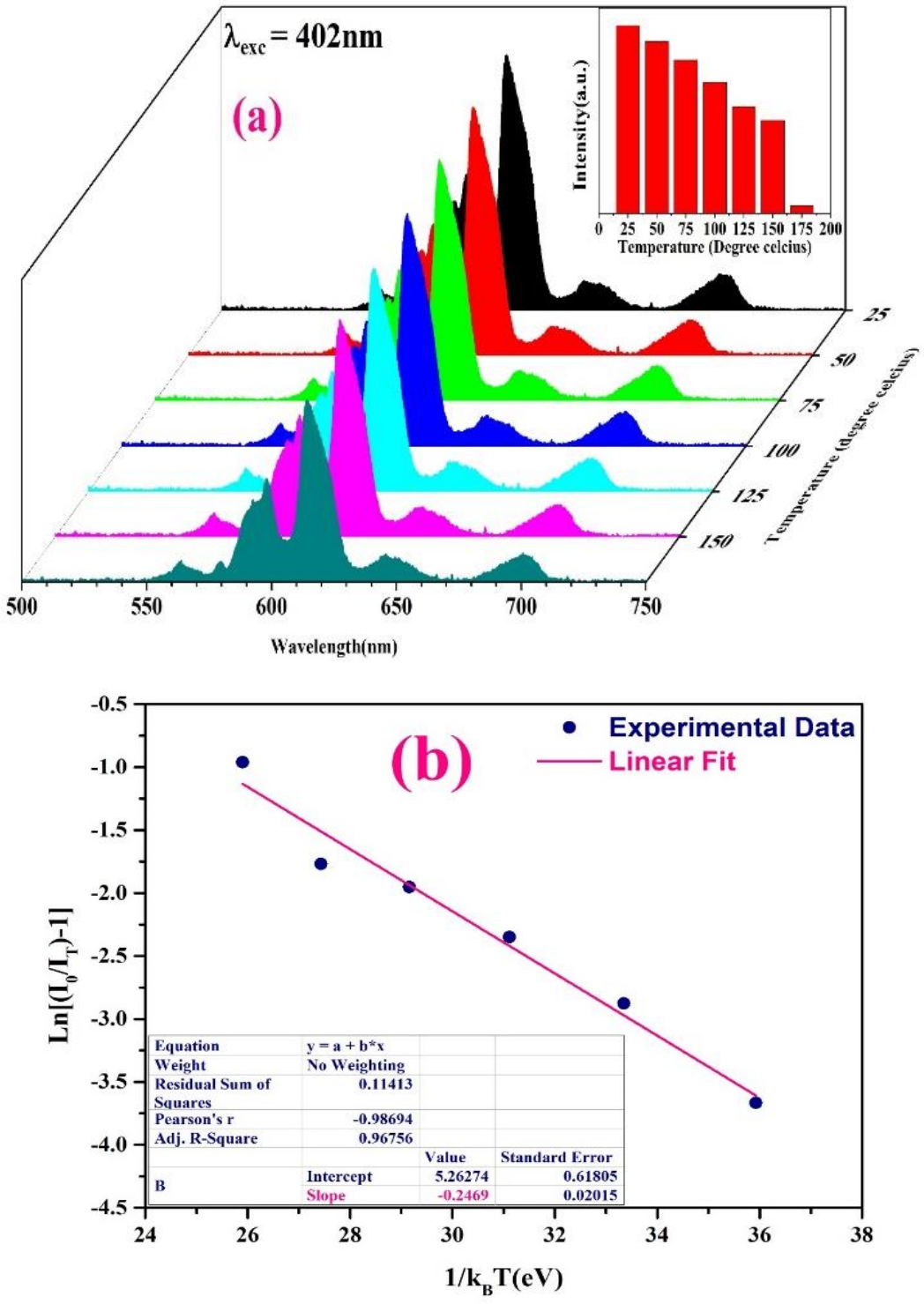

Fig. 3.15. (a) Temperature-dependent PL emission of Sm2Eu5 glass under 402 nm excitation (b) Variation of $\ln[(I_0/I_T)-1]$ versus $1/k_BT$ for emission at 613 nm under 402 nm excitation.

L. Zhao et al. [82] reported phosphors whose intensity decreases to 55% at a temperature of 225 °C. This indicates that the thermal stability of synthesized glass is relatively more. The activation energy *(ΔE)* is another important parameter used to measure thermal stability for the as prepared glass. With the help of Arrhenius equation, the activation energy *(ΔE)* can be estimated by using the following equation[81]:

$$I_T = \frac{I_0}{1+A\exp\left(-\frac{\Delta E}{k_B T}\right)} \tag{3.9}$$

Where I_0 and I_T are the PL emission intensities for the $^5D_0 \rightarrow {}^7F_2$ transition at initial and at temperature T(K), k_B is Boltzmann's, and A *is* arbitrary constants.

To find the value of ΔE, a graph is linearly fitted between Ln[(I_0/I_T)-1] and $1/k_BT$ and the slope of this plot give the ΔE as shown in Fig. 3.15(b). Thus, the value of ΔE appeared at 0.247 eV, which is relatively high as compared to the value reported by others [81]. Relatively such a high value of activation energy for the as-synthesized Sm^{3+}/Eu^{3+} co-doped KZABS glass promises high thermal stability and suitability for high powered optoelectronic device applications such as w-LEDs.

3.4. Conclusions

In this chapter, FT-IR and Raman reveals the OH content and phonon energies of the host glass. From PL excitation, emission and decay profiles, it was confirmed that thermally stable Sm-Eu co-doped glasses show intense red emission and posses energy transfer via dipole-dipole interaction. All the aforementioned results finally reveal the suitability of the Sm-Eu co-doped KZABS glasses for visible photonic applications such as red component in w-LEDs.

Chapter 4

Effective energy transfer from Dy^{3+} to Tb^{3+} ions in thermally stable KZABS glasses for intense green-emitting device applications

This chapter deals with the preparation of KZABS glasses co-doped with Dy^{3+}/Tb^{3+} ions and characterized by using various spectroscopic techniques such as PL, PL decay and TD-PL to understand the utility of the titled glasses for visible green emitting photonic device applications. An efficient energy transfer has been observed from Dy ions to Tb ions resulting in enhancing the green emission suitable for visible photonic device applications. The TD-PL studies conducted on the titled glasses reveals their thermal stability. All the studies finally reveal the superiority of Dy^{3+}/Tb^{3+} co-doped KZABS glasses for their usage as a green emitter suitable for the fabrication of w-LEDs and green visible display devices.

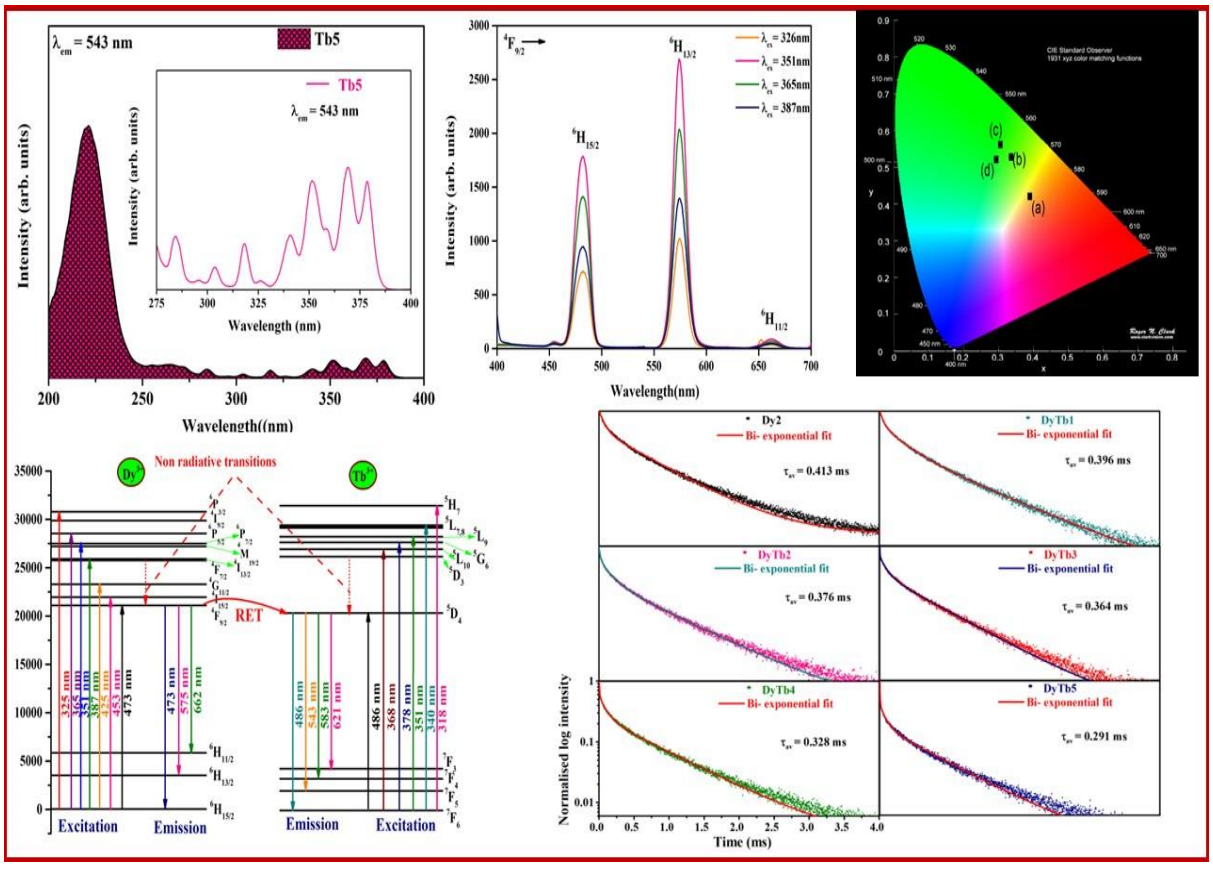

4.1 Introduction

The notable progress of the spectral features of RE ions has become an intense research area due to their numerous applications in optical communications, display devices, sensors, optical waveguides, lasers, SSL and w-LEDs. The generation of white light became a global research interest in past decades due to its vast contribution to optical device technology, mainly w-LEDs [2,32,44,83,84]. The key features of w-LEDs like high luminescence efficiency and no usage of fossil fuels are replacing incandescent and fluorescent lamps [85]. Out of various fabrication techniques, the RGB phosphor method is the most appropriate method to produce w-LEDs due to their high quantum efficiency, lesser size, and environmentally suitable conditions [7]. To enhance CRI, either n-UV LED combined with RGB phosphors or blue LED with red and green (RG) phosphor is preferred. However, the n-UV LED chip is considered a better solution for pumping the phosphor as they offer higher luminous efficiency when compared with the blue LED chip [86]. The inorganic oxides are considered one of the best choices for white light emission using RGB phosphors due to their high chemical stability and luminescence efficiency. Among these RGB phosphors, the phosphors such as $Ca_8ZnLa(PO_4)_7:Tb^{3+}$ and $NaCaPO_4:Tb^{3+}$ have been investigated for the green color in the development of RGB phosphor-converted n-UV-LEDs [87,88]. The green emitting phosphors generally have either an excitation band in UV-B (280−315 nm) or UV-C (100−280 nm) regions. Therefore, there is an extreme requirement for n-UV excitable green colored phosphors [89]. However, there are some drawbacks to using epoxy resin for coating RGB phosphors to construct w-LEDs. Usage of epoxy resins results in the degradation of output in terms of color rendering index, lifetime, and stability with time [9,10]. Therefore, it is necessary to develop cost effective phosphor-free w-LED that can emit white light with improved luminous efficiency and color rendering index with stable color temperature [85].

Our group has recently been actively involved in synthesizing and characterizing various host glasses doped with different RE ions suitable for various photonic applications [72,90–92]. The main moto of the work reported in this chapter is to prepare a glass host with relatively less phonon energies and quite suitable for giving intense visible emissions (doped with suitable RE ions for RGB color emissions) needed to fabricate phosphor free w-LEDs.

Out of various RE ions, Tb^{3+} ion is suitable to produce green emission corresponding to the transition $^5D_4 \rightarrow {}^7F_5$ and is useful for SSL technology, plasma display panels and solar cells [93]. Because of the potential applications of Tb^{3+} ions in diversified fields, researchers are paying considerable attention towards the enhancement of the intense green emission from Tb^{3+} ions by co-doping with various RE ions such as Sm^{3+}[94], Eu^{3+}[95], Ce^{3+} and Dy^{3+}[96] as sensitizers. Out of these ions, Dy^{3+} is well-known sensitizer to activate Tb^{3+} ions [93,97,98]. Tb^{3+} ions have a $^5D_4$ level which can be easily populated by the Dy level ($^4F_{9/2}$), and energy transfer occurs between these two ions [98]. There are several investigations related to sensitization of green emission shown by Tb^{3+} ions with Dy^{3+} ions in different kinds of glassy hosts such as phosphates [98], borates [96], silicates [93], borosilicate's [12] and many more. The spectral properties of RE ions depends upon the local surroundings, phonon energy and coordination of the host matrix. Among various types of glasses, borosilicate glass is a prominent choice due to their special features like extraordinary brightness, high thermal stability, richness in transparency, high solubility of RE ions and relatively lesser melting point. In chapter 3, we have already been discussed the importance of the host matrix.

Our main intention in this chapter is to understand the suitability of KZABS glasses co-doped with Dy^{3+} and Tb^{3+} ions for effective sensitization of the green emission shown by Tb^{3+} ions useful for green emitting photonic device applications. With the help of XRD, the non-crystalline behavior of the as synthesized glasses has been confirmed. Visible emission spectral features, lifetime and energy transfer efficiency of the titled glasses were determined by using

PL and PL decay profiles. TD-PL studies has also been conducted on the as synthesized glass to understand the thermal stability of the glass.

4.2 Experimental work

4.2.1 Sample preparation

Dy-Tb co-doped KZABS glasses were synthesized by using the melt-quenching method as discussed earlier in section 2.1. The details of the chemical composition used to prepare the Dy-Tb co-doped KZABS glasses and their terminology are as given below:

KZABS: $50B_2O_3 + 30\ SiO_2 + 10Al_2O_3 + 5ZnO + 5K_2CO_3$

Dy1: $50B_2O_3 + 30\ SiO_2 + 10Al_2O_3 + (4.75\text{-}y)\ ZnO + 5K_2CO_3 + 0.25Dy_2O_3$

Dy2: $50B_2O_3 + 30\ SiO_2 + 10Al_2O_3 + (4.5\text{-}y)\ ZnO + 5K_2CO_3 + 0.5Dy_2O_3$

Dy3: $50B_2O_3 + 30\ SiO_2 + 10Al_2O_3 + (4.25\text{-}y)\ ZnO + 5K_2CO_3 + 0.75Dy_2O_3$

Dy4: $50B_2O_3 + 30\ SiO_2 + 10Al_2O_3 + (4\text{-}y)\ ZnO + 5K_2CO_3 + 1.0Dy_2O_3$

Dy5: $50B_2O_3 + 30\ SiO_2 + 10Al_2O_3 + (3.75\text{-}y)\ ZnO + 5K_2CO_3 + 1.25Dy_2O_3$

Dy6: $50B_2O_3 + 30\ SiO_2 + 10Al_2O_3 + (3.5\text{-}y)\ ZnO + 5K_2CO_3 + 1.5Dy_2O_3$

Dy7: $50B_2O_3 + 30\ SiO_2 + 10Al_2O_3 + (3.25\text{-}y)\ ZnO + 5K_2CO_3 + 1.75Dy_2O_3$

Tb1: $50B_2O_3 + 30\ SiO_2 + 10Al_2O_3 + (4.75\text{-}y)\ ZnO + 5K_2CO_3 + 0.25Tb_4O_7$

Tb2: $50B_2O_3 + 30\ SiO_2 + 10Al_2O_3 + (4.5\text{-}y)\ ZnO + 5K_2CO_3 + 0.5Tb_4O_7$

Tb3: $50B_2O_3 + 30\ SiO_2 + 10Al_2O_3 + (4.25\text{-}y)\ ZnO + 5K_2CO_3 + 0.75Tb_4O_7$

Tb4: $50B_2O_3 + 30\ SiO_2 + 10Al_2O_3 + (4\text{-}y)\ ZnO + 5K_2CO_3 + 1.0Tb_4O_7$

Tb5: $50B_2O_3 + 30\ SiO_2 + 10Al_2O_3 + (3.75\text{-}y)\ ZnO + 5K_2CO_3 + 1.25Tb_4O_7$

$50B_2O_3 + 30\ SiO_2 + 10Al_2O_3 + (4.5\text{-}y)\ ZnO + 5K_2CO_3 + 0.5Dy_2O_3 + yTb_4O_7$

Where y = 0.25, 0.5, 0.75, 1.0 and 1.25

For convenience the co-doped glass samples are abbreviated as DyTb0.25, DyTb0.5, DyTb0.75, DyTb1.0 and DyTb1.25 based on the concentration of Tb^{3+} ions from 0.25 to 1.25 mol% respectively.

4.2.2 Sample characterization

The glassy nature of the as-prepared glasses has been confirmed by the XRD measurements recorded for an un-doped glass. The PL excitation, emission and decay profiles explore the optical and luminescent properties of the synthesized glasses. The temperature dependent emission profiles have been recorded to check the thermal stability of the as prepared glasses. All these characterizations have been done using the same instruments discussed in chapter 3.

4.3 Results and discussion

4.3.1 XRD Analysis

To know the glassy nature of as synthesized samples, XRD profiles were recorded for an un-doped as well as Dy-Tb co-doped KZABS glasses as indicated in Fig. 4.1. XRD patterns for all samples do not contain any sharp peak depicted the amorphous nature. Addition of RE ions do not influence the nature of glasses.

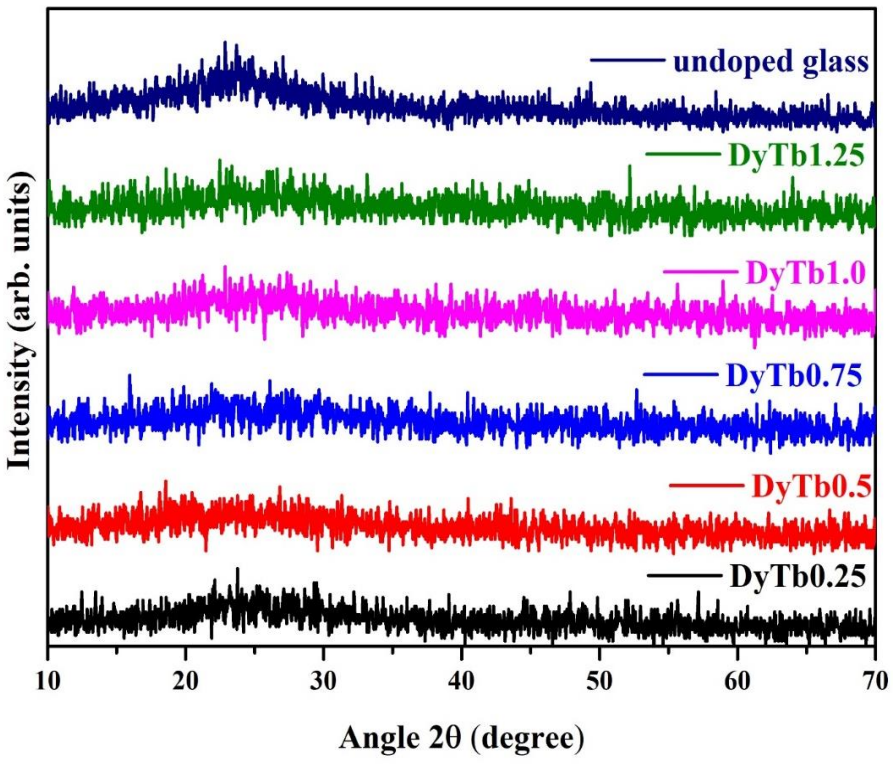

Fig. 4.1. XRD spectra recorded for an un-doped as well as Dy^{3+}/Tb^{3+} co-doped KZABS glasses

4.3.2 PL spectral studies

4.3.2.1 PL analysis of Dy^{3+} doped KZABS glasses

PL analysis of the as synthesized glasses reflects their suitability for the potential application such as display devices, SSL and w-LEDs, etc. Fig. 4.2 illustrates the PL excitation spectra of KZABS glasses doped with Dy^{3+} ions recorded under 575 nm emission wavelength in the range 300-500 nm. From Fig. 4.2, it can be observed that, Dy^{3+} ions exhibit eight excitation bands in all the glasses at 325, 338, 351, 365, 387, 426, 453 and 473 nm pertaining to $^6H_{15/2} \rightarrow {}^6P_{3/2}$, $^4I_{9/2}$, $^6P_{7/2}$, $^6P_{5/2} + {}^4M_{19/2}$, $^4F_{7/2} + {}^4I_{13/2}$, $^4G_{11/2}$, $^4I_{15/2}$ and $^4F_{9/2}$ transitions respectively [12,99].

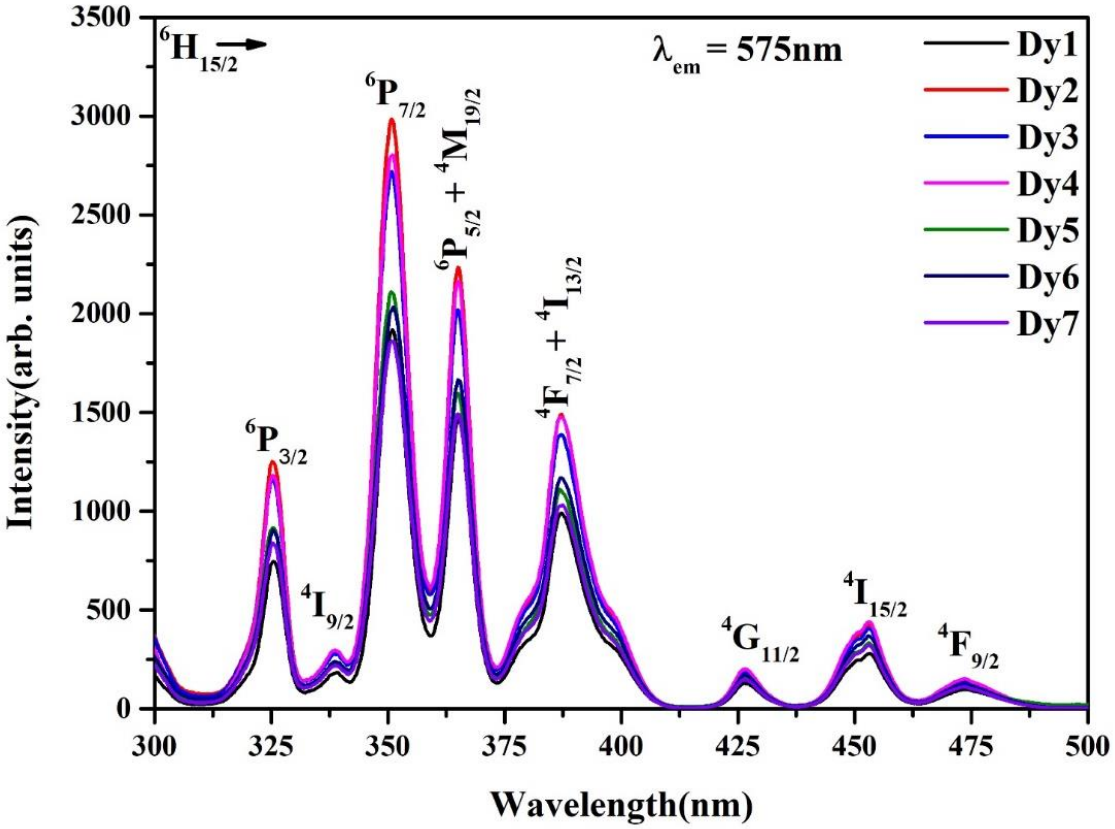

Fig. 4.2. Excitation spectra of Dy^{3+} ions doped KZABS glasses under 575 nm emission wavelength

Among all the excitation transitions, the one observed at 351 nm is relatively more intense and is suitable for exciting a greater number of doped ions from the ground state. By taking 351 nm as excitation wavelength, PL emission was recorded for all Dy^{3+} doped glasses and placed

in Fig. 4.3. Dy^{3+} ions exhibit three emission band at 482, 575 and 662 nm pertaining to the transitions $^4F_{9/2} \rightarrow {}^6H_{15/2}$, $^6H_{13/2}$ and $^6H_{11/2}$ respectively.

From Fig. 4.3, it was noticed that the optimum concentration of Dy was found to be 0.5 mol% (Dy2 glass) in KZABS glasses, and the same has been depicted in the inset of Fig. 4.3. In Dy^{3+} doped glasses, $^4F_{9/2} \rightarrow {}^6H_{15/2}$ (blue) transition observed at 482 nm is a magnetic dipole and $^4F_{9/2} \rightarrow {}^6H_{13/2}$ (yellow) transition observed at 575 nm is an electric dipole in nature. The intensity ratio of yellow (electric dipole) to blue (magnetic dipole) or Y/B ratio is used to explore the crystal field environment around the Dy^{3+} ions site [48]. The values of Y/B ratio are 1.41, 1.44, 1.50, 1.51, 1.50, 1.50 and 1.51 for Dy1, Dy2, Dy3, Dy4, Dy5, Dy6 and Dy7 respectively. The values of Y/B ratio are greater than one suggesting the fact that there is no centre of symmetry around the Dy^{3+} ions sites in the as-prepared glasses. It creates charge separation, which enhances the probability of the electric dipole transition intensity (yellow) dominating the magnetic dipole transition (blue) intensity in the presently investigated glasses investigated Dy^{3+} ions doped KZABS glasses

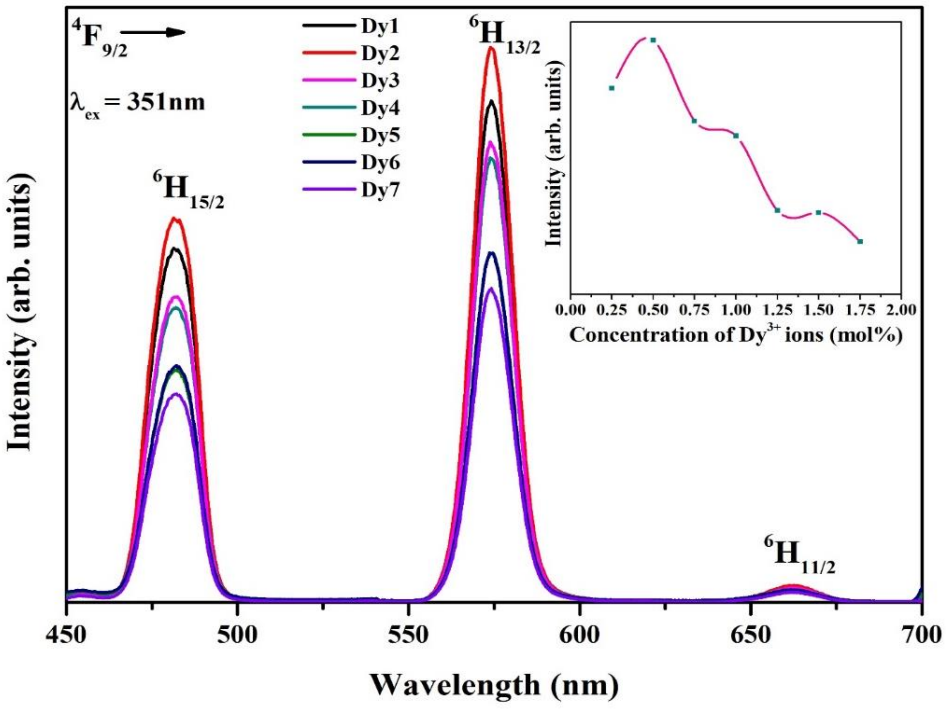

Fig. 4.3. Optimization of Dy^{3+} ion in KZABS glass under 351 nm excitation wavelength (Inset: Emission intensity variation with Dy^{3+} ion concentration for 575 nm emission peak)

M. Vijayakumar et al. [97], reported a similar type of behaviour of Dy^{3+} ions in Dy^{3+}/Tb^{3+} co-doped zinc lead fluoroborophosphate glasses. S. Kaur et al. [85] also reported similar behaviour for Dy^{3+} doped borate glasses. Fig. 4.4 show PL emission recorded for the optimized Dy2 glass under different excitation wavelengths and concluded that 351nm is quite suitable for effective excitation of Dy^{3+} ions in KZABS glasses.

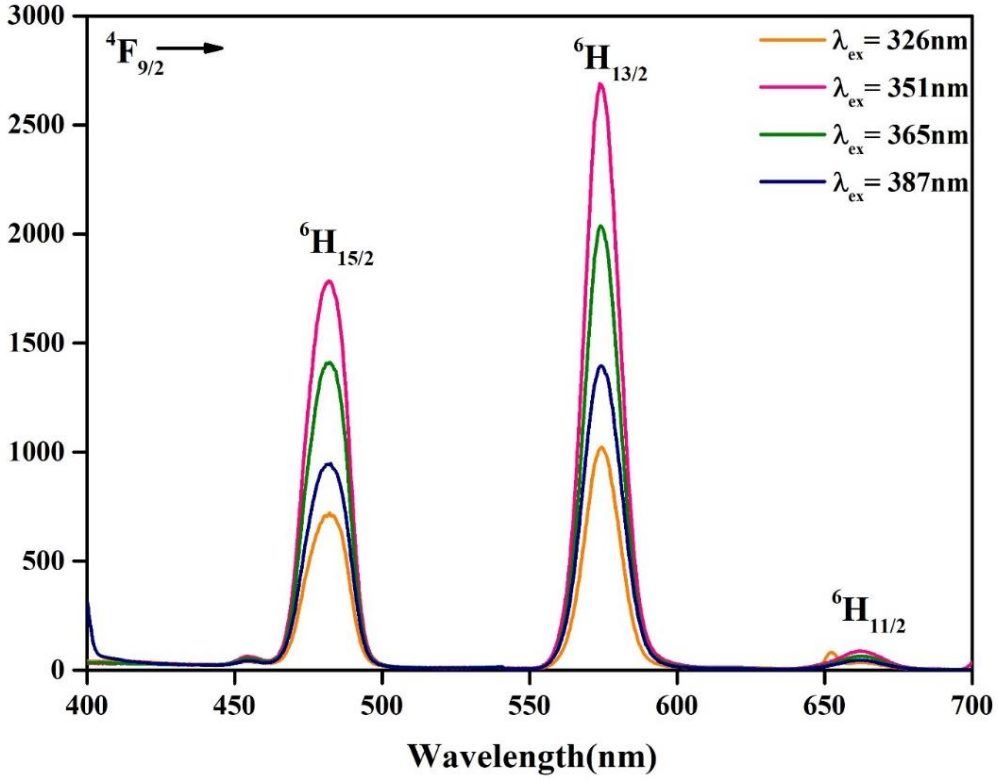

Fig. 4.4. PL emission for Dy2 (0.5mol% of Dy^{3+}) glass under different excitation wavelengths.

4.3.2.2 PL analysis of Tb^{3+} doped KZABS glasses

Fig. 4.5 illustrates the excitation spectrum of 1.25 mol% Tb^{3+} ions doped KZABS glass recorded under 543 nm emission wavelength. The detected excitation peaks divided in two groups, one is 4*f*-5*d* transitions and other is 4*f*-4*f* transitions [100]. Further f-d transitions are classified in two categories: parity allowed and parity forbidden. The strongest excitation band observed at 220 nm is origination from $^7F_6(4f^8)$-$^7E(4f^75d^1)$ is spin allowed and band originating from $^7F_6(4f^8)$-$^9E(4f^75d^1)$ at 284 & 303 are spin forbidden [95,101]. The excitation band corresponds to 4*f*-4*f* transitions are present at 318, 340, 351, 368 and 378 nm pertaining

transitions $^7F_6 \rightarrow {}^5H_7$, $^5G_2$, $^5L_9$, $^5L_{10}$ and $^5G_6$ respectively [101–103] and their magnified image has been placed in inset of Fig. 4.5. S. Kaur et al. [101] reported Tb^{3+} doped calcium aluminozincate phosphors which contains excitation pertaining to two type of transitions like 4*f*-5*d* and 4*f*-4*f*.

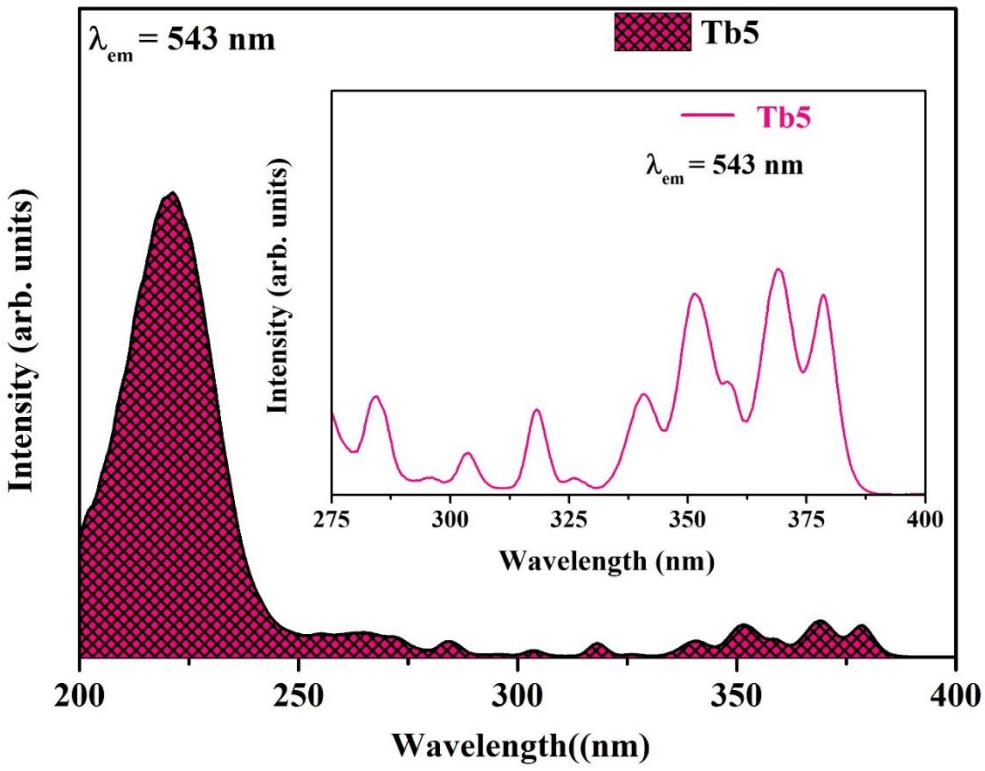

Fig. 4.5. Excitation spectrum of Tb^{3+} (1.25 mol%) doped KZABS glass under 543 nm emission wavelength (Inset: Magnified image of weaker excitation bands in the range 275-400 nm)

Fig. 4.6 displays the emission profiles of KZABS glasses for varying concentration of Tb^{3+} ion recorded under 220 nm excitation wavelength. The emission spectra consist four peaks situated at 488, 543, 586 and 621 nm pertaining to $^5D_4 \rightarrow {}^7F_6$, $^7F_5$, $^7F_4$ and $^7F_3$ transitions respectively. Furthermore, $^5D_4 \rightarrow {}^7F_6$ (blue emission) transition is electric dipole (ED) in nature which is subjected to crystal field symmetry and local environment, while $^5D_4 \rightarrow {}^7F_5$ (Green emission) transition is magnetic dipole (MD) in nature and need not depend on crystal field strength [104]. As the intensity ratio I_{ED}/I_{MD} describes the irregular behavior of doping ions in the host, for all terbium doped glasses, I_{ED}/I_{MD} (blue to green) ratio has been estimated and found to be 0.332, 0.307, 0.302, 0.308 and 0.300 for Tb1, Tb2, Tb3, Tb4 and Tb5 glasses respectively.

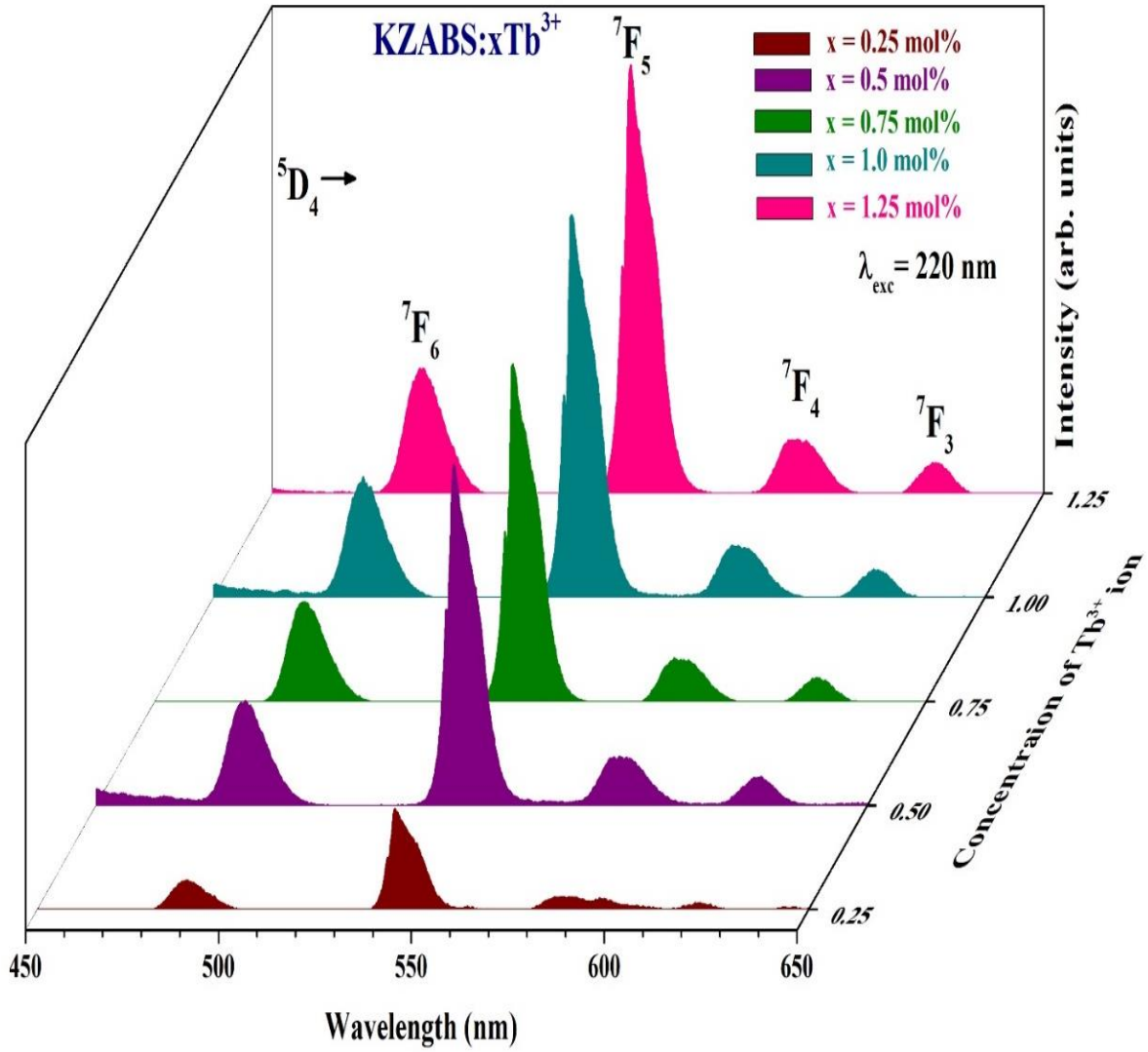

Fig. 4.6. Emission spectra of Tb^{3+} doped KZABS glasses for varying concentration of Tb^{3+} ions (0.25, 0.5, 0.75, 1.0 and 1.25 mol%) under 220 nm excitation wavelength.

4.3.2.3 PL analysis of Dy^{3+}/Tb^{3+} doped KZABS glasses

To know the luminescence features of Dy-Tb co-doped KZABS glasses, excitation and emission spectral profiles have been recorded under suitable wavelengths. Fig. 4.7 depicts the excitation profile of Dy^{3+}/Tb^{3+} co-doped DyTb1.0 (0.5 mol% of Dy^{3+} and 1.0 mol% of Tb^{3+} ion) glass under (a) 575 nm and (b) 543 nm emission wavelength. The excitation spectrum recorded at 575 nm exhibits various peaks at 325, 351, 365, 387, 425, 453 and 473 nm pertaining to the transitions of $^6H_{15/2} \rightarrow {}^6P_{3/2}$, $^6P_{7/2}$, $^6P_{5/2}$, $^4I_{13/2}$, $^4G_{11/2}$, $^4I_{5/2}$ and $^4F_{9/2}$ Dy^{3+} ions respectively as illustrated in Fig. 4.7(a).

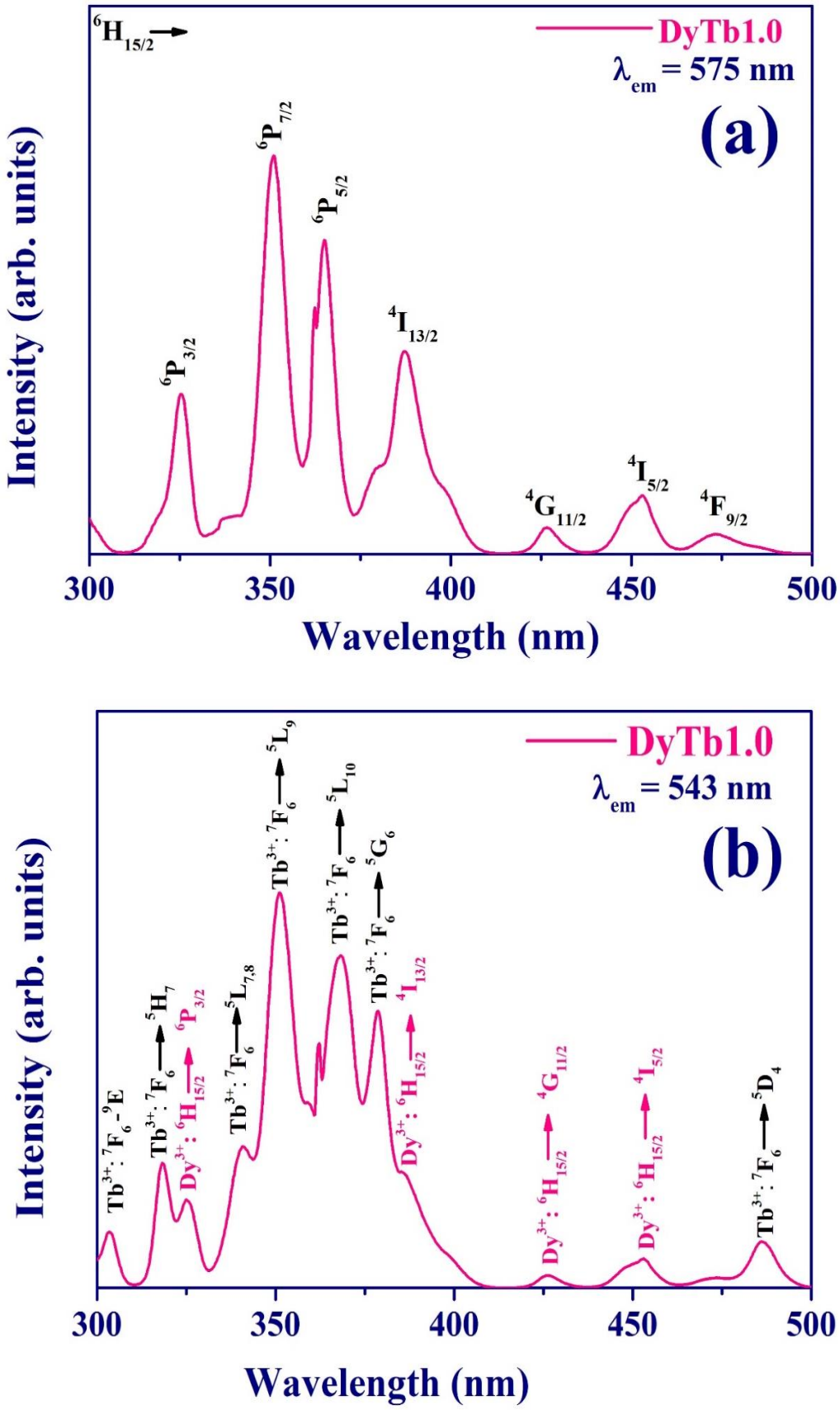

Fig. 4.7. Excitation spectrum of Dy^{3+}/Tb^{3+} co-doped DyTb1.0 (1.0 mol% of Tb^{3+}) glass under (a) 575 nm and (b) 543 nm emission wavelength

As shown in Fig. 4.7(b) the excitation spectrum recorded under 543 nm emission wavelength of Tb^{3+} ions show eleven excitation bands; seven are assigned to Tb^{3+} ions and four bands are assigned to Dy^{3+} ions. Excitation band due to 4f-5d transition of Tb^{3+} ions observed at 303 nm corresponding to $^7F_6 \rightarrow {}^9E$ (spin forbidden) transition [101]. The remaining six bands observed at 318, 340, 351, 367, 378 and 486 nm corresponding to $^7F_6 \rightarrow {}^5H_7$, $^5L_{7,8}$, $^5L_9$, $^5L_{10}$, $^5G_6$ and $^5D_4$ transitions are due to 4f-4f transitions respectively [105–107]. The four excitation bands (shown in pink color) due to Dy^{3+} ions observed at 325, 386, 426 and 452 nm are assigned to $^6H_{15/2} \rightarrow {}^6P_{3/2}$, $^4I_{13/2}$, $^4G_{11/2}$ and $^4I_{5/2}$ transitions respectively [85]. The presence of excitation bands due to Dy^{3+} ions while recording under Tb^{3+} emission wavelength 543 nm indicates the occurrence of energy transmission from Dy^{3+} to Tb^{3+} ions [97,98].

In Fig. 4.2 and 5, it was observed that 351 nm for Dy^{3+} ions and 220 nm for Tb^{3+} ions are the intense excited bands useful to record the emission spectral measurements for the Dy-Tb co-doped glasses. Fig. 4.8(a) shows the emission profiles for the Dy-Tb co-doped glasses recorded under 351 nm emission wavelength.

It consists seven emission peaks: four corresponding to Tb^{3+} ions and three corresponding to Dy^{3+} ions. The peaks due to the Tb^{3+} ions are situated at 486, 543, 583 and 621 nm and the peaks due to Dy^{3+} ions are situated at 473, 575 and 662 nm. The corresponding transitions have been already discussed in section 3.2.1 and 3.2.2 of chapter 4 respectively. In Fig. 4.8(a) it is conspicuous that, with increase in Tb^{3+} ion concentration, the intensity of peaks corresponding to Tb^{3+} ions continuously increasing whereas the intensity of the peaks corresponding to Dy^{3+} ions are continuously decreasing. This signifies the energy transfer from Dy^{3+} to Tb^{3+} ions.

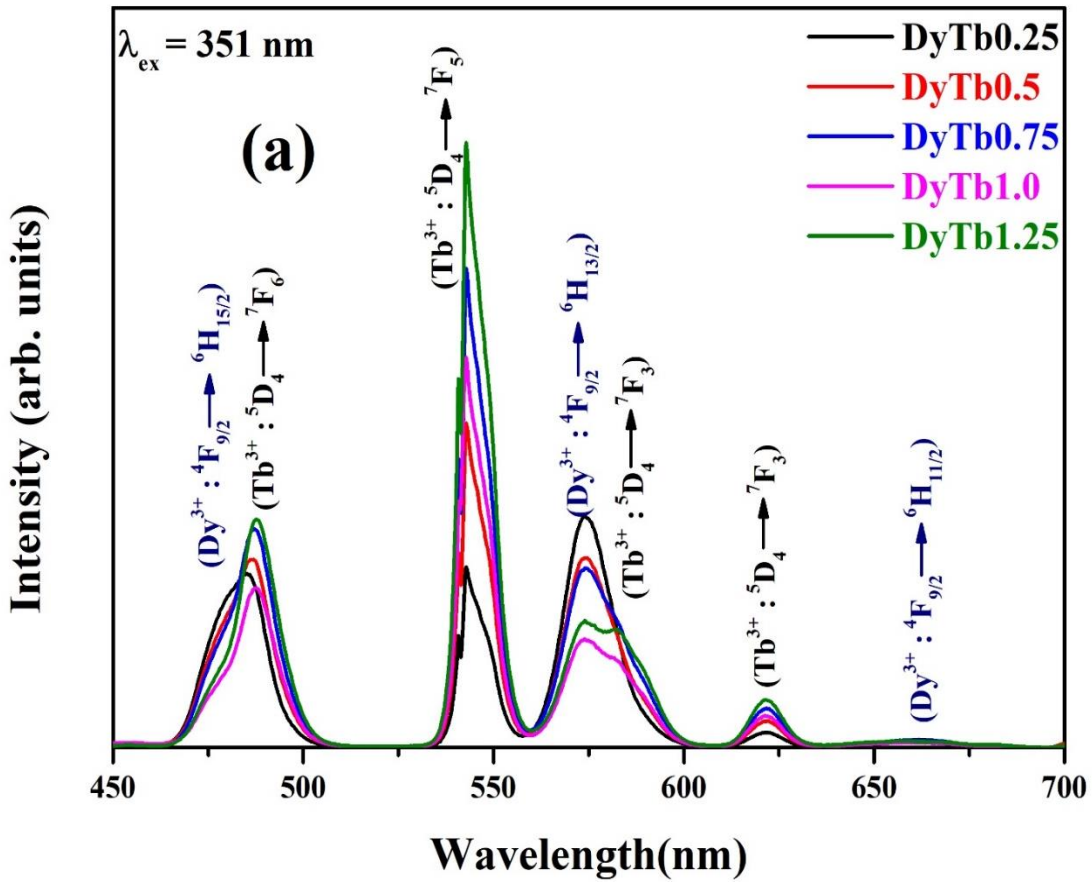

Fig. 4.8. (a) PL emission of Dy^{3+}/Tb^{3+} co-doped glasses under 351 nm excitation wavelength

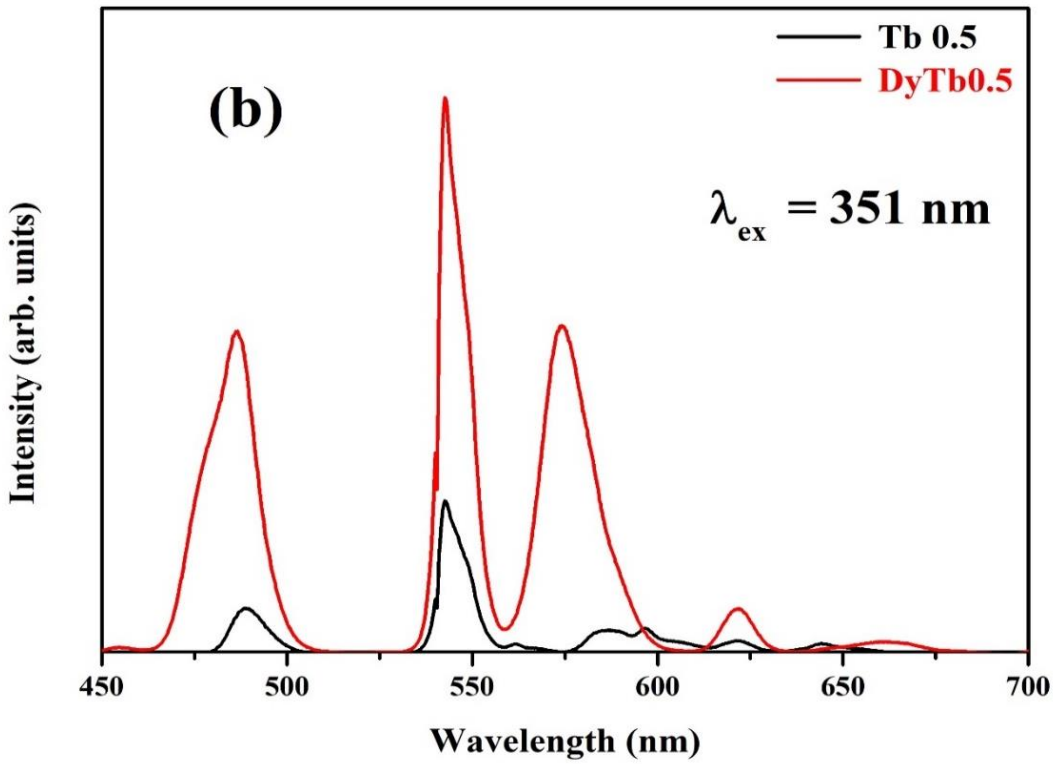

Fig. 4.8. (b) PL emission of KZABS glass doped with 0.5 mol% of Tb^{3+} ion concentration with and without Dy^{3+} ions concentration recorded under 351 nm excitation wavelength.

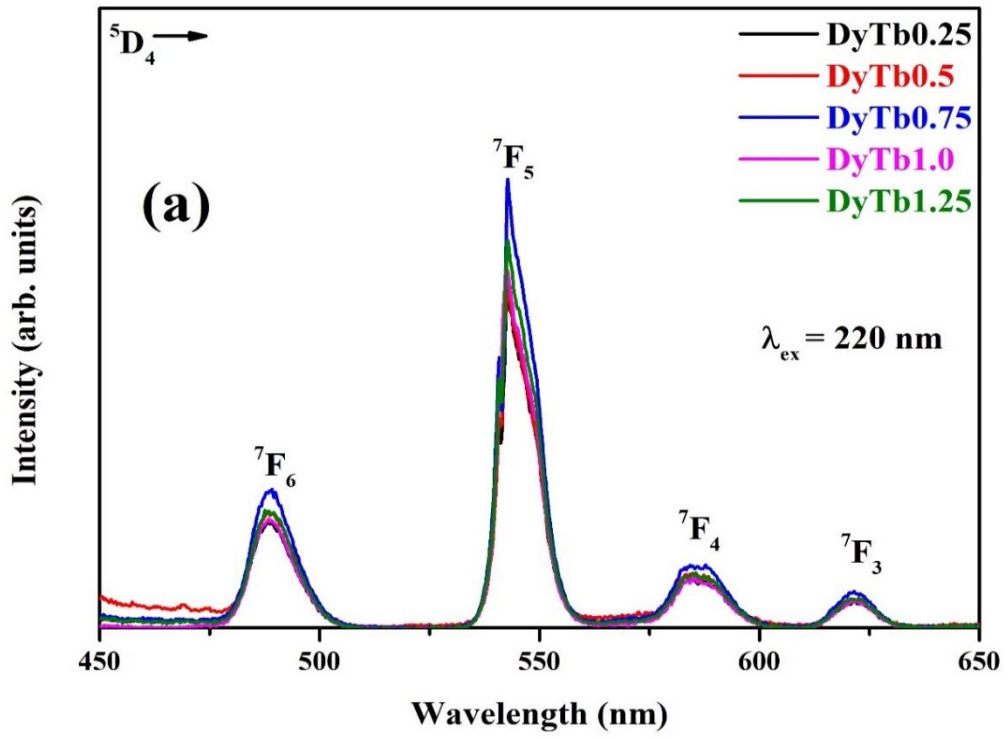

Fig. 4.9. (a) PL emission of Dy^{3+}/Tb^{3+} co-doped glasses under 220 nm excitation wavelength

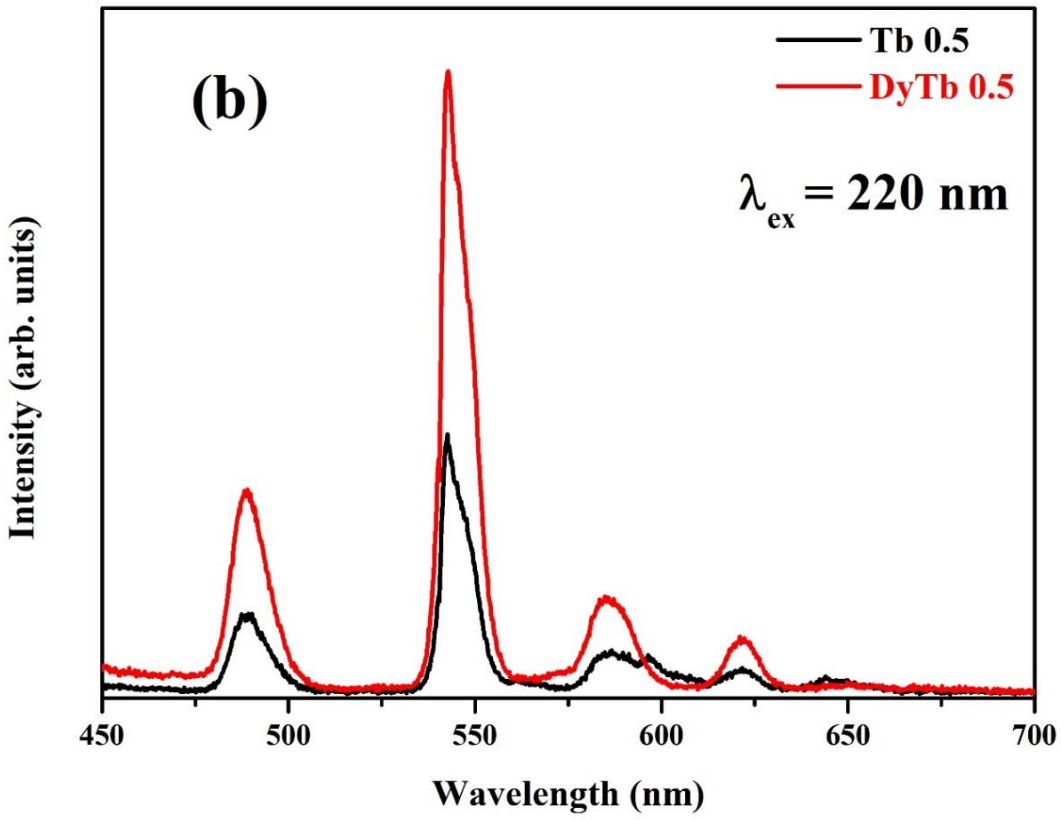

Fig. 4.9. (b) PL emission of KZABS glass doped with 0.5 mol% of Tb^{3+} ion concentration with and without Dy^{3+} ions recorded under 220 nm excitation wavelength.

To know the back transfer of energy from Tb^{3+} to Dy^{3+} ions, we have recorded the emission spectral profiles under 220 nm (Tb^{3+} ions) excitation wavelength and are shown in Fig. 4.9 (a). It contains the emission peaks of Tb^{3+} ions only without any peak pertaining to Dy^{3+} ions. This observation nullifies the possible reverse energy transfer from Tb^{3+} to Dy^{3+} ions in the as prepared glasses [93]. This allows us to contemplate that, under 351 nm excitation wavelength, the Dy^{3+}/Tb^{3+} co-doped KZABS glasses are giving optimum green color emission. Fig. 4.8 (b) and Fig. 4.9 (b) illustrates the PL emission spectra of KZABS glass doped with 0.5 mol% of Tb^{3+} ions with and without Dy^{3+} ions recorded under 351 and 220 nm excitation wavelength respectively.

From these two figures it is conspicuous that, addition of Dy^{3+} ions (sensitizer) help in enhancing the intensity of green emission shown by Tb^{3+} ions (activator). This clearly demonstrates the role played by a sensitizer (Dy ions) in enhancing the emission properties of the activator (Tb ions) in the as prepared glasses. There are several reported papers on Dy^{3+}/Tb^{3+} co-doped ions in literature out of which some host materials contain energy transfer from Dy^{3+} to Tb^{3+} ions only [93] whereas some observed energy transfer from Dy^{3+} to Tb^{3+} ions as well as from Tb^{3+} to Dy^{3+} ions [12,97]. In present work, back transfer of energy from Tb^{3+} to Dy^{3+} ions is not observed.

4.3.3 Energy transfer mechanism and decay profiles

The PL investigations conducted on Dy-Tb co-doped KZABS glasses clearly indicate the occurrence of energy transfer from Dy^{3+} ions to Tb^{3+} ions under 351 nm excitation.

From the energy level diagram shown in Fig. 4.10, it can be visualized that, $^4F_{9/2}$ level (Dy^{3+}) is nearly 500 cm^{-1} larger that the $^5D_4$ level (Tb^{3+}) ion, so the probability of transferring the photons from Dy^{3+} to Tb^{3+} ion is much more than the reverse process [96].

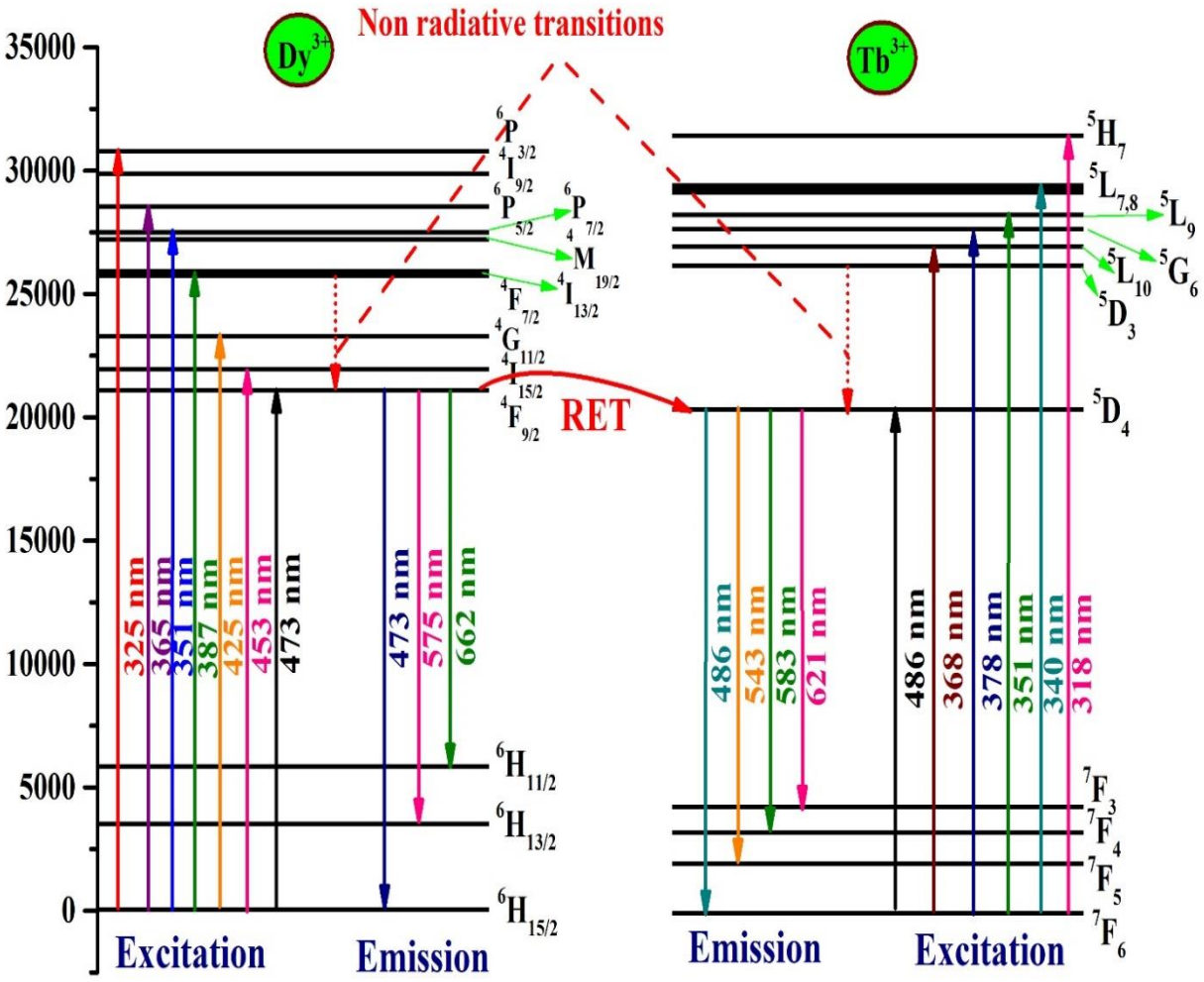

Fig. 4.10. Partial energy level diagram showing all excitation, emission and resonance energy transfer (RET) between Dy^{3+} and Tb^{3+} ions in KZABS glasses.

When Dy^{3+}/Tb^{3+} co-doped samples are excited under 351nm wavelength, energy transfer occurs from Dy^{3+} to Tb^{3+} ions as shown in the energy level diagram (Fig. 4.10) and the below equation:

$$^7F_6\,(Tb^{3+}) + {}^4F_{9/2}\,(Dy^{3+}) \rightarrow {}^5D_4\,(Tb^{3+}) + {}^6H_{15/2}\,(Dy^{3+})$$

The energy transfer efficiency from Dy^{3+} to Tb^{3+} ions has been calculated form the PL emission profiles placed in Fig. 4.8(a) by employing the following equation [108]:

$$\eta = 1 - \frac{I_D}{I_D + I_T} \qquad (4.1)$$

Where I_D and I_T are PL intensities of emission peaks at 575 and 543 nm respectively.

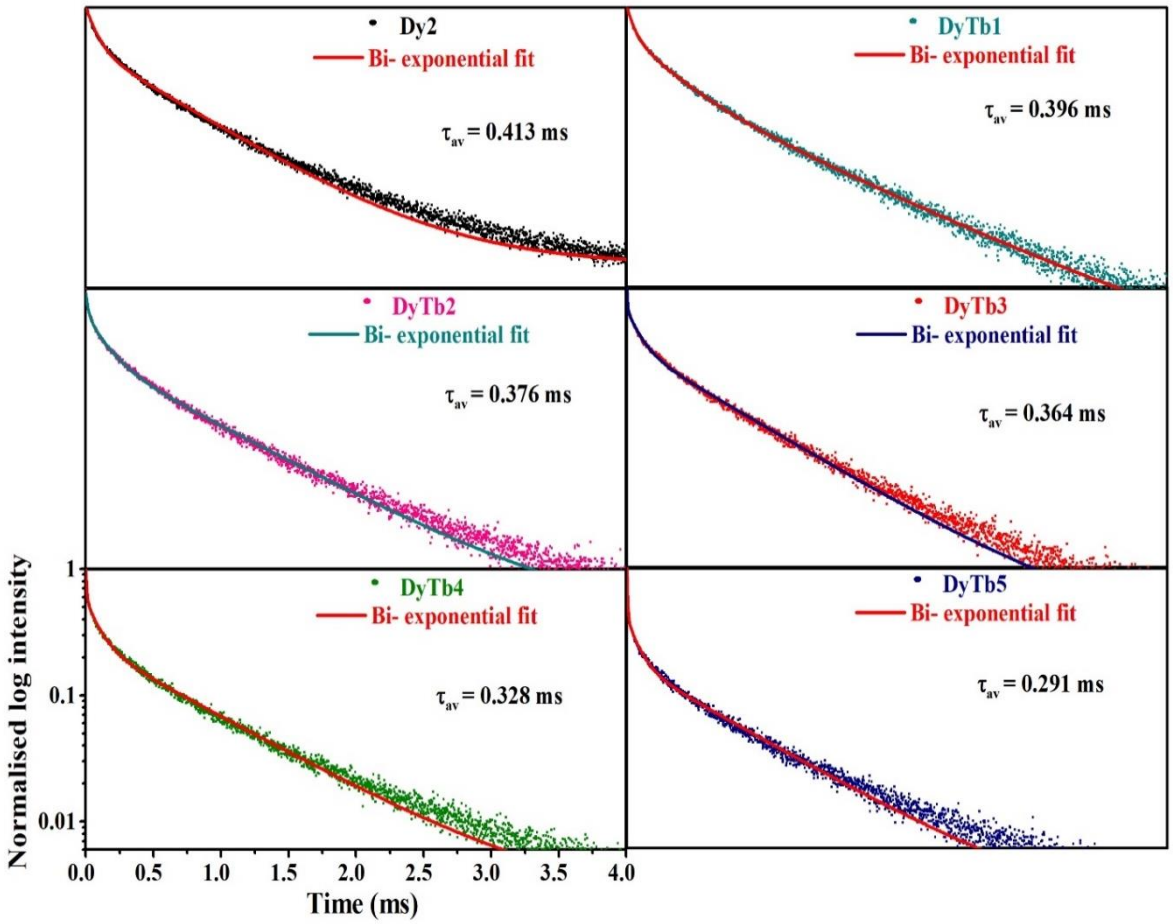

Fig. 4.11. Decay curves for Dy2 glass and Dy^{3+}/Tb^{3+} co-doped KZABS glasses recorded at 575 nm under 351 nm excitation wavelength

The estimated energy transfer efficiencies are found to be 43 and 85% for DyTb0.25 (0.5 mol% of Dy^{3+} and 0.25 mol% of Tb^{3+}) and DyTb1.25 (0.5 mol% of Dy^{3+} and 1.25 mol% of Tb^{3+}) glasses respectively. The energy transfer efficiencies obtained in the present investigation are relatively higher than the value reported by D. Ramachari for Dy^{3+}/Tb^{3+} co-doped oxyfluorosilicate glass-ceramics [108]. Under 351 nm excitation, the energy transfer takes place from Dy level ($^4F_{9/2}$) to Tb level ($^5D_4$). The energy transfer from Dy ions to Tb ions has been further confirmed by the decay profiles shown in Fig. 4.11. As shown in Fig. 4.11, the decay profiles are showing bi-exponential nature. The bi-exponential nature of the decay curves has been successfully explained by using the equation (3.2), earlier described in chapter 3.

Table 4.1

Average lifetime (τ_{avg}), energy transfer efficiency (η_T), energy transfer parameter (Q), acceptor-ion concentration (N_0), critical transfer distance (R_0) and donor–acceptor interaction parameter (C_{DA}) for Dy^{3+}/Tb^{3+} co-doped KZABS glasses.

Sample ID	**Concentration of Tb^{3+} ion (mol%)**	**τ_{avg} (ms)**	***Q***	***N_0*(10^{20} ions/ cm^3)**	***R_0* (Å)**	***C_{DA}*(10^{-44} cm^6 s^{-1})**
Dy	0	0.413	-	-	-	-
DyTb0.25	0.25	0.396	1.99	3.94	2.28	34.5
DyTb0.5	0.5	0.376	2.71	5.25	2.30	36.1
DyTb0.75	0.75	0.364	5.52	6.56	2.71	95.8
DyTb1.0	1.0	0.328	6.81	7.88	2.73	101.1
DyTb1.25	1.25	0.291	7.98	9.19	2.74	102.1

It was observed from Fig. 4.11 that the average lifetime values are decreasing with Tb^{3+} ion concentration and are found to be in range 0.291 - 0.413 ms as given in Table 4.1. These values were estimated by following equation (3.3).

The decay profiles are found to be best fitted for s=6 in I-H model (as earlier discussed in chapter 1) with fitting factor $R^2 = 0.993$ as shown in Fig. 4.12. This study finally allows us to contemplate that, the energy transfer occur from Dy^{3+} to Tb^{3+} ions via dipole - dipole interaction in as synthesized glasses. Our result is also in consonance with the result reported for Dy-Tb co-doped glasses in literature [97].

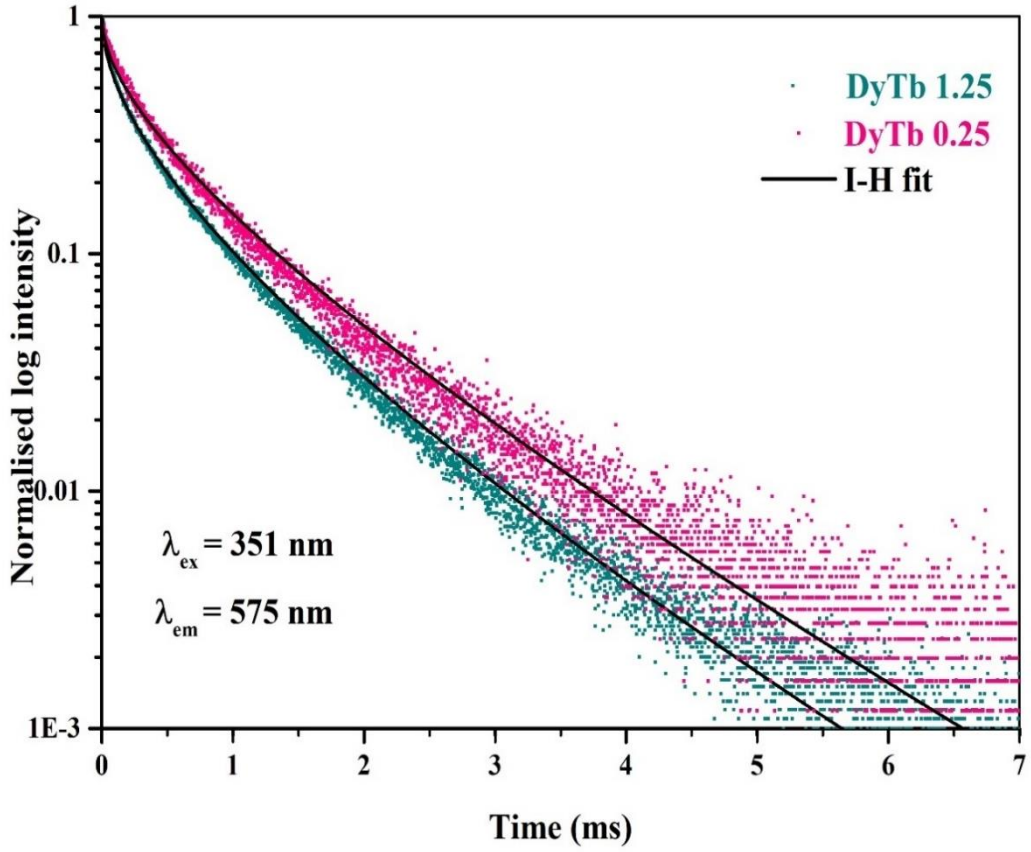

Fig. 4.12**.** Decay curves fitted with the I-H model (S = 6) for DyTb0.25 and DyTb1.25 glasses under 351 nm excitation

Table 4.2

CIE co-ordinates for Dy^{3+}/Tb^{3+} co-doped KZABS glasses under different excitation wavelengths**.**

Abbreviations in CIE diagram	Sample ID	Excitation Wavelength (nm)	CIE Co-ordinates	
			x	y
(a)	Dy2	351	0.392	0.402
(b)	Tb2	220	0.338	0.511
(c)	DyTb1.25	351	0.306	0..544
(d)	DyTb1.25	220	0.295	0.504

The values of Q, N_0, R_0 and C_{DA} have been estimated by following equations (3.6 and 3.7) and placed in Table 4.1. Increasing values of these parameters with Tb^{3+} ion concentration signifies the dominancy of energy transfer [80]. Above mentioned results obtained for the glasses investigated in the present work are in agreement with the already reported papers in literature [93,96,98,108].

4.3.4 TD-PL studies

In order to check the luminescent properties of the as prepared glasses with temperature and their utility in optical devices, the TDPL for DyTb1.25 (Dy^{3+} 0.5 mol% and Tb^{3+} 1.25 mol%) has been recorded in range 25 -175°C under 351 nm excitation and placed in Fig. 4.13. It was observed that with rise in temperature, the emission intensity continuously falls down without any change in their peak position. As shown in Fig. 4.13, the thermal quenching may be due to the temperature dependent non-radiative relaxations. As per equation (3.8), the non-radiative relaxation probability rate (R) will increase with temperature which ultimately increase the probability of non-radiative relaxations and thus emission intensity decreases as shown in Fig. 4.13. The emission intensity retains 79% at 175°C as compared to initial temperature (25°C). This signifies the temperature sustainability of the as synthesized glass [109]. Activation energy (ΔE) is also another significant parameter used to measure thermal stability for the as prepared glass. It can be be determined with the help of Arrhenius equation (earlier mentioned as equation 3.9).

To find the value of ΔE, a graph is linearly fitted between $Ln[(I_0/I_T)-1]$ and $1/k_BT$ and slope of this plot gives the ΔE as shown in the inset of Fig. 4.13. Thus, the value of ΔE (0.196 eV) observed in the present work indicates the thermal stability of the Dy^{3+}/Tb^{3+} co-doped KZABS glasses suitable for high powered optoelectronic devices applications such as w-LEDs.

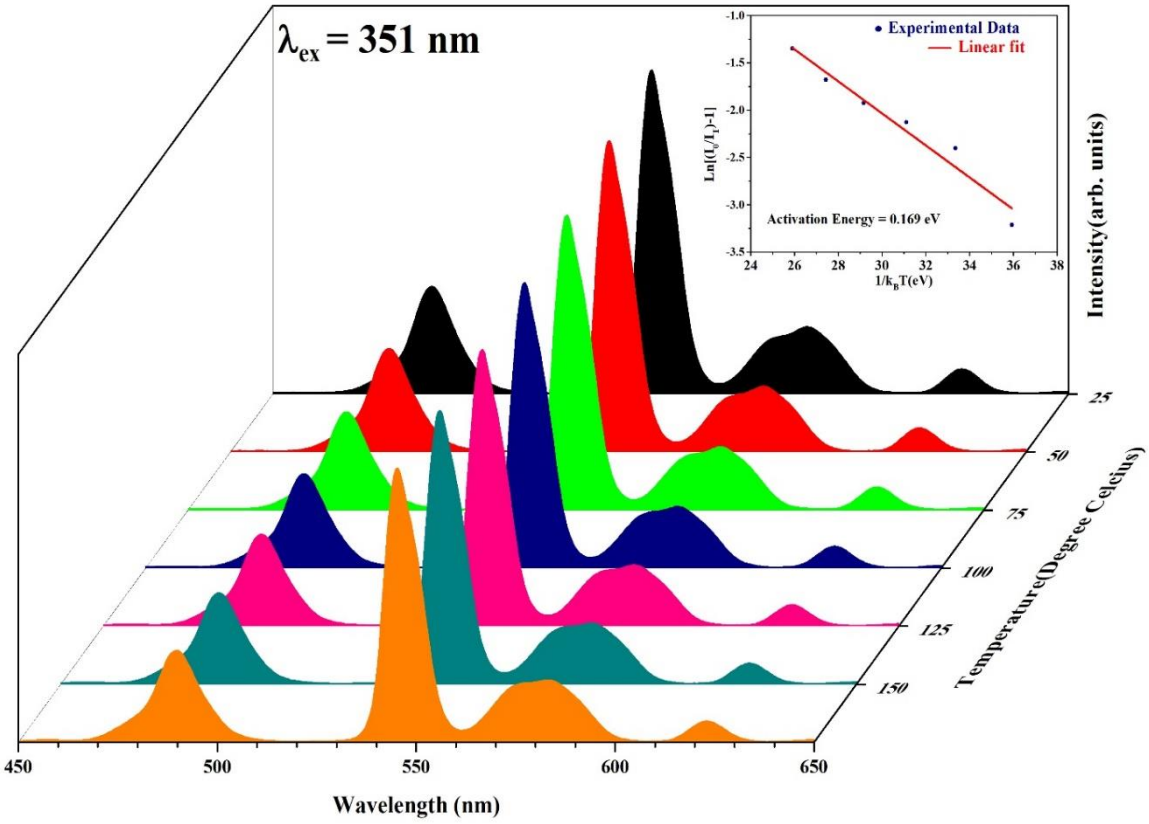

Fig. 4.13. TDPL emission of DyTb5 glass under 351 nm excitation (Inset: Variation of $\ln[(I_0/I_T)-1]$ versus $1/k_BT$ for emission at 543 nm under 351 nm excitation)

4.3.5 Colorimetric Properties

Further, to understand the colorimetric properties of the Dy^{3+}/Tb^{3+} co-doped glasses, the CIE 1931 color chromaticity diagram has been prepared and depicted as shown in Fig. 4.14. The CIE points calculated by using the earlier mentioned procedure in section 1.12 has been placed in Fig. 4.14. The CIE coordinates corresponding to the letters (a), (b), (c) and (d) (shown in Fig. 4.14) at different excitation wavelengths have been placed in Table 4.2. It was observed that, addition of Dy^{3+} ions to Tb^{3+} ions help to obtain optimum green emission. As shown in Fig. 4.14, the CIE color coordinates are gradually shifting towards deep green color from single doped [(a) & (b)] to co-doped [(c) and (d)] glasses. This result is also in consonance with the result reported in literature [97,98,108].

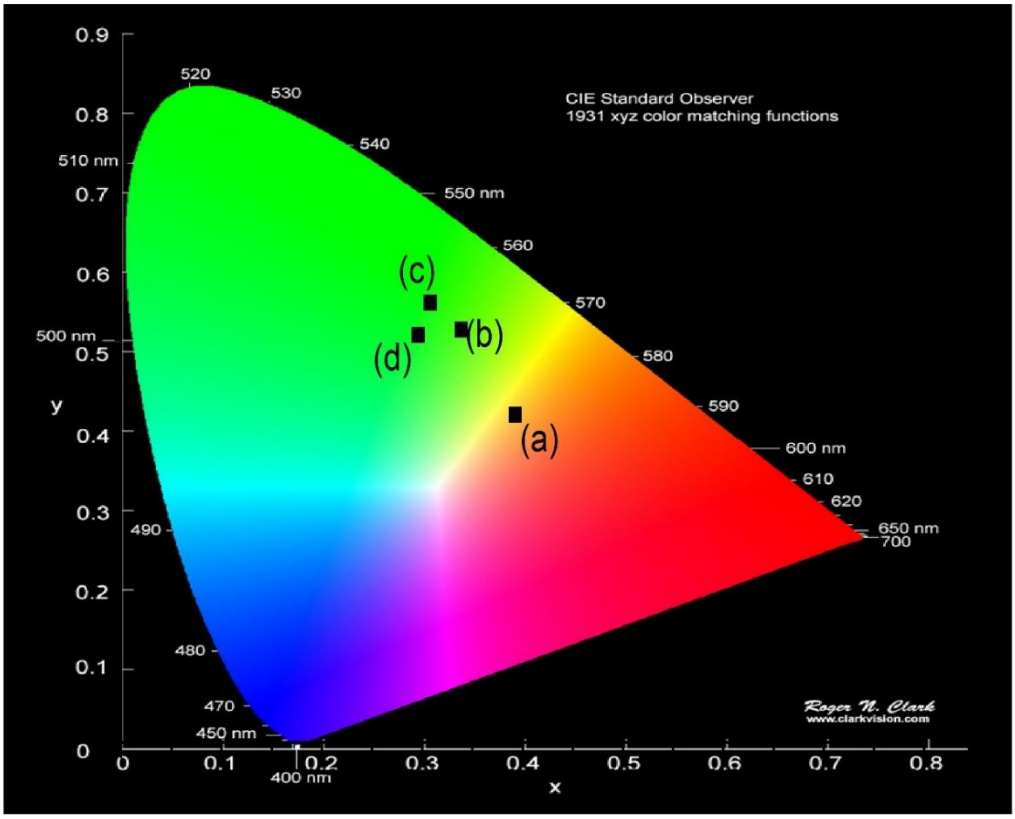

Fig. 4.14. CIE chromaticity diagram for Dy^{3+}/Tb^{3+} co-doped KZABS glasses under 351 nm excitation.

4.4.Conclusions

From PL studies of thermally stable Dy-Tb codoped glasses an unidirectional energy transfer is observed from Dy^{3+} to Tb^{3+} ions via dipole-dipole interaction. The CIE color coordinates are gradually shifting towards deep green color from single doped to co-doped glasses. The luminescent spectral analysis of Dy-Tb co-doped glasses finally allows us to contemplate the superior nature of the as prepared glasses for various green emitting photonic device applications.

Chapter 5

Color tunable photoluminescence in KZABS:Tm^{3+} glasses under different sources of excitation for Photonic Applications

This chapter includes the PL and PL decay properties of Tm^{3+} doped KZABS glasses. PL spectral properties show blue and red colors under different excitation wavelengths. The I-H model well fitted to non-exponential decay curves of Tm^{3+} doped KZABS glasses confirms the energy transfer between Tm^{3+}-Tm^{3+} ions as dipole-dipole in nature. Under 359 and 466 nm excitation wavelength, the titled glasses show CIE coordinates falling in deep-blue and deep-red color, respectively. A good color tunability can be seen from the blue to the red region under different excitation wavelengths. All the studies finally reveal the superiority of Tm^{3+} doped KZABS glasses for their usage in blue/red-emitting photonic devices needed to fabricate photonic devices such as w-LEDs.

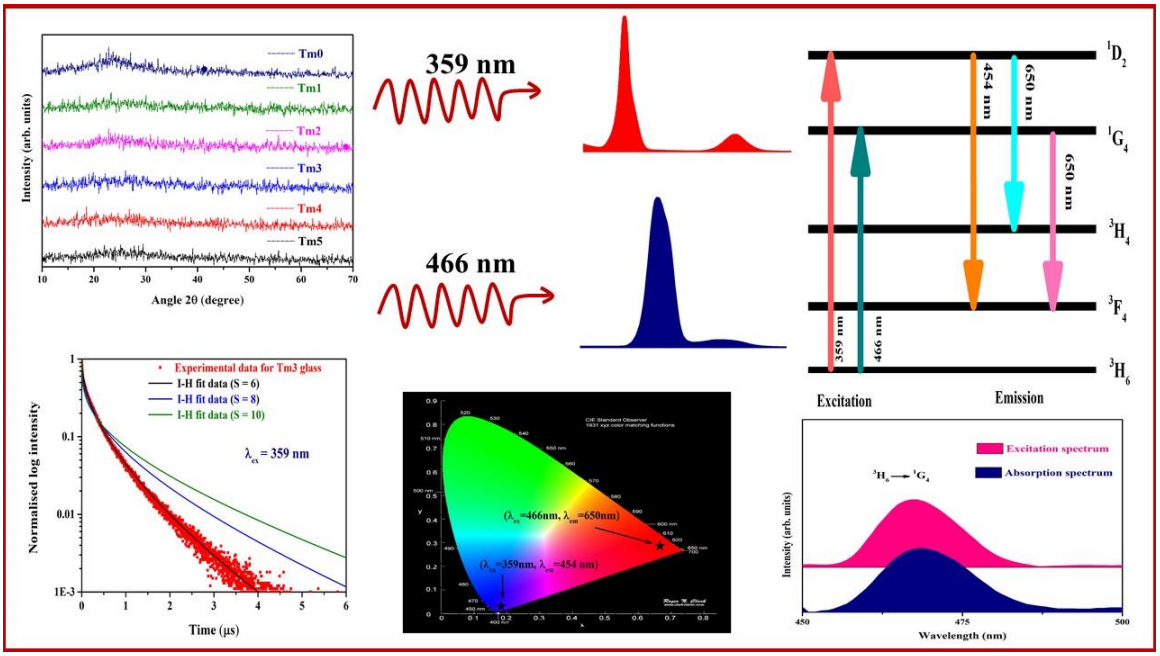

5.1. Introduction

RE ions doped crystalline and non-crystalline systems and white light have become a superior choice for researchers in the last few decades because of their wide range usage in the areas of SSL technology, photovoltaics, optical devices, laser systems, and display devices [11,110,111]. The generation of white light and advantages of RE doped glasses over phosphor materials have been earlier discussed in chapter 3 and 4. As we have selected the RGB method to produce white light, we need three prime colors to produce white light. We have already studied the suitability of KZABS glasses for visible red and green photonic device applications by doping them suitably with Sm^{3+}/Eu^{3+} [36] and Dy^{3+}/Tb^{3+} [111] ions in chapter 3 and chapter 4 respectively. Now, we want to explore the same host glass for blue color emission.

A large number of RE ions have been examined such as Eu^{3+} [7], Sm^{3+} [1], Pr^{3+} [13], Nd^{3+} [44], Tb^{3+} [110], Ho^{3+} [15] and Tm^{3+} [112] in different glasses. Tm^{3+} is one of the good choices for blue color emission because, under UV excitation, Tm^{3+} ions are excited to the $^1D_2$ state and return to the $^3H_6$ state through the $^3F_4$ state emitting blue light (465 nm). Several host matrices have been investigated to combine RE ions with traits such as high thermal stability, chemical durability and low phonon energy [112–115]. A large number of Tm^{3+} doped glasses have been investigated in silicates [115], borates [112], phosphates [114] and germinates [113] glasses.

In this chapter, we want to investigate Tm^{3+} doped KZABS glasses for blue color emission. Ultimately our target is to study the suitability of the KZABS host glass as an alternate for epoxy-free w-LED device applications in the SSL industry. The fascinating results obtained from our systematic investigations of KZABS host glass for its suitability to emit visible red and green colors prompted us to investigate the same host further to understand its capability to emit visible blue colors and color tunability [3,29]. For this, KZABS glasses were prepared with varying concentrations of Tm^{3+} ions and studied their PL performance under different

excitation wavelengths. PL spectral features help us to identify the color tunability from the blue to red region by changing the source of excitation. The PL decay measurements have also been carried out to measure the experimental lifetimes and understand the nature of interaction responsible for energy transfer among the Tm^{3+} ions using the I-H model.

5.2. Experimental section

5.2.1. Synthesis of glasses

KZABS: xTm^{3+} (x = 0, 0.25, 0.5, 0.75, 1.0 and 1.25) glasses were synthesized by employing melt-quenching method as discussed in chapter 2 and shown in Fig. 2.1. with the following chemical composition:

$50B_2O_3 + 30\ SiO_2 + 10Al_2O_3 + (4.5\text{-}x)\ ZnO + 5K_2CO_3 + xTm_2O_3$; Where x = 0, 0.25, 0.5, 0.75, 1.0 and 1.25 mol% are abbreviated as Tm0, Tm1, Tm2, Tm3, Tm4 and Tm5 respectively.

5.2.2. Characterization

We have used the same techniques as earlier discussed in chapter 3 and to record the XRD, PL excitation, emission and decay profiles, and TD-PL emission profiles. Further we analyzed this to check the suitability of the as prepared glasses in photonic device applications.

5.3. Results and discussion

5.3.1. XRD spectral measurements

To examine the non-crystalline nature of the titled glasses, XRD investigations have been performed for KZABS: xTm^{3+} (x = 0, 0.25, 0.5, 0.75, 1.0 and 1.25) glasses and are depicted in Fig. 5.1. From Fig. 5.1., it is conspicuous that all the glass samples (doped and undoped) prepared in the present work show a broad hump around an angle of 24 degrees rather than sharp peaks. The absence of sharp peaks speaks about the amorphous nature of the KZABS glasses irrespective of the RE ion concentration doped in them.

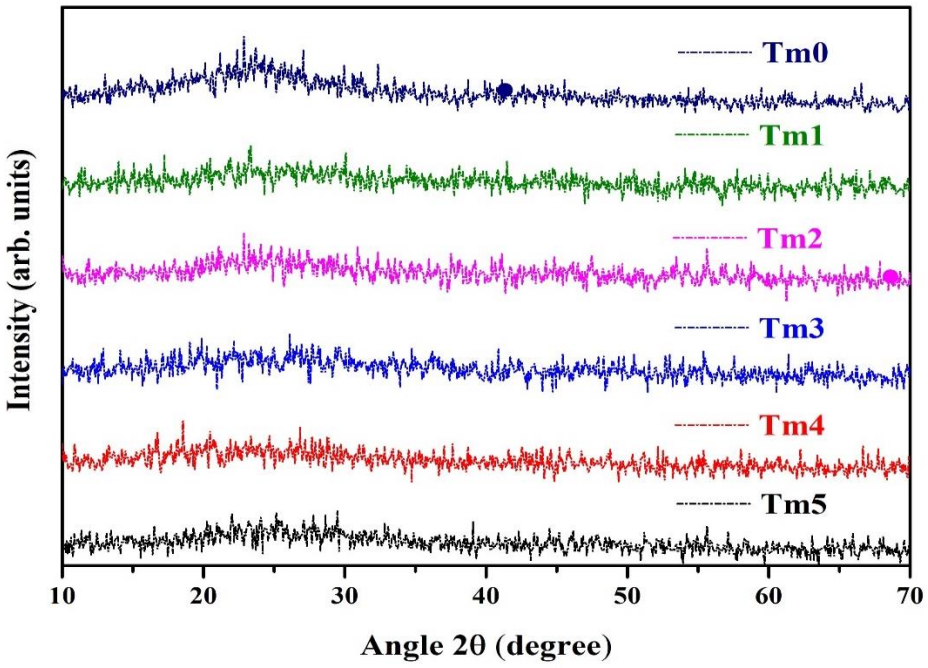

Fig. 5.1. XRD spectra recorded of KZABS: xTm^{3+} (x = 0, 0.25, 0.5, 0.75, 1.0 and 1.25 mol%) glasses.

5.3.2. UV-Vis-NIR spectroscopy

The absorption spectrum of Tm^{3+} ions (0.75 mol%) doped KZABS glass recorded from 400 to 1800 nm wavelength range has been displayed in Fig. 5.2.

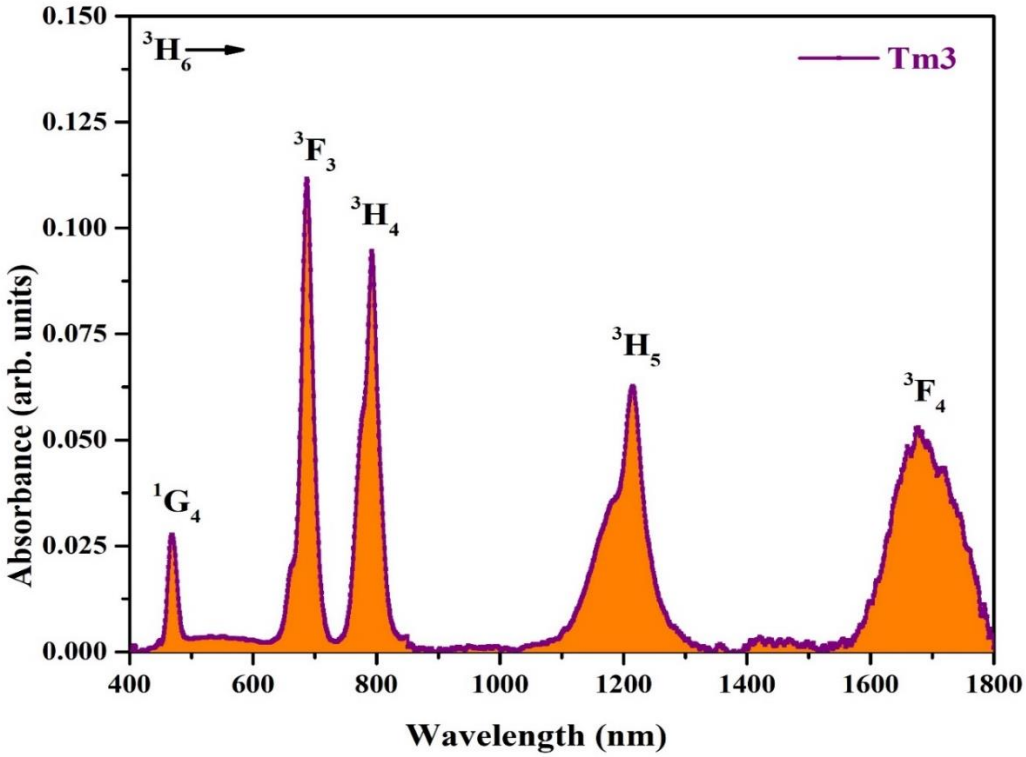

Fig. 5.2. The absorption spectrum of Tm3 glass in UV-Vis-NIR region.

The absorption spectra recorded for other Tm^{3+} ions doped KZABS glasses are the same in band positions except for some variation in their intensities. It consists of five absorption peaks situated at 470, 688, 794, 1216 and 1679 nm about the $^3H_6 \rightarrow {}^1G_4$, $^3F_3$, $^3H_4$, $^3H_5$ and $^3F_4$ transitions respectively [116].

The E_g values for the titled glasses were estimated by plotting a Tauc plot graph as shown in Fig. 5.3. by using the data given by Eq. (2.5), described in chapter 2. The E_g values were relatively high and nearly constant in the range of 2.95 to 2.99 eV for the titled glasses. Such relatively high bandgap values obtained for the as-prepared glasses indicate their suitability for multifunctional photonic device applications [16].

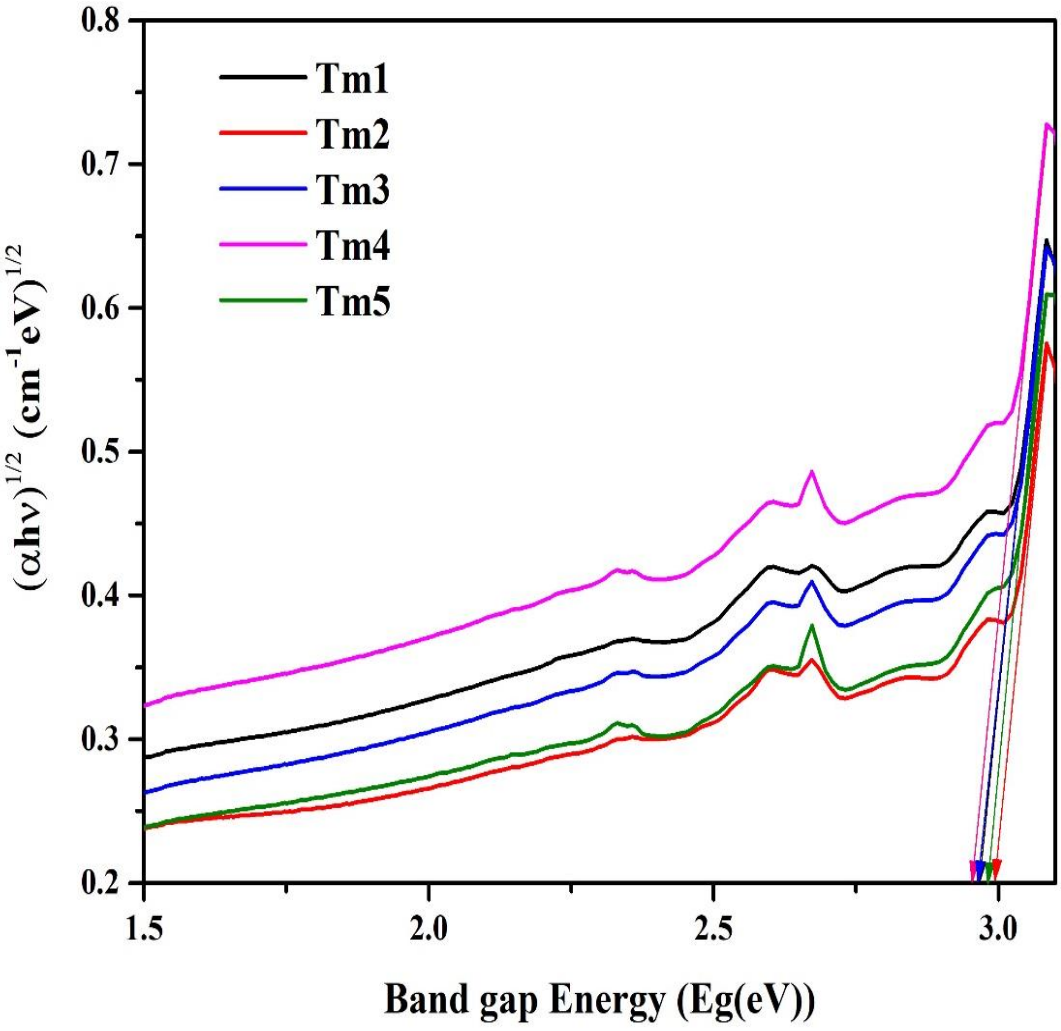

Fig. 5.3. Tauc plot for direct optical band gap of Tm^{3+} doped KZABS glasses.

5.3.3. PL analysis under different excitation wavelengths

The PL emission intensity depends on the doping content of RE ions and excitation wavelength. The as-synthesized glasses have been analyzed by varying the excitation wavelengths, and it was observed that the titled glasses portray different colored emissions under different excitation wavelengths. The excitation spectrum that has been recorded for Tm^{3+} ions (0.75 mol%) doped KZABS glass by fixing the emission monochromator at 454 nm is depicted in Fig.5.4. The excitation spectra for the other doped KZABS glasses are the same in band position except for some variation in the intensity of individual peaks, and hence they were not shown in Fig. 5.4.

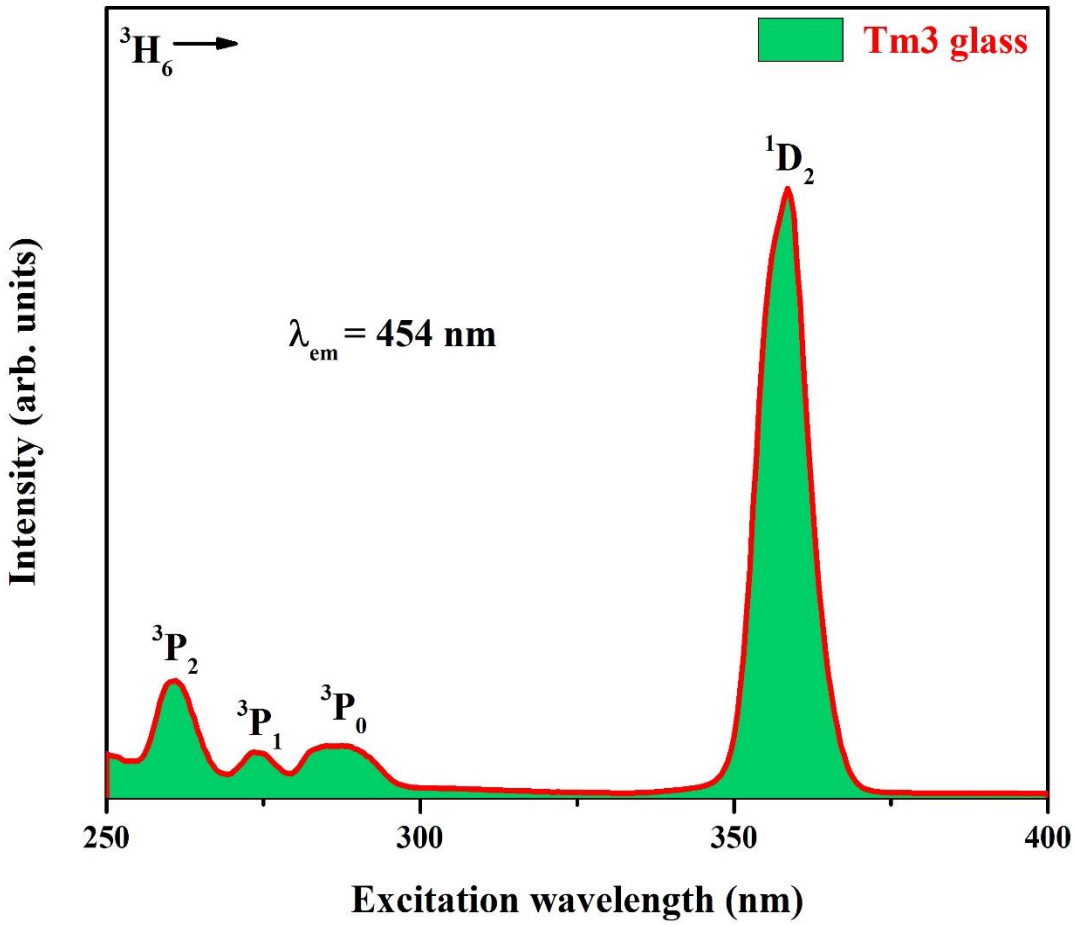

Fig. 5.4. The excitation spectrum of Tm3 glass under 454 nm emission wavelength.

From Fig. 5.4, it is observed that the excitation spectrum consists of four excitation peaks situated at 260, 274, 286 and 359 nm are attributed to $^3H_6 \rightarrow {}^3P_2$, $^3P_1$, $^3P_0$ and $^1D_2$ transitions

respectively [118]. Out of these, $^3H_6 \rightarrow {}^1D_2$ (359 nm) is relatively high in intensity and is quite suitable to read the PL emission spectra of the titled glasses. By keeping the light intensity monochromator at 359 nm, all Tm^{3+} doped samples were scanned for PL emission spectra. Fig. 5.5 shows the PL emission spectra read for the titled glasses under 359 nm excitation wavelength. It contains two emission peaks at 454 and 476 nm attributed to $^1D_2 \rightarrow {}^3F_4$ and $^1G_4 \rightarrow {}^3H_6$ transitions, respectively [118]. From Fig. 5.5, it is observed that the emission intensity of all peaks escalates up to a certain value with the Tm^{3+} ion concentration. Further, it starts decreasing even when we increase Tm^{3+} ion concentration. This happens due to the quenching effect of concentration [49].

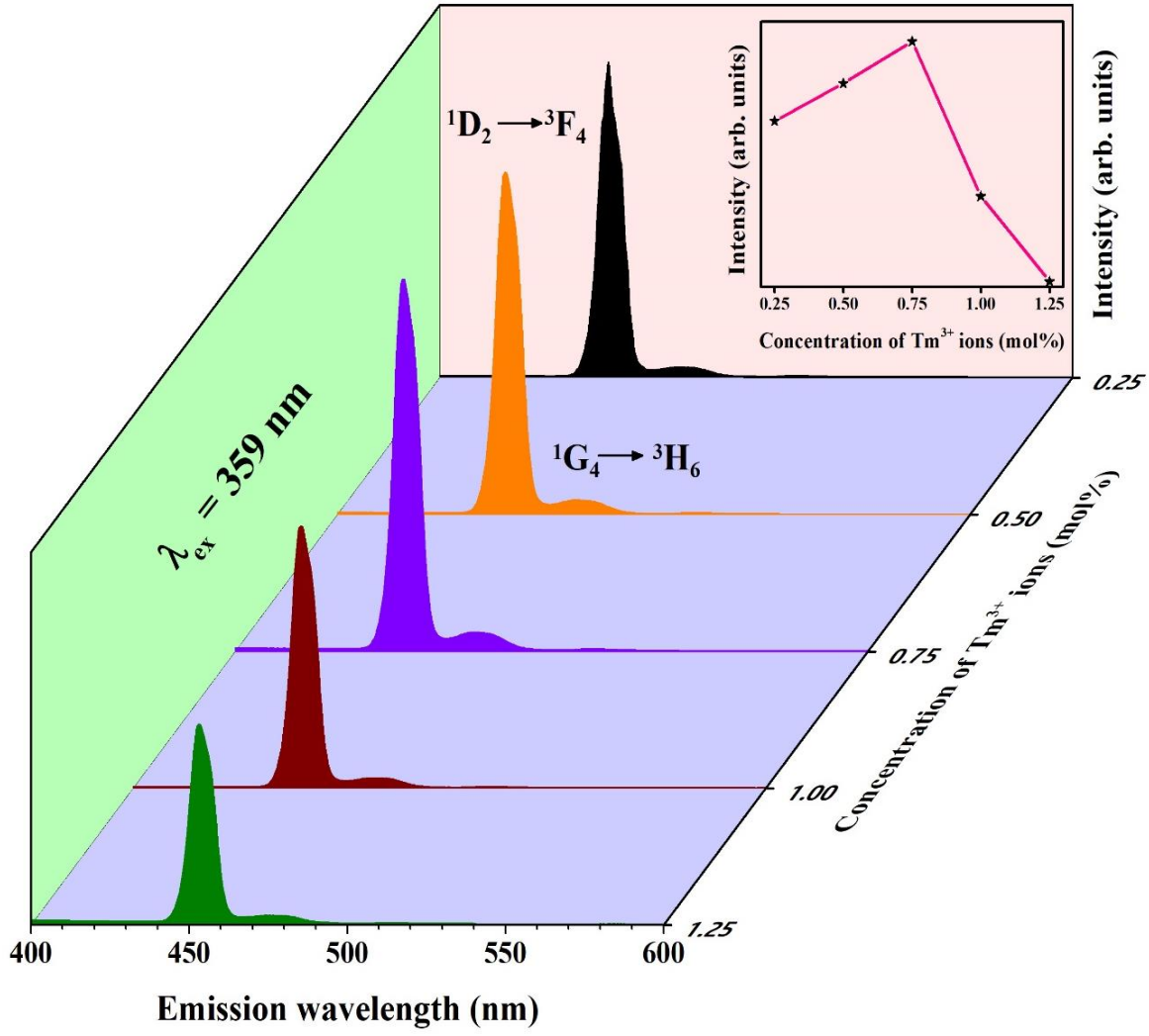

Fig. 5.5. Optimization of Tm^{3+} ion in KZABS glass under 359 nm wavelength (Inset: Intensity of the transition $^1D_2 \rightarrow {}^3F_4$ (454 nm) versus concentration of Tm^{3+} ion).

The inset of Fig. 5.5 represents the variation of emission intensity of the transition $^1D_2 \rightarrow {}^3F_4$ (454 nm) versus the concentration of Tm^{3+} ion. Thus, the optimized content of Tm^{3+} ion in KZABS host glass is 0.75 mol% which is already abbreviated as Tm3 glass in section 2.1. Fig. 5.5 contains a sharp peak at 454 nm (blue) due to a large number of photons returning to the $^3F_4$ state under 359 nm excitation. This allows us to contemplate that KZABS glasses activated with Tm^{3+} ions are apt as intense visible blue color emitters useful in designing epoxy free w-LEDs.

Further, to check the emission variability and hence the color tunability of KZABS glass doped with Tm^{3+} ions, the excitation spectrum of Tm^{3+} ions (0.75 mol%) doped KZABS glass has been studied by adjusting the emission monochromator at 650 nm as shown in Fig. 5.6.

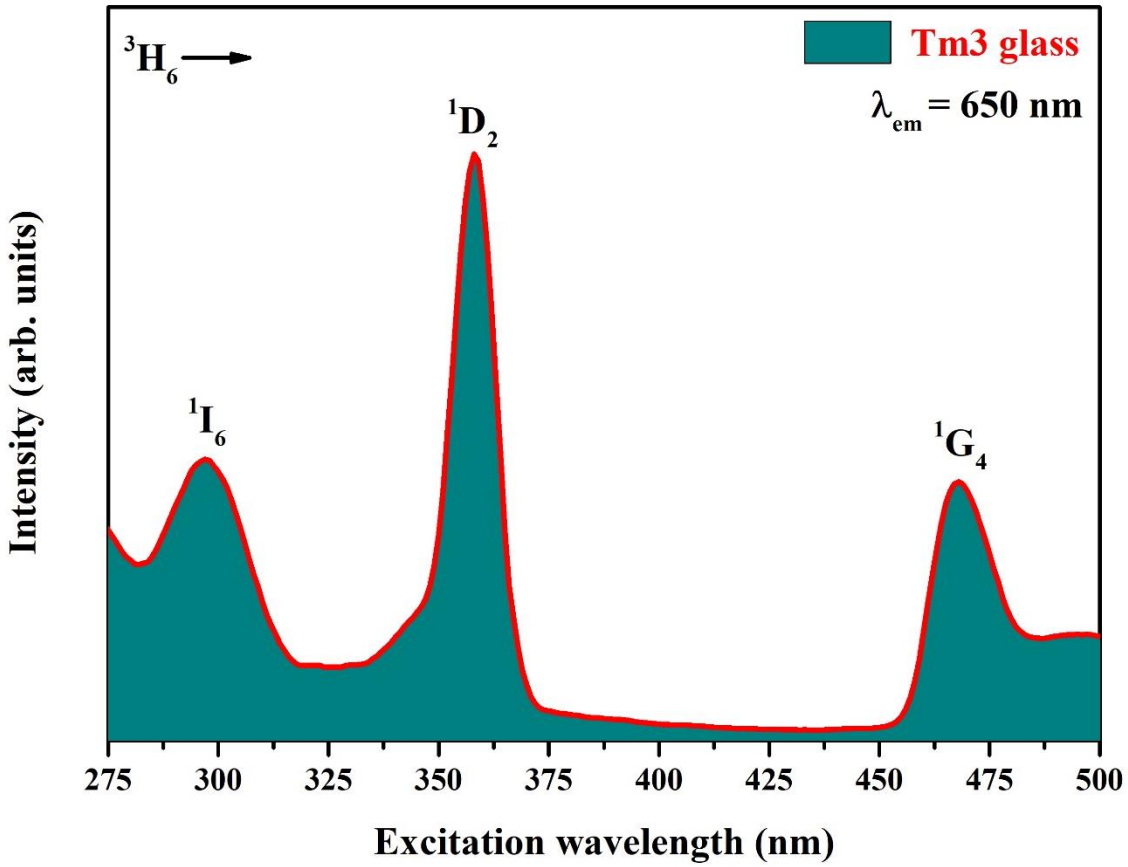

Fig. 5.6. The excitation spectrum of Tm3 glass under 650 nm emission wavelength.

As shown in Fig. 5.6, the titled glasses show three excitation peaks situated at 297, 359 and 466 nm attributed to $^3H_6 \rightarrow {}^1I_6$, $^1D_2$ and $^1G_4$ transitions, respectively. Out of these, $^3H_6 \rightarrow {}^1D_2$

(359 nm) is highly intense, and the PL performance of the titled glasses under 359 nm has already been reported in Fig. 5.5. To know about the PL performance of the titled glasses under the excitation wavelength other than 359 nm, we have investigated their PL performance under 297 nm ($^3H_6 \rightarrow {}^1I_6$) and 466 nm ($^3H_6 \rightarrow {}^1G_4$) excitation wavelengths also. Under 297 nm excitation, the titled glasses need not show any visible emission. However, the titled glasses show emission under 466 nm excitation wavelength as depicted in Fig. 5.7. From Fig. 5.7, it is observed that two emission peaks were present at 650 and 783 nm corresponding to transitions ($^1G_4 \rightarrow {}^3F_4$, $^1D_2 \rightarrow {}^3H_4$) and ($^1G_4 \rightarrow {}^3H_5$, $^3H_4 \rightarrow {}^3H_6$) respectively [16]. Under 466 nm, the $^1D_2$ and $^1G_4$ levels of Tm^{3+} ions in the titled glasses are getting depopulated simultaneously, resulting in visible red emission.

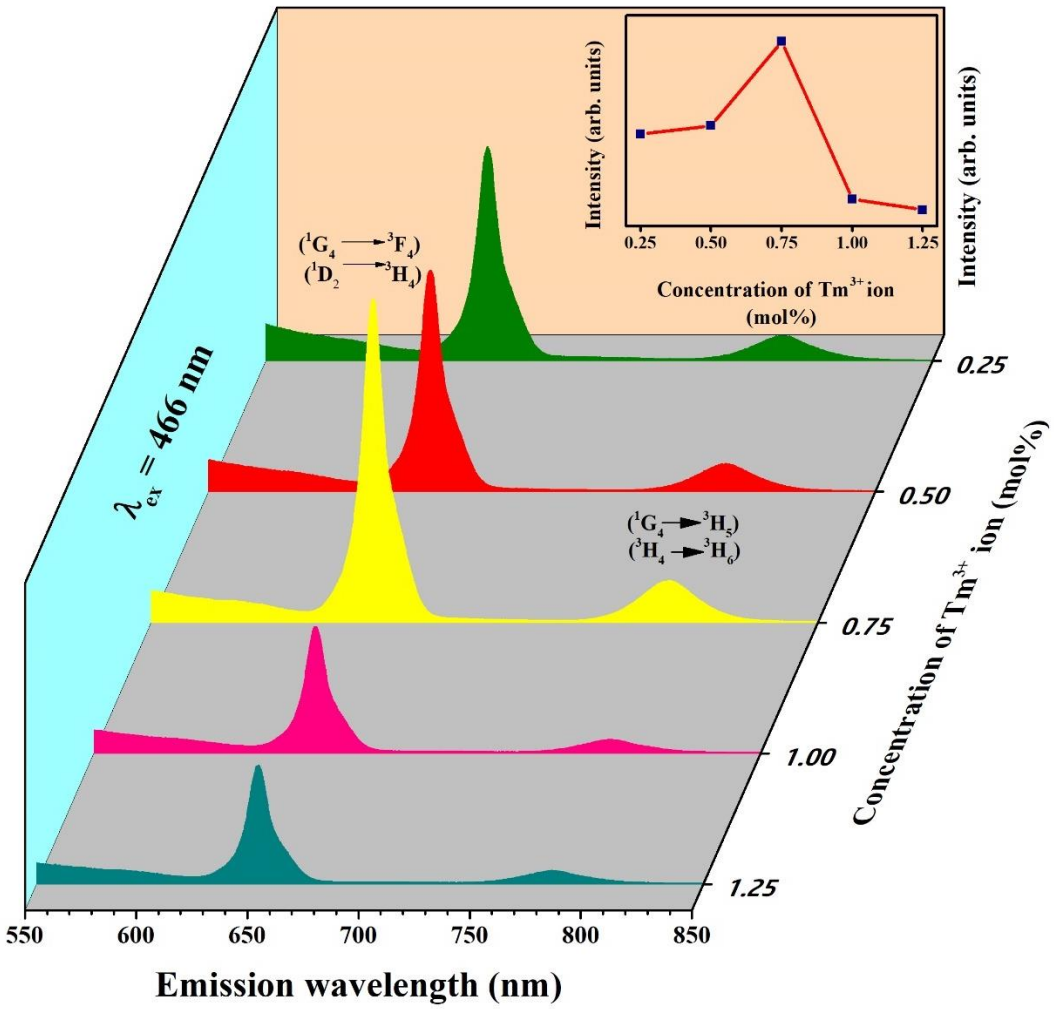

Fig. 5.7. Optimization of Tm^{3+} ions in KZABS glass under 466 nm wavelength (Inset: Intensity of the peak situated at 650 nm wavelength versus concentration of Tm^{3+} ion).

The inset of Fig. 5.7 again conveys the same information (0.75 mol% is the optimum concentration) as that of the inset shown in Fig. 5.5. The PL spectral analysis concluded that the as-prepared glasses could be utilized for blue and red color emitting applications by exciting under different wavelengths. A good color tunability can be achieved as we go from 359 nm to 466 nm.

5.3.4. Spectral overlap of $^3H_6 \rightarrow {}^1G_4$ transition

Fig. 5.8 depicts the spectral overlap observed between absorption and excitation spectra of Tm^{3+} doped KZABS glasses. The transition $^3H_6 \rightarrow {}^1G_4$ has been observed at 466 nm in the excitation spectrum of Tm3 glass shown in Fig. 5.6, and the same has been observed in the absorption spectrum of Tm3 glass at 470 nm as already demonstrated in Fig. 5.2. Thus, some energy transfer has been observed between Tm^{3+}- Tm^{3+} ions [119]. This can be further explained by Dexter's theory, which helps us find the energy transfer mechanism.

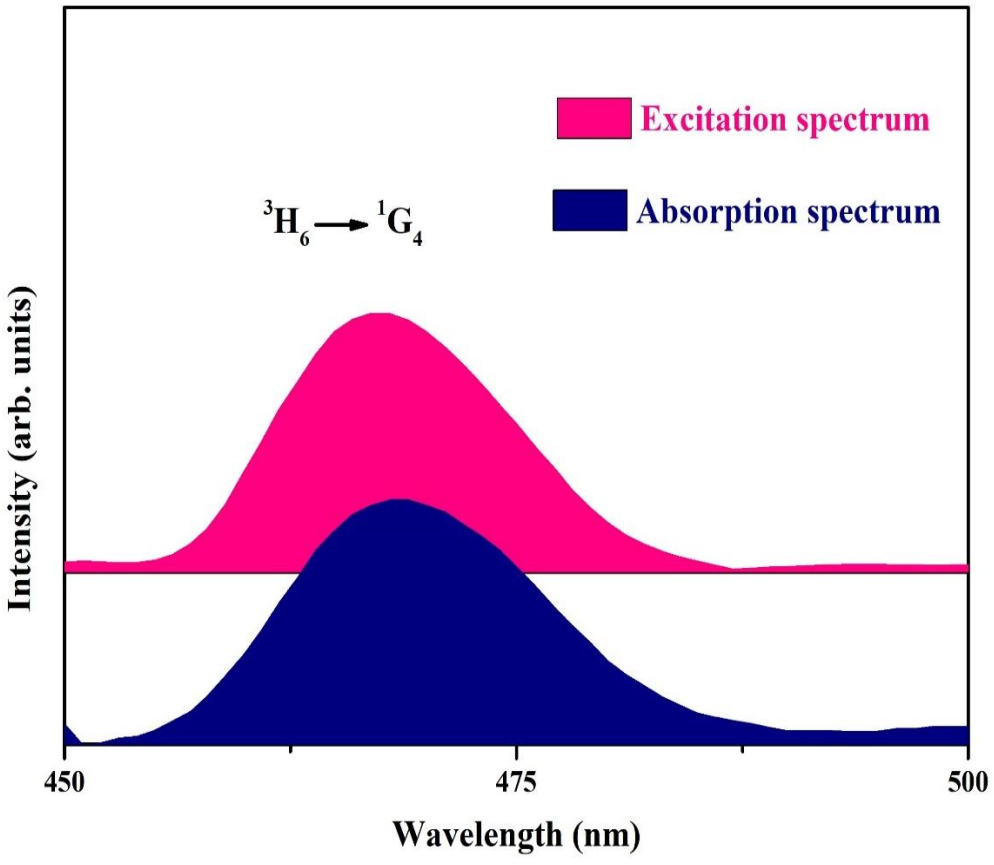

Fig. 5.8. Spectral overlap was observed between excitation and absorption spectra for the $^3H_6 \rightarrow {}^1G_4$ transition.

5.3.5. Energy transfer mechanism and decay profiles

The literature shows that energy transfer between RE ions occurs through three general methods: radiative energy transfer, energy transfer through exchange interactions, and energy transfer through multipolar interaction. As the average value of the lifetime decays with Tm3+ ion content, a radiative transfer can be discarded in the present work. The transfer of energy through exchange interaction is feasible only when the critical distance between the RE ions is nearly about 5Å [120]. Estimating the distance for energy transfer between Tm^{3+} ions is not an easy task. It needs advanced software and techniques. Generally, for the random distribution of RE ions, the average distance (D_c) between the RE ions can be estimated as [118]:

$$D_C = \left(\frac{3}{4\pi N}\right)^{1/3} \qquad (5.1)$$

In the present case, the average distance between Tm^{3+} - Tm^{3+} ions estimated is 23.8Å which is much larger than 5Å. Therefore, the multipole interaction may be the most appropriate in the present case. Further, to elucidate more about the multipolar interaction type involved in the titled glasses for the energy transfer process, the Dexter theory has been applied to PL emission recorded under 359 and 466 nm, as shown in Fig. 5.9 (a and b).

According to the Dexter theory, the probability of energy transfer via multipolar interaction between activator ions depends on the value of S. The relation between PL emission intensity and corresponding doping concentration is already discussed in equation (1.1 and 1.2) in chapter 1.

A graph is plotted between the $log\left(\frac{I}{x}\right)$ and $log(x)$ to find the value of *s.* The slope of the graph will be equal to the value of *s/3*. The value of *s* comes out to be 5.52 and 5.48 under 359 and 466 nm respectively, as shown in Fig. 5.9 (a and b). In both cases, the value of *s* equals six, which implies that energy transfer occurs through dipole-dipole interaction between activator ions.

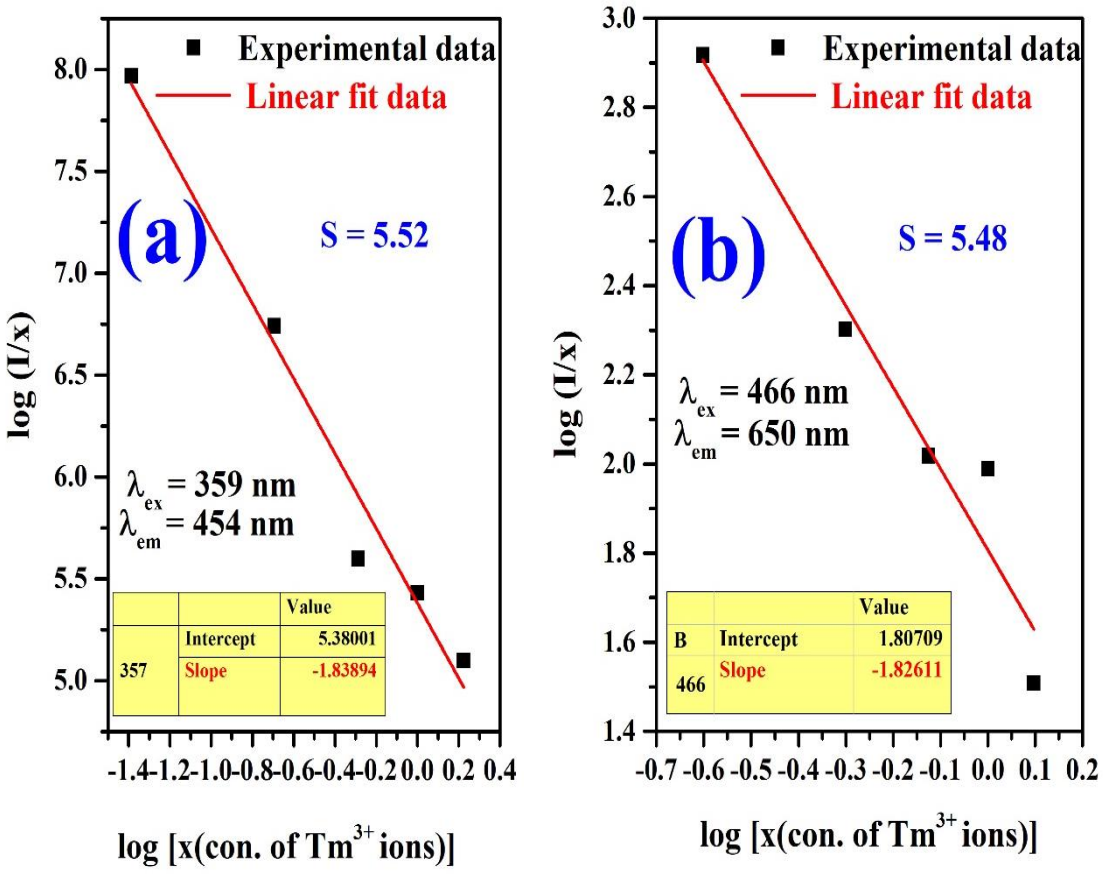

Fig. 5.9. Plot of log (I/x) versus log (x) for Tm^{3+} doped KZABS glasses under (a) 359 nm (b) 466 nm excitation wavelengths.

Based on the observed PL spectrum and using Carnall's paper [121], a schematic energy level diagram is represented in Fig. 5.10, in which Tm^{3+} ions are first excited to the higher energy levels and then return to the various lower levels either through radiative or non-radiative transitions. Some energy is transferred from an excited Tm^{3+} ion to lower excited or non-excited Tm^{3+} ions. The solid lines represented the excitation and emission transitions, and dotted red color lines represented the non-radiative transitions included in this energy transfer process, as shown in Fig. 5.10. In the present case, Tm^{3+} ions in $^1D_2$ and $^1G_4$ states are donors, and Tm^{3+} ions in $^3H_4$ and $^3H_6$ are acceptor ions.

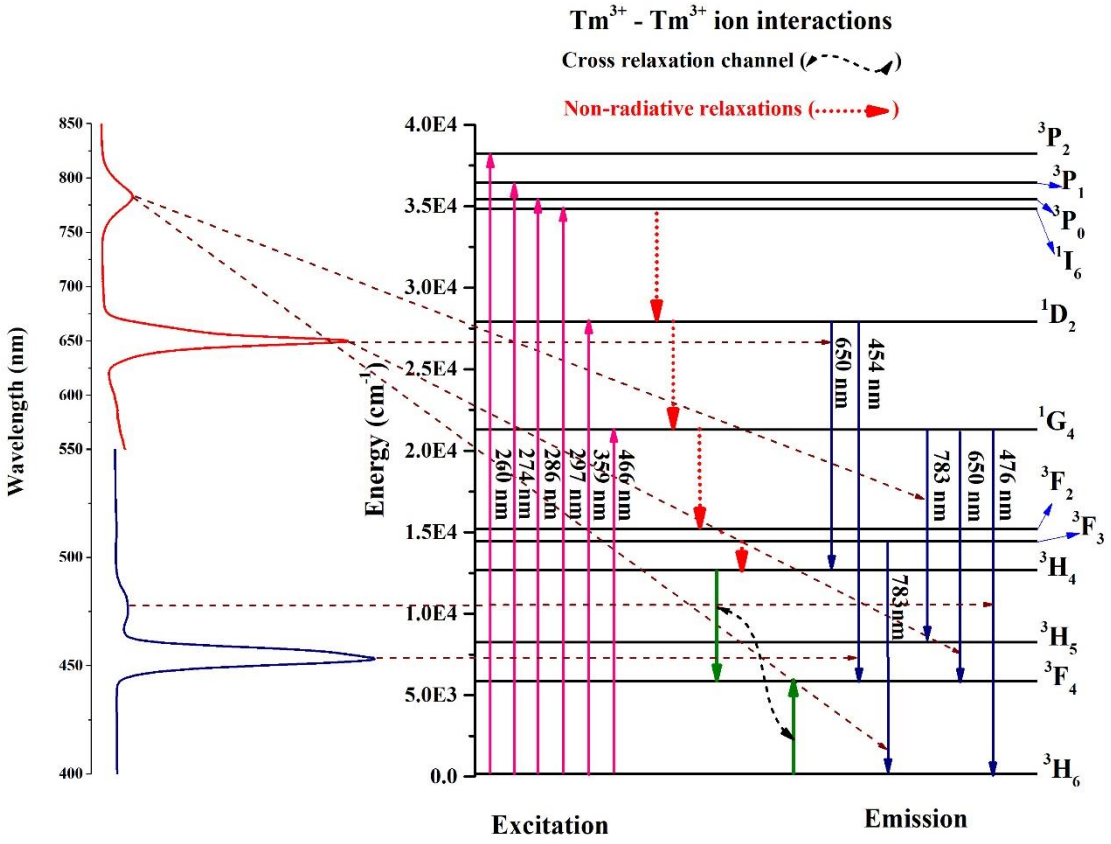

Fig. 5.10. Partial energy level diagram and possible non-radiative relaxations in Tm^{3+} doped KZABS glasses.

For further exploration of energy transfer and Tm^{3+} - Tm^{3+} ion interaction, the PL decay profiles for KZABS: xTm^{3+} (x = 0.25, 0.5, 0.75, 1.0 and 1.25) glasses were recorded under 359 nm excitation by monitoring 454 nm emission wavelength as depicted in Fig. 5.11. The PL decay profiles shown in Fig. 5.11 are well fitted to the following non-exponential (tri-exponential) expression given below [111]:

$$I = I_0 + A_1 \exp(-t/\tau_1) + A_2 \exp(-t/\tau_2) + A_3 \exp(-t/\tau_3) \quad (5.2)$$

Where I_0 and I are the emission intensities at time zero and t; A_1, A_2 and A_3 are constants of fitting; τ_1, τ_2 and τ_3 are the PL decay factors of an experimental lifetime. From the decay features shown in Fig. 5.11, it is conspicuous that the average experimental lifetime values are descending with an escalation in the concentration of Tm^{3+} ions in the titled glasses. The

observed lifetimes measured using the following equation are found to be in the range 185 - 526 μs and are placed in Table 5.1 [78]:

$$\tau_{av} = \frac{a_1\tau_1^2+a_2\tau_2^2+a_3\tau_3^2}{a_1\tau_1+a_2\tau_2+a_3\tau_3} \quad (5.3)$$

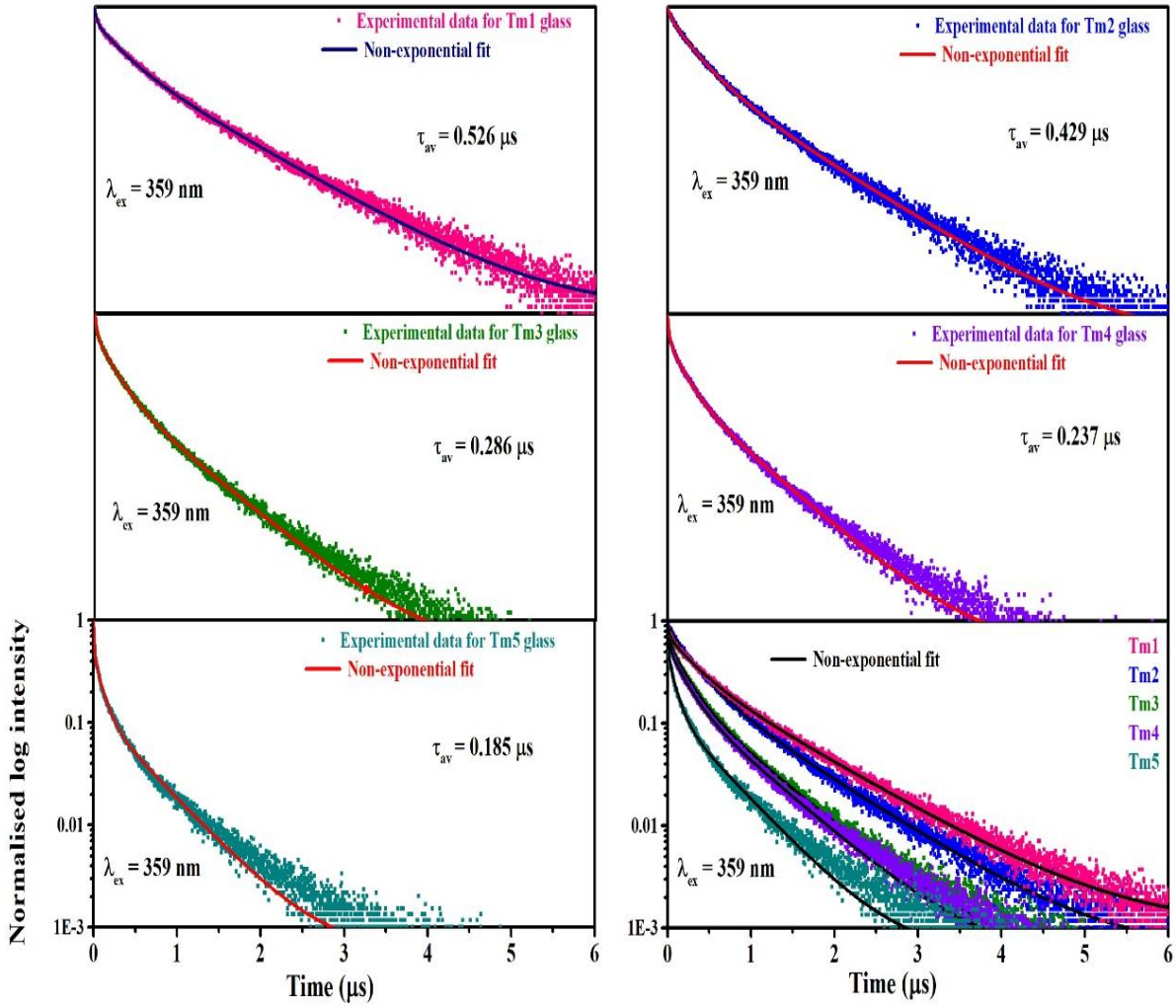

Fig. 5.11. Decay curves for Tm^{3+} doped KZABS glasses recorded under 359 nm excitation wavelength

The I-H model was applied to the PL decay curves to identify the Tm^{3+} - Tm^{3+} ion interaction. The PL decay profiles were fitted with I-H model shown in Fig. 5.12. According to the I-H model (by applying equation 1.4), the electric dipole-dipole interaction is responsible for energy transfer between Tm^{3+} ions via non-radiative transitions in as-synthesized glasses, similar to the already reported Tm^{3+} doped glasses [118]. The values of the parameters Q, N_0, R_0 and C_{DA} have been calculated using equations (3.6 and 3.7) and presented in Table 5.1.

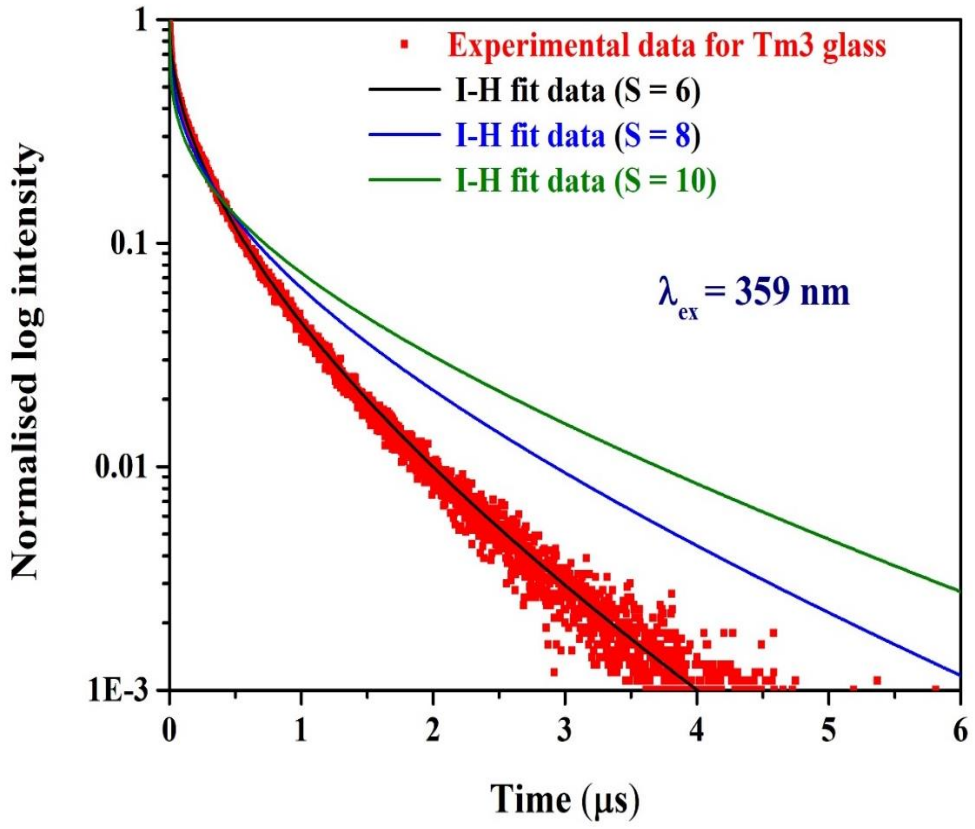

Fig. 5.12. Decay curve of Tm3 glass fitted with I-H model for S = 6, 8 and 10 under 359 nm excitation wavelength.

Table 5.1

Average lifetime (τ_{avg}), energy transfer parameter (Q), acceptor-ion concentration (N_0), critical transfer distance (R_0) and donor-acceptor interaction parameter (C_{DA}) for Tm^{3+} doped KZABS glasses.

Glass samples	τ_{avg} (μs)	Q	N_0 (10^{21} ions/cm^3)	R_0 (Å)	C_{DA} (10^{-45} cm^6 s^{-1})
Tm 1	526	3.24	4.70	4.60	33.46
Tm 2	429	4.01	9.36	3.93	12.93
Tm 3	286	5.34	13.95	3.78	10.33
Tm 4	237	6.96	18.50	3.76	9.98
Tm 5	185	7.80	22.99	3.63	8.11

5.3.6. Colorimetric properties

To check the color tunability from blue to the red region for Tm^{3+} doped KZABS glasses, CIE 1931 chromaticity diagram has been used. CIE chromaticity coordinates can be estimated with the help of emission spectra using trichromatic color values and their spectral distribution [36]. Fig. 5.13 represents the CIE chromaticity diagram with two color coordinates for optimized KZABS glass (0.75 mol% of Tm^{3+} ion). The CIE coordinate for optimized glass lies in the blue region under 359 nm excitation monitoring via 454 nm emission.

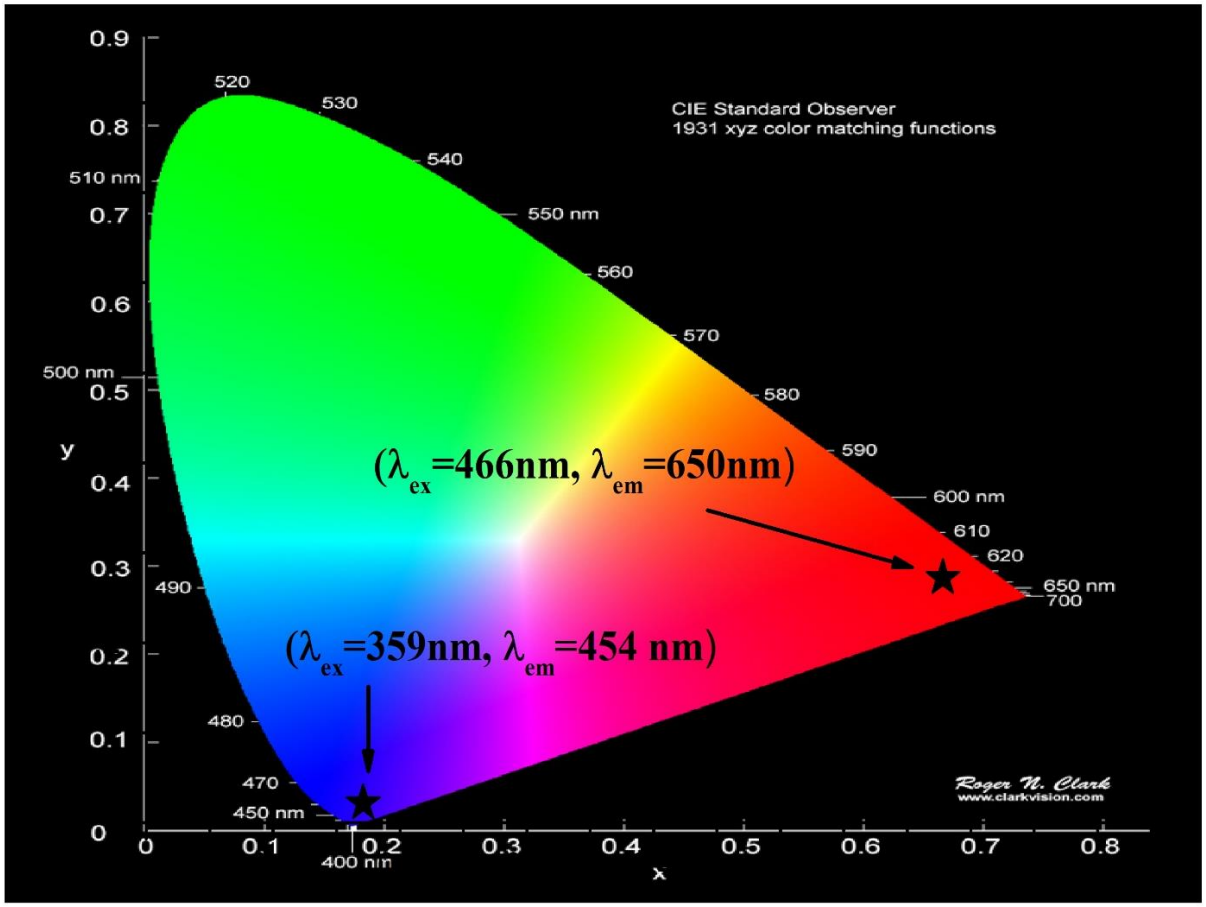

Fig. 5.13. CIE color coordinates of Tm3 glass under 359 and 466 nm excitation wavelengths.

The color coordinates lie in the deep-red region if the same sample is excited under 466 nm excitation with 650 nm emission. A good color tuning can be seen with the variation of excitation wavelength in the as-prepared KZABS glasses. The color coordinates estimated for the optimized KZABS glass are presented in Table 5.2.

For the better consideration of different color emissions, CP values can be estimated by using the equation (1.11). The CP of optimized glass was 96% under 359 nm excitation and 93.8% under 466 nm, indicating a pure blue region under 359 nm and red under 466 nm respectively.

Table 5.2

Colorimetric values for Tm3 glass under 359 and 466 nm excitation wavelengths.

Excitation wavelength (nm)	CIE chromaticity coordinates (X,Y)	Color purity (%)
359	0.172, 0.021	96
466	0.628, 0.272	93.8

5.4 Conclusions

From the results discussed earlier, it was concluded that by exciting the KZABS glass sample under two different wavelengths, good color tunability can be achieved. All these investigations represent the suitability of as-prepared glasses in photonic devices such as w-LEDs as well as blue or red color emitting applications.

Chapter 6

Tunable photoluminescence studies of KZABS:RE^{3+} (RE^{3+} = Tm^{3+}, Tb^{3+} and Sm^{3+}) glasses for w-LEDs based on energy transfer

In this chapter, KZABS: RE^{3+} (Tm^{3+}, Tb^{3+}, and Sm^{3+}) glasses were characterized through PL emission and PL decay to demonstrate red (Sm^{3+}), green (Tm^{3+}/Tb^{3}) and blue (Tm^{3+}/Tb^{3+}) colors simultaneously and white light realization by varying the Sm^{3+} ion concentration under 356 nm excitation. The energy transfer mechanism from Tm^{3+} to Tb^{3+} ($^{1}G_4$ to $^{5}D_4$), Tm^{3+} to Sm^{3+} ($^{1}G_4$ to $^{4}G_{7/2}$), and Tb^{3+} to Sm^{3+} ($^{5}D_4$ to $^{4}G_{7/2}$) are confirmed by the lifetime values. CIE coordinates and CCT values were observed near the standard white light (0.333, 0.333, and 5500 K). The results obtained reveal that Tm^{3+}/Tb^{3+}/Sm^{3+} tri-doped KZABS glasses could be a potential candidate for the fabrication of visible RGB luminescent materials, display devices and w-LEDs.

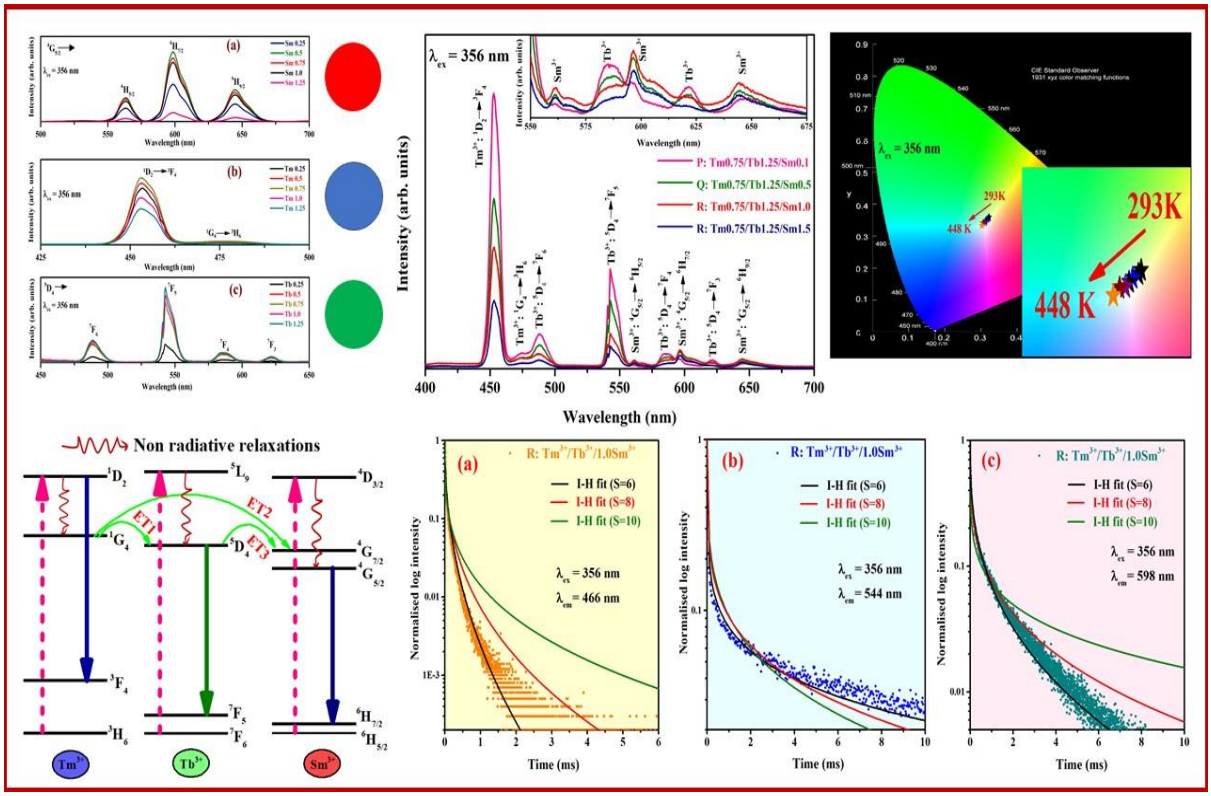

6.1. Introduction

Light-emitting diodes (LEDs) are seeking the devotion of the investigators in subsequent illumination sources because of their extensive properties like low energy consumption, long lifecycle, large efficiency (more than 80% energy saver), high stability, eco-friendly, and many more [1–3]. As we have discussed in previous chapters that how the white light surpassed the other conventional lighting technologies such as incandescent and fluorescent bulbs. Why did we prefer RGB approach for producing white light? How phosphor materials degrade the efficiency and quality of the devices? How the glass-based LEDs can be a better replacement for phosphor-based LEDs? How RE ions play a crucial role in lighting technology? All of these questions have been addressed in previous chapters. In previous chapters, we used KZABS glasses to investigate the emission properties of various RE ions in order to emit individual primary colors. In this chapter, we will try to produce white color emission by combining these three prime colors in same host glass.

Out of various RE ions, Tm^{3+}, Tb^{3+}, and Sm^{3+} ions are suitable to emit red, green, and blue colors corresponding to $^1D_2 \rightarrow {}^3F_4$ ($\approx$ 455 nm), $^5D_4 \rightarrow {}^7F_5$ ($\approx$ 545 nm), and $^4G_{5/2} \rightarrow {}^6H_{7/2}$ ($\approx$ 600 nm) transitions respectively [23]. So, white light may be obtained by combining these three ions in a single host. Following the accessible literature, it was discovered that white colour emission is a genuine issue, and this has prompted us to work on $Tm^{3+}/Tb^{3+}/Sm^{3+}$ tri-doped host glasses.

Many researchers have investigated different RE ions as active ions to produce white light in various glasses such as borate [122], silicate [115], germanate [113], phosphate [114], borosilicate [123], and tellurides [41]. The illumination of a particular colour emission may be subject to the primary matrix, the kind of dopant ion, and its concentration. We thought of combining Tm^{3+}, $Tb^{3+,}$ and Sm^{3+} ions in different ratios as dopants in same host glass to achieve the expected white light.

We have fabricated KZABS glass using and studied its suitability for visible red, green, and blue color photonic device applications by doping them suitably with Sm^{3+}/Eu^{3+} [36], Dy^{3+}/Tb^{3+} [111], and Tm^{3+} [124] ions earlier mentioned in previous chapters.

In this chapter, $Tm^{3+}/Tb^{3+}/Sm^{3+}$ tri-doped KZABS glasses were prepared and characterized through various techniques to understand their usage in w-LEDs and other colored photonic device applications. The glassy nature of the titled glasses has been revealed by using an x-ray diffractometer (XRD). The PL emission and PL decay have been studied for singly doped KZABS: RE^{3+} (RE^{3+} = Tm^{3+}, $Tb^{3+,}$ and Sm^{3+}) as well as $Tm^{3+}/Tb^{3+}/Sm^{3+}$ tri-doped KZABS glasses under suitable excitation wavelengths. The TD-PL emission helps us to determine thermal stability and color stability with a temperature rise. The efficiency and mechanism of energy transfer between RE^{3+} ions (RE^{3+} = Tm^{3+}, $Tb^{3+,}$ and Sm^{3+}) have been discussed. Furthermore, the I-H model was applied to understand the energy transfer mechanisms involved between the different RE ions.

6.2. Experimental section

KZABS glasses doped with different RE^{3+} ions were synthesized with the help of the melt-quenching process. Table 6.1 contains the detailed composition of singly optimized glasses and all tri-doped glasses with their abbreviations. The previously indicated methodologies were used to characterise all glass samples prepared for this purpose. The PL excitation, emission, and deca profiles are the primary emphasis, and a thorough analysis has been performed. The TD-PL profiles were obtained to assess thermal stability using the same apparatus described in Chapter 3.

Table 6.1

Composition details with sample abbreviations for the as-prepared KZABS glasses.

Sample ID	B_2O_3	SiO_2	Al_2O_3	ZnO	K_2O	Tm_2O_3	Tb_4O_7	Sm_2O_3
KZABS0	50	30	10	5	5	-	-	-
a	50	30	10	4.25	5	0.75	-	-
b	50	30	10	3.75	5	-	1	-
c	50	30	10	4.5	5	-	-	0.5
P	50	30	10	3.15	5	0.75	1	0.1
Q	50	30	10	2.75	5	0.75	1	0.5
R	50	30	10	2.25	5	0.75	1	1.0
S	50	30	10	1.75	5	0.75	1	1.5

6.3. Results and discussion

6.3.1. XRD analysis

XRD investigation is a pre-requisite tool to know the structural behaviour of the materials. Here we have performed XRD measurements on un-doped, singly doped KZABS:RE^{3+} (RE^{3+} = Tm^{3+}, Tb^{3+} and Sm^{3+}) and tri-doped $Tm^{3+}/Tb^{3+}/Sm^{3+}$ KZABS glasses. The XRD pattern of all the glasses shows a similar kind of trend; hence, we have shown only the XRD patterns for a few of the glasses. None of the spectra shown in Fig. 6.1 have a sharp peak signifying the glassy nature of the titled glasses. This also allows us to affirm that the addition of RE ions to the host glass need not show any change in its glassy nature.

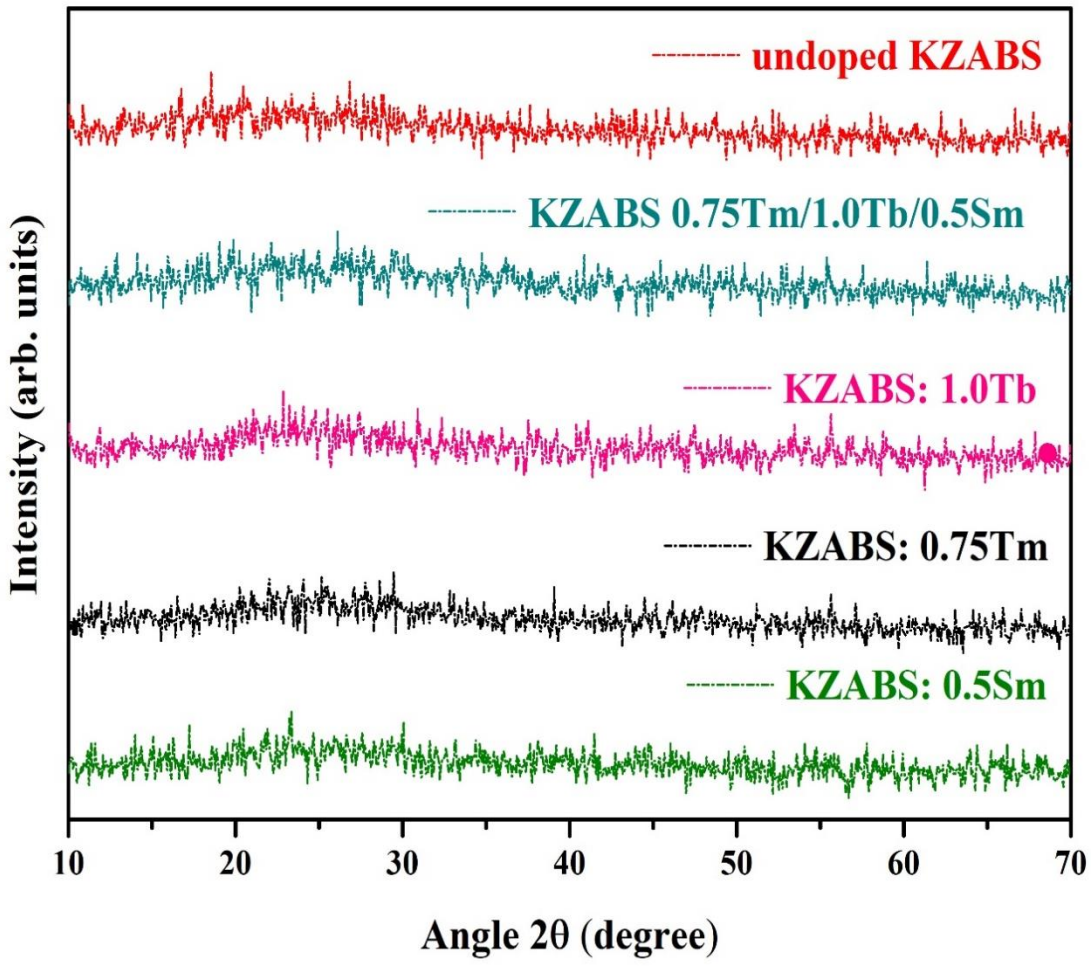

Fig. 6.1. XRD spectra recorded for an undoped, singly doped KZABS: RE^{3+} (RE^{3+} = Tm^{3+}, Tb^{3+} and Sm^{3+} ions) and tri-doped $Tm^{3+}/Tb^{3+}/Sm^{3+}$ KZABS glasses

6.3.2. PL analysis

6.3.2.1. PL investigations of singly doped KZABS: RE^{3+} (RE^{3+} = Tm^{3+}, Tb^{3+} and Sm^{3+}) glasses

PL is a spectroscopic technique that is useful to understand the spectral features of a material and reveal the information pertaining to the intensity of light that the materials can emit for a certain wavelength. PL spectra can be recorded as a function of either excitation or emission wavelength. In the present work, PL excitation spectrum has been recorded first to select best suitable excitation wavelength for further characterization of the material. Fig. 6.2 show the excitation spectra of singly doped KZABS: RE^{3+} (RE^{3+} = Tm^{3+}, $Tb^{3+,}$ and Sm^{3+}) glasses by

monitoring their respective emission wavelengths. As the excitation spectra for the remaining concentration of the individual ion doped into KZABS glass are identical in peak position but some variation in their intensity, they were not shown in Fig. 6.2. As can be observed from Fig. 6.2, the excitation spectrum recorded for 1 mol% of Tb^{3+} ions doped KZABS glass (shown by green line) monitored under 544 nm emission wavelength show various excitation peaks in the range 250-310 nm due to $^7F_6$ ($4f^8$) - ^9E ($4f^75d^1$) transitions and the remaining at 320, 342, 354, 371 and 381 nm due to $^7F_6 \rightarrow {}^5H_7$, $^5G_2$, $^5L_9$, $^5L_{10}$ and $^5G_6$ transitions respectively [101–103].

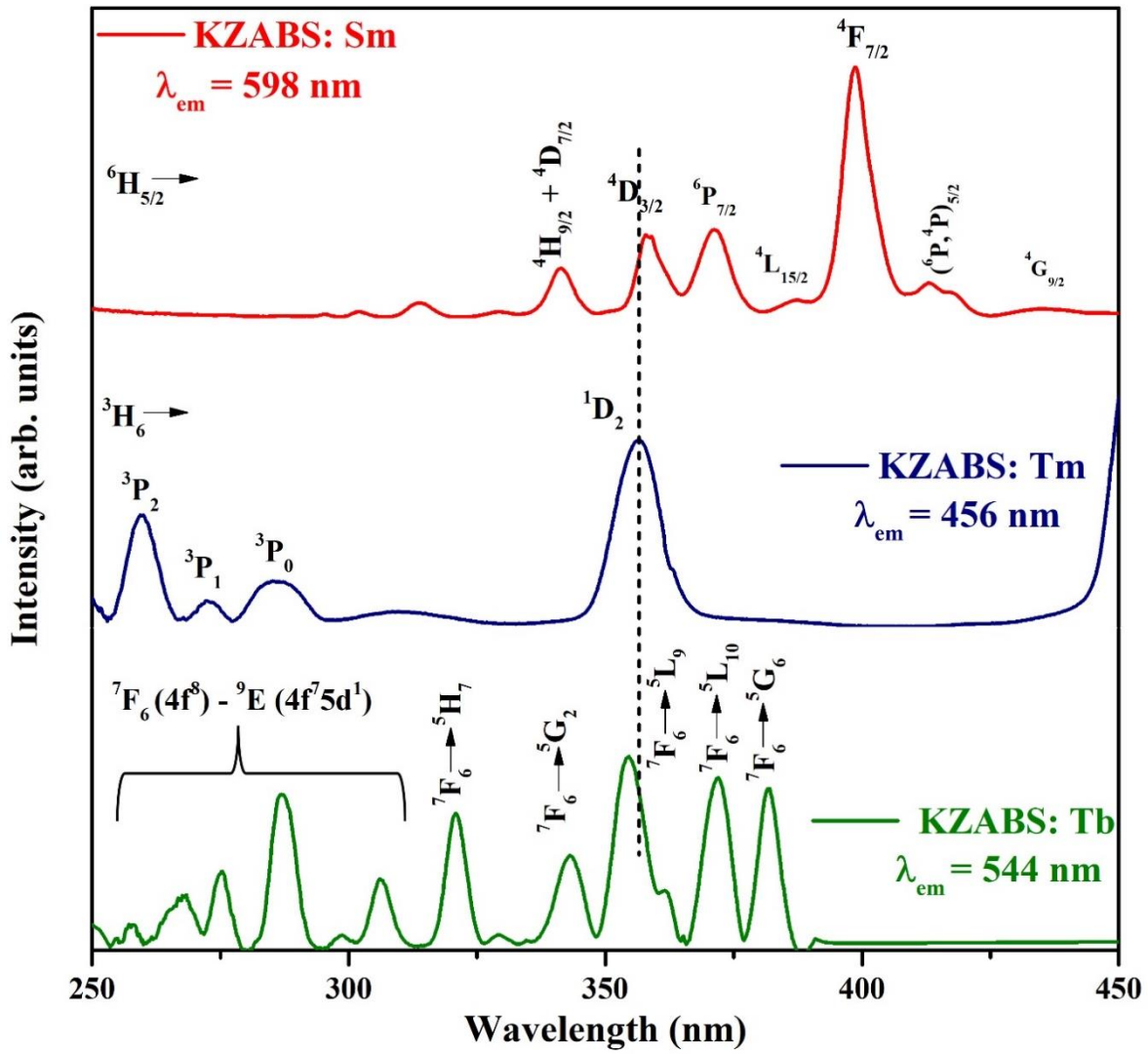

Fig. 6.2. The excitation spectra for singly doped KZABS: RE^{3+} (RE^{3+} = Tm^{3+}, Tb^{3+} and Sm^{3+}) glasses at their respective emission wavelengths

The Fig. 6.2. also reveal the excitation bands of 0.75 mol% of Tm^{3+} ions doped KZABS glasses (shown by blue line) examined under 456 nm emission wavelength that contains four excitation bands originated at 260, 272, 286, and 356 nm attributed to the $^3H_6 \rightarrow {}^3P_2$, $^3P_1$, $^3P_0$ and $^1D_2$ respectively [118]. The same figure shows the excitation spectrum of 0.5 mol% of Sm^{3+} ions in KZABS glasses (shown by red line) recorded at 598 nm emission wavelength which contains several excitation peaks situated at 341, 358, 371, 387, 399, 413 and 435 nm corresponding to $^6H_{5/2} \rightarrow {}^4H_{9/2} + {}^4D_{7/2}$, $^4D_{3/2}$, $^6P_{7/2}$, $^4L_{15/2}$, $^4F_{7/2}$, $(^6P, {}^4P)_{5/2}$ and $^4G_{9/2}$ transitions respectively [111]. In all these spectra shown in Fig. 6.2., it is conspicuous that one typical excitation peak appearing nearly at 356 nm is an effective excitation wavelength to record the PL emission spectra of the titled glasses.

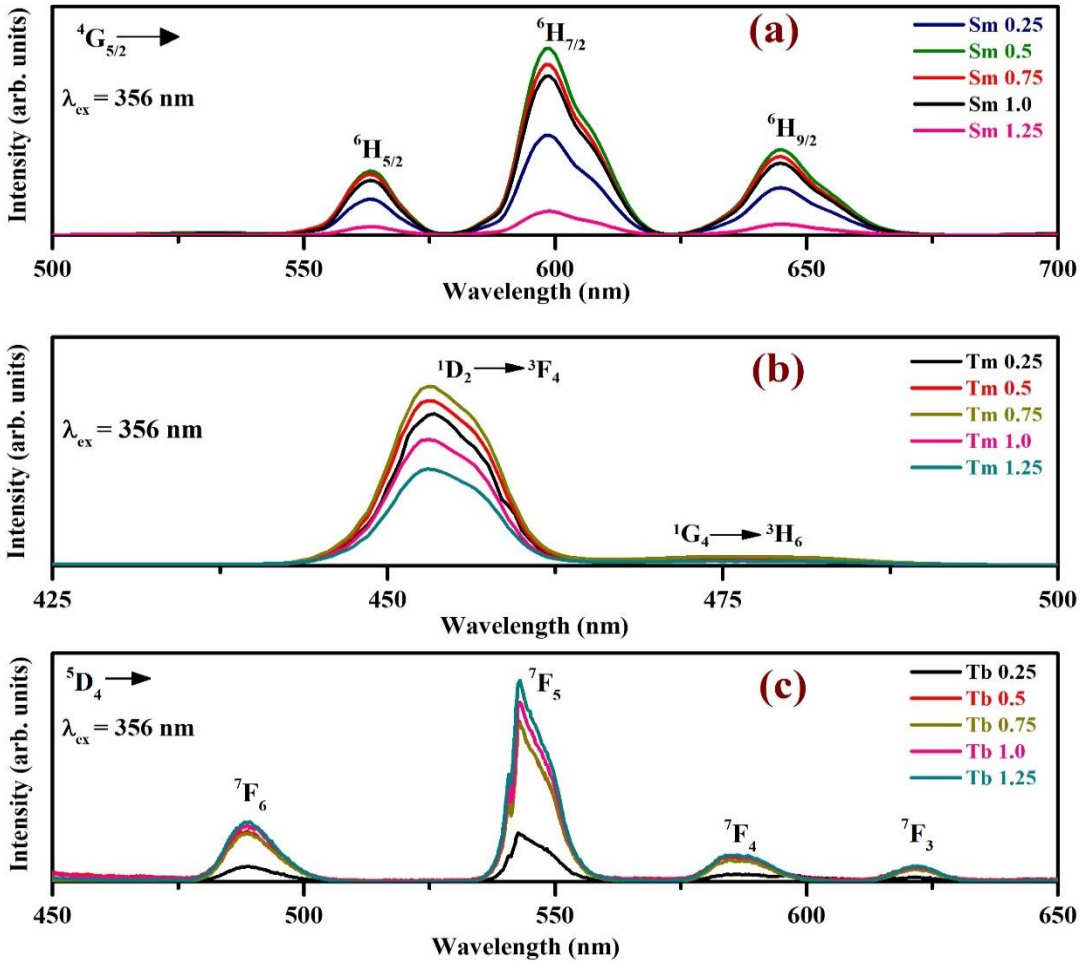

Fig. 6.3. The emission profiles for singly doped KZABS: RE^{3+} (RE^{3+} = Tm^{3+}, Tb^{3+} and Sm^{3+}) glasses under 356 nm excitation wavelength

The PL emission profiles recorded for singly doped KZABS: RE^{3+} (RE^{3+} = Tm^{3+}, $Tb^{3+,}$ and Sm^{3+}) glasses by fixing the excitation monochromator at 356 nm are shown in Fig. 6.3 (a-c). Fig. 6.3(a) shows the emission spectra of KZABS: xSm^{3+} (x = 0.25, 0.5, 0.75, 1.0 and 1.25) glasses that consists of three peaks at 563, 598 and 645 nm pertaining to the $^4G_{5/2} \rightarrow {}^6H_{5/2}$, $^6H_{7/2}$ and $^6H_{9/2}$ transitions respectively. The transitions pertaining to $^4G_{5/2} \rightarrow {}^6H_{5/2}$ and $^6H_{9/2}$ are magnetic dipole and electric dipole in nature respectively as per the selection rule ($\Delta J = 0$ and ± 2, J is angular momentum). As the Sm^{3+} ion concentration increases the emission intensity of the as-prepared glasses initially increases up to 0.5 mol% and further decreases due to concentration quenching effect [33–35]. Fig. 6.3 (b) shows the emission spectra for KZABS: xTm^{3+} (x = 0.25, 0.5, 0.75, 1.0 and 1.25) glasses having two emission bands at 456 and 474 nm attributed to the $^1D_2 \rightarrow {}^3F_4$ and $^1G_4 \rightarrow {}^3H_6$ transitions respectively [118]. Considering the quenching effect, we have seen that the optimum concentration in KZABS: Tm^{3+} glasses is found to be at 0.75 mol%. In Fig. 6.3 (c), it can be visualized that Tb^{3+} doped KZABS glasses have four bands initiating from the ground state $^5D_4$ to the excited states $^7F_{6,5,4\&3}$ at 489, 544, 587 & 622 nm respectively [104]. The concentration effect seems to be absent in Tb^{3+} doped glasses. So, we randomly choose one concentration for further study (1 mol% for Tb^{3+} ions in present work). As observed from Fig. 6.3, Tm^{3+}, $Tb^{3+,}$ and Sm^{3+} ions emit blue, green, and reddish-orange colors under the same excitation. We decide to combine all these three RE ions in an appropriate ratio which may lead to giving white light emission under 356 nm UV excitation.

6.3.2.2.PL investigations of tri-doped KZABS: $Tm^{3+}/Tb^{3+}/xSm^{3+}$ glasses

Here we are using the common wavelength (356 nm) to excite the tri-doped KZABS: $Tm^{3+}/Tb^{3+}/xSm^{3+}$ (x = 0.1, 0.5, 1.0 and 1.5) glasses. Fig. 6.4. illustrates many peaks corresponding to all the three RE ions at 456 (Tm^{3+}), 474 (Tm^{3+}), 488 (Tb^{3+}), 544 (Tb^{3+}), 562 (Sm^{3+}), 586 (Tb^{3+}), 598 (Sm^{3+}), 621 (Tb^{3+}) and 644 nm (Sm^{3+}). The transitions ascribed to

these bands are the same as already discussed in section 6.3.2.1. A slight variation is observed in band positions compared to the singly doped glasses. As the intensity of Tm^{3+} peak observed at 456 nm is relatively more intense than the other peaks, we have magnified the image observed from 550-675 nm range as shown in the inset of the same figure.

An interesting pattern observed in Fig. 6.4 is that the strength of bands pertaining to Tm^{3+} and Tb^{3+} ions drastically diminished, although the peaks ascribed to the Sm^{3+} ions are growing.

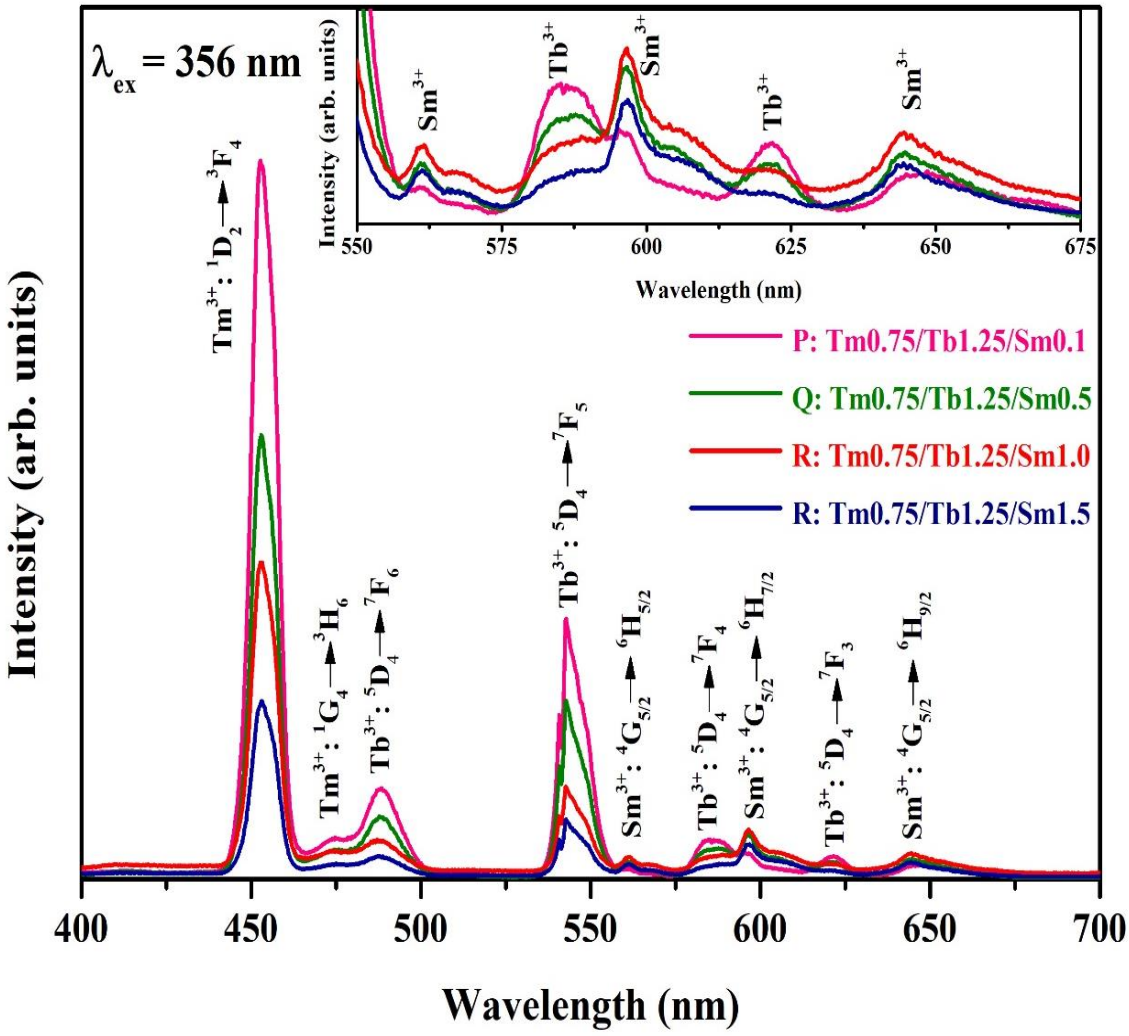

Fig. 6.4. The emission profiles for tri-doped KZABS: $Tm^{3+}/Tb^{3+}/xSm^{3+}$(x = 0.1, 0.5, 1.0 and 1.5) glasses under 356 nm excitation wavelength

We have plotted the intensity of peaks situated at 456 (blue region), 544 (green region), and 598 nm (reddish-orange region) versus Sm^{3+} ions concentration to check their variation with

Sm^{3+} ion content as shown in Fig. 6.5. From Fig. 6.5, it is conspicuous that with increase in Sm^{3+} ion concentration, there might be a transfer of energy from Tm^{3+} & Tb^{3+} ions to Sm^{3+} ions and the combined emission gives white light emission under 356 nm excitation. Furthermore, the energy transfer process from Tm^{3+} & Tb^{3+} ions to Sm^{3+} ions in the titled glasses can be better understood by drawing an energy level diagram between the involved RE^{3+} ions.

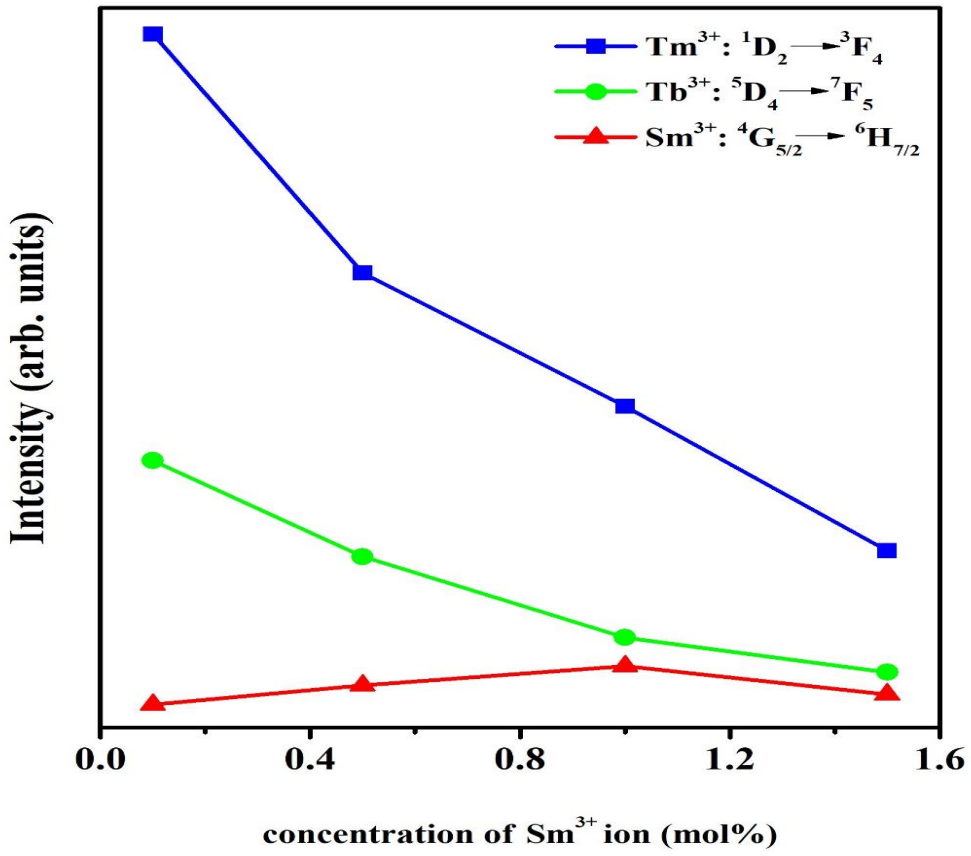

Fig. 6.5. Variation of the intensity of the peaks originated at 456 nm (blue), 544 nm (green) and 598 nm (red) versus the concentration of Sm^{3+} ions for the as-prepared glasses.

6.3.3. Energy transfer mechanism analysis

For better recognizing the energy transfer processes involved in tri-doped KZABS glasses, an energy level diagram is plotted between RE^{3+} (RE^{3+} = Tm^{3+}, Tb^{3+}, and Sm^{3+}) ions as shown in Fig. 6.6. The energy transfer routes named ET1, ET2, and ET3 can be visualized from the diagram involved as:

ET1: Tm^{3+} ($^1G_4$) → Tb^{3+} ($^5D_4$); ΔE ≈ 800 cm^{-1}

ET2: Tm^{3+} ($^1G_4$) → Sm^{3+} ($^4G_{7/2}$); ΔE ≈ 1300 cm^{-1}

ET3: Tb^{3+} ($^5D_4$) → Sm^{3+} ($^4G_{7/2}$); ΔE ≈ 500 cm^{-1}

It may be noticed that $^1G_4$ energy level of Tm^{3+} ions is approximately 800 and 1300 cm^{-1} larger than the $^5D_4$ level of Tb^{3+} and $^4G_{7/2}$ level of Sm^{3+} ions respectively and $^5D_4$ (Tb^{3+}) is 500 cm^{-1} higher than of $^4G_{7/2}$ (Sm^{3+}) level. This show the possibility of photons transfer from Tm^{3+} to Tb^{3+} and Sm^{3+} ions and Tb^{3+} to Sm^{3+} ions [96]. When as- prepared tri-doped samples were excited under 356 nm wavelength, energy conversion between RE^{3+} (RE^{3+} = Tm^{3+}, $Tb^{3+,}$ and Sm^{3+}) ions as per the following equation:

$$^1G_4\,(Tm^{3+}) + {}^7F_6\,(Tb^{3+}) \rightarrow {}^5D_4\,(Tb^{3+}) + {}^3H_6\,(Tm^{3+}) \quad (6.1)$$

$$^1G_4\,(Tm^{3+}) + {}^6H_{5/2}\,(Sm^{3+}) \rightarrow {}^4G_{7/2}\,(Sm^{3+}) + {}^3H_6\,(Tm^{3+}) \quad (6.2)$$

$$^5D_4\,(Tb^{3+}) + {}^6H_{5/2}\,(Sm^{3+}) \rightarrow {}^4G_{7/2}\,(Sm^{3+}) + {}^7F_6\,(Tb^{3+}) \quad (6.3)$$

The energy transfer efficiencies from Tm^{3+} to Tb^{3+} & Sm^{3+}, Tb^{3+} to Sm^{3+} ions have been estimated from the PL emission spectra (shown in Fig. 6.4) by using the following expressions [108]:

$$\eta_1 = 1 - \frac{I_{Tm}}{I_{Tm}+I_{Tb}} \quad (6.4)$$

$$\eta_2 = 1 - \frac{I_{Tm}}{I_{Tm}+I_{Sm}} \quad (6.5)$$

$$\eta_3 = 1 - \frac{I_{Tb}}{I_{Tb}+I_{Sm}} \quad (6.6)$$

Where I_{Tm}, I_{Tb} and I_{Sm} are PL emissive intensities of bands situated at 456, 544, and 598 nm respectively.

The calculated energy transfer efficiencies for glass R (KZABS: 0.75Tm^{3+}/1Tb^{3+}/1Sm^{3+}) are 47, 28, and 40%, corresponding to ET1, ET2, and ET3 routes respectively.

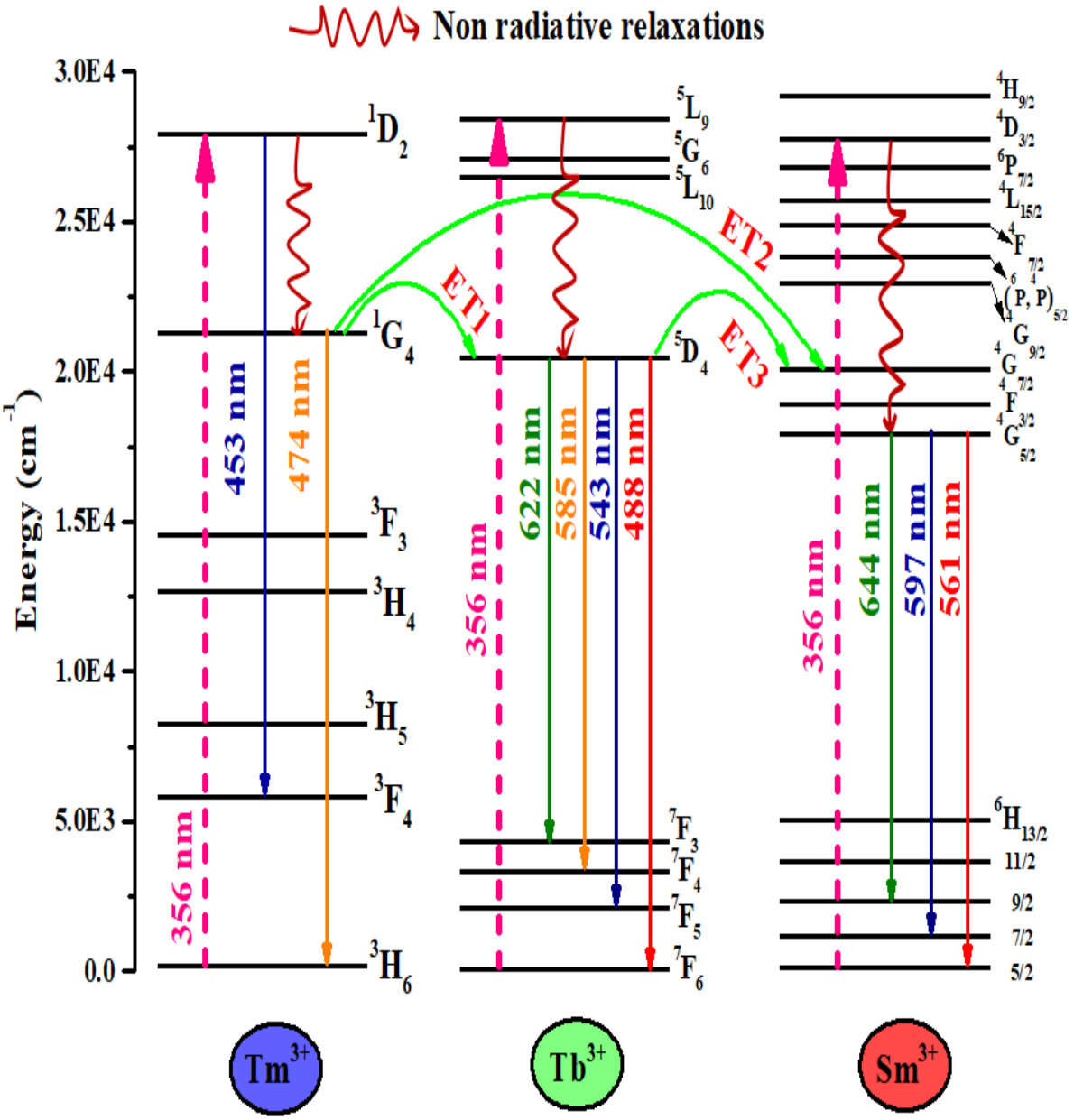

Fig. 6.6. Partial energy level diagram for tri-doped KZABS glasses showing their excitation and emission transitions, including various energy transfer processes via non-radiative relaxations

6.3.4. PL decay curves analysis

The decay curves were investigated for the as-synthesized glasses under their respective emission wavelengths monitoring via 356 nm excitation wavelength to understand more about energy transfer, as shown in Fig. 6.7. The decay profiles for optimized singly doped with Tm^{3+}, Tb^{3+} and Sm^{3+} were recorded under their prominent emissions 456, 544, and 598 nm respectively, as illustrated in Fig. 6.7 (a, b & c). The decay profiles for tri-doped glasses have also been recorded under 456, 544, and 598 nm as depicted in Fig. 6.7. (d, e & f).

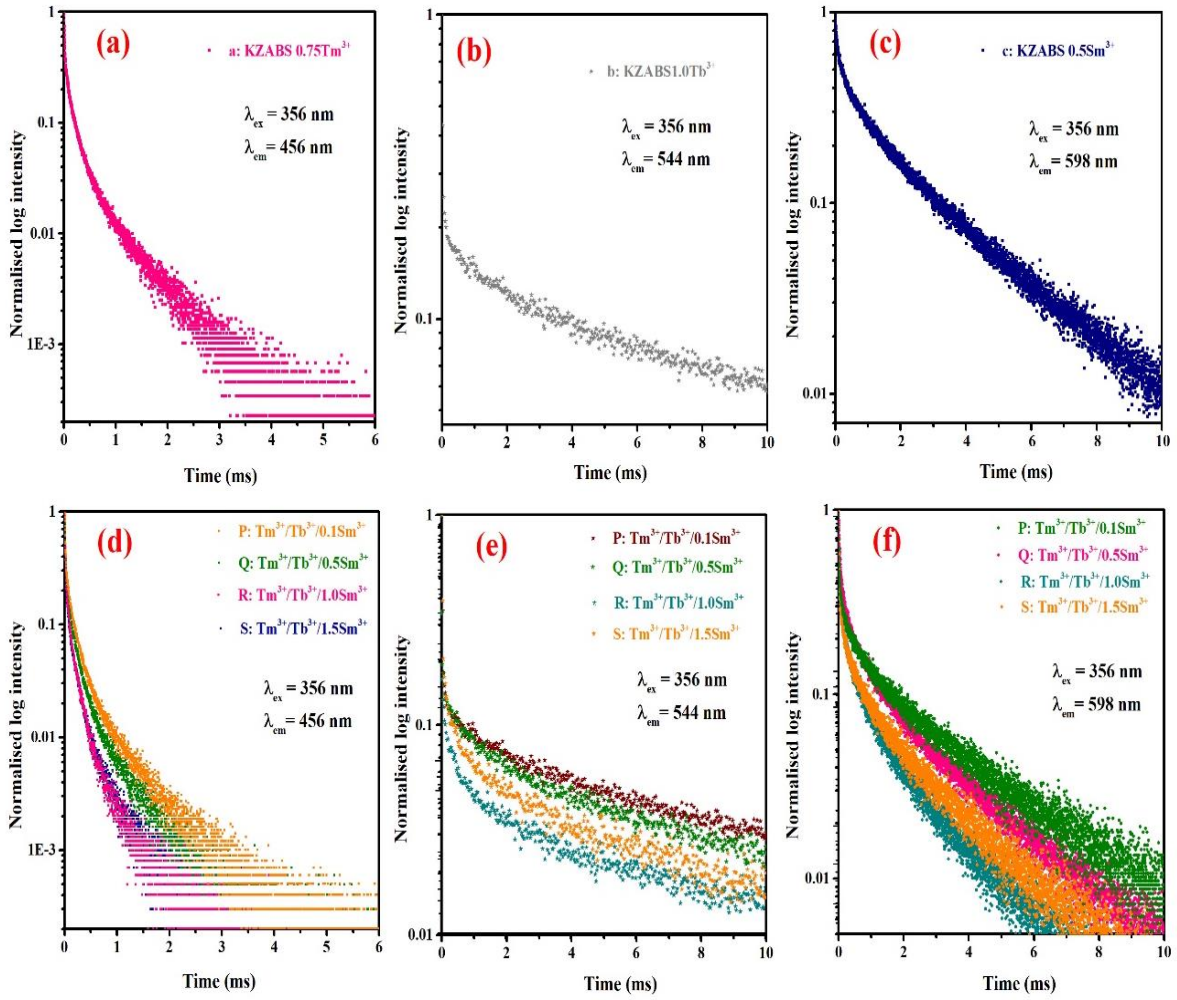

Fig. 6.7. PL decay profiles monitoring via their respective emissions for singly doped glasses [(a)Tm^{3+} under 456 nm (b) Tb^{3+} under 544 nm (c) Sm^{3+} under 598 nm] and tri-doped glasses at (d) 456 nm (e) 544 nm and (f) 598 nm wavelengths.

The non-exponential character of the decay profiles has been confirmed by applying the equation (3.2) The average lifetime (τ_{av}) values were tabulated in table 6.2, as estimated by using the expression (3.3).

Table 6.2

Average lifetime (τ_{av} (ms)) values for the as-prepared glasses under 356 nm excitation wavelength monitoring via different emission wavelengths

Sample ID	λ_{em} = 456 nm	λ_{em} = 544 nm	λ_{em} = 598 nm
a	0.594	-	-
b	-	0.426	-
c	-	-	1.39
P	0.428	0.412	0.985
Q	0.379	0.391	0.893
R	0.238	0.303	0.768
S	0.243	0.284	0.794

It was observed that the average lifetime values are decreasing with increase in Sm^{3+} ion content for tri-doped glasses under different emission wavelengths. When we compare emission wavelengths, it is observed that the lifetime values are lower under 456 and 544 nm emission wavelengths when compared to the 598 nm emission wavelength. It may conclude that energy transfer occurs somewhere more prominent in 456 and 544 than 598 nm emission for tri-doped glasses.

The earlier explained non-exponential decay curves were found best fitted for S=6 in the I-H model as shown in Fig. 6.8. It signifies that the dipole-dipole interaction is responsible for energy transfer via all routes ET1, ET2 & ET3 in the as-synthesized glasses. It is observed that the value of Q and Ro changes with the Sm^{3+} ion concentration and their emission wavelengths.

It demonstrates that energy transfer from one ion to another depends on their concentration and the emission and excitation wavelengths. These values can be used further to obtain donor-acceptor interaction parameter (C_{DA}) as per the equations (3.6 and 3.7)

The values of these parameters for glass R under different emission wavelengths have been depicted in Table 6.3.

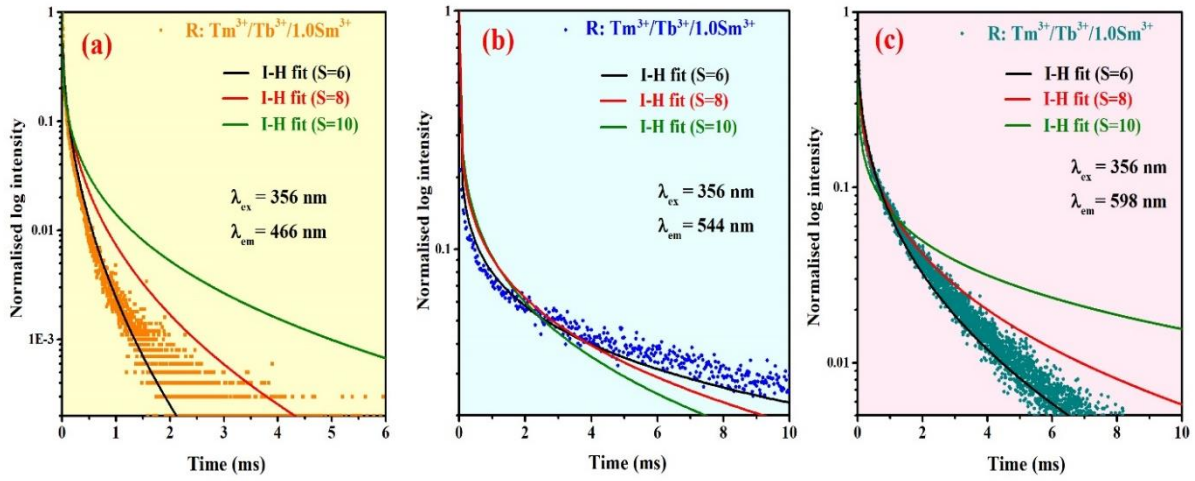

Fig. 6.8. PL decay profiles fitted with I-H model for S = 6, 8 & 10 under different emission wavelengths for tri-doped glass R

6.3.5. TD-PL analysis

The emission profiles of KZABS: $0.75Tm^{3+}/1Tb^{3+}/1Sm^{3+}$ glass (say R) have been recorded under 356 nm excitation to check their variations with temperature in the range 298-448 K as shown in Fig. 6.9. We have seen that the luminescence intensity of titled glass slightly decreases with temperature rise. When the temperature reaches 448 K, the integrated illumination intensity retained 87% compared to 298 K, more significant than the earlier values reported in the literature [109]. It points out the relatively good thermal stability of the titled glass in the range 298-448 K. one more typical parameter to recognize the thermal stability is the activation energy (ΔE) that may be estimated by using equation (3.9), earlier mentioned in chapter 3.

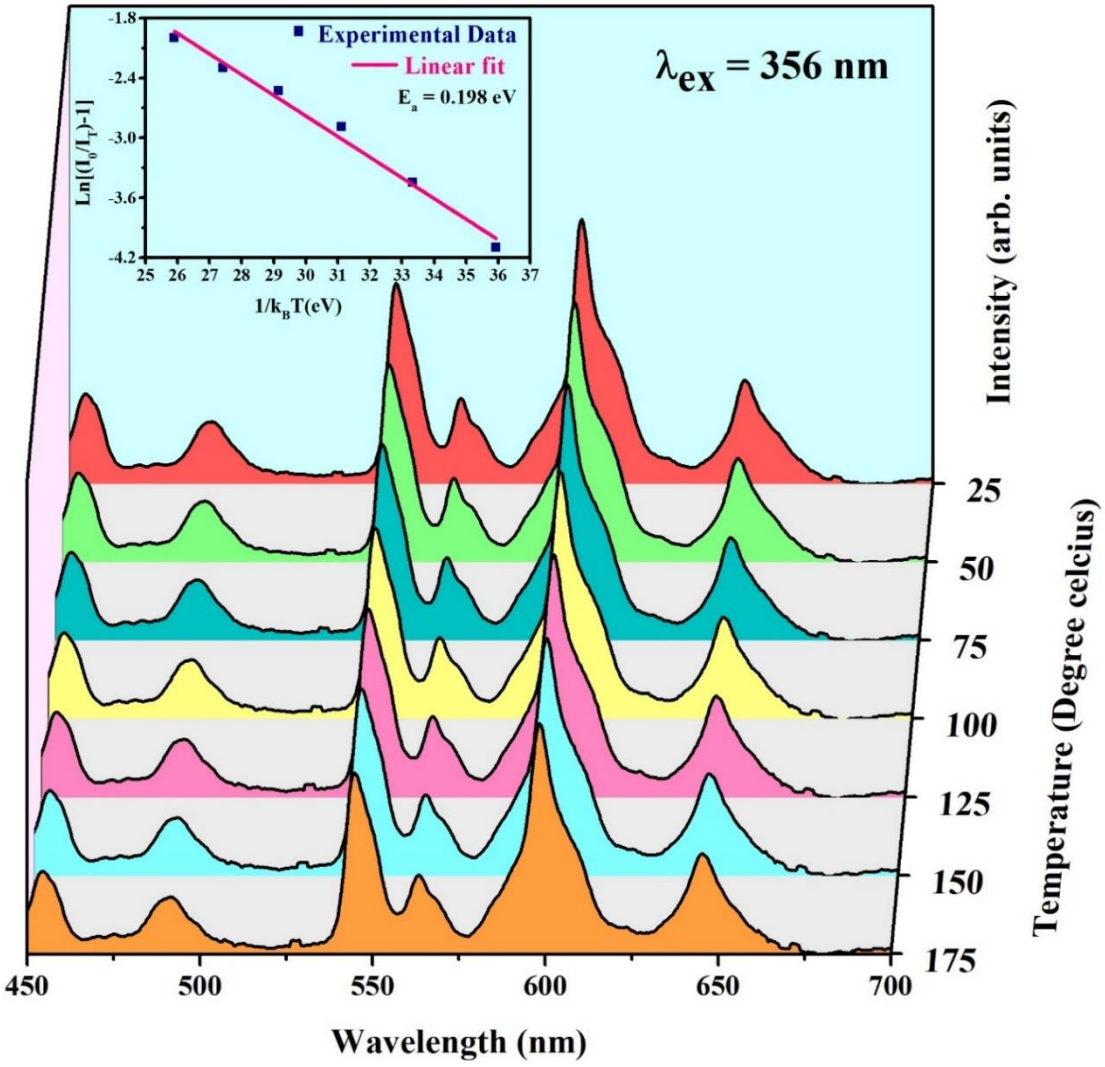

Fig. 6.9. Temperature-dependent PL emission for glass R: KZABS $Tm^{3+}/Tb^{3+}/1.0Sm^{3+}$ under 356 nm excitation (Inset: Variation of $\ln[(I_0/I_T)-1]$ versus $1/k_BT$ for a most illuminated peak at 598 nm under 356 nm excitation)

Equation (3.9) can be simplified as:

$$ln\left(\frac{Io}{I_T}-1\right)=\frac{-\Delta E}{k_BT}+ln\,C \qquad (6.7)$$

Here C is an arbitrary constant. The value of ΔE was found to be 0.198 eV from the slope of the linear fit of equation (6.7) as illustrated in the inset of Fig. 6.9, which is relatively less than the earlier published values in the literature [81].

6.3.6. Colorimetric properties

The CIE 1931 chromaticity diagram has been used to check the actual color emitted by the as-prepared glasses a, b, c, P, Q, R, and S, as shown in Fig. 6.10(a). The corresponding CIE coordinates and CCT values given in Table 6.3 were obtained via their PL emission spectra shown in Fig. 6.3.(a-c) and Fig. 6.4 utilizing the trichromatic color values and their spectral distribution [36]. From Fig. 6.10.(a & b), it is clear that CIE points for singly doped KZABS: RE^{3+}(RE^{3+} = Tm^{3+}, Tb^{3+}, and Sm^{3+}) glasses lies in blue, green and red color respectively and for tri-doped KZABS: $Tm^{3+}/Tb^{3+}/xSm^{3+}$ (x = 0.1, 0.5, 1.0 and 1.5) glasses lies near to standard white region (0.33, 0.33).

Table 6.3

Energy transfer parameter (Q), acceptor-ion concentration (N_0), critical transfer distance (R_0) and donor-acceptor interaction parameter (C_{DA}) for tri-doped glass R under different emission wavelengths.

Emission wavelength (nm)	**Q**	**N_0 (10^{20} ions/cm^3)**	**R_0(Å)**	**C_{DA} (10^{-45} cm^6 s^{-1})**
456	28.23	6.56	4.66	251
544	17.25	6.56	3.96	93
598	11.48	6.56	3.45	41

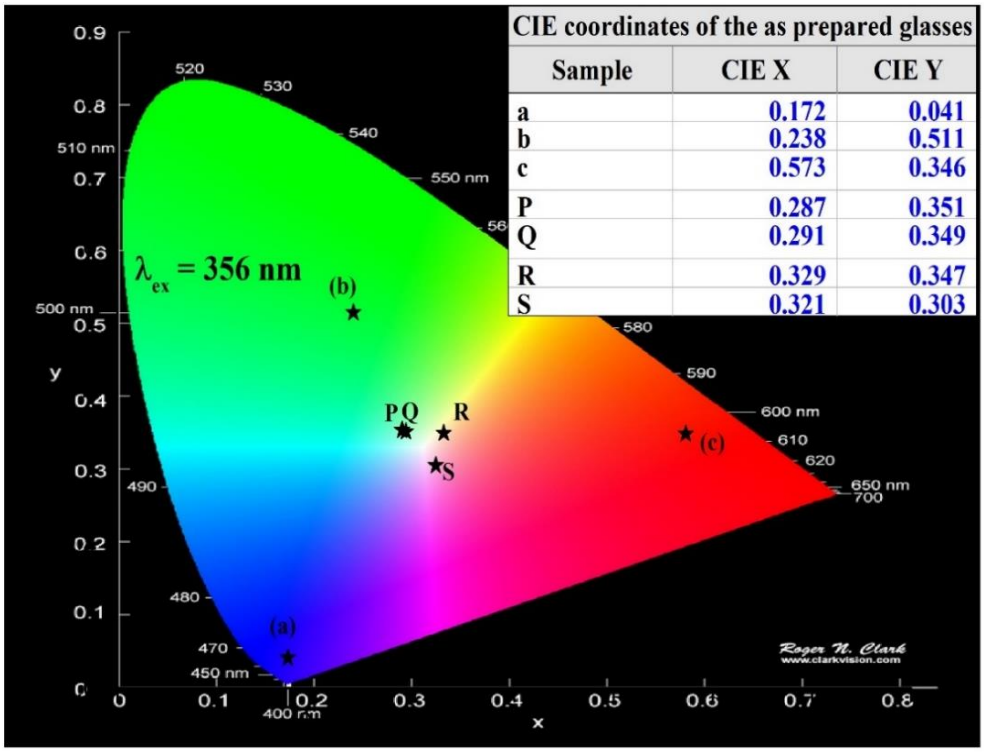

Fig. 6.10. (a) CIE chromaticity diagram for singly doped and tri-doped KZABS glasses under 356 nm excitation wavelength

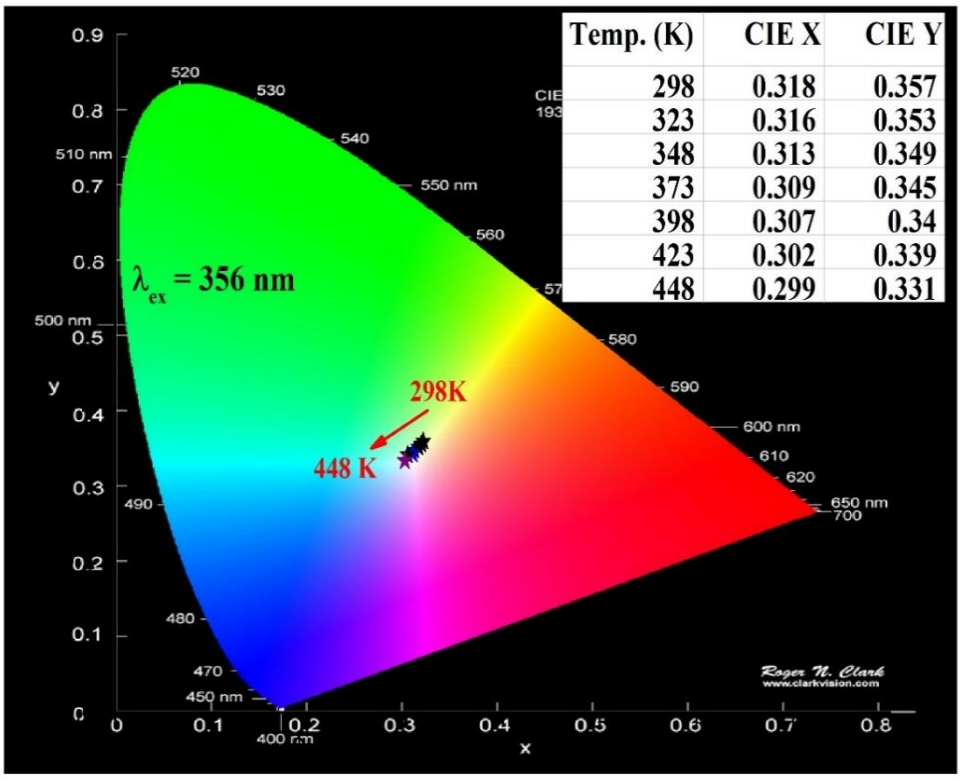

Fig. 6.10. (b) CIE chromaticity diagram for glass R using the TD-PL emission spectra

It is pointed out that the glass KZABS: $Tm^{3+}/Tb^{3+}/1Sm^{3+}$ (R) has CIE points (0.329, 0.347) and CCT (5653K), which are almost near to the ordinary white light (0.33, 0.33, and 5500 K). Thus, tri-doped KZABS: $Tm^{3+}/Tb^{3+}/1Sm^{3+}$ (R) glass can be a promising material for the fabrication of w-LEDs.

6.4. Conclusions

The recorded PL and PL decay profiles show a good amount of energy transfer between Tm^{3+}, Sm^{3+} and Tb^{3+} ions via non-radiative dipole-dipole interaction in thermally stable KZABS glasses. CIE coordinates and CCT values for glass R were observed to be (0.329, 0.347, and 5653K) near the standard white light (0.333, 0.333, and 5500 K). These results suggest that $Tm^{3+}/Tb^{3+}/Sm^{3+}$ KZABS glasses could be a potential candidate for fabricating RGB photonic devices and w-LEDs.

Chapter 7
Conclusions and Future Scope

This chapter summarises the general research work described in this thesis, including the conclusive results drawn from the findings. This chapter also examines the prospect of the present investigation or how it can be expanded and applied to other research areas in the future. Furthermore, we intend to prepare glass-ceramics using the same composition as the present system and evaluate their luminescence features.




7.1 Summary

This thesis reports the structural, optical and photoluminescent properties of KZABS glasses doped with different RE ions suitable for lighting applications especially w-LEDs. In the present work, First we check the individual prime color emission in KZABS glass by adding suitable RE ions into it. Further we combine all three colors to produce white light. Here we summarise the work discussed in previous chapters one by one.

Chapter 3 reports the structural, physical, optical and PL characteristics of Sm-Eu co-doped KZABS glasses prepared by employing the sudden quench method. A broad hump shown by XRD recorded for KZABS host glass confirms the glassy nature of the as-synthesized glass. The presence of functional groups like OH bonding, B-O-B bending, and stretching vibrations in BO_3 and BO_4 tetrahedral units in a KZABS host glass has been confirmed by FT-IR and Raman techniques. Raman spectrum recorded for an un-doped KZABS host glass reveal the phonon energy of host glass as 466 cm^{-1}. Relatively less OH content (52.21 ppm) estimated from the FT-IR spectral features & relatively less phonon energy calculated from the Raman spectrum observed by the host glass speaks about the superior luminescence quality of the host glass. From the PL and PL decay curves, it was concluded that the optimum concentration of Sm^{3+} ion in KZABS borate glass is 0.5 mol% and Sm^{3+} ion transfers a good amount of energy to the Eu^{3+} ion. Dexter theory and I-H model explains that the energy transfer from Sm^{3+} ion to Eu^{3+} ion via non-radiative dipole-dipole interaction. With increase in Eu^{3+} ion concentration, energy transfer efficiency and probability rates are increasing and average lifetime values are decreasing. This again confirming the energy transfer from Sm^{3+} to Eu^{3+} ion. Thus, co-doping of the Sm^{3+}/Eu^{3+} ions lead to the transfer of a good amount of energy and Sm^{3+} ion becomes an efficient sensitizer for Eu^{3+} ions. The CIE coordinates move towards the red region on increasing the Eu^{3+} ion concentration gradually. Further, the TD-PL promises for the good thermal stability of Sm^{3+}/Eu^{3+} co-doped KZABS glass. All the aforementioned results finally

reveal the suitability of the Sm-Eu co-doped KZABS glass for visible photonic applications such as red component in w-LEDs.

In Chapter 4, the Dy^{3+}, Tb^{3+}, Dy^{3+}/Tb^{3+} doped glasses have been effectively prepared by melt-quench method. The amorphous nature of the as prepared glasses has been confirmed by the XRD studies. The green emission of Tb^{3+} (543nm) ions in Dy-Tb co-doped glasses are found to be increasing with increase in Tb^{3+} ion content under 351 nm excitation wavelength. In co-doped glasses, an unidirectional energy transfer has been observed from Dy^{3+} to Tb^{3+} ions. The energy transfer efficiency was found to be 43 and 85% for DyTb0.25 (0.5 mol% of Dy^{3+} and 0.25 mol% of Tb^{3+}) and DyTb1.25 (0.5 mol% of Dy^{3+} and 1.25 mol% of Tb^{3+}) glasses respectively. The I-H model applied to the bi-exponential decay curves reveals the energy transfer process from Dy^{3+} to Tb^{3+} ions via dipole-dipole in nature. The average lifetime values are decreasing with increase in Tb^{3+} ion content and varies from 0.413ms to 0.291ms. This decrease in lifetime values with increase in Tb^{3+} ion content has been attributed to cross relaxation process. Activation energy determined from TD-PL is accounting for the thermal stability of the as-synthesized glasses. The CIE color coordinates are gradually shifting towards deep green color from single doped to co-doped glasses. The luminescent spectral analysis of Dy-Tb co-doped glasses finally allows us to contemplate the superior nature of the as prepared glasses for various green emitting photonic device applications.

In chapter 5, the PL behavior of Tm^{3+} doped KZABS glasses prepared via the melt-quenching process has been studied. XRD pattern confirms the glassy nature of both doped and undoped glasses. The as-prepared glasses emit two different colors blue and red when examined under two different excitation wavelengths 359 and 466 nm respectively. In both cases, the optimum concentration was found to be 0.75 mol%. High bandgap values estimated from absorption spectra are in the range 2.95-2.99eV which are good values for the present glasses to use in optoelectronic devices. A spectral overlap that has been observed between absorption spectra

and excitation spectra creates a scope for the energy transfer between Tm^{3+} - Tm^{3+} ions. Further, Dexter's theory applied to the PL features confirms this energy transfer process as dipole-dipole in nature. This result is also in consonance with the I-H model applied to the PL decay profiles of the titled glasses. The calculated CIE points for optimized glass under two different excitation wavelengths 359 and 466 nm indicate the intense blue and red colors respectively. For both blue and red emissions CP was found to be 96% and 93.8% respectively which indicates the brightness of the emitted colors. Thus, by exciting the KZABS glass sample under two different wavelengths, good color tunability can be achieved. All these investigations represent the suitability of as-prepared glasses in photonic devices such as w-LEDs as well as blue or red color emitting applications.

In chapter 6, we have prepared singly and tri-doped KZABS: RE^{3+} (RE^{3+} = Tm^{3+}, Tb^{3+} and Sm^{3+}) glasses. We have demonstrated various characterization techniques to determine the acceptability of the titled glasses. XRD measurements revealed the glassy nature of as-prepared glasses. From PL, it was observed that the KZABS glasses tri-doped with Tm^{3+}/Tb^{3+}/Sm^{3+} could emit RGB colors simultaneously, and white light may be realized by varying the Sm^{3+} ion content under the 356 nm excitation. The energy transfer confirmed via PL emissions between RE^{3+} ions through the possible roots asTm^{3+} to Tb^{3+} (ET1: $^1G_4$ to $^5D_4$), Tm^{3+} to Sm^{3+} (ET2: $^1G_4$ to $^4G_{7/2}$), and Tb^{3+} to Sm^{3+} (ET3: $^5D_4$ to $^4G_{7/2}$). The decreasing values of the average lifetime with Sm^{3+} ion concentration support the energy transfer and estimated energy transfer efficiencies are 47, 28, and 40% for ET1, ET2, and ET3 processes. The non-exponential decay curves well fitted with the I-H model reveal the mechanism involved in energy transfer is dipole-dipole interaction. The thermal stability of as-prepared glasses can be assured through TDPL measurements and correspondingly estimated CIE coordinates.CIE coordinates and CCT values for glass R were observed to be (0.329, 0.347, and 5653K) near the standard white

light (0.333, 0.333, and 5500 K). These results suggest that $Tm^{3+}/Tb^{3+}/Sm^{3+}$ KZABS glasses could be a potential candidate for fabricating RGB photonic devices and w-LEDs.

7.2 Future Perspectives:

- To calculate the radiative properties of the as-prepared glasses to extend their utility in laser applications.
- To study the up-conversion luminescence of Tm^{3+}/Yb^{3+} co-doped KZABS glasses for the red laser applications.
- To convert the KZABS glasses to glass-ceramics by heat treatment (e.g., for 8 hours, 12 hours, 16 hours and 20 hours) and to understand their luminescence efficiency.
- To explore the sol-gel synthesis method to improve the luminescence and crystallinity in glass-ceramics.

References:

[1] M. Zhao, Y. Liu, S. Ma, D. Liu, K. Wang, Investigation of energy transfer mechanism and luminescence properties in Eu3+ and Sm3+ co-doped ZnWO4 phosphors, J. Lumin. 202 (2018) 57–64. https://doi.org/10.1016/j.jlumin.2018.05.030.

[2] N. Deopa, S. Kaur, A. Prasad, B. Joshi, A.S. Rao, Spectral studies of Eu3+ doped lithium lead alumino borate glasses for visible photonic applications, Opt. Laser Technol. 108 (2018) 434–440. https://doi.org/10.1016/j.optlastec.2018.07.010.

[3] S. Kaur, A.S. Rao, M. Jayasimhadri, B. Sivaiah, D. Haranath, Synthesis optimization, photoluminescence and thermoluminescence studies of Eu3+ doped calcium aluminozincate phosphor, J. Alloys Compd. 802 (2019) 129–138. https://doi.org/10.1016/j.jallcom.2019.06.169.

[4] J. Cho, J.H. Park, J.K. Kim, E.F. Schubert, White light-emitting diodes: History, progress, and future, Laser Photonics Rev. 11 (2017). https://doi.org/10.1002/lpor.201600147.

[5] H. Ji, L. Wang, M.S. Molokeev, N. Hirosaki, R. Xie, Z. Huang, Z. Xia, O.M. Ten Kate, L. Liu, V. V. Atuchin, Structure evolution and photoluminescence of Lu3(Al,Mg)2(Al,Si)3O12:Ce3+ phosphors: New yellow-color converters for blue LED-driven solid state lighting, J. Mater. Chem. C. 4 (2016) 6855–6863. https://doi.org/10.1039/c6tc00966b.

[6] G. Li, J. Lin, Recent progress in low-voltage cathodoluminescent materials: Synthesis, improvement and emission properties, Chem. Soc. Rev. 43 (2014) 7099–7131. https://doi.org/10.1039/c4cs00109e.

[7] S.H. Lee, J.S. Yu, Synthesis and luminescence properties of Eu3+ doped BaGd 2Ti4O13 phosphors, Mater. Res. Bull. 50 (2014) 354–358. https://doi.org/10.1016/j.materresbull.2013.11.009.

[8] K.N. Kumar, L. Vijayalakshmi, J. Choi, J.S. Kim, Efficient red-luminescence of CaLa2ZnO5 phosphors co-doped by Ce3+ and Eu3+ ions, J. Alloys Compd. 787 (2019) 711–719. https://doi.org/10.1016/j.jallcom.2019.02.105.

[9] V. Uma, M. Vijayakumar, K. Marimuthu, G. Muralidharan, Luminescence and energy transfer studies on Sm 3 þ / Tb 3 þ codoped telluroborate glasses for WLED applications TBLT2S, J. Mol. Struct. 1151 (2018) 266–276. https://doi.org/10.1016/j.molstruc.2017.09.053.

[10] S. Ye, F. Xiao, Y.X. Pan, Y.Y. Ma, Q.Y. Zhang, Phosphors in phosphor-converted white light-emitting diodes: Recent advances in materials, techniques and properties, Mater. Sci. Eng. R Reports. 71 (2010) 1–34. https://doi.org/10.1016/j.mser.2010.07.001.

[11] Y.Y. Dikhtyar, D. V. Deyneko, D.A. Spassky, B.I. Lazoryak, S.Y. Stefanovich, A novel high color purity blue-emitting Tm3+-doped β-Ca3(PO4)2-type phosphor for WLED application, Optik (Stuttg). 227 (2021) 166027. https://doi.org/10.1016/j.ijleo.2020.166027.

[12] K.A. Bashar, W.L. Fong, K.A. Haider, S.O. Baki, M.H.M. Zaid, M.A. Mahdi, Optical studies on Tb 3 + : Dy 3 + singly and doubly doped Borosilicate glasses for white light and solid state lighting applications, J. Non. Cryst. Solids. 534 (2020) 119943. https://doi.org/10.1016/j.jnoncrysol.2020.119943.

[13] V. Hegde, C.S.D. Viswanath, N. Chauhan, K.K. Mahato, S.D. Kamath,

Photoluminescence and thermally stimulated luminescence properties of Pr3+-doped zinc sodium bismuth borate glasses, Opt. Mater. (Amst). 84 (2018) 268–277. https://doi.org/10.1016/j.optmat.2018.06.064.

[14] N. Wantana, E. Kaewnuam, Y. Ruangtaweep, D. Valiev, S. Stepanov, K. Yamanoi, H.J. Kim, J. Kaewkhao, Radio, cathodo and photoluminescence investigations of high density WO3-Gd2O3-B2O3 glass doped with Tb3+, Radiat. Phys. Chem. 164 (2019) 108350. https://doi.org/10.1016/j.radphyschem.2019.108350.

[15] S. Mahamuda, K. Swapna, P. Packiyaraj, A. Srinivasa Rao, G. Vijaya Prakash, Visible red, NIR and Mid-IR emission studies of Ho3+ doped Zinc Alumino Bismuth Borate glasses, Opt. Mater. (Amst). 36 (2013) 362–371. https://doi.org/10.1016/j.optmat.2013.09.023.

[16] R. Sharma, A. Prasad, S. Kaur, N. Deopa, R. Rani, M. Venkateswarlu, A.S. Rao, Spectroscopic properties of deep red emitting Tm3+ doped ZnPbWTe glasses for optoelectronic and laser applications, J. Non. Cryst. Solids. 516 (2019) 82–88. https://doi.org/10.1016/j.jnoncrysol.2019.04.032.

[17] K. Siva Rama Krishna Reddy, K. Swapna, M. Venkateswarlu, S. Mahamuda, A.S. Rao, Thermal, Up-Conversion and Near-Infrared Luminescence studies of Erbium ions doped Alkaline-Earth Boro Tellurite glasses, Solid State Sci. 97 (2019). https://doi.org/10.1016/j.solidstatesciences.2019.106016.

[18] S. Nayab Rasool, L. Rama Moorthy, C.K. Jayasankar, Spectroscopic Investigation of Sm3+ doped phosphate based glasses for reddish-orange emission, Opt. Commun. 311 (2013) 156–162. https://doi.org/10.1016/j.optcom.2013.08.035.

[19] Y. Ye, S. Wang, H. An, White-light emission and chromaticity characterization of

Dy3+ doped fluoride glass for standard white light source, J. Non. Cryst. Solids. 526 (2019) 119697. https://doi.org/10.1016/j.jnoncrysol.2019.119697.

[20] F. Grum, R.F. Witzel, P. Stensby, Evaluation of Whiteness., J Opt Soc Am. 64 (1974) 210–215. https://doi.org/10.1364/JOSA.64.000210.

[21] K. El-Egili, Infrared studies of Na 2 O – B 2 O 3 – SiO 2 and Al 2 O 3 – Na 2 O – B 2 O 3 – SiO 2 glasses, Phys. B. 325 (2003) 340–348.

[22] A.A. Ali, Y.S. Rammah, R. El-Mallawany, D. Souri, FTIR and UV spectra of pentaternary borate glasses, Meas. J. Int. Meas. Confed. 105 (2017) 72–77. https://doi.org/10.1016/j.measurement.2017.04.010.

[23] L.K. Bharat, Y. Il Jeon, J.S. Yu, RE3+ (RE3+ = Tm3+, Tb3+ and Sm3+) ions activated Y6WO12 phosphors: Synthesis, photoluminescence, cathodoluminescence and thermal stability, J. Alloys Compd. 685 (2016) 559–565. https://doi.org/10.1016/j.jallcom.2016.05.321.

[24] R.T. Alves, C.M. Trindade, A.C.A. Silva, N.O. Dantas, A.S. Gouveia-Neto, White light generation and energy transfer in Tm3+/Tb3+/Sm3+ -doped 60TeO2. 40ZnO glasses, J. Lumin. 227 (2020) 117543. https://doi.org/10.1016/j.jlumin.2020.117543.

[25] T. Wang, S. Wang, H. Zhang, X. Zou, W. Hu, Tm3+-Dy3+-Eu3+ tri-doped transparent glass-ceramics containing NaY(MoO4)2 crystal phase: Preparation, energy transfer, warm white light emitting, Opt. Mater. (Amst). 104 (2020) 109851. https://doi.org/10.1016/j.optmat.2020.109851.

[26] P. Rekha Rani, M. Venkateswarlu, S. Mahamuda, K. Swapna, N. Deopa, A.S. Rao, Spectroscopic studies of Dy3+ ions doped barium lead alumino fluoro borate glasses,

J. Alloys Compd. 787 (2019) 503–518. https://doi.org/10.1016/j.jallcom.2019.02.088.

[27] Y.H. Nam, W.J. Chung, W. Bin Im, Phosphor in glass using β-SiAlON:Eu2+, CaAlSiN3:Eu2+ and Nd-doped silicate glass for enhanced color gamut of white LED, J. Alloys Compd. 851 (2021) 156945. https://doi.org/10.1016/j.jallcom.2020.156945.

[28] J. Steinbrück, P.W. Nolte, S. Schweizer, Far-field studies on Eu3+-doped lithium aluminoborate glass for LED lighting, Opt. Mater. X. 5 (2020) 2–6. https://doi.org/10.1016/j.omx.2019.100046.

[29] H.Y. Morshidy, M.S. Sadeq, A.R. Mohamed, M.M. EL-Okr, The role of CuCl2 in tuning the physical, structural and optical properties of some Al2O3–B2O3 glasses, J. Non. Cryst. Solids. 528 (2019) 119749. https://doi.org/10.1016/j.jnoncrysol.2019.119749.

[30] M. Rajesh, M.R. Babu, N.J. Sushma, B.D.P. Raju, Influence of Er3+ ions on structural and fluorescence properties of SiO2-B2O3- Na2Co3-NaF-CaF2 glasses for broadband 1.53 μm optical amplifier applications, J. Non. Cryst. Solids. 528 (2020). https://doi.org/10.1016/j.jnoncrysol.2019.119732.

[31] A. Prasad, A.S. Rao, G.V. Prakash, A study on up-conversion and energy transfer kinetics of KGdF4:Yb3+/Er3+ nanophosphors, J. Mol. Struct. 1205 (2020) 127647. https://doi.org/10.1016/j.molstruc.2019.127647.

[32] N. Deopa, B. Kumar, M.K. Sahu, P.R. Rani, A.S. Rao, Effect of Sm 3+ ions concentration on borosilicate glasses for reddish orange luminescent device applications, J. Non. Cryst. Solids. 513 (2019) 152–158. https://doi.org/10.1016/j.jnoncrysol.2019.03.025.

[33] T. Dilova, G. Atanasova, A.O. Dikovska, N.N. Nedyalkov, The effect of light irradiation on the gas-sensing properties of nanocomposites based on ZnO and Ag nanoparticles, Appl. Surf. Sci. (2019) 144625. https://doi.org/10.1016/j.apsusc.2019.144625.

[34] A. M. Nahhas, Introductory Chapter: Overview of ZnO Based Nano Materials and Devices, Zinc Oxide Based Nano Mater. Devices. (2019). https://doi.org/10.5772/intechopen.85969.

[35] B.Y. Huang, B.L. Feng, L. Luo, C.L. Han, Y.T. He, Z.R. Qiu, Warm white light generation from single phase Sr3Y(PO4)3:Dy3+, Eu3+ phosphors with near ultraviolet excitation, Mater. Sci. Eng. B Solid-State Mater. Adv. Technol. 212 (2016) 71–77. https://doi.org/10.1016/j.mseb.2016.07.017.

[36] Ravita, A. S.Rao, Effective sensitization of Eu3+ visible red emission by Sm3+ in thermally stable potassium zinc alumino borosilicate glasses for photonic device applications, J. Lumin. (2021) 118689. https://doi.org/10.1016/j.jlumin.2021.118689.

[37] T. Nazari Aliabadi, P. Alizadeh, Microstructure and dielectric properties of CCTO glass-ceramic prepared by the melt-quenching method, Ceram. Int. 45 (2019) 19316–19322. https://doi.org/10.1016/j.ceramint.2019.06.182.

[38] A.M. Abd-Elnaiem, G. Abbady, A thermal analysis study of melt-quenched Zn5Se95 chalcogenide glass, J. Alloys Compd. 818 (2020) 152880. https://doi.org/10.1016/j.jallcom.2019.152880.

[39] G. Singh, R. Vaish, Melt quenched V2O5/BiVO4 composite: A novel and promising adsorbent and photocatalyst, Mater. Chem. Phys. 240 (2020) 122238. https://doi.org/10.1016/j.matchemphys.2019.122238.

[40] A. Lenarciak, N.A. Wójcik, P. Kupracz, J. Strychalska-Nowak, Z. Sobczak, M. Prześniak-Welenc, J. Karczewski, R.J. Barczyński, Thermal, electrical, and magnetic properties of Fe2O3–PbO–SiO2 glass prepared by traditional melt-quenching and twin roller fast-cooling methods, J. Phys. Chem. Solids. 135 (2019). https://doi.org/10.1016/j.jpcs.2019.05.007.

[41] A. Kaur, A. Khanna, L.I. Aleksandrov, Structural, thermal, optical and photo-luminescent properties of barium tellurite glasses doped with rare-earth ions, J. Non. Cryst. Solids. 476 (2017) 67–74. https://doi.org/10.1016/j.jnoncrysol.2017.09.025.

[42] G. El-Damrawi, A.M. Abdelghany, A.H. Oraby, M.A. Madshal, Structural and optical absorption studies on Cr2O3 doped SrO-P2O5 glasses, Spectrochim. Acta - Part A Mol. Biomol. Spectrosc. (2019) 117840. https://doi.org/10.1016/j.saa.2019.117840.

[43] M.A.K. El-Fayoumi, M. Farouk, Structural properties of Li-borate glasses doped with Sm3+ and Eu3+ ions, J. Alloys Compd. 482 (2009) 356–360. https://doi.org/10.1016/j.jallcom.2009.04.021.

[44] R.A. Talewar, S. Mahamuda, K. Swapna, A.S. Rao, Sensitization of Yb3+ by Nd3+ emission in alkaline-earth chloro borate glasses for laser and fiber amplifier applications, J. Alloys Compd. 771 (2019) 980–986. https://doi.org/10.1016/j.jallcom.2018.08.270.

[45] H. George, N. Deopa, S. Kaur, A. Prasad, M. Sreenivasulu, M. Jayasimhadri, A.S. Rao, Judd-Ofelt parametrization and radiative analysis of Dy3+ ions doped Sodium Bismuth Strontium Phosphate glasses, J. Lumin. 215 (2019) 116693. https://doi.org/10.1016/j.jlumin.2019.116693.

[46] S.K. Lenkennavar, M.K. Kokila, B. Eraiah, Spectroscopic investigation of different

nano metals doped to lead sodium calcium borate glasses, Mater. Today Proc. (2020). https://doi.org/10.1016/j.matpr.2020.02.235.

[47] C. Gautam, A. Madheshiya, A. Kumar Singh, K. Kishor Dey, M. Ghosh, Synthesis, optical and solid NMR studies of strontium titanate borosilicate glasses doped with TeO2, Results Phys. 16 (2020) 102914. https://doi.org/10.1016/j.rinp.2019.102914.

[48] Y. Zhang, C. Lu, L. Sun, Z. Xu, Y. Ni, Influence of Sm2O3 on the crystallization and luminescence properties of boroaluminosilicate glasses, Mater. Res. Bull. 44 (2009) 179–183. https://doi.org/10.1016/j.materresbull.2008.03.004.

[49] S. Kaur, N. Deopa, A. Prasad, R. Bajaj, A.S. Rao, Intense green emission from Tb 3 + ions doped zinc lead alumino borate glasses for laser and w-LEDs applications, Opt. Mater. (Amst). 84 (2018) 318–323. https://doi.org/10.1016/j.optmat.2018.07.020.

[50] R. Sharma, A.S. Rao, Photoluminescence study of Sm3+ doped Zinc Lead Tungsten Tellurite glasses for reddish-orange photonic device applications, Opt. Mater. (Amst). 84 (2018) 375–382. https://doi.org/10.1016/j.optmat.2018.07.035.

[51] P. Du, J.S. Yu, red-emitting phosphors with ultrabroad excitation band for white light-emitting diodes, Sci. Rep. 3 (2017) 1–10. https://doi.org/10.1038/s41598-017-12161-5.

[52] G. Fan, X. Wang, X. Qiu, D. Fan, R. Hu, Z. Tian, Luminescent properties of orange-red emitting phosphors NaGd(MoO4)(WO4):Sm3+ for white LED, Opt. Mater. (Amst). 91 (2019) 363–370. https://doi.org/10.1016/j.optmat.2019.02.023.

[53] F. Ahmadi, A. Asgari, Spectroscopic investigation of Sm3+ doped sulfophosphate glasses for visible photonic applications, J. Non. Cryst. Solids. 505 (2019) 406–413. https://doi.org/10.1016/j.jnoncrysol.2018.11.023.

[54] S. Park, T. Vogt, Near UV excited line and broad band photoluminescence of an anion-ordered oxyfluoride, J. Am. Chem. Soc. 132 (2010) 4516–4517. https://doi.org/10.1021/ja909486j.

[55] H. Xi, S. Chen, Intense red emission and two-way energy transfer in Sm 3 + , Eu 3 + co-doped NaLa (WO 4) 2 phosphors, Mater. Res. Bull. 111 (2019) 140–145. https://doi.org/10.1016/j.materresbull.2018.11.004.

[56] M.E. Alvarez-Ramos, R.C. Carrillo-Torres, R. Sánchez-Zeferino, U. Caldiño, J. Alvarado-Rivera, Co-emission and energy transfer of Sm3+ and/or Eu3+ activated zinc-germanate- tellurite glass as a potential tunable orange to reddish-orange phosphor, J. Non. Cryst. Solids. 521 (2019) 119462. https://doi.org/10.1016/j.jnoncrysol.2019.119462.

[57] S.R. Yashodha, N. Dhananjaya, C. Manjunath, Synthesis and photoluminescence properties of Sm3+ doped LaOCl phosphor with reddish orange emission and it's Judd- Ofelt analysis, Mater. Res. Express. 7 (2020). https://doi.org/10.1088/2053-1591/ab57a6.

[58] S. Arunkumar, K. Marimuthu, Concentration effect of Sm3+ ions in B2O 3-PbO-PbF2-Bi2O3-ZnO glasses - Structural and luminescence investigations, J. Alloys Compd. 565 (2013) 104–114. https://doi.org/10.1016/j.jallcom.2013.02.151.

[59] S. Das, A. Amarnath Reddy, S. Ahmad, R. Nagarajan, G. Vijaya Prakash, Synthesis and optical characterization of strong red light emitting KLaF4:Eu3+ nanophosphors, Chem. Phys. Lett. 508 (2011) 117–120. https://doi.org/10.1016/j.cplett.2011.04.029.

[60] L. Liang, H. Wu, H. Hu, M. Wu, Q. Su, Enhanced blue and green upconversion in hydrothermally synthesized hexagonal NaY1-xYbxF4:Ln3+ (Ln 3+ = Er3+ or Tm3+),

J. Alloys Compd. 368 (2004) 94–100. https://doi.org/10.1016/j.jallcom.2003.07.010.

[61] M.R. Ahmed, B. Ashok, S.K. Ahmmad, A. Hameed, M.N. Chary, M. Shareefuddin, Infrared and Raman spectroscopic studies of Mn2+ ions doped in strontium alumino borate glasses: Describes the role of Al2O3, Spectrochim. Acta - Part A Mol. Biomol. Spectrosc. 210 (2019) 308–314. https://doi.org/10.1016/j.saa.2018.11.053.

[62] M.A. Azooz, H.A. ElBatal, Preparation and characterization of invert ZnO–B2O3 glasses and its shielding behavior towards gamma irradiation, Mater. Chem. Phys. 240 (2020) 122129. https://doi.org/10.1016/j.matchemphys.2019.122129.

[63] R. Boda, M. Shareefuddin, M.N. Chary, R. Sayanna, FTIR and Optical Properties of Europium Doped Lithium Zinc Bismuth Borate Glasses, Mater. Today Proc. 3 (2016) 1914–1922. https://doi.org/10.1016/j.matpr.2016.04.092.

[64] В.М. Денисов, Л.Т. Денисова, О.В. Кучумова, Л.Г. Чумилина, Смачивание золота расплавами системы Bi 2 O 3 –B 2 O 3 , Неорганические Материалы. 50 (2014) 228–232. https://doi.org/10.7868/s0002337x1402002x.

[65] S.M. Abo-Naf, FTIR and UV-VIS optical absorption spectra of gamma-irradiated MoO 3-doped lead borate glasses, J. Non. Cryst. Solids. 358 (2012) 406–413. https://doi.org/10.1016/j.jnoncrysol.2011.10.013.

[66] E.S. Moustafa, Y.B. Saddeek, E.R. Shaaban, Structural and optical properties of lithium borobismuthate glasses, J. Phys. Chem. Solids. 69 (2008) 2281–2287. https://doi.org/10.1016/j.jpcs.2008.04.020.

[67] H. Ebendorff-Heidepriem, W. Seeber, D. Ehrt, Dehydration of phosphate glasses, J. Non. Cryst. Solids. 163 (1993) 74–80. https://doi.org/10.1016/0022-3093(93)90647-G.

[68] J. Suresh Kumar, K. Pavani, A. Mohan Babu, N. Kumar Giri, S.B. Rai, L.R. Moorthy, Fluorescence characteristics of Dy3+ ions in calcium fluoroborate glasses, J. Lumin. 130 (2010) 1916–1923. https://doi.org/10.1016/j.jlumin.2010.05.006.

[69] B.B. Kale, A. Jha, S.K. Apte, P. V. Adhyapak, D.P. Amalnerkar, Removal of OH impurities from GeS2 by reactive atmosphere and its glass preparation, Mater. Chem. Phys. 78 (2003) 330–336. https://doi.org/10.1016/S0254-0584(01)00551-X.

[70] M.R. Ahmed, K.C. Sekhar, A. Hameed, M.N. Chary, M. Shareefuddin, Role of aluminum on the physical and spectroscopic properties of chromium-doped strontium alumino borate glasses, Int. J. Mod. Phys. B. 32 (2018). https://doi.org/10.1142/S0217979218500959.

[71] P. Pascuta, R. Lungu, I. Ardelean, FTIR and Raman spectroscopic investigation of some strontium-borate glasses doped with iron ions, J. Mater. Sci. Mater. Electron. 21 (2010) 548–553. https://doi.org/10.1007/s10854-009-9955-7.

[72] V.M. Krishna, S. Mahamuda, R.A. Talewar, K. Swapna, M. Venkateswarlu, A.S. Rao, Dy3+ ions doped oxy-fluoro boro tellurite glasses for the prospective optoelectronic device applications, J. Alloys Compd. 762 (2018) 814–826. https://doi.org/10.1016/j.jallcom.2018.05.191.

[73] K. Swapna, S. Mahamuda, A. Srinivasa Rao, S. Shakya, T. Sasikala, D. Haranath, G. Vijaya Prakash, Optical studies of Sm3+ ions doped Zinc Alumino Bismuth Borate glasses, Spectrochim. Acta - Part A Mol. Biomol. Spectrosc. 125 (2014) 53–60. https://doi.org/10.1016/j.saa.2014.01.025.

[74] R. V. Perrella, M.G. Manfré, R.R. Gonçalves, G.H. Silva, J.H. Faleiro, H.P. Barbosa, C.A. de Oliveira, M.A. Schiavon, J.L. Ferrari, Dipole-dipole energy transfer

mechanism to the blue-white-red color-tunable emission presented by CaYAlO4:Tb3+,Eu3+ biocompatibility material obtained by the simple and low cost of chemical route, Mater. Chem. Phys. 247 (2020). https://doi.org/10.1016/j.matchemphys.2020.122855.

[75] W.T. Carnall, P.R. Fields, K. Rajnak, Electronic Energy Levels of the Trivalent Lanthanide Aquo Ions. III. Tb 3+ , J. Chem. Phys. 49 (1968) 4447–4449. https://doi.org/10.1063/1.1669895.

[76] R.A. Talewar, S. Mahamuda, K. Swapna, M. Venkateswarlu, A.S. Rao, Spectroscopic studies of Sm3+ ions doped alkaline-earth chloro borate glasses for visible photonic applications, Mater. Res. Bull. 105 (2018) 45–54. https://doi.org/10.1016/j.materresbull.2018.04.033.

[77] P.R. Rani, M. Venkateswarlu, S. Mahamuda, K. Swapna, N. Deopa, A.S. Rao, G.V. Prakash, SC, Mater. Res. Bull. (2018). https://doi.org/10.1016/j.materresbull.2018.10.033.

[78] K. Li, X. Liu, Y. Zhang, X. Li, H. Lian, J. Lin, Host-sensitized luminescence properties in CaNb2O6:Ln3+ (Ln3+ = Eu3+/Tb3+/Dy3+/Sm3+) phosphors with abundant colors, Inorg. Chem. 54 (2015) 323–333. https://doi.org/10.1021/ic502493c.

[79] W.J. Yang, L. Luo, T.M. Chen, N.S. Wang, Luminescence and energy transfer of Eu- and Mn-coactivated CaAl 2Si2O8 as a potential phosphor for white-light UVLED, Chem. Mater. 17 (2005) 3883–3888. https://doi.org/10.1021/cm050638f.

[80] S. Mahamuda, K. Swapna, M. Venkateswarlu, A. Srinivasa Rao, S. Shakya, G. Vijaya Prakash, Spectral characterisation of Sm3+ ions doped Oxy-fluoroborate glasses for visible orange luminescent applications, J. Lumin. 154 (2014) 410–424.

https://doi.org/10.1016/j.jlumin.2014.05.017.

[81] J. Sun, D. Cui, Synthesis, structure, and thermally stable luminescence of Dy 3+-doped Na3YSi2O7 host compound, J. Am. Ceram. Soc. 97 (2014) 843–847. https://doi.org/10.1111/jace.12703.

[82] L. Zhao, D. Wang, C. Chen, Y. Wang, Synthesis and photoluminescence properties of novel CaB6O10:RE3+ (RE = Ce, Tb, Dy, Eu) phosphors under ultraviolet excitation, Mater. Res. Bull. 70 (2015) 817–821. https://doi.org/10.1016/j.materresbull.2015.06.024.

[83] R.T. Alves, C.M. Trindade, A.C.A. Silva, N.O. Dantas, White light generation and energy transfer in Tm 3 þ / Tb 3 þ / Sm 3 þ -doped, J. Lumin. 227 (2020) 117543. https://doi.org/10.1016/j.jlumin.2020.117543.

[84] H. George, N. Deopa, S. Kaur, A. Prasad, M. Sreenivasulu, M. Jayasimhadri, A.S. Rao, Judd-Ofelt parametrization and radiative analysis of Dy3+ ions doped Sodium Bismuth Strontium Phosphate glasses, J. Lumin. 215 (2019) 116693. https://doi.org/10.1016/j.jlumin.2019.116693.

[85] S. Kaur, A.K. Vishwakarma, N. Deopa, A. Prasad, M. Jayasimhadri, A.S. Rao, SC, Mater. Res. Bull. (2018). https://doi.org/10.1016/j.materresbull.2018.04.002.

[86] V. Singh, A. Kumar, C.M. Mehare, H. Jeong, S.J. Dhoble, ur na, Opt. - Int. J. Light Electron Opt. (2019) 163733. https://doi.org/10.1016/j.ijleo.2019.163733.

[87] Y.L. Van Kien, N.R. Liu, A high-performance 94 GHz double-balanced up-conversion mixer for imaging radar sensors in 90 nm CMOS, Analog Integr. Circuits Signal Process. 87 (2016) 21–33. https://doi.org/10.1007/s10470-016-0710-8.

[88] D. V Deyneko, V.A. Morozov, A.A. Vasin, S.M. Aksenov, Y. Yu, S. Yu, B.I. Lazoryak, The crystal site engineering and turning of cross-relaxation in green-emitting β -Ca 3 (PO 4) 2 -related phosphors, J. Lumin. 223 (2020) 117196. https://doi.org/10.1016/j.jlumin.2020.117196.

[89] K. Rawat, A.K. Vishwakarma, K. Jha, Thermally stable Ca 2 Ga 2 SiO 7 : Tb 3 + green emitting phosphor for tricolor w- LEDs application, Mater. Res. Bull. 124 (2020) 110750. https://doi.org/10.1016/j.materresbull.2019.110750.

[90] N. Deopa, A.S. Rao, Photoluminescence and energy transfer studies of Dy 3 + ions doped lithium lead alumino borate glasses for w-LED and laser applications, J. Lumin. 192 (2017) 832–841. https://doi.org/10.1016/j.jlumin.2017.07.052.

[91] N. Deopa, A.S. Rao, S. Mahamuda, M. Gupta, M. Jayasimhadri, D. Haranath, G.V. Prakash, SC, J. Alloys Compd. (2017). https://doi.org/10.1016/j.jallcom.2017.03.020.

[92] L.R. Moorthy, Judd ± Ofelt parametrization and radiative transitions analysis of Tm 3 ‡ doped alkali chloroborophosphate glasses, 12 (1999) 0–6.

[93] P. Dharmaiah, C.S.D. Viswanath, C. Basavapoornima, K. Venkata, C. Kulala, S. Hong, Luminescence and energy transfer in Dy 3 + / Tb 3 + co-doped transparent oxy fl uorosilicate glass-ceramics for green emitting applications, Mater. Res. Bull. 83 (2016) 507–514. https://doi.org/10.1016/j.materresbull.2016.06.044.

[94] E.F. Huerta, O. Soriano-romero, A.N. Meza-rocha, S. Bordignon, A. Speghini, Lithium-aluminum-zinc phosphate glasses activated with Sm 3 þ , Sm 3 þ / Eu 3 þ and Sm 3 þ / Tb 3 þ for reddish-orange and white light generation, 846 (2020). https://doi.org/10.1016/j.jallcom.2020.156332.

[95] Z. Liu, X. Sun, S. Xu, J. Lian, X. Li, Z. Xiu, Q. Li, D. Huo, J. Li, Tb 3 + - and Eu 3 + - Doped Lanthanum Oxysulfide Nanocrystals . Gelatin-Templated Synthesis and Luminescence Properties, (2008) 2353–2358. https://doi.org/10.1021/jp0764687.

[96] J. Pisarska, A. Kos, E. Pietrasik, W.A. Pisarski, Energy transfer from Dy 3 þ to Tb 3 þ in lead borate glass, Mater. Lett. 129 (2014) 146–148. https://doi.org/10.1016/j.matlet.2014.05.035.

[97] M. Vijayakumar, K. Viswanathan, K. Marimuthu, Structural and optical studies on Dy 3 þ : Tb 3 þ co-doped zinc lead fl uoro- borophosphate glasses for white light applications, J. Alloys Compd. 745 (2018) 306–318. https://doi.org/10.1016/j.jallcom.2018.02.211.

[98] Green to white tunable light emitting phosphors : Dy 3 þ / Tb 3 þ in zinc phosphate glasses, 64 (2017) 33–39. https://doi.org/10.1016/j.optmat.2016.11.033.

[99] R. Liu, M. Chen, X. Zhu, Y. Zhou, F. Zeng, Z. Su, Luminescent properties and structure of Dy 3 þ doped germanosilicate glass, J. Lumin. 226 (2020) 117378. https://doi.org/10.1016/j.jlumin.2020.117378.

[100] C. Po, S.A.A. Eu, C.T. Phosphors, K. Li, M. Shang, D. Geng, H. Lian, Y. Zhang, J. Fan, J. Lin, Synthesis , Luminescence , and Energy-Transfer Properties of, 4 (2014). https://doi.org/10.1021/ic500545y.

[101] S. Kaur, A.S. Rao, M. Jayasimhadri, V.V. Jaiswal, D. Haranath, Tb3+ ion induced colour tunability in calcium aluminozincate phosphor for lighting and display devices, J. Alloys Compd. 826 (2020) 154212. https://doi.org/10.1016/j.jallcom.2020.154212.

[102] D.R. Taikar, S. Tamboli, S.J. Dhoble, Optik Synthesis and photoluminescence

properties of red , green, Opt. - Int. J. Light Electron Opt. 142 (2017) 183–190. https://doi.org/10.1016/j.ijleo.2017.05.095.

[103] L.P. Singh, N.P. Singh, S.K. Srivastava, Terbium doped SnO2 nanoparticles as white emitters and SnO2:5Tb/Fe3O4 magnetic luminescent nanohybrids for hyperthermia application and biocompatibility with HeLa cancer cells, (2015) 6457–6465. https://doi.org/10.1039/c4dt03000a.

[104] S.K. Gupta, P.S. Ghosh, A.K. Yadav, N. Pathak, A. Arya, S.N. Jha, D. Bhattacharyya, R.M. Kadam, Luminescence Properties of SrZrO 3 / Tb 3 + Perovskite : Host-Dopant Energy-Transfer Dynamics and Local Structure of Tb 3 +, (2016). https://doi.org/10.1021/acs.inorgchem.5b02639.

[105] K.C. Sobha, LUMINESCENCE OF, AND ENERGY TRANSFER Tb3+ IN NASICON-TYPE PHOSPHATE, 51 (1996) 1263–1267.

[106] M.N. Huang, Y.Y. Ma, X.Y. Huang, S. Ye, Q.Y. Zhang, Spectrochimica Acta Part A : Molecular and Biomolecular Spectroscopy The luminescence properties of Bi 3 + sensitized Gd 2 MoO 6 : RE 3 + (RE = Eu or Sm) phosphors for solar spectral conversion, 115 (2013) 767–771. https://doi.org/10.1016/j.saa.2013.06.111.

[107] M. Vijayakumar, K. Marimuthu, Effect of Tb 3 + concentration on Sm 3 + doped lead fl uoro-borophosphate glasses for WLED applications, J. Non. Cryst. Solids. 447 (2016) 45–54. https://doi.org/10.1016/j.jnoncrysol.2016.05.028.

[108] D. Ramachari, L.R. Moorthy, C.K. Jayasankar, Energy transfer and photoluminescence properties of Dy 3 þ / Tb 3 þ co-doped oxy fl uorosilicate glass – ceramics for solid-state white lighting, Ceram. Int. 40 (2014) 11115–11121. https://doi.org/10.1016/j.ceramint.2014.03.136.

[109] M.K. Sahu, H. Kaur, B. V Ratnam, J.S. Kumar, M. Jayasimhadri, Structural and spectroscopic characteristics of thermally stable Eu 3 + activated barium zinc orthophosphate phosphor for white LEDs, Ceram. Int. 46 (2020) 26410–26415. https://doi.org/10.1016/j.ceramint.2020.07.263.

[110] V. Singh, Ravita, S. Kaur, A.S. Rao, H. Jeong, Green-emitting Tb3+ doped LaP3O9 phosphors for plasma display panel, Optik (Stuttg). 244 (2021) 167323. https://doi.org/10.1016/j.ijleo.2021.167323.

[111] Ravita, A.S. Rao, Effective energy transfer from Dy3+ to Tb3+ ions in thermally stable KZABS glasses for intense green emitting device applic, J. Lumin. 239 (2021) 118325. https://doi.org/10.1016/j.jlumin.2021.118325.

[112] Y.C. Ratnakaram, D. Thirupathi Naidu, A. Vijaya Kumar, J.L. Rao, Characterization of Tm3+ doped mixed alkali borate glasses - Spectroscopic investigations, J. Phys. Chem. Solids. 64 (2003) 2487–2495. https://doi.org/10.1016/j.jpcs.2003.06.001.

[113] B.M. Walsh, N.P. Barnes, D.J. Reichle, S. Jiang, Optical properties of Tm3+ ions in alkali germanate glass, J. Non. Cryst. Solids. 352 (2006) 5344–5352. https://doi.org/10.1016/j.jnoncrysol.2006.08.029.

[114] A. Kermaoui, F. Pellé, Synthesis and infrared spectroscopic properties of Tm3+-doped phosphate glasses, J. Alloys Compd. 469 (2009) 601–608. https://doi.org/10.1016/j.jallcom.2008.02.024.

[115] X. Wang, K. Li, C. Yu, D. Chen, L. Hu, Effect of Tm2O3 concentration and hydroxyl content on the emission properties of Tm doped silicate glasses, J. Lumin. 147 (2014) 341–345. https://doi.org/10.1016/j.jlumin.2013.11.025.

[116] Ł. Marek, M. Sobczyk, W. Wrzeszcz, Relaxation dynamics of excited states of Tm3+ ions in TeO2-ZnO-Na2O-Y2O3 glasses, J. Rare Earths. 37 (2019) 1188–1195. https://doi.org/10.1016/j.jre.2019.03.011.

[117] A. Okasha, A.M. Abdelghany, S.Y. Marzouk, The influence of Ba2+ and Sr2+ ions with the Dy3+ ions on the optical properties of lead borate glasses: Experimental and Judd-Ofelt comparative study, J. Mater. Res. Technol. 9 (2020) 59–66. https://doi.org/10.1016/j.jmrt.2019.10.029.

[118] I.I. Kindrat, B. V Padlyak, R. Lisiecki, V.T. Adamiv, Optical spectroscopy and luminescence properties of a Tm3+-doped LiKB4O7 glass, J. Non. Cryst. Solids. 521 (2019) 119477. https://doi.org/10.1016/j.jnoncrysol.2019.119477.

[119] C. Xu, Y. Song, H. Guan, Y. Sheng, P. Ma, X. Zhou, Z. Shi, H. Zou, The photoluminescence, thermal properties and tunable color of Na1-: XAl1+2 xSi1-2 xO4: X Ce3+/Tb3+/Dy3+ via energy transfer: A single-component multicolor-emitting phosphor, Phys. Chem. Chem. Phys. 19 (2017) 22197–22209. https://doi.org/10.1039/c7cp02789c.

[120] S. Kaur, M. Jayasimhadri, A.S. Rao, A novel red emitting Eu3+doped calcium aluminozincate phosphor for applications in w-LEDs, J. Alloys Compd. 697 (2017) 367–373. https://doi.org/10.1016/j.jallcom.2016.12.150.

[121] W.T. Carnall, P.R. Fields, K. Rajnak, Electronic energy levels of the trivalent lanthanide aquo ions. IV. Eu 8+, J. Chem. Phys. 49 (1968) 4424–4442. https://doi.org/10.1063/1.1669893.

[122] L. Zur, J. Pisarska, W.A. Pisarski, Terbium-doped heavy metal glasses for green luminescence, J. Rare Earths. 29 (2011) 1198–1200. https://doi.org/10.1016/S1002-

0721(10)60626-6.

[123] M. Kumar, A.S. Rao, Concentration-dependent reddish-orange photoluminescence studies of Sm3+ ions in borosilicate glasses, Opt. Mater. (Amst). 109 (2020) 110356. https://doi.org/10.1016/j.optmat.2020.110356.

[124] Ravita, A.S. Rao, Color tunable photluminescence in KZABS: Tm3+ glasses under different sources of excitation for photonic appllications, Jiurnal of Non-Crystalline Solids. 565 (2022).

CURRICULUM VITAE

Ravita (Gold medalist)
Research Scholar
Delhi technological university
Delhi-110042
Contact No: +91-8059558925
Email: ravitapilania64@gmaill.com

Educational Qualification

Degree	Year of Passing	Board/University	Percentage/CGPA
Ph.D	2022	DTU, Delhi	Thesis submitted
M.Sc	2016	DCRUST, Murthal,	85
B.Sc	2014	MDU, Rohtak	73.8
12^{th}	2011	HBSE, Bhiwani	94.8

Awards & Experience:

- Prestigious performance in board
- Gold medal at the post-graduation level
- Awarded “DST Inspire Fellowship” in August 2018
- CSIR-UGC NET-JRF, June 2019
- Best Poster award for presenting a poster entitled “Photoluminescence studies of Sm3+/Eu3+ co-doped KZABS Glasses for optoelectronic device applications” International network of OSA students (IONS-2020), February 29-2^{nd} March 2020 at Indian Institute of Technology, Delhi-110016
- Commendable research award for excellence in research in 2021

Skills

- Patience and understanding
- Enthusiasm and friendliness
- Critical thinking and Time management
- Good handling in high-temperature furnaces and various characterization equipments

LIST OF PUBLICATIONS

1. "Effective Sensitization of Eu^{3+} Visible Red emission by Sm^{3+} in thermally stable Potassium Zinc Alumino Borosilicate Glasses for Photonic Device Applications"

   Ravita, *A. S. Rao*

   Journal of Luminescence, 244 (2022) 118689 (I.F. = 4.171)

2. "Effective energy transfer from Dy^{3+} to Tb^{3+} ions in thermally stable KZABS glasses for intense green-emitting device applications"

   Ravita, *A. S. Rao*

   Journal of Luminescence, 239 (2021) 118325 (I.F. = 4.171)

3. "Color tunable photoluminescence in KZABS: Tm^{3+} glasses under different sources of excitation for photonic applications"

   Ravita, *A. S. Rao*

   Journal of Non-Crystalline Solids, 585 (2022) 121532 (I.F. = 4.458)

4. "Tunable photoluminescence studies of KZABS: RE^{3+} (RE^{3+} = Tm^{3+}, Tb^{3+} and Sm^{3+}) glasses for w-LEDs based on energy transfer"

   Ravita, *A. S. Rao*

   Accepted in Journal of Luminescence, manuscript ID: LUMIN-D-22-00843
   (I.F. = 4.171)

5. "Green-emitting Tb^{3+} doped LaP_3O_9 phosphors for the plasma display panel"

   V. Singh, ***Ravita****, S. Kaur, A.S. Rao, H. Jeong*

   Optik, 244 (2021) 167323 (I.F. = 2.840)

6. "Spectral characteristics of Tb^{3+} doped ZnF2–K2O–Al2O3–B2O3 glasses for epoxy-free tricolour w-LEDs and visible green laser applications"

   A. Kumar, Anu, M.K. Sahu, ***Ravita,*** *S. Dahiya, N. Deopa, A. Kumar, R. Punia, A.S. Rao*

   Journal of luminescence, 43 (2017) 118676 (I.F. = 4.171)

7. "Effect of Annealing on Structural Properties of Fe3O4 Ferrite Nanoparticles"

   Ravita, *Amita, A. Kumar, P.S. Rana*

   Journal of Computational and Theoretical Nanoscience, 24 (2018) 5748-5751, (I.F. = 1.3)

8. "Luminescent studies on Sm^{3+} doped Alkali Zinc Alumino Borosilicate (AZABS) Glasses for w-LED Applications"

   Rajat Bajaj, Pooja Rohilla, Aman Prasad, ***Ravita,*** *Ankur Shandilya, A.S. Rao*

   Communicated to Journal of non-crystalline solids, (I.F. = 4.538)

9. "Luminescent studies on Tm^{3+}/Dy^{3+}/Eu^{3+}doped Potassium Zinc Alumino Borosilicate (KZABS) glasses for color tunability and warm white light generation"

   Ravita, *Aman Prasad, A.S. Rao*

   Communicated to Journal of Luminescence, (I.F. = 4.171)

10. "Cool white light generation from thermally stable Dy^{3+} doped CABS glasses for epoxy-free lighting applications"

    Ravita, *Aman Prasad, Pooja Rohilla, Rajat Baja, Ankur Shandilya, A.S. Rao*

    Communicated to Optical materials, (I.F. = 3.754)

CONFERENCES ATTENDED

- Attended and presented a poster entitled "Luminescence Properties of Sm^{3+} Doped KZABS glasses for w-LEDs" in an International Conference on Atomic, molecular, optical and nanophysics with applications (CAMNP-2019), December 18 - 20th, 2019 at Delhi Technological University, Delhi-110042
- Attended and presented a poster entitled "Photoluminescence studies of Sm^{3+}/Eu^{3+} co-doped KZABS glasses for optoelectronic device applications" in an International network of OSA students (IONS-2020), February 29-2nd March 2020 at Indian Institute of Technology, Delhi-110016
- Attended and presented poster entitled "Effective energy transfer between Dy3+-Dy3+ ion interactions in thermally stable KZABS glasses for yellow color emission useful in a white light generation" in International Conference on Recent Advances in Functional Materials (RAFM-2022), 14-16th March 2022 at ARSD College University of Delhi, Delhi-110021

Journal of Luminescence 244 (2022) 118689

Contents lists available at ScienceDirect

Journal of Luminescence

journal homepage: www.elsevier.com/locate/jlumin

Effective sensitization of Eu^{3+} visible red emission by Sm^{3+} in thermally stable potassium zinc alumino borosilicate glasses for photonic device applications

Ravita, A.S. Rao *

Department of Applied Physics, Delhi Technological University, Bawana Road, New Delhi, 110 042, India

A B S T R A C T

Sm^{3+}/Eu^{3+} co-doped thermally stable potassium zinc alumino borosilicate glasses prepared by melt quenching method have been characterized by using spectroscopic techniques to understand their luminescence behavior. For an undoped glass, the XRD pattern recorded confirms the amorphous nature whereas FT-IR and Raman spectrum confirms the functional groups present. Addition of Sm^{3+} ions as a sensitizer makes the as prepared glasses more efficient for display devices. The mechanism of the energy transfer from Sm^{3+} to Eu^{3+} ion has been observed through non-radiative process. The non-exponential time decay curves are giving decreasing lifetimes with increase in Eu^{3+} ion concentration confirms the energy transfer. The calculated CIE points for the glasses move towards the red region with increase in the concentration of Eu^{3+} ions under the UV excitation. All the results obtained contemplate the suitability of the as prepared glasses for photonic device applications such as w-LEDs, solar cells and display devices.

1. Introduction

Synthesis and characterization of rare earth (RE) ions doped glasses attracted many scientific groups phenomenally due to their significant and widespread applications in fascinating fields like lasers, optical fiber amplifiers, display devices and solid-state lighting (SSL) devices such as w-LEDs [1–4]. Usage of RE doped glasses in SSL technology, especially in w-LEDs, is quite interesting because of their special characteristics like high brightness, less power consumption, financial viability and environment friendly nature [5–7]. Owing to these characteristic features, many researchers are paying attention to the RE doped glasses [8–12]. In literature, several types of glasses such as fluoride, tellurite, halide, borate, silicate and borosilicate glasses have been investigated by the researchers for the aforementioned applications [13–15]. Among these, borate glasses have proved to be a competent candidate for device applications in ultraviolet optics, optical triggers, semiconductors, biomaterials and temperature dependent sensors [15]. Further, these materials could be used as optical device substrates in reflecting windows owing to their special properties like thermal stability, less reactivity, high transparency and high mechanical strength [16,17]. Many types of dopants have been used, like transition metals, heavy metals and RE ions [3,18]. When it comes to high luminescence, RE ions are a unique and better choice as dopants. Broadly, the use of RE ions have seen in all kinds of optical devices like optical fibers, optical detectors, optical amplifiers, and color displays [19,20]. RE metals are a group of 17 elements including Scandium and Yttrium within the lanthanide family. RE ions are extremely important for optical and magnetic behavior due to their 4f valence shell. Out of these, trivalent europium (Eu^{3+}) ion has six 4f valence electrons showing intense red emission in the visible range. Eu^{3+} doped materials are employed in solid-state lasers, w-LEDs, color displays and communication devices [7,21–24].

At present, w-LEDs can be fabricated by various methods. The first method is by exciting a yellow phosphor with a blue LED (or) near-ultraviolet (n-UV) LEDs [24]. Such types of phosphors exhibit relatively low color rendering index (CRI), correlated color temperature (CCT) due to the absence of a red component [25]. CRI defines the quality of the devices; high CRI value means high color emission or good quality of the devices. The more generalized way to fabricate w-LEDs is to combine tricolor (red, green and blue) LEDs, as they have better color stability, color temperature as compared to the blue LED chip based w-LEDs [26]. However, in phosphor-based LEDs, epoxy resins are required which degrade the devices with time. To avoid these problems, people are searching for glass based LEDs [27,28]. The greatest advantage of glass-based LEDs is easy to prepare, financially supportive and no epoxy resins required. Among the three prime colors needed to produce white light, red one is more important for natural white light. Eu^{3+} ions are the good red emitters to explore the photoluminescence in a suitable host. The addition of trivalent Samarium (Sm^{3+}) ion makes it more

* Corresponding author.
E-mail address: drsrallam@gmail.com (A.S. Rao).

https://doi.org/10.1016/j.jlumin.2021.118689
Received 27 July 2021; Received in revised form 15 December 2021; Accepted 16 December 2021
Available online 18 December 2021

Journal of Luminescence 239 (2021) 118325

Contents lists available at ScienceDirect

Journal of Luminescence

journal homepage: www.elsevier.com/locate/jlumin

Effective energy transfer from Dy^{3+} to Tb^{3+} ions in thermally stable KZABS glasses for intense green emitting device applications

Ravita, A.S. Rao *

Department of Applied Physics, Delhi Technological University, Bawana Road, New Delhi, 110 042, India

ARTICLE INFO

Keywords:
Glasses
Photoluminescence
Energy transfer
Decay curves
CIE coordinates
Photonic devices

ABSTRACT

Potassium Zinc Alumino Borosilicate (KZABS) glasses co-doped with Dy^{3+}/Tb^{3+} ions have been synthesized by employing a sudden melt quenching technique. To check the luminescence behavior, the as prepared glasses were characterized by employing spectroscopic tools like photoluminescence (PL) excitation and emission, temperature dependent PL and PL decay to see the energy transfer between Dy^{3+} and Tb^{3+} ions and optimum green emission suitable for photonic applications. The XRD spectra reveals the amorphous nature of the as prepared KZABS glasses. PL spectral features show optimum green emission and confirms energy transfer from Dy^{3+} to Tb^{3+} ions. With the help of temperature dependent PL, glasses were found to be thermally stable. The decay profiles recorded show bi-exponential nature and demonstrates the energy transfer that took place from Dy^{3+} to Tb^{3+} ions. The Inokuti- Hirayama (I–H) model confirms the interaction involved in energy transfer process as dipole-dipole in nature. The CIE coordinates are found to be shifting gradually towards intense green region with increase in activator concentration (Tb^{3+}) under the optimized sensitizer (Dy^{3+}) concentration. It is also observed that, the CIE coordinates shifting towards intense green region when the as prepared KZABS glasses are excited with suitable excitation wavelengths of both sensitizer and activator. All the studies finally reveal the superiority of Dy^{3+}/Tb^{3+} co-doped KZABS glasses for their usage in green emitting photonic device applications such as w-LEDs and display devices.

1. Introduction

The notable progress of the spectral features of rare earth (RE) ions have become an intense research area due to their numerous applications in optical communications, display devices, sensors, optical waveguides, lasers, solid-state lighting (SSL) and w-LEDs. The generation of white light became a global interest of research in past decades due to their huge contribution in optical device technology mainly w-LEDs [1–5]. The key features of w-LEDs like high luminescence efficiency, no usages of fossil fuels are responsible for the replacement of the incandescent and fluorescent lamps [6]. Out of various techniques of fabrication, the RGB phosphor method is most appropriate method to produce w-LEDs due to their high quantum efficiency, lesser size and environmentally suitable conditions [7]. To enhance color rendering index (CRI), either *n*-UV LED in combination with RGB phosphors or blue LED with red and green (RG) phosphor is preferred. However, *n*-UV LED chip is considered as a better solution for pumping the phosphor as they offer higher luminous efficiency when compared with blue LED chip [8]. The inorganic oxides are considered as one of the best choices for white light emission using RGB phosphors due to both high chemical stability and luminescence efficiency. Among these RGB phosphors, the phosphors such as $Ca_8ZnLa(PO_4)_7:Tb^{3+}$ and $NaCaPO_4:Tb^{3+}$ have been investigated for the green color in the development of RGB phosphor converted *n*-UV-LEDs [9,10]. The green color emitting phosphors has generally an excitation band either in UV-B (280–315 nm) or UV-C (100–280 nm) region. Therefore, there is an extreme requirement of *n*-UV excitable green colored phosphors [11]. However, there are some drawbacks in the usage of an epoxy resin for coating RGB phosphors to construct w-LEDs. Usage of epoxy resins results into the degradation of output in terms of CRI, lifetime, and stability with time [12,13]. Therefore, it is needed to develop a phosphor free w-LED that can emit white light with improved luminous efficiency and CRI with stable colour temperature and cost effective in comparison to the conventional phosphor based w-LEDs [6].

In recent years, researchers found that glasses doped with RE ions are most appropriate alternatives for the epoxy resin containing phosphors. RE doped glasses become superior day by day among other materials due to their special features like easiness in shaping, fully recyclable

* Corresponding author.
E-mail addresses: drsrallam@gmail.com, drsrallam@dce.ac.in (A.S. Rao).

https://doi.org/10.1016/j.jlumin.2021.118325
Received 19 February 2021; Received in revised form 3 June 2021; Accepted 3 July 2021
Available online 14 July 2021

Journal of Non-Crystalline Solids 585 (2022) 121532

Contents lists available at ScienceDirect

Journal of Non-Crystalline Solids

journal homepage: www.elsevier.com/locate/jnoncrysol

Color tunable photoluminescence in KZABS: Tm^{3+} glasses under different sources of excitation for photonic applications

Ravita, A.S. Rao *

Department of Applied Physics, Delhi Technological University, Bawana Road, New Delhi 110042, India

ARTICLE INFO

Keywords:
Borosilicate Glasses
Photoluminescence
Energy transfer
Decay curves
CIE coordinates

ABSTRACT

Potassium Zinc Alumino Borosilicate (KZABS) glasses doped with Tm^{3+} ions have been prepared by using a melt quenching process and further investigated through various spectroscopic tools such as optical absorption, photoluminescence (PL) excitation, PL emission, and PL decay measurements. The non-crystalline nature of the as-prepared glasses was confirmed by XRD measurements. PL spectral properties show blue and red colors under different excitation wavelengths. The absorption spectrum recorded in the UV-Vis-NIR range reveals the high bandgap energy. The Inokuti-Hirayama (I-H) model well fitted to non-exponential decay curves confirms the energy transfer between Tm^{3+}-Tm^{3+} ions as dipole-dipole in nature. Under 359 and 466 nm excitation wavelength the titled glasses are showing CIE coordinates falling in deep blue and deep red color, respectively. A good color tunability can be seen from the blue to the red region under different excitation wavelengths. All the studies finally reveal the superiority of Tm^{3+} doped KZABS glasses for their usage in blue/red-emitting photonic devices needed to fabricate photonic devices such as w-LEDs.

1. Introduction

Rare-Earth (RE) ion doped crystalline and non-crystalline systems become a prominent choice for research in the last few decades because of their wide use in the areas of solid-state lighting (SSL), photovoltaics, optical devices, laser systems, and display devices [1–3]. In modern SSL technologies, white-light-emitting diodes (w-LEDs) are interesting devices because of their outstanding performance such as less power consumption, more lifetime, high efficiency, high stability, eco-friendly, and many more [4–6]. A Commercial way to attain white light is to mix yellow and blue emissions. The most common source used for blue color is Gallium-based semiconductor chips [7] and for yellow color is yttrium-aluminum-garnet doped with Ce^{3+} ions (YAG: Ce^{3+}) [8]. The light produced by this method is in contrast with natural light and has some limitations such as low color stability, less efficiency, correlated color temperature (CCT), and thermal stability. Color stability and CCT values speak a lot about the performance of the device. Because of the red component deficiency, the aforementioned problem arises [9]. These problems can be solved by using phosphor-based LEDs. White light can be achieved by using tricolor (red, green, and blue abbreviated as RGB) LEDs in an appropriate ratio [10,11]. Pronounced LEDs become good replacements for traditional lights because of their durability and high efficiency. The main concern with phosphor-based LEDs is their high synthesis temperature and the epoxy resin requirement, which results in the degradation of units in terms of lifetime, health risks (due to high temperature), and efficiency [12,13]. Oxidative degradation is also the main problem with RGB phosphor. Also, the modern SSL applications were limited by the rapid degradation of blue color as the blue light was absorbed by red and green light hence resulting in poor blue emission [1]. $BaMgAl_{10}O_{17}:Eu^{2+}$ is the well-known commercial phosphor emitting blue color but it has some drawbacks such as high temperature, oxidative degradation due to which the performance of the device reduces with time [14]. To overcome these difficulties, RE doped glasses can be appropriate alternatives because of easy fabrication techniques, economic and environment friendly, and especially no epoxy resin required in it [15–20].

RE doped host matrices are extensively explored having potential applications in the field of light emission due to their 4f valence shell [21,22]. Lanthanide family with scandium and yttrium comes under RE metals. RE ions exist in their most stable 3+ oxidation state having high stability because 4f orbital is well shielded by $5s^2 5p^6$ octet. Each RE ion has different emission properties due to its unique electronic energy distribution. A large number of RE ions have been examined such as Eu^{3+} [10], Sm^{3+} [4], Pr^{3+} [17], Nd^{3+} [23], Tb^{3+} [2], Ho^{3+} [15], and

* Corresponding author.
E-mail address: drsrallam@dce.ac.in (A.S. Rao).

https://doi.org/10.1016/j.jnoncrysol.2022.121532
Received 22 January 2022; Received in revised form 22 February 2022; Accepted 25 February 2022
Available online 4 March 2022

Optik - International Journal for Light and Electron Optics 244 (2021) 167323

Contents lists available at ScienceDirect

Optik

journal homepage: www.elsevier.com/locate/ijleo

Original research article

Green-emitting Tb^{3+} doped LaP_3O_9 phosphors for plasma display panel

Vijay Singh [a,*], Ravita [b], Sumandeep Kaur [b], A.S. Rao [b], Hoonil Jeong [a]

[a] Department of Chemical Engineering, Konkuk University, Seoul 05029, Republic of Korea
[b] Department of Applied Physics, Delhi Technological University, Bawana Road, New Delhi 110042, India

ARTICLE INFO

Keywords:
Co-precipitation
Plasma display panel
Tb^{3+} ions
LaP_3O_9
Photoluminescence

ABSTRACT

$La_{1-x}P_3O_9:xTb^{3+}$ ($x = 0.005 \leq x \leq 0.11$) phosphors were prepared via the co-precipitation method. The crystal phase was analyzed by X-ray diffraction and the various functional groups in the host were investigated using Fourier transform infra-red (FT-IR) spectroscopy. The luminescence properties of the Tb^{3+} ions were studied using photoluminescence (PL) excitation and emission spectra. The PL analyses under ultraviolet (UV) and vacuum ultraviolet (VUV) excitation both gave almost similar results. The green emission was observed at 546 nm, corresponding to the transition $^5D_4 \rightarrow {}^7F_5$ under 251, 147 and 172 nm excitation. The optimum concentration was 0.09 mol. The calculated CIE coordinates were shifted towards the intense green region from the pale white region with increasing Tb^{3+} ion concentration. The obtained results demonstrated the potential for LaP_3O_9 as a candidate in lighting and plasma display panel (PDP) applications.

1. Introduction

Ongoing international research has improved the fabrication and design of materials which are eco-friendly, chemically stable, cheaper, thermally and mechanically stable and possessing good optical properties [1–3]. Luminescent materials incorporating rare earth (RE) ions are showcasing applications in diverse areas such as flat panel displays (FPD), solid state lighting (SSL), light-emitting diodes (LEDs) and thermal sensors [1,4–7]. For large screens, high-definition television (HDTV) is in great demand, but cathode ray tubes (CRTs) take up very large space and are bulky. Thus, FPDs such as electroluminescence display (ELD), plasma display panel (PDP) and liquid crystal display (LCD) have attracted research for the market of large screen displays. As ELD and LCD are advanced FPDs as compared to PDP, they have certain drawbacks, such as, for LCDs, restricted viewing angle, slow response speed and difficulty in assembling a screen larger than 30 inches, and for ELDs, availability restricted to neutral and multicolor ELDs specialized for some medical instruments and portable computers. Therefore, PDP has potential among the different FPDs for use in wall mounting HDTV due to its bigger size. Moreover, it consumes very low power, has a broad viewing angle, and provides fast response, along with many other advantages [8,9]. For PDPs, inert gas plasma is used to excite the primary color (red, green and blue) phosphors by vacuum ultraviolet (VUV) radiation [10].

The literature reveals that phosphors with lanthanide oxides are more efficient with a broad excitation band [11]. $LnPO_4$ is the most studied lanthanide orthophosphate [12,13]. Some reports focused on polyphosphates like LnP_3O_9 because of its special structure [14,15]. From this background, we selected LaP_3O_9 as a host material. Recently, many researchers have examined the structural and

* Corresponding author.
E-mail address: vijayjiin2006@yahoo.com (V. Singh).

https://doi.org/10.1016/j.ijleo.2021.167323
Received 21 April 2021; Accepted 28 May 2021
Available online 1 June 2021

Journal of Luminescence 244 (2022) 118676

Contents lists available at ScienceDirect

Journal of Luminescence

journal homepage: www.elsevier.com/locate/jlumin

Spectral characteristics of Tb^{3+} doped ZnF_2–K_2O–Al_2O_3–B_2O_3 glasses for epoxy free tricolor w-LEDs and visible green laser applications

A. Kumar [a], Anu [b], M.K. Sahu [b], Ravita [b], S. Dahiya [c], Nisha Deopa [a,*], Anand Malik [a], R. Punia [c], A.S. Rao [b]

[a] Department of Physics, Chaudhary Ranbir Singh University, Rohtak Bypass Road, Jind, 126102, Haryana, India
[b] Department of Applied Physics, Delhi Technological University, Bawana Road, New Delhi, 110 042, India
[c] Department of Physics, Maharshi Dayanand University, Rohtak, 124001, Haryana, India

A B S T R A C T

In the current work, a series of Zinc Potassium Alumino fluoroborate (ZKAlFB) glasses doped with different concentrations of Terbium ions (Tb^{3+}) were synthesized by employing the melt-quench technique. The spectroscopic properties of the as-prepared glass samples were examined using characterization techniques like XRD, FT-IR, DSC, UV–vis–NIR absorption and emission to unlock their utility in photonic devices. Absorption spectral information was used to determine the nature of bonding between Tb^{3+} ions and its surrounding ligands. FT-IR spectral information recorded for an undoped glass has been used to understand various functional groups present in the as-prepared ZKAlFB glass. The DSC thermogram was used to estimate glass thermal stability (ΔT) and transition temperature (Tg) of the as-prepared ZKAlFB glass. The Judd-Ofelt (J-O) intensity parameters estimated from absorption spectral data are correlated with the emission spectral profiles to estimate radiative properties. The photoluminescence (PL) intensity of the as-prepared ZKAlFBTb glasses is found to be maximum for 1 mol% of Tb^{3+} ions and beyond decreases showing concentration quenching. Using PL spectral data, the CIE color coordinates, and Correlated Color Temperature (CCT) values were evaluated to understand the suitability of the as-prepared glasses for green color emitting photonic devices. The experimental lifetime values estimated from the decay profiles are decreasing with elevation in Tb^{3+} ion concentration due to energy transfer through the cross-relaxation process. Quantum efficiency (η), emission cross-section (σ_{se}), CIE and CCT values obtained for 1 mol% Tb^{3+} ions doped ZKAlFB glass demonstrates its superiority in fabricating epoxy free tricolor w-LEDs and visible green lasers.

1. Introduction

The development of inorganic lighting technology has gained widespread consideration for the rare earth (RE) doped glasses that act as a leading idea in the construction of photonic devices, and their luminescence properties play a significant role in fabricating w-LEDs and color displays [1–5]. Further, the RE ions in glasses are optically active that can reveal diverse properties of massive significance in the field of science and technology.

[6]. The exclusive features that discriminate RE ions from other ions (transition metal ions) are their electronic enrich arrangement, which shows the shielding of 4f shell by external 5s and 5p sub-shells and in turn expedite them as optically active, revealing longer lifetime and narrow emissions [7,8]. Furthermore, RE ions activated glasses have received more attention over crystals and ceramics due to their wide in-homogeneous bandwidths, cheap production cost and high quantum efficiency [2]. They possess various auspicious applications such as optical fibers, display devices, w-LEDs, lasers, memory devices, sensors, and waveguides [3–5].

Recently, the w-LEDs have been used globally in every household, restaurant and office owing to their excellent characteristics such as environmental friendliness, longer lifespan, lower fabrication cost and higher reliability [9,10]. The w-LEDs can be fabricated by combining blue color emitting LED InGaN chip with yellow color emitting YAG: Ce^{3+} phosphor. This popular technique of producing w-LEDs is deprived of poor color rendering index (CRI) and halo-effect [11,12]. To resolve the aforesaid problems, RGB phosphors are pumped with n-UV LEDs that support in reducing the halo effect and refining the CRI value. However, both techniques provide encapsulated phosphors in an epoxy region that can deteriorate at intense excitation & temperatures, causing a decrease in its output progressively [13,14]. Therefore, glasses doped with RE ions might be considered the probable aspirants and alternatives for devising w-LEDs due to the absence of epoxy region.

The selection of the host matrix is generally known to be a critical challenge in studying the luminescence behavior of materials. Among the various oxide glass formers such as borate, borosilicate, germinate,

* Corresponding author.
E-mail address: nispectro999@gmail.com (N. Deopa).

https://doi.org/10.1016/j.jlumin.2021.118676
Received 7 April 2021; Received in revised form 26 November 2021; Accepted 9 December 2021
Available online 18 December 2021

Tunable photoluminescence studies of KZABS: RE^{3+} (RE^{3+} = Tm^{3+}, Tb^{3+} and Sm^{3+}) glasses for w-LEDs based on energy transfer

Ravita, A.S. Rao*

Department of Applied Physics, Delhi Technological University, Bawana Road, New Delhi-110 042, INDIA

ABSTRACT

Here singly and tri-doped ($Tm^{3+,}$ Tb^{3+}, and Sm^{3+}) borosilicate glasses in potassium Zinc alumino borosilicate (KZABS) glasses were prepared by using the melt quenching technique. The tri-doped as-prepared KZABS glasses were characterized through photoluminescence (PL) emission and PL decay to demonstrate red (Sm^{3+}), green (Tb^{3+}) and blue (Tm^{3+}) colors simultaneously and white light realization by varying the Sm^{3+} ion concentration under 356 nm excitation. The energy transfer mechanism from Tm^{3+} to Tb^{3+} ($^1G_4$ to $^5D_4$), Tm^{3+} to Sm^{3+} ($^1G_4$ to $^4G_{7/2}$), and Tb^{3+} to Sm^{3+} ($^5D_4$ to $^4G_{7/2}$) are confirmed by the lifetime values. The I-H model fitted with non-exponential decay curves reveals the dipole-dipole interaction. The temperature-dependent PL (TDPL) measurement and corresponding CIE points demonstrate the thermal stability of the as-prepared glasses. CIE coordinates and CCT values were observed near the standard white light (0.333, 0.333, and 5500 K). The results obtained reveal that Tm^{3+}/Tb^{3+}/Sm^{3+} tri-doped KZABS glasses could be a potential candidate for the fabrication of visible RGB luminescent materials, display devices and w-LEDs.

Keywords: *Glasses, photoluminescence, energy transfer, decay curves, CIE coordinates, photonic devices*

*Corresponding author: (Prof. A.S. Rao)

E-mail IDs: drsrallam@gmail.com; drsrallam@dce.ac.in